THE CONFLATION OF BUILDING SIMULATION (BS) AND COMPUTATIONAL FLUID DYNAMICS (CFD) FOR THE PREDICTION OF THERMAL PERFORMANCE OF FACADE FOR NATURALLY VENTILATED RESIDENTIAL BUILDINGS IN SINGAPORE

WANG LIPING

(*B.Eng., MSc. Eng., Xi'an Univ. Arch. & Tech., China*)

A THESIS SUBMITTED

FOR THE DEGREE OF DOCTOR OF PHILOSOPHY

DEPARTMENT OF BUILDING

NATIONAL UNIVERSITY OF SINGAPORE

2006

Dedication

To my parents Yifang , Yanwen and my husband Qi

Acknowledgements

First of all, I would like to express my sincere thanks to my supervisor, Professor Wong Nyuk Hien, for his sound guidance and encouragement during my three and half year study in National university of Singapore. I feel grateful for having the opportunity to do research work under the direction of him. His knowledge helped me to deeply understand the problems and quickly build up my research approach.

I would like to thank my thesis committee members, Professor Lee Siew Eang, and Professor Chew Yit Lin(Michael), for providing me with valuable comments and advisement to improve my thesis. I would like to sincerely thank Professor Tham, Professor Sekhar, and Professor Cheong for their precious suggestions for me to build up this research topic.

I would like to express my special thanks to Professor Chen Qingyan, Professor Santamourious, Dr. Zhai Zhiqiang, Dr. Jiang Yi, Dr. Xu weiruan, Dr. Ery, for their precious help in the fields of natural ventilation studies. I thank Mr. Wang Junhong and Mr. Zhang Xinhuai for their tireless help during the process of running my simulation works. I also thank Dr. Henry Feriadi, Dr. Priyadarsini, Chen Yu, Jiafang, Li Shuo for their time and knowledgeable help in my thesis.

Table of Contents

Summary

Passive cooling by natural ventilation is becoming an attractive alternative to alleviate problems associated with air-conditionings such as energy shortage, sick building syndrome and global warming. Although the concept of natural ventilation is not complicated, it is a challenge to design naturally ventilated buildings as natural ventilation is difficult to control. It is important for architects and engineers to predict the performance of natural ventilation, especially in the early design and renovation stages. Unfortunately, there are no available simulation tools to accurately and quickly predict natural ventilation design in detail.

To improve evaluation quality of thermal comfort in buildings and provide facade design guidelines for naturally ventilated buildings, a program with a text-mode interface that coupled the computational fluid dynamics (FLUENT) and building simulation program (ESP-r) for long term natural ventilation prediction was developed.

In order to correctly simulate the particular spaces with CFD, boundary conditions at the integrating surface have been provided by ESP-r. Different coupling strategies, including pressure boundary conditions and velocity boundary conditions, have been investigated to provide better prediction of natural ventilation. The results on averaged indoor air temperature by coupled simulations are compared with those by building simulations alone.

Mean pressure coefficients, which have significant impacts on coupled simulations, were investigated with various turbulence models to predict outdoor airflow simulation and obtained the accurate pressure coefficients of external surface and validated with experiment results.

The coupling program was validated by a series of validation studies, including single zone cases, multi-zone cases, and field measurement studies. The results show that the coupled simulations can produce much better results than building simulation alone especially in the aspect of indoor air velocity prediction.

The integration of building simulation (BS) and computational fluid dynamics (CFD) simulation provides a way to assess the performance of natural ventilation in whole buildings, and the detailed thermal environment information in a particular space within a reasonable simulation time.

The feasibility of natural ventilation based on typical year weather data was investigated. Thermal comfort criteria for naturally ventilated residential buildings, including thermal comfort index (PMV) and thermal asymmetry, were used to evaluate various facade designs. Parametric facade design studies were carried out to provide facade design guidelines for naturally ventilated buildings in Singapore and the benefits of this coupling program were highlighted.

List of Tables

List of Figures

Chapter 1 Introduction

Facade is considered to be the meso-environment between the micro-environment of humans and the external macro-environment. It plays an important part in contributing to a productive and comfortable individual life, especially in naturally ventilated buildings. How to optimize facade designs to achieve the comfortable indoor thermal environment in naturally ventilated buildings becomes an important research area. This chapter briefly reviews the status of facade designs in hot-humid climate and the current methodologies for natural ventilation studies, and provides background for this research, and indicates the needs to provide coupling tools for quickly and accurately predicting long term natural ventilation for various facade design evaluation.

1.1 Background of natural ventilation and facade design studies

There is a growing interest in the application of natural ventilation in buildings due to the energy, indoor air quality and environmental problems associated with mechanically ventilated buildings. Various mechanical systems including heating, ventilation and air-conditioning (HVAC) systems in residential and office buildings contribute substantially to the energy consumption. As the benefits of natural ventilation, including reducing operation costs, improving indoor air quality and providing satisfactory thermal comfort in certain climates, are recognized, passive cooling of houses using natural ventilation has become an attractive alternative to alleviate the associated problems with air-conditioned buildings.

The concept of natural ventilation is well accepted and welcomed by people and designers in the world. Even in places with hot-humid climates, where air-conditioners are ordinary in both office and commercial buildings, naturally ventilated buildings are not uncommon. For example, 86% of the people in Singapore live in HDB (Housing & Development Board) residential buildings, which are designed to be naturally ventilated.

Natural ventilation is difficult to design and control although the principle itself is not difficult to understand. The excessive amount of moisture in the air and intensive solar radiation make many passive cooling design strategies difficult to implement in hot and humid regions. The success of a naturally ventilated building is decided by a good indoor climate, which influences its sustainability. Thermal performance of façade components plays an important role in determining heat gains into buildings which can determine the indoor environment, especially for buildings with low internal heat source such as residential buildings or schools. For this reason, naturally ventilated building designs in hot-humid climates need to pay more attention to orientations, shading devices, material selections, and window sizes.

The study of heat gain through facades for naturally ventilated buildings is more critical than that for air-conditioned buildings since the amount of heat gain is a significant factor influencing the indoor thermal comfort for naturally ventilated buildings. Ventilation is considered to be one of the effective means to achieve thermal comfort in naturally ventilated buildings. With the increase of air velocity, neutral temperature for thermal comfort can be increased. Another important factor that affects thermal comfort in naturally ventilated

buildings is solar heat gain, which can be controlled by shading devices. Increasing window to wall ratios can improve ventilation and indoor air quality but increase solar heat gain as well. Therefore, external shading devices become an important component to reduce solar heat gains, especially for large windows. The evaluation of thermal performance of facade designs in naturally ventilated buildings should be conducted in a comprehensive way. Arbitrarily exaggerating the effects of one particular component and neglecting the effects of others would be biased. Thermal comfort is an effective criterion to integrate the various impacts of all these facade components on indoor thermal environment.

The significant effects of dynamic outdoor climate on indoor environment increase the complexity of natural ventilation. Although there are many research works focusing on the impacts of facade components on energy consumptions in sealed mechanically ventilated buildings (e.g. Lin, 2006; *Cheung et al.*, 2005; Ozdeniz and Hancer, 2005), the knowledge of facade designs in naturally ventilated building is still deficient, especially for hot-humid climate. Therefore, optimization and comprehensive evaluation of the facade systems in naturally ventilated buildings are necessary and important for hot-humid climate.

1.2 Current methods for natural ventilation study in buildings

The methods for natural ventilation study to evaluate facade performance are categorized into three types: field measurements, controlled experiments and numerical simulations. Field measurements can only collect on site data from a few buildings, the locations of the instruments are restricted by on site conditions for the purpose of safety and security, and

uncertainties of these measurements could be significant and thus make it difficult for further data analyses. Data obtained from a controlled environment such as wind tunnel experiments and full scale model experiments are more reliable than those collected in field measurement. However, setting up and running these experiments are time consuming and high cost. The quality of the data acquired from these experiments is also limited by the accuracy of the instruments.

Numerical simulation is a cost-effective and efficient approach to predict thermal performances of facade in naturally ventilated buildings among various architecture designs. Simulation methods for natural ventilation fall into two broad categories: computational fluid dynamics (CFD) method and building simulation (BS) method. CFD simulation provides detailed spatial distributions of air velocity, air pressure, temperature, contaminant concentration and turbulence by numerically solving the governing conservation equations of fluid flows. It is a reliable tool for the evaluation of thermal environment and contaminant distributions. These results can be directly or indirectly used to quantitatively analyze the indoor environment and determine facade system performances. However, the application of CFD for natural ventilation prediction has been limited due to long computational time and excessive computer resource requirements. A calculation for a simple case of natural ventilation with reasonable solution may take a few hours using computer workstations. The lack of proper information at the boundary for CFD simulation makes the flow simulation less accurate. BS tools basically include two fundamental modules: thermal simulation and airflow network to solve the heat and mass transfer and airflow in the building systems. These tools greatly facilitate energy-efficient sustainable building designs by providing rapid

predictions of facade thermal behaviors, indoor air flow of the building and better understanding of the consequences of various design decisions. However, BS assumes the indoor air is well-mixed. It can only provide the uniform results for targeted spaces, which normally does not meet the requirements for detailed indoor environment analyses. Information provided by these two programs (CFD and BS) is complementary for advanced evaluation of building designs for thermal comfort. The integration of BS and CFD programs can eliminate a few assumptions employed in the separate applications, dramatically reduce computation time of CFD, and result in accurate and quick predictions of building performance in naturally ventilated buildings. On one hand, CFD can provide the detailed and accurate indoor air velocity and temperature distributions. On the other hand, wall surface temperatures and opening boundary conditions from BS results will provide CFD accurate and time varying boundary conditions. Therefore, it is very interesting and attractive to couple BS and CFD programs to handle natural ventilation designs. In the coupling approach, the CFD program will simulate airflow at specific time with corresponding boundary conditions with steady airflow pattern. CFD simulation in the coupling approach will only be implemented in the concerned indoor space rather than the whole building, which can save computing costs. The heat conduction part and air flow simulation in other zones will be implemented in BS program, which only needs a small fraction of the computation time. In summary, the integration of the BS and CFD simulation could provide a quick and accurate way to assess the performance of natural ventilation in whole buildings, as well as detailed thermal environmental information in some particular spaces. Therefore, there is urgent need

to provide an efficient coupling program between BS and CFD to predict natural ventilation efficiently and accurately.

1.3 Objectives of the study

This research aims to develop a methodology and program to couple CFD and BS for wind-driven natural ventilation prediction and carry out parametric studies of various facade designs to provide guidelines for naturally ventilated buildings in Singapore.

The primary objectives of the study are as follows

- Examine appropriate coupling strategies between BS and CFD for natural ventilation studies.
- Develop a coupling program with interface between BS and indoor CFD to quickly and accurately predict thermal performance of naturally ventilated rooms.
- Carry out parametrically study for the naturally ventilated residential buildings in Singapore using coupled simulations to provide facade design guidelines for HDB buildings based on thermal comfort criteria.

1.4 Scope of the study

The subjects of the expected coupling program are high-rise naturally ventilated residential buildings. Although both buoyancy effect and wind pressure are forces for natural ventilation, only wind force is considered in this study since the temperature difference between indoor and outdoor is not significant for natural ventilated residential buildings in Singapore.

For parametric facade design studies, the study focuses on four significant parameters: orientations, window to wall ratios and lengths of shading devices and building material properties. A series of parametric simulations by varying the window to wall ratios, shading devices and room orientations for various building designs are carried out using the coupled CFD and BS simulations. Thermal comfort results based on the results of coupled simulations are used to analyze the effects of physical parameters on indoor environment. The impacts of physical parameters of façade on indoor thermal comfort are evaluated by the percentage (or number) of unsatisfactory (or satisfactory) hours of thermal comfort, PMV index (Predicted Mean Vote) and thermal asymmetry near to the facade in the typical design period (a typical hour, a typical week, a typical day, or a typical year).

A program with a text-mode interface that couples BS and CFD is designed to accurately and efficiently predict thermal comfort in natural ventilation designs. The expected simple and accurate turbulence modeling method can save computational cost for external airflow simulation for the purpose of obtaining pressure coefficient values. By applying the coupling programs to façade design in naturally ventilated buildings, design guidelines are developed on various aspects of orientations, window sizes and positions, and shading devices.

1.5 Thesis Outline

Chapter 1 briefly reviews status of facade designs in hot-humid climate and the current methodologies for natural ventilation studies and provides the background of this research, and indicates the need to provide coupling tools which can quickly and accurately to predict long term natural ventilation to evaluate various facade designs.

Chapter 2 reviews the evolution of simulation methods for building performance prediction and current status of facade design studies and thermal comfort criteria for hot-humid climate, highlights the advantages of integration of BS and CFD and indicates the necessity to couple between BS and CFD to evaluate facade designs in naturally ventilated buildings.

Chapter 3 introduces the two fundamental modules of BS (thermal simulation and multi-zone airflow program) including the governing equations, boundary conditions, iteration methods of building simulation.

Chapter 4 introduces the fundamentals of computational fluid dynamics. Different turbulence models in CFD are reviewed and applied to predict pressure coefficients of external surfaces.

Chapter 5 compares different coupling strategies and provides detailed coupling methodology and procedures for natural ventilation prediction. Validations have been done with full CFD simulations and field measurements.

Chapter 6 investigates the feasibility of natural ventilation in Singapore, and summarizes the criteria for facade assessments in naturally ventilated buildings. The evaluation works have been done with the coupling program based on thermal comfort index for various facade designs and with the building simulation program based on thermal asymmetric criterion for naturally ventilated buildings. The facade design guidelines are developed based on parametric studies.

Chapter 7 summarizes the main findings obtained from this study and some limitations and further perspectives are discussed.

Chapter 2 Literature review

Chapter 2 reviews methods for building performance prediction, façade design and thermal comfort studies. Two main knowledge gaps are highlighted: 1) coupling program between building simulation (BS) and computational fluid dynamics (CFD) for indoor thermal environment prediction and 2) façade design optimization in naturally ventilated residential buildings.

2.1 Methods for building performance prediction

2.1.1 Building simulation

Built environment is a complex system with several sub-systems interacting with each other. Continuous energy transfer processes take place among the building's inter-connected regions such as rooms, walls, windows, ducts, etc. Traditionally, building service engineers rely on manual calculations using required design conditions based on analytical formulations and many simplified assumptions, which frequently led to oversized plants and poor thermal performances.

The research activities on building simulation can be traced back to the 1960's and 1970's, when the fundamental theory and algorithms of heat transfer and load estimation were laid on. Thermal response factor method (Mitalas and Stephenson, 1967; Stephenson and Mitalas 1967) is commonly used by most of building simulation programs to model transient heat transfer processes through building envelope and between internal surface and the room. Another method for modeling transient heat transfer processes is the control volume approach.

In this approach, discretized conservation equations are applied for finite regions (air volume, surfaces, material components, air flow components and plant components) and solved numerically (Clarke, 1977).

Detailed and long-term decisions in design and operation, for the purpose of indoor thermal comfort and energy saving for the buildings, require speedy computational program for designers and engineers to appraise various design approaches for envelope and mechanical systems. Thermal simulation program is the basic module in most of the current integrated building simulation tools. Most of current building simulation programs like EnergyPlus (Crawley, 2000), ESP-r (Clarke, 1988) and TAS (EDSL, 1989) apply heat balance method to deal with simultaneous presence of multiple heat transfer processes including conduction, convection and radiation. Multiple heat processes are simplified with one-dimension assumption, so that heat conductions, convections and solar radiations connected with weather data can be easily considered in thermal simulation and the calculation of thermal process can be done in a relatively fast fashion.

As more emphases have been put on economic and environmental constraints, “green or sustainable” buildings, which can provide a healthy and comfortable built environment with the reduction of negative impacts on environment and energy consumption, become the theme of building sectors in the 90s. Meanwhile, building simulation program is required in the whole design-build-operation process. Integration works between thermal simulation with other simulation modules such as airflow network, artificial lighting and daylighting, shading are conducted to make building simulation a powerful and multifunctional simulation tool

suite. The dynamic combination between thermal program and airflow network can expand the applications of building simulation tools into indoor air quality and passive cooling studies.

Coupling between thermal conditions and airflow network is implemented in this stage. Therefore, buoyancy effect induced by temperature difference and indoor air temperature affected by the infiltration and inter-zone airflows can be predicted (Beausoleil – Morrison, 2001). Building simulation software, such as ESP-r and TAS, integrate airflow simulation into the simulator engine for better prediction. The multi-zone airflow model COMIS (LBNL, 1988) was combined with DOE-2 (LBNL, 1982) and BLAST (Hittle, 1979) to become the new building simulation program EnergyPlus. Multizone airflow models rely on a lumped-parameter method, which idealizes a building as a collection of well-mixed zones, connected through discrete flow paths. Multi-zone airflow simulations are governed by pressure-flow algebraic equation for airflow components, mass balance equation at the nodes and hydrostatic pressure variations in the zones (Feustel, 1999). Newton-Raphson method is used to solve the set of non-linear mass conservation equations in the program (Herrin, 1990) and the specialized algorithm and program structures greatly reduce the computational cost (Lorenzetti, 2002). However, there are two main deficiencies in multi-zone airflow model: first, accuracy of flow prediction through the components is limited by the simple algebraic governing equations; second, the momentum (Navier-stokes) equations and turbulence models are not involved in multi-zone airflow program because of the well-mixed assumption. Therefore, multi-zone airflow program cannot accurately predict detailed airflows and coupled multi-zone and thermal module can not accurately determine indoor air temperature

further as heat convection cannot be properly considered. Coupled simulations between building simulation and computational fluid dynamics (CFD) can be a promising way for better prediction of building performance.

2.1.2 Computational Fluid dynamics

CFD has become a vital technique, and has been widely applied in the fields of aerodynamics, electronic engineering, hydrodynamics, turbomachinery, chemical engineering, marine engineering, biological engineering, environmental engineering and building technology (Versteeg & Malalasekera, 1995). The application of CFD in building technologies can be summarized into three important categories: outdoor airflow simulation for wind load analyses, indoor airflow simulation for indoor temperature and velocity prediction, and both indoor and outdoor airflow simulation for natural ventilation.

2.1.2.1 Outdoor airflow simulation

Simulating external airflow around buildings is a complicated task in fluid dynamics because the flow is typically separated and various vortices are generated around the buildings. Reynolds-averaged Navier–Stokes models (RANS) are widely used in engineering and industries for turbulence airflow simulations. Holmbom (1982) predicted turbulence flows over two-dimensional obstacles immersed in a boundary layer with a mathematical numerical model. It was concluded that the distorted shear flows approaching and passing over block geometry can be divided into three basic flow regions: the displacement zone, the upstream separation zone, and the wake zone. A recirculation flow region which extends approximately 8 step heights downstream was created behind the obstacle. Häggkvist, *et al.* (1989) simulated

the pressure field around buildings with the general equation solver PHOENICS, using the standard k-ε turbulence model. For a single house, the calculation domain was about 14 house heights (h) high and the distance from the domain inlet (vertical) boundary to the house was about 5h and the downstream distance to the domain outlet boundary was about 12h. In this case, it was important to define the computational domain large enough to avoid interaction between the recirculation zones and the boundaries.

The inaccuracies of RANS for external airflow simulation models were pointed out by several researchers (Shuzo *et al.*,1990; Tamura *et al.*,1997; Lakehal & Rodi,1997). The inaccuracies were due to overestimation of turbulence kinetic energy around the frontal corner and unsuccessful reproduction of Karman's vortex street behind the bluff body (Murakami *et al.*, 1990). The length of the recirculation region and velocities in the recirculation region behind the model were over-predicted in the case of the $k-\varepsilon$ model. To overcome the above deficiencies in RANS, large eddy simulation (LES) was used for external airflow prediction (Jiang & Chen, 2001; Jiang *et al*, 2003). The results of large eddy simulation showed good agreement with experiment data (Jiang & Chen, 2001). In addition, unsteady RANS modeling for external airflow was performed by Iaccarino *et al.* (2003) and the results showed good agreement with experiment data. Recently, Burnett *et al.* (2005) used the standard $k-\varepsilon$ model to simulate a typical high rise residential building in Hong Kong for external surface pressure coefficients to evaluate wind-driven ventilation inside the flats and their 2D LES results were used to verify the standard $k-\varepsilon$ turbulence model results for external simulations.

In environmental designs, outdoor airflow simulations can be used for environmental design on the aspect of outdoor thermal comfort, urban heat island mitigation, and particle dispersion. One of the important applications of outdoor airflow simulation is to obtain pressure coefficients (Cp) of external surfaces to provide boundary conditions for airflow network in building simulations and further coupled simulation between BS and CFD. Although large eddy simulation and unsteady $k-\varepsilon$ model can provide more accurate pressure coefficient predictions, the computation burden with these models is high. It is important to apply proper turbulence model to help engineers or researchers quickly and accurately predict Cp. However, no specific research has been done to compare the pressure coefficients predicted by different turbulence modeling methods (including the standard $k-\varepsilon$ model, Renormalization group (RNG) model, realization $k-\varepsilon$ model, Reynolds stress model).

2.1.2.2 Indoor airflow simulation

Indoor airflow simulations are normally used for air conditioned rooms when the inlet and outlet boundary conditions are given or for naturally ventilated rooms when the boundary conditions of apertures can be estimated.

Chen (1995) studied five two-equation k-ε models: the standard k-ε model, a low Reynolds-number k-ε model, a two-layer k-ε model, a two-scale k-ε model, and a RNG k-ε model. The performance of the five models in predicting natural convection, forced convection, and mixed convection in rooms, as well as in an impinging jet flow was evaluated. The results indicated that the anisotropic turbulence found in indoor air flow cannot be predicted with any of these models. The results indicated that both standard and the RNG k-ε

models were very stable but the RNG model is more accurate than the standard k-ε model for indoor airflow computations.

Chen and Xu (1998) proposed a new fast zero-equation model to simulate indoor air velocity, temperature and contaminant concentrations in rooms. The new zero-equation model was validated for the cases of natural convection, forced convection, mixed convection and displacement ventilation in a room. Indoor airflow simulation with new model can be 10 times faster than the standard k-ε model.

2.1.2.3 Both indoor and outdoor airflow simulation

In order to predict natural ventilation, full CFD simulations (indoor and outdoor airflow simulation) are required and computational domains should be large enough to make sure that turbulence is fully developed at computational boundaries. However, both unsteady RANS and LES modeling are computationally intensive and require large amount of computer memory. For a study of indoor airflow in a building apartment, LES for both indoor and outdoor airflow prediction may require three months of computing time on a high performance workstation (Jiang & Chen, 2002). Therefore, the requirements for intensive computing resources and time cost make the unsteady RANS and LES inappropriate for complex building cluster modeling. The standard k-ε model and the RNG k-ε model were used by Evola & Popov (2005) to simulate cross ventilation and single sided ventilation inside and around a cubic room. Their results indicated that the difference between RNG and LES results for airflow rate prediction inside the rooms was not significant when both compared with experiment data (Jiang et al, 2003), and thus RNG model was recommended

to be used for the assessment of ventilation rate and the air distribution inside a room. Similar to Lakehal & Rodi (1997), they also pointed out that RANS turbulence model failed to determine the correct velocity components near the horizontal surfaces.

One of the difficulties for natural ventilation prediction is the inconsistent requirements of grid size for indoor and outdoor simulations. The grid size for outdoor simulations in a large domain cannot be very small due to computer capacity. However, the grid size for indoor airflow simulation should be fine enough to model detailed indoor environment (Chen, 2004). Therefore, an economic way for natural ventilation is to decouple the outdoor and indoor airflow simulation for accurate results. Zhai *et al.* (2000) decoupled outdoor flow modeling from indoor airflow modeling to reduce the computation burden. Chen (2004) illustrated a few architectural indoor and outdoor environment designs with the aids of CFD simulations. The method that the indoor airflow and outdoor airflow should be separately simulated was put forward. For natural ventilation designs, the outdoor airflow simulation can provide flow information as boundary conditions for the indoor airflow simulation.

2.1.3 Integration of BS and CFD

Based on the above literature reviews for build simulation (BS) and computational fluid dynamics (CFD), it can be concluded that both BS and CFD have their own disadvantages. Due to the well-mixed zone assumption in BS, detailed indoor environment cannot be provided. In addition, the accuracy of multi-zone airflow model is constrained by the simple flow-pressure governing equations for various components and lacking momentum equations for indoor airflow. On the one hand, solar radiation cannot be easily considered within current

CFD models and CFD simulations require high computation cost, especially when grid size requirements for various computational domains are inconsistent, such as the case in indoor and outdoor airflow simulation and heat conduction simulation. On the other hand, BS model heat transfer and radiation processes based on heat balance methods and CFD can predict reliable detailed airflow for outdoor and indoor. Therefore, the integration of BS and CFD simulation is becoming an active research area in recent years.

The research work for integration of BS and CFD can be divided into two categories according to the coupling purposes: thermal environment predictions for air-conditioned rooms and for naturally ventilated rooms.

2.1.3.1 Integration works for air-conditioned buildings

To accurately evaluate energy loads for air conditioned room, several building simulation programs have been internally or externally coupled with CFD simulation program on the thermal aspect (Negrao, 1995; Srebric *et al.*, 2000; Beausoleil-Morrison, 2001; Zhai, 2003; Djunaedy, 2005).

Negrao(1995) built in a CFD code into the ESP-r building simulation program. For each time-step, ESP-r performed a thermal calculation to establish boundary conditions, such as inlet air velocity and temperature, including the surface heat flux, for CFD calculation. CFD then used these boundary conditions to calculate the detailed air velocity, air temperature, and surface convection coefficients. Once the CFD solution converges, it passed the results back to ESP-r to complete the whole building and plant calculations. The surface convection coefficients from CFD were then fed back to ESP-r to perform the detailed heating and

cooling load calculations.

Srebric et al. (2000) coupled a CFD code with the energy analysis program ACCURACY (Chen, 1988), which calculates the hourly heating and cooling loads based upon the energy balance method. At first, ACCURACY calculated the wall surface temperatures and A/C supply air velocity based on the cooling load required for that space, CFD then used those results to perform the airflow simulations and to calculate the convection coefficients for ACCURACY.

Beausoleil-Morrison (2001) developed an adaptive convection algorithm to improve the accuracy of the heat convection for building simulation program ESP-r. The appropriate heat convective coefficients can be calculated based on the dynamic conflation program. The integration between ESP-r and CFD for air-conditioned rooms was further improved based on Negrao (1995) by adding zero-equation turbulence model and wall functions in the built in CFD program.

Zhai (2003) introduced several coupling methods to integrate thermal simulation in EnergyPlus and CFD simulation (MIT-CFD). Thermal simulation program can provide building energy loads and interior surface temperatures of building envelopes to CFD as boundary conditions while CFD predicts convective heat transfer coefficient more accurately to help energy simulation to calculate energy consumption. The comparison of the simulated results with experimental data showed that the results of the integrated building simulation were closer than those by separated energy simulation and computational simulation.

Except the internal integration between BS and CFD by taking CFD as a module for BS, Djunaedy (2005) externally coupled the ESP-r thermal simulation with commercial CFD software FLUENT. The viability of the external coupling method in achieving the integrated multi-domain building simulation tools has been investigated. This research indicated that the external coupling method could provide the results as good as the internal coupling using external coupling approach.

2.1.3.2 Integration works for natural ventilated buildings

Although, the integration methods for air-conditioned buildings to accurately estimate energy consumption in buildings are well studied by many researchers, there are limited investigation on the integration of CFD simulation and building simulation for naturally ventilated buildings for better thermal comfort.

Negrao (1995) built in a CFD module to couple with airflow network module in ESP-r internally by exchanging boundary conditions. However, the internal coupling application is constrained by the requirement of cubic simulation domain, maximum grid sizes and computational time and convergence issues.

Carrilho-da-Graca, *et al.* (2002) used a coupled, transient simulation approach to model heat transfer and airflow in the apartments in Beijing and Shanghai. Wind-driven ventilation was simulated using CFD for each outside wind direction and velocity. The surface convection coefficients used as boundary condition for thermal analyses were calculated from the near-wall air velocity using experimental correlations suggested by Chandra and Keresteciogl(1984). Carrilho-da-Graca, *et al.* used isothermal CFD calculations to avoid the

heavy computational burden of using CFD for detailed airflow and indoor surface temperatures. As they stated that thermal buoyancy effects were much smaller than wind driven pressure in naturally ventilated residential buildings, the coupling approach that airflow simulation was independent of thermal simulation by assuming uniform indoor air temperature was adopted. Occupant thermal comfort was evaluated using Fanger's comfort model. The results showed that night cooling might replace air-conditioning systems for a significant part of the cooling season in Beijing, but with a high condensation risk. But for Shanghai, neither night cooling nor daytime ventilation can be considered successful.

Sreshthaputra (2003) coupled DOE-2 program with transient HEATX (3D-CFD simulation program) for natural ventilation to analyze the heat transfer and airflow performance of an unconditioned 100-year-old Buddhist temple in an urban area of Bangkok, Thailand. Two variables were coupled between the two programs during the calibration process. On one hand, the amount of outside air infiltration specified by air change rate (ACH) in DOE-2 is specified according to CFD results. The CFD simulation was used to estimate the maximum ventilation rate to be supplied to DOE-2 by multiplying the maximum air velocity across the windows with the total area of the windows. On the other hand, the interior surface convection coefficient for each surface based on CFD results will be transfer to DOE-2 when the temperature difference for indoor air temperature between DOE-2 and CFD are larger than 1 degree. Since the whole year dynamic simulation is estimated to take very long time (730 days approximately) with the coupled simulation, the method where average values of the air exchange rates and the corresponding convection coefficients were obtained from the coupled simulation of two selected days was adopted. These average values were used by

DOE-2 to perform the annual hourly calculations. However, although the computational domain has included the outdoor surrounding area, the domain was not large enough to accurately estimate the airflow for both indoor and outdoor. CFD program applied for both indoor and outdoor computational domain largely increases the computational cost.

Tan (2005) externally coupled between PHOENICS and Multi-zone model program-MultiVent for natural ventilation. However, the coupling program cannot well predict wind-driven natural ventilation alone. Good accuracy of the integration could only be obtained when buoyancy effects are involved in natural ventilation. Nevertheless, currently, there is no available coupling program to accurately and efficiently predict wind-driven natural ventilation. The main driving force of natural ventilation for high-rise residential buildings is the wind. In order to investigate thermal performance of high-rise residential buildings, it is important to achieve coupled simulations for wind-driven natural ventilation.

2.2 Facade design and thermal comfort studies

2.2.1 Facade design parameters

Successful facade designs by considering the thermal property of construction materials, window sizes, shading, and building orientations, can be an optimum modifier to achieve better indoor thermal comfort with minimum energy usages, although local climate is important in determining the potential of applying natural ventilation in certain regions. Optimum thermal performance design for building envelope and high energy efficiency

design for conventional energy systems are the two significant issues for relieving high energy demands for building operations (Zhu and Lin, 2004).

For naturally ventilated buildings, Sreshthaputra *et al.* (2004) used coupled simulations between DOE-2 and 3D CFD simulations for improving indoor thermal comfort in an unconditioned old Buddhist temple in Thailand. Several strategies were put forward to improve the indoor thermal comfort include applying a low absorption roof coating, adding ceiling insulation, increasing the sunshade at the building's exterior surfaces and nighttime-only ventilation. Lin, *et al.* (2004) studied Chinese traditional vernacular dwellings, where the sun shading and insulation are put in the first place for design and natural ventilation provide a better indoor thermal environment.

Several façade design studies have been done for air-conditioned buildings. Cheung *et al.* (2005) investigated an integrated design approach, considering wall insulation, glazing type, color of external wall, window size and external shading for high-rise apartments in Hong Kong in order to reduce the cooling requirement. The results showed a reduction of 31.4% in annual required cooling energy and 36.8% in peak cooling loads with optimum facade design in air-conditioned buildings. Ozdeniz and Hancer (2005) evaluated 14 different roof constructions for warm climate with the consideration of thermal comfort and energy consumption. Lin (2006) analyzed the impacts of facade designs on cooling loads with a series of DOE2.0 simulations. Their results suggested that facade design parameters which closely related to opening and shading such as window to wall ratios, shading devices and orientations account for approximately 80% to 90% air conditioning energy consumption.

Construction material, windows and shading devices are important components for facade.

2.2.1.1 Construction material properties

Thermal properties of construction materials, which affect the rate of heat transfer in and out of a building and consequently the indoor thermal conditions and comfort of the occupants, are thermal conductivity, resistance, transmittance, surface characteristics with respect to radiation –absorptivity, reflectivity and emissivity, heat capacity and transparency to radiation of different wavelengths (Givoni, 1981).

Thermal conductivity of a material determines the heat flow in unit time by conduction through unit thickness of a unit area of the material, across a unit temperature gradient.

Thermal conductance of the element is given by:

$$c = \frac{\lambda}{d}$$

Where c (W/m^2℃)indicates thermal conductance of the element, λ (W/m℃)is thermal conductivity of the material and d (m) is thickness of the element.

The overall thermal resistance of wall to heat flow between the air on either side is given by:

$$R = 1/h_i + \sum d_i/\lambda_i + 1/h_e$$

Where h_i (W/m^2℃) is internal convective heat transfer coefficient, h_e is the external convective heat transfer coefficient(W/m^2℃) .The reciprocal of thermal resistance R is termed thermal transmittance.

The surface characteristics with respect to radiation include absorptivity (α), reflectivity (r) and emissivity (ε). The color of a surface gives a good indication of its absorptivity of solar radiation. The absorptivity of solar radiation decreases with the lightness of color.

$$r = 1 - \alpha$$

For a grey body, absorptivity and emittance are equal for any specific wavelength. In this study, a light colored façade surface was chosen to simplify the model.

The term heat capacity of wall refers to the amount of heat required to elevate the temperature of a unit volume of the wall, or unit area of the surface, by one degree. They are namely volumetric heat capacity of material, Cv, and heat capacity of the wall, Cw. Under the condition of fluctuation, when the structure is heated and cooled periodically as a result of variation in outdoor temperature and solar radiation, the heat capacity has a decisive effect in determining indoor thermal conditions.

Properly considering the properties of construction materials can improve indoor thermal comfort and reduce energy consumption. Building design and comfort study in Bangladesh by Mallick (1996) indicated rooms with thicker walls tend to be more comfortable, particularly in the hot and dry period between March and June. In the study performed in Hong Kong, it was found that the cooling loads could be reduced by 1.8% by moving the extruded polystyrene (EPS) insulation from inside to outside the external walls. The reduction in peak cooling loads, achieved by adding extra thermal mass, does not show a linear relationship with the amount of thermal mass added (Cheung *et al.*, 2005). Bojic and Yik (2005) studied the impacts of external wall construction on cooling energy for high-rise residential buildings

in Hong Kong by using simulation program HTB2. The results showed that envelope insulation would be effective in reducing the annual space cooling loads up to 38% but had the possibility of increasing the peak cooling loads. Reducing thermal capacity would largely increase peak cooling loads.

In Singapore, the current facade construction material standard for air-conditioned buildings is that ETTV (Envelope Thermal Transfer Value) should not exceed 50W/m^2 . The equation for ETTV calculation is as follows (BCA, 2004).

$$ETTV = 12(1\text{-}WWR)\ U_w + 3.4(WWR)U_f + 211(WWR)(SF)(CF)$$

Where WWR: window-to-wall ratio

U_w : thermal transmittance of opaque wall (W/Km^2) – wall U-value

U_f : thermal transmittance of fenestration (W/Km^2) --- fenestration U-value

CF: correction factor for solar heat gain through fenestration

SC: shading coefficients of fenestration

However, for naturally ventilated buildings in Singapore, building regulations in Singapore (P.W.D., 1979) only specify that the U value of any external wall in non-air conditioned building should not be more than 3.5 W/m^2 K. There are no facade design guidelines for better indoor thermal comfort.

2.2.1.2 Window sizes

Window characteristic have important impacts on the effectiveness of ventilative cooling. Reed (1953) investigated indoor flow pattern and air speed via wind tunnel experiments. The results showed that maximum air speed within a building is acquired when the outlet is larger

than the inlet. Givonni (1978) proposed a correlation based on experimental data, to calculate the average indoor air velocity with the ratio of the opening's area to wall area and the reference external wind speed. Melaragno (1982) has proposed the average and maximum indoor air velocity values for window to wall ratios of 0.66 and 1. Tantasavasdi *et al.* (2001) explored the potential of using natural ventilation as a passive cooling system for new house designs in Thailand. It was found that the inlet aperture area should be around 20% of the floor area to achieve adequate natural ventilation for an acceptable comfort level. Gritzki *et al*. (2004) investigated the air exchange in a room with different windows and window geometries using both experiment and CFD simulation to get reliable data for the air change rate and air exchange efficiency for natural ventilation. The results showed that the ventilation efficiency depends on the opening angle of the window and the attainable air change rate is a function of the temperature difference and opening angle of the window.

2.2.1.3 Shading devices

Appropriate external shading devices can control the amount of solar radiation transmitted into the room to largely reduce cooling loads and improve indoor thermal comfort.

Muniz (1985) investigated the effect of external shading devices on air flow pattern, thermal comfort and daylighting, for tropical hot-humid climate via a low-speed wind tunnel and an artificial skydome. Bouchlaghem(2000) presented a computer model to simulate the thermal performance of the building, taking into account window shading devices. The simulation results by Cheung *et al.*(2005) indicated that the longer the shading devices, the greater the reductions in both annual required cooling energy and peak cooling load for high-rise

apartments in hot and humid climates. Corrado (2004) evaluated the influence of the geometry of window-shading device system on the final performance of the system itself using the mean shading factor, which is defined as the ratio of the global solar radiation received on the window in presence of shading devices to the global solar radiation.

Most of the current literatures are on the investigation of facade design optimization for air-conditioned building for the purpose of minimizing energy consumptions. Very few studies have been done for improving naturally ventilated buildings, especially for hot-humid climate. Consequently, it is necessary to apply coupled simulations to do the parametric studies for facade design evaluation of naturally ventilated residential buildings.

2.2.2 Thermal comfort studies for naturally ventilated buildings

In order to effectively evaluate various facade designs for naturally ventilated buildings, it is a primary task to find suitable criteria for assessments. In the aspect of thermal performance, the function and purpose of naturally ventilated buildings is to provide comfortable indoor thermal environment for residents, including indoor air temperature, air velocity, mean radiant temperature and relative humidity. Appraisements on various facade designs should be comprehensive and not biased to emphasize on any particular facade component. Therefore, thermal comfort for naturally ventilated buildings is the idealized criteria for this comprehensive evaluation.

The comfort expectations are subjective. It is important to know that the comfort expectations of tropical population and people from temperate or cold climate are different. A few

thermal comfort studies were carried out in tropics. Nicol and Humphreys (1973) presented the results of field studies in the UK, India, Iraq and Singapore. It is noted that temperatures well above 30 ℃ are not considered uncomfortable in some cases. Dutt et al. (1992) investigated thermal comfort in a naturally ventilated dining room of a students' hall in Singapore. Tropicalized PMV index is proposed based on mean condition in the survey (583 respondents) with mean air temperature 29.8 ℃, mean radiant temperature 30.1 ℃ and mean humidity 75%. Thermal comfort analyses indicate that the mean indoor velocity 0.47 m/s is associated with the Predicted Mean Vote of 0.74, which amounts to three quarters of the way along between "neutral" and slightly warm" on the 7-point scale. Mallick (1996) did thermal comfort study of occupants living in urban housing in Bangladesh. The results showed that people can endure high temperature and very high humidity for comfort. It is quite interesting to see that there is no apparent effect of humidity on changes in comfort sensations.

Many studies indicate that thermal comfort predictions for air-conditioned room is not suitable for naturally ventilated rooms because of adaptive activities and different thermal perception. Baker and Standeven (1996) suggested that adaptive activities/exercises are important to meet thermal satisfaction of the occupants. Thermal comfort zone for passive natural ventilation might be extended by adaptive opportunities. Brager and De Dear (1998) pointed out that an adaptive model could eliminate the need to get the information of clothing patterns of the future, unknown occupants by taking account of the feedback loop between discomfort and purposive behavioral thermoregulation. De Dear and Brager (1998) found that the biases between PMV and ASHRAE vote were generally smaller for the air conditioned

buildings than for the naturally ventilated buildings. Many published literatures showed that the human thermal sensation in a naturally ventilated environment is much better than that in a mechanically controlled thermal environment. (Fanger and Toftum, 2002; Xia *et al*., 1999). De Dear and Brager (2002) believed that thermal perception of those who live or work in naturally ventilated buildings –both preferences as well as tolerances –is likely to extend over a wider range of temperatures than are currently reflected in the old ASHRAE Standard 55 comfort zone. Nicol and Humphreys (2002) explained the origin and development of the adaptive approach to thermal comfort. The adaptive principle is that people react in ways which tend to restore their comfort if a change occurs such as to produce discomfort. They pointed out that the comfort zone may be as narrow as $\pm 2^{\circ}C$ in a situation where there is no possibility of changing clothing or activity and where air movement cannot be used. In situations where these adaptive opportunities are available and appropriate the comfort zone may be considerably wider. Nicol (2004) conducted field studies in hot-humid tropical climates. It was found that the international standard for indoor climate, ISO7730 based on Fanger's predicted mean vote equation, does not adequately describe comfort conditions when buildings are not mechanically heated or cooled. ISO7730 overestimates the occupant response on the ASHRAE scale at high temperatures and underestimates it at low temperatures.

Current available models for thermal comfort prediction for naturally ventilated buildings for hot-humid climate are summarized as follows:

1) Fanger & Toftum

The Fanger and Toftum model is an extension of the PMV model that includes an expectancy factor for use in non-air-conditioned building (Fanger & Toftum, 2002). They explained the main reason for the deviation between PMV prediction (Fanger, 1970) and actual feeling in naturally ventilated buildings is low expectations and overestimation of a metabolic rate. The new adjusted PMV model (Fanger & Toftum, 2002) is to multiple the predicted PMV values with expectancy factors (0.7 for Singapore). Accordingly, the upper temperature limits adjusted for expectation for 20% dissatisfied (PMVE=0.85) was changed to 29.4 ºC.

2) ANSI/ASHRAE Standard 55-2004

ASHRAE Standard (2004) provided the alternative method to predict acceptable thermal conditions for naturally conditioned spaces, developed from a global database of 21,000 measurements taken primarily in office buildings. In the approach, thermal responses in naturally ventilated space are linked with the outdoor climate and two sets of operative temperature limits—one for 80% acceptability and one for 90% acceptability are included in the diagram "Acceptable operative temperature ranges for naturally conditioned spaces"(ASHRAE standard, 2004). The application of this method, operable windows that can be adjusted by the occupants are required. Metabolic rates range from 1.0 met to 1.3 met and occupants can adapt their clothing according to thermal conditions. The required indoor operative temperature limits for 90% acceptability and 80% acceptability are listed in Table 2.1, which is calculated based on outdoor air temperature of the typical year in Singapore. However, the estimation of thermal comfort using this method is limited with mean monthly outdoor air condition.

When the difference between radiant and air temperature is less than 4 ºC, the operative temperature is calculated by the following equation,

$$T_{op} = At_a + (1 - A)t_r \quad (2.2)$$

Where t_a =air temperature;

t_r = radiant temperature

A= 0.5 (<0.2m/s); 0.6(0.2-0.6m/s); 0.7(0.6-1m/s)

Table 2.1 Required indoor operative temperature limits for naturally ventilated spaces in Singapore base on ASHRAE Standard 55-2004

Month		Jan	Feb	Mar	Apr	May	Jun
Mean monthly outdoor air temperature (℃)		26.74	26.97	27.48	27.75	28.52	28.16
80% acceptability	MIN	22.66	22.70	22.85	22.93	23.30	23.12
	MAX	29.65	29.75	29.88	29.94	30.20	30.08
90% acceptability	MIN	23.80	23.90	24.10	24.20	24.40	24.34
	MAX	28.72	28.80	28.90	28.95	29.20	29.08
Month		Jul	Aug	Sep	Oct	Nov	Dec
Mean monthly outdoor air temperature (℃)		28.45	28.01	27.99	27.64	27.17	26.70
80% acceptability	MIN	23.30	23.00	23.00	22.90	22.76	22.66
	MAX	30.20	30.00	30.00	29.91	29.80	29.65
90% acceptability	MIN	24.40	24.30	24.30	24.16	23.98	23.80
	MAX	29.20	29.00	29.00	28.93	28.84	28.72

3) Thermal comfort studies in National University of Singapore for naturally ventilated residential buildings

Feriadi (2003) developed a thermal comfort prediction chart and fuzzy thermal comfort model suitable for naturally ventilated buildings in the tropics based on 1063 data collected through field surveys in Singapore and Indonesia. Wong and Khoo (2003) did a field study in a fan-ventilated classrooms in Singapore. Their results showed that the ASHRAE standard 55 is not applicable in free-running buildings in the local climate. The adjusted PMV model by Fanger and Jorn Tofttum (2002), which incorporates two common forms of adaptation:

namely, reducing activity pace and expectation, also showed discrepancy in predicting actual thermal sensations, especially at lower temperatures. Thermal comfort regression model (Wang and Wong, 2005a) for naturally ventilated residential buildings has been derived from 538 field survey data in Singapore

$$PMV = -11.7853 + 0.4232 \times Temp - 0.57889V \quad (2.3)$$

where, *Temp* (℃)indicates the indoor air temperature and *V* (m/s)refers to indoor air velocity measured at 1.2 m above the ground. The term *PMV* refers to the average (mean) response of a group exposed to a given climatic conditions rather than individual responses. As relative humidity is highly correlated with dry bulb temperature, the impacts of variation of dry bulb temperature on thermal comfort can indirectly indicate the effects of relative humidity changes on thermal comfort. In another aspect, relative humidity in hot-humid climate is always in the high level (above 60%). Therefore, the parameter relative humidity is not involved in the regression model. clo and met are normally standard for residential buildings in Singapore. The clo-value is around 0.34-0.5 as people tends to adjust their clothes at home for better thermal comfort and met is equal to 1.0. Dry bulb temperature and air velocity are parameters for thermal comfort prediction. The acceptable thermal condition can be achieved when PMV ranges from -1.3 to 1.1 (Feriadi et al, 2003). Therefore, the upper limit of indoor discomfort is set to be PMV=1.1.

2.3 Summary of literature reviews

Different methods for building performance prediction and facade design evaluation including facade design studies and thermal comfort as the criteria for appraisements are reviewed in this chapter. The existing literatures have shown that the coupled simulation

between BS and CFD is a promising way to improve the accuracy of indoor thermal condition prediction with less computing efforts. Facade design optimization can provide occupants comfortable thermal environment with less energy usage. However, it has been noticed that several fundamental issues have not been solved yet. Several of the major issues are listed below.

1) Most of the current BS and CFD coupling efforts have been focused on the development of specific coupling methods for air-conditioned buildings. Several problems in the coupling of BS and CFD programs for natural ventilation still have not been addressed. For example,

- Which data exchanging methods and strategies are more suitable for natural ventilation design processes?
- How to realize the connection between boundary conditions of building openings and local weather conditions and building characteristics?
- How to automatically simulate long term natural ventilation with less computing efforts?

Finding the solutions for these problems for coupling program in naturally ventilated buildings is extremely important to provide accurate and fast prediction for natural ventilation.

2) In the past facade design studies, less concerns have been shown on facade designs for naturally ventilated buildings, especially for hot-humid climate. However, the optimization of

naturally ventilated facade designs can obtain comfortable thermal environment without usage of air-conditioning or with the less usage of air-conditioning for energy saving.

Most of available studies for natural ventilation focused on particular components and neglected the influences of other factors. Nevertheless, a comprehensive way on facade design investigation for naturally ventilated building is necessary to correctly evaluate the combined effects of the major factors.

The main reason for very few facade studies on natural ventilation can be attributed to the lack of appropriate simulation tools for investigation since the airflow network in building simulation tools cannot accurately predict ventilation profiles in buildings and CFD simulations for both indoor and outdoor prediction need a lot computational efforts. Therefore, the coupled simulation tool works as a bridge between thermal comfort criteria and facade design optimizations for naturally ventilated buildings.

Chapter 3 Fundamentals of building simulations –ESP-r

This chapter presents an understanding of theory and methodology of two key modules in building simulation program ESP-r: thermal simulation and multi-zone airflow simulation, which are basic modules in current coupled simulation studies. The governing equations for thermal and airflow simulation are described. The boundary conditions and numerical methods to solve the set of governing equations in building simulation are introduced.

3.1 Introduction of ESP-r

Among all these building simulation tools, ESP-r (Environmental Systems performance, Research version) (http://www.esru.strath.ac.uk/Programs/ESP-r.htm) is one of the research-oriented building simulation tools, which enables powerful analyses of thermophysical processes, artificial lighting, 2D and 3D conduction, moisture exchanges, air flow, and shading devices of buildings with or without plant and control systems. Control volume numerical method is used in ESP-r. In this method, building and plant systems are spatially discretized into a number of inter-connected finite regions holding uniform properties (Clarke, 2001). Central to the model is its matrix equation processor, which is designed to accommodate variable time-stepping, control and the treatment of complicated systems, to solve the heat and mass conservation algebraic equations, representing the state of the whole system in time and space (Hensen, 1991) and according to characteristics of governing equations, different solvers are employed for subsystem matrices (air flow network,

plant network). The theories and the validity of ESP-r has been contributed and continuously evolved by Clarke (1977), Tang (1985), Hensen(1991), Aasem(1993), Negrao (1995), Nakhi(1995), Chow(1995), MacQueen(1997), Kelly(1998), Hand(1998), and Beausoleil – Morrison (2001).

The source code of ESP-r is open and the summarized index of ESP-r code is available on line (http://www.esru.strath.ac.uk/Programs/ESP-r_CodeDoc/). ESP-r is composed of about twelve modules as following, each contributing particular technique to the building simulation process: Project manager, Simulator (including thermal simulation alone and airflow network simulation), Results analysis, Stand alone mass flow simulation (including the network flow and CFD simulation), Stand alone plant simulation, Climate analysis, etc. Figure 3.1 shows the relationship between the program and modules which form the simulation environment. In normal use, the three main modules, the project manager module (prj), the simulator module (bps) and the Results analysis module (res), are used to investigate building performance to assess the consequences of any change to system design. The first module (prj) supports interactive definition of the whole building systems including building (geometry, construction material, and operation schedule, shading obstruction), airflow network, plant network and control systems with the access of databases (climate, event profiles, plant components, window properties, etc) and shading and insolation prediction and view factors, etc and provide user's access to the interface of the other two modules: the simulator module (bps) and the Results analysis module (res). The simulator module (bps) performs the simulation of energy thermal simulation for envelope heat transfer and plant heat exchange processing, or fluid flows or both thermal and airflow simulation and presents some

graphical facilities to monitor the residuals of variables during the simulation processes. Several modules for particular facilities contain their own (simulation engine) bps, which allows each module to be debugged independently and preserve the integrity of the system when other modules are modified or a new module is added. The third main module (res) is responsible for the analyses of the results saved by bps. Different forms of results are available: statistical analysis, graphical facilities, tabulations, result exports etc. The interactions among the three modules can be continuous in order to help the building designer make decisions.

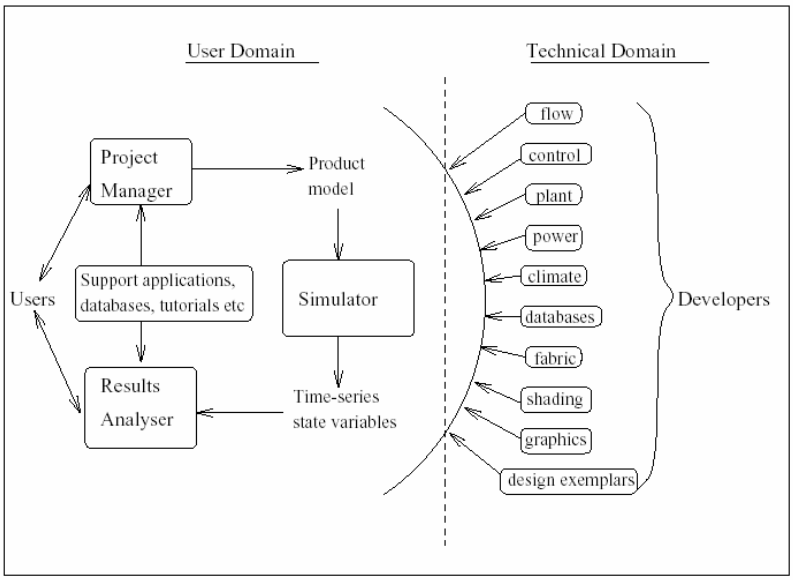

Figure 3.1 Structure of ESP-r (Source: ESRU, 2002)

Open source code, highly modular structure and both graphic and text mode interface offer unique features for further theoretical improvement and integration work with other available software. Thermal simulation and airflow network are the two fundamental components in building simulation, which are introduced in the following sections.

3.2 Thermal simulation

Building thermal simulation is the basic component of the integrated building design tool (ESP-r). In ESP-r, the building is discretized by representing air volumes (such as rooms), opaque and transparent fabric components (wall, windows, roofs, floors), solid-fluid interfaces (such as the internal and external surfaces of walls and windows), and plant components (such as boilers and heat exchangers) with nodes. Heat balance method is applied to each finite volume and therefore, each control volume is linked with others by conservation equation with the means of conduction, convection, radiation and fluid flow (Clarke, 2001).

The conservation of any transport process can be interpreted by the first law of thermodynamics: the change in internal energy of a system is equal to the heat added to the system minus the work done by the system. Therefore, the heat balance method can be written in the following form:

$$\dot{Q}_s = \dot{Q}_{cond} + \dot{Q}_{conv} + \dot{Q}_R + \dot{Q}_{mf} + \dot{Q}_g \qquad (3.1)$$

Where

$\dot{Q}_s$ -- The rate of heat storage in the control volume

$\dot{Q}_{cond}$ -- Heat exchange rate in the form of heat conduction between the control volume and environment.

$\dot{Q}_{conv}$ -- Heat exchange rate in the form of heat convection between the surface of control volume and environment.

$\dot{Q}_R$ -- Heat exchange rate in the form of radiation between the control volume and environment.

$\dot{Q}_{mf}$ -- Heat exchange rate in the form of inter-zone fluid to fluid heat exchange

$\dot{Q}_{g}$ -- Internal heat generation rate within the control volume

Therefore, each inter-connected uniform finite region, including multiple construction layers, internal and external zone surfaces, room air volumes, working fluid and plant components, can be written in the form of Equation 3.1.

The general differential conservation equation for each control volume P, assuming thermal properties of each region is only time dependent, can be written as:

$$\underset{\text{heat storage rate in control volume}}{\rho_P C_P V_P \frac{dT_P}{dt}} = \underset{\text{heat conduction item}}{q_{con} A} + \underset{\text{heat convection item}}{\sum_{c=1;c\neq P}^{n} h_{c,P} A (T_c - T_P)} + \underset{\text{heat radiation item}}{\sum_{s=1;s\neq P}^{m} h_{s,P} A (T_s - T_P)} + \underset{\text{heat exchange by inter zone airflow}}{\sum_{f=1;f\neq P}^{k} v_{f,P} \rho_{f,P} C_{f,P} (T_f - T_P)} + \underset{\text{heat generation in control volume}}{q_v V_P} \quad (3.2)$$

where T_P (℃) represents the temperature of the region P; ρ_P (kg/m^3)is the density of the region P; V_P(m^3) is the volume of the region P; q_{con}(W/m^2) is the heat flux through conduction; A (m^2) is the section area; C_P(J/kg • ℃) is the specific heat capacity of the region P, k (W/mK) is the thermal conductivity. $h_{c,P}$(W/m^2 • ℃) is the heat transfer coefficient between region c and P. n indicates the number of heat convection flowpaths between region P and surrounding regions c. $h_{s,P}$(W/m^2 • ℃) is the inter-surface radiation coefficient between region s and P. m indicates the number of longwave flowpaths between region P and surrounding surfaces s. $v_{f,P}$ (m^3/s) is the inter-region volume flow rate relative to volume P, $C_{f,P}$ is the specific heat capacity of the inflow, $\rho_{f,P}$ is the density of the inflow, k indicates the number of interzone flowpaths between region P and surrounding regions f. q_v (W/m^3) is

heat generation per unit volume ie from cooling or heating systems or solar radiation. The heat balance discretised equation express the thermal interactions between the region status at the end of the time step and the region present status at the beginning of the time step and neighbors, the resulting equation set links all heat flowpaths over time and space.

The established conservative discretization equations can be generalized in matrix notation(3.3).

$$[A][T^{n+1}] = [B][T^{n}] + C = Z \qquad (3.3)$$

where A is a non-homogeneous sparse matrix of coefficients of node temperature and heat generation terms on the left of the conservation equations at the end of time-step. T^{n+1} is the vector of unknown nodal temperatures and heat generation at the end of time-step. B represents a sparse matrix of coefficients of node temperature and heat generation at the beginning of time-step. T^{n} is the vector of known nodal temperatures and heat generation at the beginning of time-step. The matrix C holds a column matrix of boundary excitations. Matrix C represents the present values and the known boundary excitations. Therefore, the complicated simultaneous multi-heat processes including conduction, convection, and radiation, mass exchange can simply be represented by the linear matrix correlation for numerical solution. In order to obtain the solutions within the lowest computing time, the overall system matrix is partitioned into a number of sub-matrices and direct methods for solving linear matrix equation are used for each partitioned matrix (Clarke, 2001).

3.3 Multi-zone Airflow simulation

Multi-zone modeling is widely used to predict ventilation driven by wind pressure, buoyancy, or mechanical forces for incompressible steady flow. The multi-zone airflow model used in ESP-r was developed by Cockcroft (1979) and Hensen (1991). Infiltration and natural ventilation through the leakages and openings and air distribution within the connected zones can be solved in multi-zone models. Within the model, the building and air handling systems are decretized by a set of nodes representing rooms (or parts of rooms), equipment connection points, ambient conditions etc. The node paths to represent airflow paths, and pressure drops are connected by components corresponding to discrete fluid flow passages including doors, windows, cracks, conduits, junctions and controller, pumps, fans, etc. The mass conservation equations based on empirical flow-pressure functions for airflow paths are solved in successive time steps to yield airflow distributions within fluid flow network. Iterative methods for multi-zone models are used to adjust the unknown nodal pressure conditions till mass conservation within the network can be reached.

3.3.1 Node definition

The fluid flow (air or water) nodes in the network can be defined by four types in the airflow network: boundary nodes with known pressure, boundary nodes with wind pressure, internal nodes with unknown pressure and internal nodes with known pressure. The defined network is established by connecting a number of internal and boundary nodes. The nodes for multi-zone model are required to define fluid type, node type, a referenced geometric height, static pressure and temperature. For boundary nodes, total pressure should be pre-known

either for the cases with mechanical ventilation or for wind induced natural ventilation. Pressure at an internal node is normally unknown and mass balance equations must be satisfied with the set of internal nodes.

3.3.2 Flow component definition

There are several options to describe these airflow characteristics: power law models, orifice models, stairwell and shaft models, and two-way flow models. The flow component types in multi-zone model in ESP-r are summarized by Henson (1991). Mass flow rate for each component is governed by a function of the pressure differences of connected nodes. Each model requires specific data to describe the airflow characteristics of the opening. The form of flow-pressure equation to estimate mass flow rate through components can be generalized by Equation (3.4) (Clarke, 2001).

$$\dot{m} = ka(\Delta P)^x \qquad (3.4)$$

Where ΔP is the pressure difference of connected nodes through the component, k is an empirical constant, a represents characteristic dimension of the component, and x is an empirical component. For instance, the mass flow rates (kg/s) for commonly used component—orifices in natural ventilation can be determined by

$$\dot{m} = C_d A\sqrt{2\rho\Delta P} \qquad (3.5)$$

C_d is the discharge coefficient, which normally use 0.65 for turbulent flows; A is the opening area (m^2), ΔP is the pressure difference across the opening (Pa) and ρ is the density of the inflow.

3.3.3 Boundary conditions with wind pressure

When boundary conditions are induced by wind pressure, in order to connect the free stream wind conditions (wind speed and wind direction) and the influence of surrounding buildings to external boundary surfaces at a particular level, vertical wind velocity profile and dimensionless pressure coefficients are required for airflow network program.

3.3.3.1 Wind profile models

In the airflow network, there are three types of wind profiles to map the free stream wind speed with the local wind velocity by a reduction factor, which is the ratio between this local reference wind speed and free stream wind speed as read from the climate file.

- Power law wind profile (Liddament 1986)

$$\frac{v_l}{v_{10}} = k z_l^{\,a} \qquad (3.6)$$

Where v_{10} is the free stream wind speed measured at a standard height of 10m; v_l is local wind velocity at the height of z_l m ; k and a are terrain dependent parameters.

- Logarithmatic wind profile (Simiu and Scanlan 1986)

$$\frac{v_l}{v_m} = \left(\frac{z_{0,l}}{z_{0,m}}\right)^{0.1} \left(\ln\frac{z_l - d_l}{z_{0,l}} / \ln\frac{z_m - d_m}{z_{0,m}}\right) \qquad (3.7)$$

Where v_l is the local wind speed at a height z_l above the ground; v_m is free stream wind speed at the height z_m above the ground; $z_{0,i}$ is a terrain dependent roughness length; d_i is a terrain dependent displacement length.

- LBL model wind profile (Liddament 1986)

$$\frac{v_l}{v_m} = \frac{\alpha_l (z_l / 10)^{r_l}}{\alpha_m (z_m / 10)^{r_m}} \qquad (3.8)$$

Where v_l is the local wind speed at a height z_l above the ground; v_m is free stream wind speed at the height z_m above the ground; α_i and r_i are terrain dependent constants.

The typical values for terrain parameters for each model are summarized in Table 3.1 (Clarke, 2001).Wind profile models are only valid for heights from ($20*z_0$+d) and to 60-100m, and the wind speed and the direction below ($20*z_0$+d) is strongly influenced by individual obstacles, and can only be predicted through wind tunnel experiments or simulations with a CFD model (Hensen, 1991).

Table 3.1 Values for terrain parameters (Clarke, 2001)

Terrain	k	a	$z_{0,i}$	d_i	α_i	r_i
Open flat country	0.68	0.17	0.03	0.0	1.00	0.15
Country, scattered wind breaks	0.52	0.20	0.1	0.0		
Rural			0.5	0.7h	0.85	0.20
Urban	0.35	0.25	1.0	0.8h	0.67	0.25
City	0.21	0.33	>2.0	0.8h	0.47	0.35

h is the height of the building (m)

3.3.3.2 Pressure coefficients

A set of wind pressure coefficients, which vary according to wind directions and orientations of the building surface, are significantly affected by surrounding obstructions. Accurate prediction of this parameter is one of the most significant and difficult aspects of airflow

modeling as it is taken as the opening boundary condition and cannot be calculated by theoretical means alone (Hensen, 1991). The pressure coefficients of external surface temperature can be calculated by the following equation:

$$C_p = \left(\frac{p - p_\infty}{1/2 \rho V_r^2} \right) \qquad (3.9)$$

Where p (N/m^2) is the surface pressure, p_∞ (N/m^2) is the pressure at free stream and V_r is the reference wind speed at reference level r, which is usually equal to the building height. Typically, a pressure coefficient set is composed of 16 values at 22.5 degree intervals to reflect the characteristics of the building and surroundings. The azimuth is required to define the surface orientation and angles are recorded clockwise from north so that north is 0^o, east is 90^o and south is 180^o. In the case of an up and down zone, the azimuth has no meaning and may be set to zero. Published experimental data are used in ESP-r airflow network as the collection of standard pressure coefficients sets for typical designs, which are applicable for low-rise buildings (less than 3 stories). For high-rise building, the original pressure coefficient file is not sufficient.

Airflow network simulation for natural ventilation requires the knowledge of the exterior pressure distributions and empirical coefficients to compute the pressure and velocity values within the interior nodes. However, it is difficult to estimate those data because they are strongly dependent on the building's form and surrounding conditions, which vary from case to case. Accurate knowledge of the wind pressure distribution over the building envelope is important to predict indoor environment for natural ventilation in buildings.

3.3.4 Airflow network solution

Mass conservation equation is required to be obeyed at each internal node. Therefore, for quasi-steady conditions without considering non-flow processes by adding or removing fluid for the zone, the sum of mass flows for an internal node should be equal to zero.

$$R_i = \sum_k \dot{m}_{k,i} = 0 \quad (3.10)$$

Where R_i (kg/s) indicates the residual of the sum of mass flow rate in zone i; $\dot{m}_{k,i}$ (kg/s) is the mass flow rate between zone k and zone i; and k indicates the zone number connected with zone i.

The initial pressure for each internal node is assigned and the flow for each connection is determined by appropriate flow-pressure equation as a function of current pressure differences. Iterative approach is used to solve a set of nonlinear equations with Newton-Raphson (N-R) method and the node pressure is corrected until the nodal mass residual reach certain convergence criteria.

In the N-R method, a new estimate of the vector of all node pressures, {P}, is computed from the current estimate of pressure {P}*, by

$$\{P\} = \{P\}^* - \{C\} \quad (3.10)$$

Where the node correction vector, {C}, is determined by the matrix relationship

$$\{J\}\{C\} = \{R\} \quad (3.11)$$

LU decomposition method, which is numerically stable, is used to obtain the pressure correction vector {C}. Where{R} is a vector of nodal mass flow residuals with element given by

$$R_i = \sum_k \dot{m}_{k,i} \qquad \text{(kg /s)} \qquad (3.12)$$

and {J} is a Jacobian matrix and the diagonal elements are given by:

$$J_{i,i} = \sum_k \frac{\partial \dot{m}_{k,i}}{\partial \Delta P_{k,i}} \qquad \text{(kg /s Pa)} \qquad (3.13)$$

Where $\dot{m}_{k,i}$ (kg/s) is airflow rate between zone k and zone i, and $\triangle P_{k,i}$ is pressure difference (Pa) between zone k and zone i.

The off-diagonal elements of Jacobian matrix given by

$$J_{i,k} = \sum_1^M -\left(\frac{\partial \dot{m}_{k,i}}{\partial \Delta P_{k,i}}\right); \qquad \text{(kg /s Pa)} \qquad (3.14)$$

M is the number of connections between node i and node k. Therefore, the summation of the terms in each row of the Jacobian matrix is equal to zero.

Mass conservation at each zone provides the convergence criterion for the N-R iterations. When conservation is satisfied for all zones for the current system pressure estimate, the solution has converged. In practice, it is sufficient when mass flow rate residuals are smaller than a certain convergence limit. In multi-zone airflow network in ESP-r, there are two optional criteria for convergence: ERRMAX and FLOWMAX (Henson, 1991). N-R iteration will stop when the maximum percentage residual for all the nodes is smaller than ERRMAX or maximum absolute residual is smaller than FLOMAX

$$\left(\frac{\left| \sum_k \dot{m}_{k,i} \right|}{\sum_k \left| \dot{m}_{k,i} \right|} \right)_{\max} \leq \frac{ERRMAX}{100} \qquad (3.15)$$

$$\left(\left| \sum \dot{m}_k \right| \right)_{\max} \leq FLOMAX \quad (kg/s) \qquad (3.16)$$

3.4 Discussion

In this chapter, the fundamental issues for two basic simulation modules in building simulation program ESP-r have been reviewed and discussed. The governing equations, boundary conditions and numerical solutions of thermal simulation module and airflow network module are introduced. Although there are more than 200 building simulation programs in the world (http://www.eere.energy.gov/buildings), the basic models in most of the programs are quite similar. ESP-r is one of the best available building simulation programs that has been widely used and validated.

However, the current building simulation programs have limitations in natural ventilation prediction. With the mixed assumption in building simulation, detailed indoor environment evaluation cannot be obtained for naturally ventilated building designs. In addition, the air flow profile cannot be accurately predicted and described without the involvement of momentum equations and turbulence equations in multi-zone airflow models. Consequently, the accuracy of natural ventilation prediction is limited by the idealized assumptions and simplified governing equations. The biggest advantage of building simulation is to provide a

way to predict indoor environment with a fast speed. Therefore, building simulation can be considered as a starting point to further improve the prediction method for natural ventilation.

As mentioned in Chapter 2, Negrao (1995), and Beausoleil-M. (2001) internally coupled ESP-r and CFD module mainly to improve the accurate of energy consumption prediction in HVAC systems. For internal coupling between ESP-r and CFD, a module CFD was build into the ESP-r for simulation and only one model is to be built for the coupled simulation. Matrix formation in each module (thermal analysis, airflow network or CFD) is affected due to data exchange in each time step. However, the internal coupling between ESP-r and CFD strictly limited simulation geometry and the number of grids, and the parallel computing techniques used in current state-of-the-science CFD codes for speedy computation also cannot be employed. There is no internal CFD module is built inside building simulation for external coupling between ESP-r and CFD. The changes of source code can be minimized. Simulation models should be built separately in CFD and ESP-r. Data exchanges for boundary conditions are needed to bridge the two programs. Djunaedy (2005) externally coupled ESP-r and CFD for energy consumption prediction, but the problem of coupling ESP-r and CFD for accurately predicting natural ventilation is not solved.

Chapter 4 Fundamentals of Computational fluid dynamics

In this chapter, the fundamental governing equations and boundary conditions for computational fluid dynamics and various turbulence models for indoor airflow and outdoor airflow are introduced. The techniques for outdoor airflow simulation are discussed and different turbulence models are applied to outdoor airflow simulation. The purpose of outdoor airflow simulation is to find a suitable turbulence model for outdoor airflow simulation to calculate the mean pressure coefficients for building simulation.

Computational fluid dynamics (CFD) has already become a significant tool in designing or enhancing our understanding of fluid dynamics in the fields of science and engineering. CFD techniques can be applied to simulate realistic fluid problems, which are difficult or costly to be solved analytically and experimentally. Currently, there are several widely used commercial CFD tools, such as PHOENICS, FLUENT, CFX, and STAR-CD. The governing equations and turbulence models being solved in these tools are essentially the same. The commercial CFD software FLUENT is a popular general-purpose package used in many research and industrial areas. In this study, FLUENT is used to couple with building simulation ESP-r.

4.1 Governing equations and numerical methods of fluid airflow

The properties of fluid flows (such as air velocity, pressure, temperature and turbulence characteristics) in spatial and temporal distribution are governed by three conservative laws of fluid flows: mass conservation, momentum equation (Newton's second law) and energy conservation. The differential governing equations for a control volume in a Cartesian coordinate system can be written as:

Mass conservation equation (continuity equation)

$$\frac{\partial \rho}{\partial t} + div(\rho U_i) = 0 \qquad (4.1)$$

where U_i represents velocity component in each perpendicular coordinate direction x_i (i=1,2,3), t is the time, and div is the divergence operator.

Momentum conservation equation (unsteady Navier-Stokes equation)

$$\frac{\partial(\rho U_i)}{\partial t} + div(\rho U_i U_j) = -\frac{\partial P}{\partial x_i} + div(\mu grad U_i) + B_i \qquad (4.2)$$

where U_i and U_j are velocity components in x_i and x_j directions, t is the time, P is the pressure, μ is the molecular dynamic viscosity, B_i is the body force and *grad* is the gradient operator.

Energy equation

$$\frac{\partial(\rho h)}{\partial t} + div(\rho U_i h) = div(\lambda grad T) + S_h \qquad (4.3')$$

where T is the air temperature, λ is the thermal conductivity of air, ρ is the air density, S_h is the net source term in the fluid.

For the idea gas, liquid and solid, $h = c_p T$, and c_p is the specific heat of air at constant pressure. The governing equation can be rewritten as:

$$\frac{\partial(\rho T)}{\partial t} + div(\rho U_i T) = div(\Gamma grad T) + S_T \quad (4.3)$$

where $\Gamma = \lambda / c_p = \eta / \mathrm{Pr}$ is the temperature viscous diffusion coefficient, Pr is the Prandtl number, S_T is the net source term in the fluid.

General transport equation

The governing equations can be generalized by denoting the dependent variables, such as the enthalpy, the temperature, or velocity components, with a general variable ϕ in the governing equations.

$$\frac{\partial(\rho\phi)}{\partial t} + div(\rho U_i \phi) = div(\Gamma_\phi grad\phi) + S \quad (4.4)$$

where Γ is diffusion coefficient and *S* is source term.

4.2 Turbulence modeling

The governing equations, applicable for laminar flow and turbulence flow, are a set of coupled non-linear partial differential equations and are very difficult to directly solve these governing equations for fully turbulence flow because of high velocity fluctuations in time and space, which needs very fine meshes and extremely high speed work stations to describe processes at all turbulence eddy length scales. The most widely used method for turbulence flow is to solve Reynolds averaged governing equations with the complements of other turbulence models to represent turbulence characteristics.

According to the principle of Reynolds average, the time-averaged value for any dependent variable is defined by

$$\bar{\phi} = \frac{1}{\Delta t}\int_t^{t+\Delta t} \phi(t)dt \quad (4.5)$$

The relationship among the instant value of variable ϕ, the time-averaged value $\bar{\phi}$, and fluctuation value can be expressed as:

$$\phi = \bar{\phi} + \phi' \qquad (4.6)$$

By replacing the dependent variables in the above governing equations (4.1) (4.2) (4.3) using the averaged and fluctuation values, the Reynolds-averaged governing equations can be written as:

Continuity equation

$$\frac{\partial(\rho u_i)}{\partial x_i} = \frac{\partial(\rho u_i')}{\partial x_i} = 0 \quad (4.7)$$

where u_i and u_i' are the Reynolds averaged and turbulence fluctuant velocity component respectively, in three perpendicular coordinate directions x_i(i=1,2,3).

Momentum equations

$$\frac{\partial(\rho u_i)}{\partial t} + \frac{\partial(\rho u_i u_j)}{\partial x_j} = -\frac{\partial P}{\partial x_i} + \frac{\partial}{\partial x_j}(\mu \frac{\partial u_i}{\partial x_j} - \rho\overline{u_i' u_j'}) + B_i \quad (4.8)$$

where u_i and u_j are the Reynolds-averaged velocity components in x_i and x_j directions. Comparing with governing equation (4.2), the additional item $\rho\overline{u_i' u_j'}$ is added into Reynolds averaged equation after the process of time averaging for second order item. This extra stress, called Reynolds stresses, represents the turbulence influence on the mean airflow.

Energy equation

$$\frac{\partial(\rho T)}{\partial t} + \frac{\partial(\rho u_j T)}{\partial x_j} = \frac{\partial}{\partial x_j}(\Gamma \frac{\partial T}{\partial x_j} - \rho\overline{u_j' T'}) + S_T \qquad (4.9)$$

where T is the Reynolds-averaged air temperature. $\rho\overline{u_j' T'}$, called turbulent heat flux, has been added in the Reynolds-averaged equation, representing the turbulence influence on the mean air temperature.

Similarly, the time average transport equation derived from generalized transport equation (4.4) for other scalar ϕ can be expressed by,

$$\frac{\partial(\rho\bar{\phi})}{\partial t}+\frac{\partial(\rho u_j\bar{\phi})}{\partial x_j}=\frac{\partial}{\partial x_j}(\Gamma_\phi\frac{\partial\bar{\phi}}{\partial x_j}-\rho\overline{u_j'\phi'})+S \qquad (4.10)$$

For the set of Reynolds-averaged equations, there are six additional unknown Reynolds stresses $\rho\overline{u_i'u_j'}$ in the time averaged momentum equation and the extra three turbulence heat fluxes terms $\rho\overline{u_j'T'}$ in the time average temperature equations after the process of time-averaging operations. Therefore, the set of governing equations are not closed. Accurate predictions of Reynolds stresses and turbulence scalar fluxes are the main tasks for turbulence modeling.

To close the system of time averaging flow governing equations, the classic Boussinesq assumption (Equation 4.11), which employs the analogy between viscous stresses in Newton‘s viscosity law and Reynolds stresses in Reynolds-averaged N-S equation to link Reynolds stresses to the mean rates of deformation, is used to built up the traditional turbulence models (zero equation model, $k-\varepsilon$ model, Reynolds stress equation model, etc.)

$$\tau_{i,j}=-\rho\overline{u_i'u_j'}=\mu_t(\frac{\partial u_i}{\partial x_j}+\frac{\partial u_j}{\partial x_i}) \qquad (4.11)$$

where μ_t (Pa s) is the turbulent or eddy viscosity

Similarly, by analogy, turbulent scalar fluxes (Equation 4.12), such as turbulent heat and concentration fluxes, can be proportional to the gradient of the mean value of the transported quantity.

$$-\rho\overline{u_j'\phi'} = \Gamma_t \frac{\partial \bar{\phi}}{\partial x_j} \qquad (4.12)$$

Where Γ_t is the turbulent diffusivity

By applying Equation (4.11) and (4.12) to the Reynolds-averaged governing equations, we can obtain the new sets of Reynolds-averaged momentum equation and temperature equation:

$$\frac{\partial(\rho u_i)}{\partial t} + \frac{\partial(\rho u_i u_j)}{\partial x_j} = -\frac{\partial P}{\partial x_i} + \frac{\partial}{\partial x_j}\left[(\mu + \mu_t)\frac{\partial u_i}{\partial x_j}\right] + B_i \qquad (4.13)$$

$$\frac{\partial(\rho T)}{\partial t} + \frac{\partial(\rho u_j T)}{\partial x_j} = \frac{\partial}{\partial x_j}\left[\left(\frac{\mu}{\sigma} + \frac{\mu_t}{\sigma_t}\right)\frac{\partial T}{\partial x_j}\right] + S_t \qquad (4.14)$$

Therefore, the determination of eddy viscosity μ_t becomes the main task for various classic turbulence models. These turbulence models are further classified according to the number of differential equations used to solve the turbulent quantities. The commonly used RANS (Reynolds average Navier-Stokes), zero equation model, RSM (Reynolds Stress model) and LES (Large eddy simulation) for building technology are introduced in the following section.

4.2.1 The Standard $k-\varepsilon$ two-equation models

The standard $k-\varepsilon$ model (Launder & Spalding, 1974) is a semi-empirical model based on an isotropic eddy-viscosity concept by introducing the turbulence kinetic energy (k) and its dissipation rate (ε) transport equations. The turbulence viscosity in standard $k-\varepsilon$ two equation model is defined by Equation 4.15

$$\mu_t = C_\mu \rho \frac{k^2}{\varepsilon} \qquad (4.15)$$

where C_μ is the empirical constant. k and ε can be determined by solving the following transport equations. The model transport equation for k is derived from the exact equation, while the transport equation for ε was obtained using physical reasoning.

$$\frac{\partial}{\partial t}(\rho k)+\frac{\partial}{\partial x_i}(\rho k u_i)=\frac{\partial}{\partial x_j}\left[(\mu+\frac{\mu_t}{\sigma_k})\frac{\partial k}{\partial x_j}\right]+G_k+G_b-\rho\varepsilon+S_k \quad (4.16)$$

and

$$\frac{\partial}{\partial t}(\rho \varepsilon)+\frac{\partial}{\partial x_i}(\rho \varepsilon u_i)=\frac{\partial}{\partial x_j}\left[(\mu+\frac{\mu_t}{\sigma_\varepsilon})\frac{\partial \varepsilon}{\partial x_j}\right]+C_{1\varepsilon}\frac{\varepsilon}{k}(G_k+C_{3\varepsilon}G_b)-C_{2\varepsilon}\rho\frac{\varepsilon^2}{k}+S_\varepsilon \quad (4.17)$$

In these equations, G_k represents the generation of turbulence kinetic energy due to the mean velocity gradients,

$$G_k=-\rho\overline{u_i'u_j'}\frac{\partial u_j}{\partial x_i} \quad (4.28)$$

G_b is the generation of turbulence kinetic energy due to buoyancy. $C_{1\varepsilon}$, $C_{2\varepsilon}$, and $C_{3\varepsilon}$ are constants in Table 4.1. σ_k and σ_ε are the turbulent Prandtl numbers for k and ε, respectively. S_k and S_ε are user-defined source terms.

Table 4.1 Model constants for standard $k-\varepsilon$ model

$C_{1\varepsilon}$	$C_{2\varepsilon}$	C_μ	σ_k	σ_ε
1.44	1.92	0.09	1.0	1.3

These default values have been determined from experiments for fundamental turbulent shear flows. The assumption for applying the standard $k-\varepsilon$ model is fully turbulent flows, whose effects of molecular viscosity are negligible.

4.2.2 RNG $k-\varepsilon$ two-equation models

Yakhot and Orszag (1986) derived the RNG-based $k-\varepsilon$ turbulence model from the instantaneous Navier-Stokes equations, using a mathematical technique called "renormalization group" (RNG) methods. RNG model was derived using a more rigorous statistical technique and its model constants are derived analytically. The model equations in their RNG form are similar to those for the standard $k-\varepsilon$ model.

The RNG $k-\varepsilon$ model transport equations for k and ε are as follows:

$$\frac{\partial}{\partial t}(\rho k)+\frac{\partial}{\partial x_i}(\rho k u_i)=\frac{\partial}{\partial x_j}\left[(\mu+\mu_t/\sigma_k)\frac{\partial k}{\partial x_j}\right]+G_k+G_b-\rho\varepsilon+S_k \quad (4.19)$$

And

$$\frac{\partial}{\partial t}(\rho\varepsilon)+\frac{\partial}{\partial x_i}(\rho\varepsilon u_i)=\frac{\partial}{\partial x_j}\left((\mu+\mu_t/\sigma_\varepsilon)\frac{\partial\varepsilon}{\partial x_j}\right)+C_{1\varepsilon}\frac{\varepsilon}{k}(G_k+C_{3\varepsilon}G_b)-C_{2\varepsilon}^{*}\rho\frac{\varepsilon^2}{k}+S_\varepsilon \quad (4.20)$$

In these equations, G_k represents the generation of turbulence kinetic energy due to the mean velocity gradient. G_b is the generation of turbulence kinetic energy due to buoyancy. The quantities σ_k and σ_ε are Prandtl numbers for k and ε, respectively S_k and S_ε are user-defined source terms. $C_{2\varepsilon}^{*}\equiv C_{2\varepsilon}+\frac{C_\mu\eta^3(1-\eta/\eta_0)}{1+\beta\eta^3}$, $\eta\equiv Sk/\varepsilon$, $S=\left(2S_{i,j}S_{i,j}\right)^{1/2}$, $S_{i,j}=\frac{1}{2}\left(\frac{\partial u_i}{\partial x_j}+\frac{\partial u_j}{\partial x_i}\right)$, $\eta_0=4.38$, $\beta=0.012$. The constants used in RNG $k-\varepsilon$ model are given in Table 4.2.

As in standard $k-\varepsilon$ models, the eddy viscosity is computed from

$$\mu_t = \rho C_\mu \frac{k^2}{\varepsilon} \quad (4.21)$$

C_μ is a constant, and the value is listed in Table 4.2.

Table 4.2 Model constants for RNG $k-\varepsilon$ model

$C_{1\varepsilon}$	$C_{2\varepsilon}$	C_μ	σ_k	σ_ε
1.42	1.68	0.0845	0.7179	0.7179

The main difference between the RNG and standard $k-\varepsilon$ models lies in the additional term R_ε in the ε equation introduced by the coefficient $C_{2\varepsilon}^*$ of ε destruction rate:

$$R_\varepsilon = \frac{C_\mu \rho \eta^3 (1-\eta/\eta_0)}{1+\beta\eta^3} \frac{\varepsilon^2}{k} \quad (4.22)$$

Therefore, the coefficient of ε destruction rate is related with flow conditions and the function of coordinates. For moderately strained flows, the RNG model tends to give results comparable to the standard $k-\varepsilon$ mode, while for rapidly strained flows, the RNG model yields a lower turbulence viscosity than the standard $k-\varepsilon$ model (FLUENT user's guide). Thus, the RNG model is more appropriate to predict turbulence flow with rapid strain.

4.2.3 Realized $k-\varepsilon$ two-equation models

The realizable $k-\varepsilon$ model was proposed by Shih *et al.* (1995) was intended to improve standard $k-\varepsilon$ models by adopting a new formula for C_μ and a new model equation for dissipation (ε) based on the dynamic equation of the mean-square vorticity fluctuation.

The modeled transport equations for k and ε in the realizable $k-\varepsilon$ model are

$$\frac{\partial}{\partial t}(\rho k) + \frac{\partial}{\partial x_j}(\rho k u_j) = \frac{\partial}{\partial x_j}\left[\left(\mu + \frac{\mu_t}{\sigma_k}\right)\frac{\partial k}{\partial x_j}\right] + G_k + G_b - \rho\varepsilon + S_k \quad (4.23)$$

and

$$\frac{\partial}{\partial t}(\rho\varepsilon)+\frac{\partial}{\partial x_j}(\rho\varepsilon u_j)=\frac{\partial}{\partial x_j}\left[\left(\mu+\frac{\mu_t}{\sigma_\varepsilon}\right)\frac{\partial\varepsilon}{\partial x_j}\right]+\rho C_1 S_\varepsilon-\rho C_2\frac{\varepsilon^2}{k+\sqrt{v\varepsilon}}+C_{1\varepsilon}\frac{\varepsilon}{k}C_{3\varepsilon}G_b+S_\varepsilon$$

(4.24)

where

$$C_1=\max\left[0.43,\frac{\eta}{\eta+5}\right],\ \eta=S\frac{k}{\varepsilon},\ S=\sqrt{2S_{ij}S_{ij}}$$

In these equations, G_k represents the generation of turbulence kinetic energy due to the mean velocity gradients. G_b is the generation of turbulence kinetic energy due to buoyancy. C_2 and $C_{1\varepsilon}$ are constants. σ_k and σ_ε are the turbulent Prandtl numbers for k and ε, respectively. S_k and S_ε are user-defined source terms.

As in other $k-\varepsilon$ models, the eddy viscosity is computed from

$$\mu_t=\rho C_\mu\frac{k^2}{\varepsilon} \qquad (4.25)$$

In realizable $k-\varepsilon$ model, C_μ is no longer constant.

$$C_\mu=\frac{1}{A_0+A_s\dfrac{kU^*}{\varepsilon}} \qquad (4.26)$$

where

$$U^*\equiv\sqrt{S_{ij}S_{ij}+\tilde{\Omega}_{ij}\tilde{\Omega}_{ij}} \qquad (4.27)$$

and

$$\tilde{\Omega}_{ij}=\Omega_{ij}-2\varepsilon_{ijk}\omega_k \qquad (4.28)$$

$$\Omega_{ij}=\overline{\Omega_{ij}}-\varepsilon_{ijk}\omega_k \qquad (4.29)$$

where $\overline{\Omega_{ij}}$ is the mean rate of rotation tensor viewed in a rotating reference frame with angular velocity ω_k. The model constants A_0 and A_s are given by

$$A_0 = 4.04, \quad A_s = \sqrt{6}\cos\Phi$$

where

$$\Phi = \frac{1}{3}\cos^{-1}\left(\sqrt{6}W\right), \quad W = \frac{S_{ij}S_{jk}S_{ki}}{\tilde{S}^3}, \quad \tilde{S} = \sqrt{S_{ij}S_{ij}}, \quad S_{ij} = \frac{1}{2}\left(\frac{\partial u_j}{\partial x_i} + \frac{\partial u_i}{\partial x_j}\right)$$

It can be seen that C_μ is a function of the mean strain and rotation rates, the angular velocity of the system rotation, and the turbulence fields (k and ε). The constants for realizable $k-\varepsilon$ model are listed in Table 4.3.

It is noted that the form of the ε equation is different from those in the standard and RNG based $k-\varepsilon$ models. The production term in the ε equation does not involve the production of *k* and the denominator of destruction term is always larger than zero. Realizable $k-\varepsilon$ model can better represent the spectral energy transfer and have non-singularity destruction term (FLUENT user's guide). This model has been validated for a wide range of flows, such as rotating homogeneous shear flows, free flows including jets and mixing layers, channel and boundary layer flows, and separate flows. For all these cases, the performance of the model has been found to be substantially better than that of the standard $k-\varepsilon$ model (Shih *et al.*, 1995). RANS modeling has been widely used is since it can give reasonable results for many industrial flows with an affordable computing cost with acceptable accuracy.

Table 4. 3 Model constants for Realizable $k-\varepsilon$ model

$C_{1\varepsilon}$	C_2	σ_k	σ_ε
1.44	1.9	1.0	1.2

4.2.4 Other methods for turbulence flow

4.2.4.1 Zero-equation model

Zero-equation model uses an algebraic formula to describe turbulence viscosity with time-averaged velocity scale. A zero-equation eddy viscosity model is newly developed by Xu (1998) based on natural and forced convection flow results by Direct Numerical Simulation(DNS), which is widely used for indoor air environment prediction.

4.2.4.2 Reynolds stress model

To eliminate the isotropic eddy viscosity assumption for $k-\varepsilon$ two equations, the Reynolds stress model (RSM) (Hanjalic and Launder, 1972） solves differential governing equations for Reynolds stresses/fluxes to obtain closure of the Reynolds-averaged equations. Although RSM has some successful applications, additional nine extra governing equations are to be solved in RSM for Reynolds stresses and Heat fluxes in three dimensional flows and a great deal of computational cost is added.

4.2.4.3 Large eddy simulation

Another important turbulence prediction method--large eddy simulation (LES) directly solves the large, energy-carrying eddies, which are affected by the boundary conditions and carry most of the Reynolds stresses and the small scale eddies are modeled with turbulence models since the small eddies tend to be isotropic. LES is appropriate to accurately solve three dimensional, time-dependent airflow problems, but requires a large-capacity, high-speed computer to study airflows related to buildings.

4.3 Numerical methods

4.3.1 Discretization method

The flow governing equations (4.1)-(4.3) with appropriate turbulence models, as well as particular boundary conditions, establish a complete system of flow equation. However, these equations are highly non-linear and strongly coupled. Therefore, the partial differential governing equations (PDE) must be solved numerically. In the numerical simulation approach, a finite number of grid points are used to represent computation domain and a series of time intervals are used to indicate continuous time. Therefore, the accurate differential equations are replaced with discrete algebraic equations that can be solved by a computer through block iteration method.

The two commonly used discretization approaches for fluid dynamic are finite difference method (Figure 4.1) and finite volume method (Figure 4.2). The finite difference method directly approximates the differential derivatives with Taylor series expansion or polynomial approximation and therefore, the numerical accuracy of the discretization is easy to be analyzed. Only structured meshing with rectangular computational domain or a combination of sub-rectangular domains can be used. Comparing with finite difference method, the finite volume method is flexible. It is based on the integral form of conservative governing equations and approximates the integrals using the Gauss theorem and replaces all cell fluxes with difference quotients and can handle the structured grids and unstructured grids. The biggest advantage of the finite volume method is that the conservation of momentum, heat and other transport quantities can be accurately achieved on each cell. Due to the obvious

physical concepts and flexibility for general complicated cases, the finite volume method is adopted in most of commercial CFD codes. A brief introduction of this algorithm is the following.

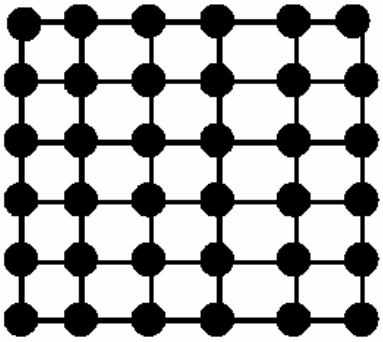

Figure 4. 1 Finite difference method

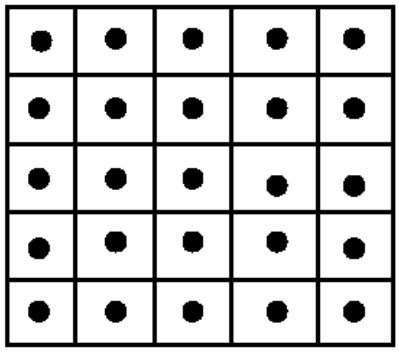

Figure 4. 2 Finite volume method

The governing equation for a general variable ϕ (velocity component, turbulence kinetic energy, turbulence dissipation, temperature, etc.) under steady state condition can be written as

$$div(\rho U_i \phi) = div(\Gamma_\phi grad\phi) + S \qquad (4.30)$$

The variables, diffusion coefficient and source items of representative governing equations are listed in Table 4.4

Table 4. 4 Governing equations represented by Eq 4.30

Equation	ϕ	Γ_ϕ	S_ϕ
Continuity	1	0	0
Momentum	U_i	$\mu + \mu_t$	$-\frac{\partial P}{\partial x_i} + B_i$
Turbulent Kinetic energy	k	$\mu + \frac{\mu_t}{\sigma_k}$	$(P + G - \varepsilon)\rho$
Dissipation rate of k	ε	$\mu + \frac{\mu_t}{\sigma_\varepsilon}$	$\rho[C_{\varepsilon 1}(P+G) - C_{\varepsilon 2}\varepsilon]\frac{\varepsilon}{k}$
Temperature	T	$\frac{\mu}{\mathrm{Pr}} + \frac{\mu_t}{\mathrm{Pr}_t}$	S_t

When $\phi = 1$, Equation (4.30) is the continuity equation. It is often associated with the pressure variable in anticipation of the so-called pressure correction equation. Pr_t is turbulent Prandtl number.

Integrating equation (4.30) over a typical control volume by applying the Gauss theory ($\int_\Omega \nabla \cdot F d\Omega = \int_S F \cdot dS$), we can obtain that

$$\oint_S (\rho U_i \Phi - \Gamma_{\phi f} \frac{\partial \Phi}{\partial x_i}) \cdot dS = \int_{\Delta v} S dV \quad (4.31)$$

The source term S is linearized as

$$S = S^c + S^P \phi_P$$

where $S_\phi^P \le 0$. This linearization is conducive to convergence of the problem.

$$\int_{\Delta v} S \, dV = S^c \Delta V + S^P \phi_P \Delta V$$

Therefore, the discretization form of the governing equations is

$$A_P \phi_P = \sum_{nb} A_{nb} \phi_{nb} - S^c \Delta V \quad (4.32)$$

where

$$A_P = \sum_{nb} A_{nb} - S^p \Delta V$$

The subscript nb refers to the neighboring points around node P. The main coefficient A_{nb} that relates the principal unknown ϕ_P to its neighboring ϕ_{nb} contains the combination contribution from convection $\rho U_j \phi$ and diffusion $-\Gamma_\phi \frac{\partial \phi}{\partial x_j}$.

4.3.2 Pressure-correction method

The discretized algebraic equations can be iterated based on the initial guessed conditions or the values from last iteration. With the assumed pressure field, the velocity distributions can

be obtained by solving velocity discretized algebraic equations. However, there are no specific governing equations for pressure and the obtained velocity may not be able to observe the continuity equations. Therefore, it is necessary to establish pressure correction governing equation for adjusting pressure field to make sure the calculated velocity field can meet the continuity equations. To couple the pressure and velocity with continuity equation, Patankar and Spalding (1972) put forward the SIMPLE (Semi-Implicit Method for Pressure Linked Equations) method for incompressible flow problems. Patankar (1980) revised the SIMPLE method by introducing pseudo-velocity to improve the coordination between velocity correction and pressure correction and speed up convergence.

4.4 Boundary conditions

The boundary conditions of the system to be simulated must be well-posed to build up a particular physical problem. All boundary conditions in the computational domain must be provided. For turbulence flow near the wall, a no-slip condition is normally adopted. Temperature or a heat flux can be specified on the wall for energy conservation equation. When the grids near the wall are not fine enough to describe the inner viscous layer, special wall treatment technique--wall function is used to calculate the solution variables near the wall for system governing equations based on corresponding quantities on the wall. There are two options available in FLUENT for wall functions: standard wall function (Launder and Spalding, 1974) and non-equilibrium wall function (Kim and Choudhury, 1995). Standard wall function is the most widely used for a broad range of fluid flow cases. Non-equilibrium wall function is used for severe pressure gradient flows involving separation, reattachment,

etc. The advantage of the application of wall function is to save computing efforts to avoid using fine meshes near the wall.

Except wall boundary conditions, the other boundary conditions for the transport variables used in the study are velocity boundary, pressure boundary, and symmetry boundary. Pressure flow may be specified at different points in the domain but the fluid pressure needs to be defined at least in one point in the flow as reference pressure. Velocity components are commonly given at the boundaries. Turbulence variables (k and ε) related parameters and temperature are also required to define the opening conditions. Symmetry boundary is used when the physical geometry has mirror symmetry and therefore the computational cost is reduced significantly.

4.5 Pressure coefficient (Cp) predictions

4.5.1 Pressure coefficient calculation methods

There are four different methods for pressure coefficient calculation: algebraic equations, site measurement, wind tunnel study, and CFD simulations.

Algebraic algorithm

Application of empirical algebraic equations is a simple and quick method to estimate pressure coefficients around buildings. Cp calculation models (Walker and Wilson, 1994; Grosso, 1992) are derived from results of wind tunnel experiments. Since the experimental data obtained from one building site may not be extended to another because of different building surroundings, the accuracy of algebraic equation method is compromised.

Site measurement

Although full-scale measurements for a building can provide reliable data, doing experiments is time consuming and it is difficult to control for investigated parameters.

Wind tunnel study

Wind tunnel is a mechanical means of producing wind under controlled environment to study the airflow around the buildings, which models an atmospheric boundary layer to generate mean velocity profile and turbulence properties around building models. Scaled models are normally used in wind tunnel to study their ventilation characteristics. One of the main functions of wind tunnel is to predict the wind pressure distributions over the external envelopes for ventilation studies. The advantages of wind tunnel measurement are that the results respond directly to the building geometric conditions and parameters can be easily modified to meet the required conditions. However, wind tunnel experiments are constrained by limited measuring points and the accuracy of the measuring instruments.

CFD simulations

Computational fluid dynamics (CFD) provides an alternative approach to calculate ventilation rate and detailed airflow distributions in and around buildings. CFD is widely used due to its informative results and, low labor and equipment costs, as a result of the development in turbulence modeling and the increase in computer speed and capacity.

Therefore, CFD simulations are applied in this study to predict accurate pressure coefficients (Cp) of external surfaces.

4.5.2 Cp prediction result comparison with experiment data

Pressure coefficients provide boundary conditions for airflow network in BS and, coupled simulations between CFD and BS for natural ventilation, which directly determine the general airflow routes. As discussed above, CFD is an appropriate and reliable method for pressure coefficient prediction. Jiang and Chen (2001) investigated the numerical simulation of large eddy simulation for airflow around a bluff body and showed good simulation results of pressure coefficient distribution comparing with wind tunnel experiment data by AIJ working group (1994). Although large eddy simulation is a more accurate method, it is more time consuming comparing with classic turbulence models. In this study, in order to find fast and accurate turbulence model for Cp prediction, different turbulence models (standard $k-\varepsilon$ model, RNG $k-\varepsilon$ model, realizable $k-\varepsilon$ model, and Reynolds stress model) are employed to predict pressure coefficients with the comparison of the experimental results available in literature (AIJ working group, 1994). Dimensions of building block are 2H×2H×1H and dimensions of the computational domain are 30H×20H×6H (Fig. 4.3). In the numerical study, the numerical number is 3.6×10^4. The total number of cells is 1,350,000 with non-structure meshes and the smallest dimensionless grid size close to the wall is 0.05. The upwind mean velocity u_0 employs a 1/4 shear flow power-law profile as the inlet boundary conditions, and the mean velocity in the other two directions are zero. The SIMPLER method in FLUENT is used to obtain the coupling between pressure and velocity distribution and second order upwind discretization scheme is used to avoid numerical diffusion. The convergence criterion of 10^{-4} is set for the residuals of all the variables. Turbulence models

standard $k-\varepsilon$ model, RNG $k-\varepsilon$ model, realizable $k-\varepsilon$ model, and Reynolds stress model are adopted respectively.

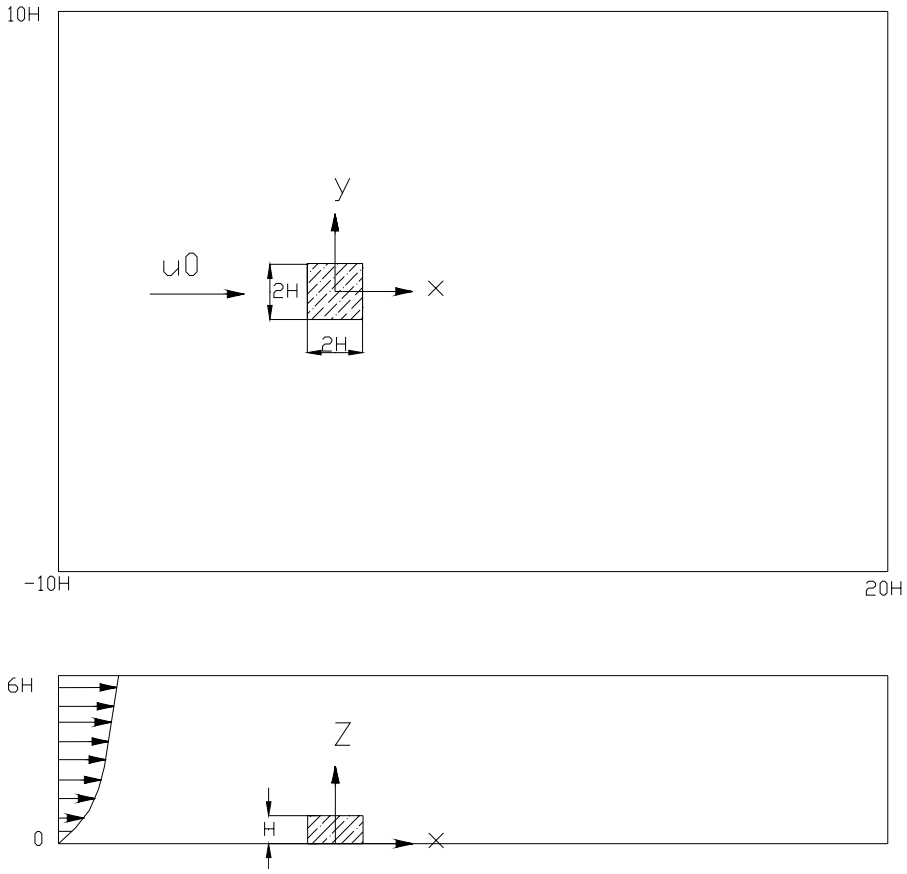

Figure 4. 3 Dimensions of the computational domain (section view and plan view)

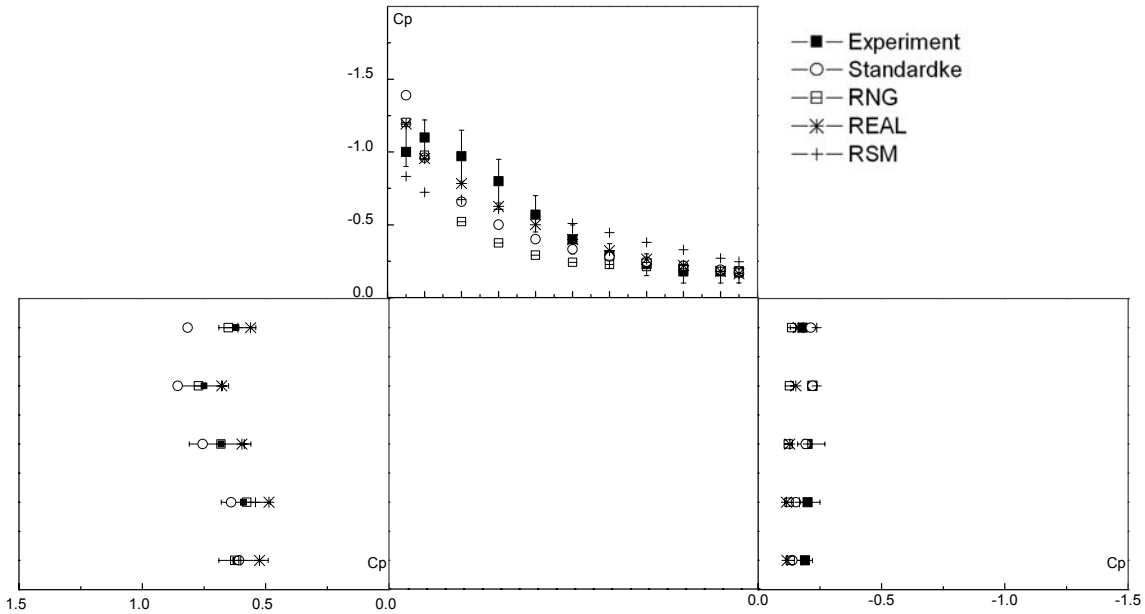

(a)

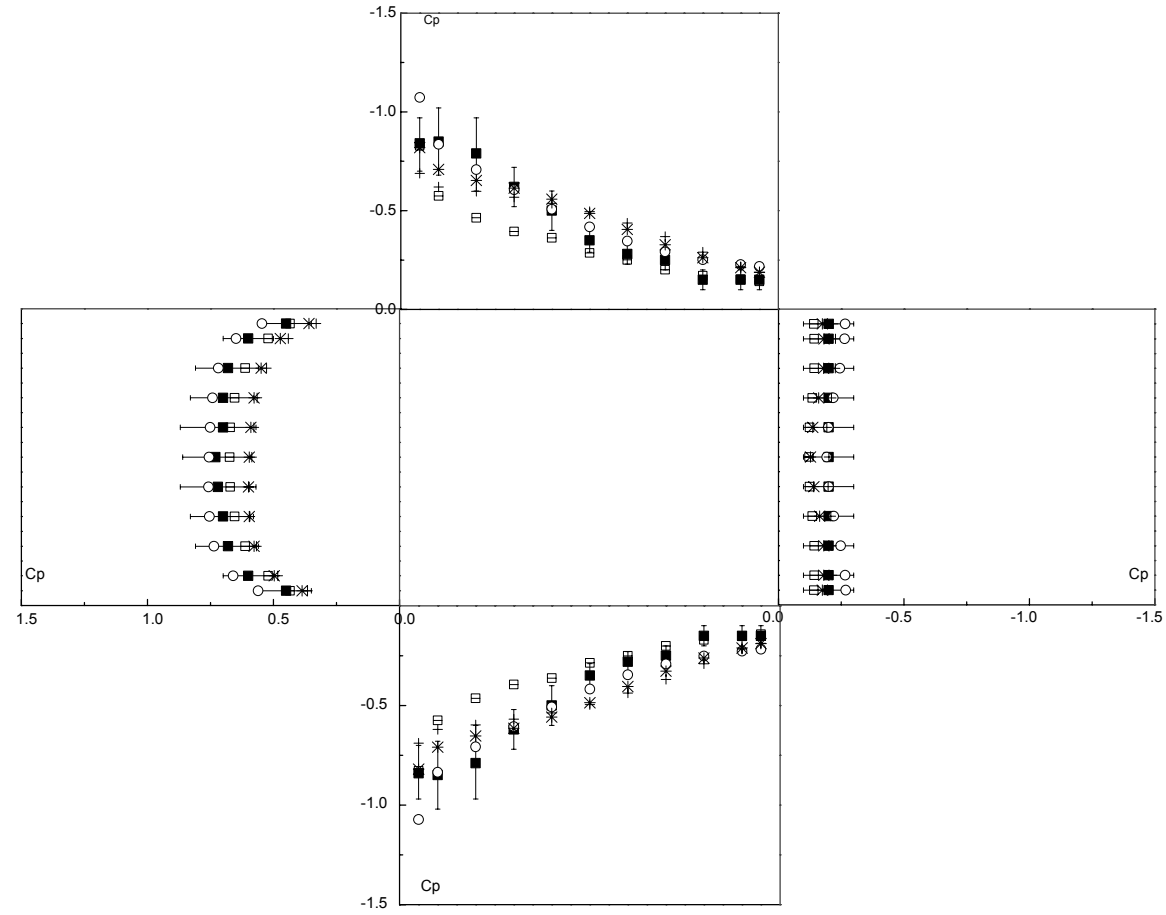

(b)

Figure 4. 4 Mean pressure coefficients on middle vertical section (a) and plan view at the height of H/2 (b) at wind direction of 0º

Pressure coefficients are calculated based on Equation 3.9 and the reference wind speed is at roof level 1H. Figure 4.4 shows the comparison of simulation results of pressure coefficients using standard $k-\varepsilon$ model, RNG $k-\varepsilon$ model, realizable $k-\varepsilon$ model and Reynolds stress model with experimental results. Pressure coefficients at leeward side are quite uniform. The four turbulence models generally show consistent results with the experiment data. For the standard $k-\varepsilon$ model, the major deficiency is that there is a rapid increase of pressure coefficients at the windward corner on the roof, while for the experiment data, pressure coefficient at the front corner is gradually increase and then decrease at the end. This can be attributed to the overestimation of turbulence kinetic energy at the location in standard $k-\varepsilon$ model (Murakami, *et al*, 1990). The prediction results with Reynolds stress model and realizable $k-\varepsilon$ model at front corner are improved. However, a great deal of computational time is required for solving additional Reynolds stress governing equation. Therefore, realizable $k-\varepsilon$ model is reliable and selected for pressure coefficient predictions to provide correct boundary conditions when studying natural ventilation in buildings.

4.6 Discussion

The fundamental issues on CFD for building airflow simulation including: governing equations, turbulence models, numerical procedure and boundary conditions are introduced in this chapter. Comparing with building simulation, CFD simulations require significant computing efforts. Therefore, for realizable complex cases, simulation works by CFD alone are costly to carry out for a whole block, especially for natural ventilation, under which both

outdoor and indoor airflow and temperature distribution are required. The integration of building simulation and computational fluid dynamics can be a promising method to provide a fast and accurate method to predict natural ventilation.

Turbulence models for prediction of pressure coefficients are also performed for a bluff body and compared with experimental results available in literature. The results indicate that realizable $k-\varepsilon$ model is appropriate turbulence model to predict pressure coefficients for boundary conditions of airflow network simulations.

Chapter 5 Indoor coupling for naturally ventilated rooms

The coupling strategies for natural ventilation between building simulation (BS) and computational fluid dynamics (CFD) are discussed and coupling methodology and procedures for natural ventilation are stated in the Chapter. Single zone cases and multi-zone cases have been used to validate coupled simulations with full CFD simulations. Field measurements for a typical naturally ventilated building are carried out for validation of coupled simulations. The main discrepancy factors have also been analyzed.

5.1 Coupling strategies

As discussed in the previous chapters, both BS and CFD have their own limitations in predicting thermal environment of naturally ventilated buildings. Building simulation programs can quickly predict the indoor environment but indoor airflow profiles cannot be accurately predicted with airflow network in BS. Firstly, detailed indoor thermal environment cannot be obtained with the well-mixed assumption in building simulation. In addition, airflow simulations in BS are governed by pressure-flow algebraic equation for airflow components, mass balance equation at the nodes and hydrostatic pressure variations in the zones (Feustel, 1999). There is no momentum equation involved in the airflow network. Thirdly, pressure coefficients normally used in BS are collected either from some wind tunnel experiment results for some typical exposed or surrounded buildings, which may not be suitable for a specific case, or from empirical equations. The total pressure of wind induced

boundary nodes are calculated based on pressure coefficients. These pressure coefficients in the building simulation databases are the average coefficients of the whole oriented wall rather than the coefficients averaged for the specific area of the orifices, which may add potential inaccuracy in multi-zone airflow simulation. Therefore, accurate indoor thermal environment for naturally ventilated buildings cannot be obtained with BS alone.

On the other hand, the CFD simulation can be regarded as a powerful simulation program which can provide detailed airflow and thermal environment information for both indoor and outdoor. However, the impacts of solar radiations are not easy to calculate in CFD and several assumptions have to be made to solve this problem. The requirements of mesh sizes for heat transfer among construction layers, indoor airflow computational domain, and outdoor airflow computational domain are inconsistent. It is still computationally intensive to simulate the whole building for both indoor and outdoor with the natural ventilation although rapid progress in computing technology has been made in recent years. In addition, lacking proper boundary conditions reduces the accuracy of flow modeling using standalone indoor CFD simulations for natural ventilation. Currently, there is no suitable simulation tool to investigate the natural ventilation for both indoor thermal environment and building design.

Coupled simulations between BS and CFD can largely reduce computation cost and improve the resolution and accuracy of the results. BS can provide interior surface temperature and pressure (or velocity) conditions for openings as boundary conditions for indoor CFD simulation and CFD predicts indoor airflow more accurately to help building simulation to calculate indoor thermal comfort levels. Generally speaking, there are two coupling methods:

static coupling and dynamic coupling for thermal and CFD simulation. The dynamic coupling process involves coupling between the two programs at every time step and the iteration between BS and CFD reaches a converged solution at each time step. The dynamic coupling improves the accuracy of thermal simulation for mechanical ventilation. However, it is computationally expensive due to the many iteration steps required to reach convergence between two programs and the dynamic coupling method may not greatly improve the overall accuracy of building simulation for natural ventilation since indoor environment prediction in BS more depends on the outdoor conditions in each time step. In fact, the dynamic coupling approach may even result in instability in multi-zone airflow simulation. As static strategy requires less computation time and thermal environment for naturally ventilated residential buildings (heat source negligible) is mainly governed by climatic conditions, static strategy is chosen to be used to couple building simulation and indoor CFD simulation for accurate and fast prediction.

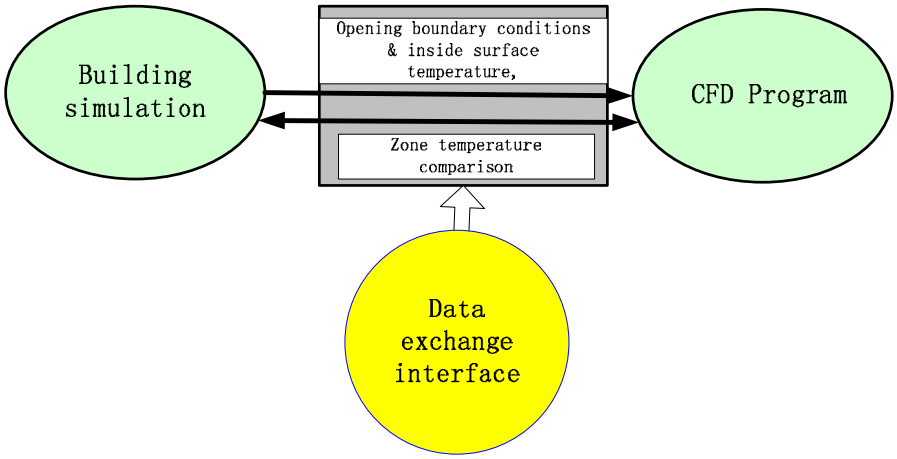

Figure 5.1 The coupling strategy between BS and CFD

Figure 5.1 shows the detailed coupling strategy between BS and CFD program. From building simulation, the inside surface temperatures for each wall are fed into indoor CFD simulation.

The detailed boundary conditions for the openings including velocity boundary conditions (or pressure boundary conditions), airflow direction, air temperature are provided for detailed indoor environment calculations. The predicted indoor average temperature by CFD simulation will be compared with zone temperature from building simulation results. A text-mode data exchange interface has been made to provide the convenient data passage between the two programs to minimize the modification to building simulation—ESP-r. Commercial software FLUENT is used as the external CFD program to couple with ESP-r. The data exchange interface has been programmed to automatically implement the data exchange between the two programs. The detailed thermal comfort prediction model for indoor environment is finally provided for evaluation in the data interface.

One of the important tasks for natural ventilation simulations is to accurately predict the indoor airflow (airflow contour, vector, and average velocity) which cannot be done by multi-zone simulation. The boundary conditions for indoor CFD simulation, obtained from building simulation results, are significant to determine the indoor airflow profile. There are two types of inlet conditions in CFD simulation for incompressible indoor airflow: pressure inlet condition and velocity inlet condition. The total pressure condition or velocity condition at openings are derived from the building simulation results.

The total pressure conditions for wind induced boundary nodes are fixed and calculated by using pressure coefficients in building simulation. The total pressure conditions in ESP-r for boundary nodes are defined as (ESRU, 2002)

$$P = Cp \times \frac{1}{2} \rho W S^2 - 9.81 \times \rho \times H \qquad (5.1)$$

$$\rho = 1.1881 \times 293.15/(273.15 + T) \qquad (5.2)$$

where P (Pa) is the total pressure of the boundary nodes (which includes stack pressure), ρ(m^2) is the outdoor air density estimated by Bussinesq approximation, which is accurate as long as actual density variation is small, WS is the wind speed at the reference height (roof height), and H (m) is the height of the boundary nodes.

If pressure-inlet boundary conditions are used, the opening with larger pressure value will be taken as pressure-inlet, the other opening with smaller value will be taken as pressure-outlet. If the internal opening is taken as inlet, the inlet direction is normal to the boundary. Otherwise, the wind direction will be taken as inlet direction for external openings. The internal opening as a component between two zones adopts the calculated average pressure value between the neighboring zones as the opening pressure value.

The velocity at the opening can be calculated directly from the following equation as in ESP-r:

$$V_{i,j} = \frac{\dot{m}_{i,j}}{\rho \cdot A} \qquad (5.3)$$

where $V_{i,j}$ (m/s) represents the component velocity from the i^{th} node to j^{th} node, $\dot{m}_{i,j}$ (kg/s) is the total mass flow rate between i^{th} node and j^{th} node, ρ (kg/m^3)is the air density from the zone where the air flows into, and A (m^2) is the component area.

If the velocity-inlet boundary conditions are used, the one with positive signal for i^{th} zone is taken as velocity inlet, the other one is taken as outflow. Similar to pressure boundary

conditions, if the internal opening is taken as velocity inlet, the inlet direction is normal to the boundary. Otherwise, the wind direction will be taken as inlet direction for external openings.

5.2 Coupling procedures

The static coupling strategy is adopted for wind-driven natural ventilation between ESP-r and FLUENT simulation and the internal surface temperature and opening boundary conditions obtained from BS are fed into CFD simulations. The coupling procedures compose of five main steps as shown in Figure 5.2.

The text-mode interface, comprising five categories, was programmed for automatically running the coupled simulations.

a) Model and climatic data preparation. Before carrying out coupling program, both building simulation model and CFD simulation model are required to be setup. Building simulation model comprises the geometric information, construction thermal properties, and airflow network for the whole building, while CFD simulation model needs only the information of the space to be simulated. The particular climatic file is required to be prepared, including the information of file location, intended simulation period, time interval etc.

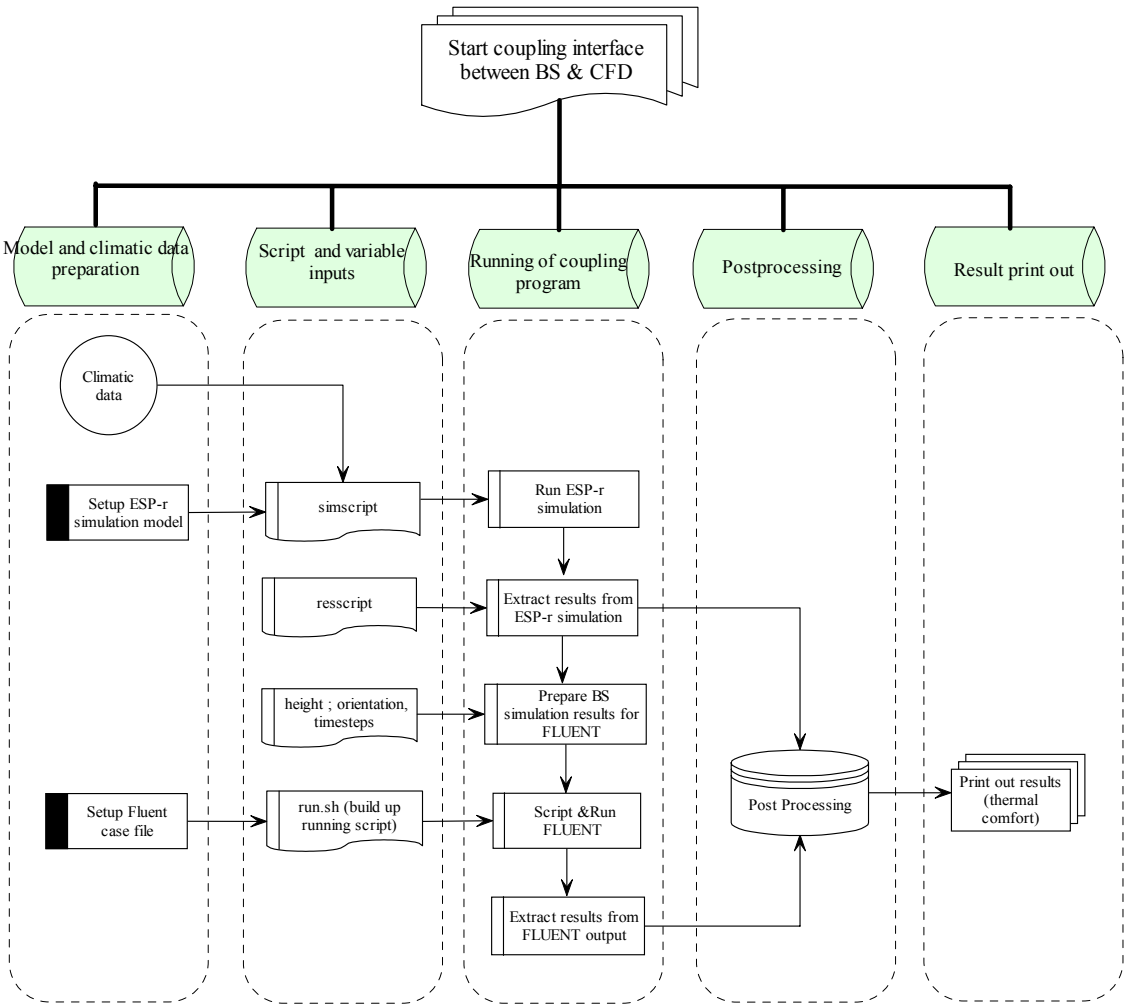

Figure 5.2 Coupling procedures between ESP-r and FLUENT for naturally ventilated residential buildings

b) Script and variable inputs. Two input files (simscript, resscript), a variable input data set of interested room information (height, orientation, simulation timesteps) and one script program (run.sh) are involved. 'simscript', serving as the input for running ESP-r, prepares the required information for running ESP-r including the location of configuration file, the climatic data file, particular files for simulation results, simulation periods, simulation interval. 'resscript' is used as the input for extracting required parameter results from simulation results to extract zone temperature, mean radiant temperature, surface temperature, total pressure of openings, outdoor ambient temperature, wind speed, wind direction, etc. The

script ‘run.sh’ is to generate FLUENT running script for each time interval. All the boundary conditions related to building simulation results are to be automatically input into FLUENT for time series cases. The pressure conditions for openings are compared, the opening with large pressure boundary condition is set to be inlet and the one with small pressure is set to be outlet. The required results from CFD are also prepared to be extracted.

c) Running of coupling program. The running of coupling program is the core of the coupling interface, which invokes all the five categories in sequences. The first step is to run ESP-r simulation according to the required configuration file, simulation period, and climatic file recorded in ‘simscript’ input file and to generate simulation results. The second step is to save the required parameters for each individual file from simulation results. The third step is to prepare results for FLUENT. The program (‘code’) is used to open each required parameter result file obtained from BS, and extract the useful information to organize the idealized input file for the execution of FLUENT. The ‘code’ includes characteristics of the particular calculation unit, such as height of the unit, facing orientation. In order to solely consider the wind pressure, the effects of stack pressure are removed in the results preparation. The temperature unit is converted from ℃ to K. Wind incident angles are indicated by x and y components. In the forth step, the script file (‘script’) with the aids of ‘run.sh’ is generated for running FLUENT. After running FLUENT, an output file is to be generated for averaged indoor temperature and averaged indoor air velocity.

d) Post-processing. The program (environment) is used to summarize the useful results from coupled simulation such as temperature, velocity, relative humidity and mean radiant temperature, etc.

e) Result printout. Thermal comfort data and statistic analyzing results, for example, satisfactory thermal comfort percentage, are printed out.

Coupled simulations can be done automatically using the program interface. In the following section, coupled simulation results are to be further validated with full CFD simulations and field measurement studies. For each indoor CFD simulation within coupled simulations, non-slip wall boundary conditions, pressure inlet and pressure outlet boundary conditions, standard $k-\varepsilon$ model with wall function and SIMPLE algorithm are adopted. If the internal opening is taken as inlet, the inlet direction is normal to the boundary. Otherwise, the wind direction will be taken as inlet direction for external openings. 10^{-6} for energy equation and 10^{-4} for momentum, $k-\varepsilon$ equations are the criteria for convergence. Mesh independence is checked by running FLUENT with finer mesh for each case and no significant differences were found.

5.3 Coupling strategy comparison and validation with full CFD simulation

Both single zone scenarios and multi-zone scenarios by using coupling programs have been tested and verified with full CFD simulations in this section. The prominent advantages with coupled simulations are to largely reduce computing cost comparing with full CFD simulation

and provide detailed indoor thermal profile comparing with BS. For each scenario, two cases, perpendicular wind with wind direction 0°(N) and angular wind with wind direction 45°(NE), are selected for modeling. The modeling times are 2nd Jan 18:30 and 1st Jan 12:30 in the year 2001 to represent different climate conditions. The climatic conditions for the two cases are extracted from the Singapore weather file are summarized in Table 5.1.

Table 5.1 Climatic data

Time	Wind Direction (0°N; 90°E)	Wind Speed (m/s)	Temperature (℃)	Relative Humidity
Case 1: 2nd Jan 18:30	0	1.7	25	92
Case 2: 1ST Jan 12:30	45	5.8	29	76

5.3.1 Single zone scenarios

A single zone room with two opposite windows on both north and south facing walls is used in this validation study. Generally speaking, the geometric layout is used to represent typical room layout of residential buildings. Normally, there are two openings in the room: one opening on the external wall (façade) and another opposite opening (window or door) connected with another room (zone). For the single zone studies, both of the openings are on the opposite external walls and two single zone scenarios vary in the location of the openings.

5.3.1.1 Scenario 1

The dimension of the room is 3mx5mx3m (LxWxH), with direct opposite openings 2mx1m (WxH), shown in Figure 5.3. Indoor CFD simulation and ESP-r building simulation are processed with this single zone. The full CFD computation domain is shown in Figure 5.4 and 5.5. Both indoor and outdoor airflows are calculated simultaneously. The velocity-inlet

boundary condition for full CFD simulation uses the 1/4 shear flow profile to model the atmospheric boundary layer. Pressure-outlet boundary condition is adopted for the full CFD simulation domain.

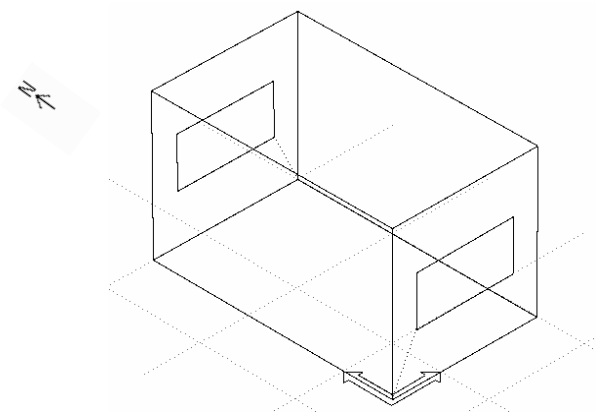

Figure 5.3 A single zone room with two opposite window layout (scenario 1)

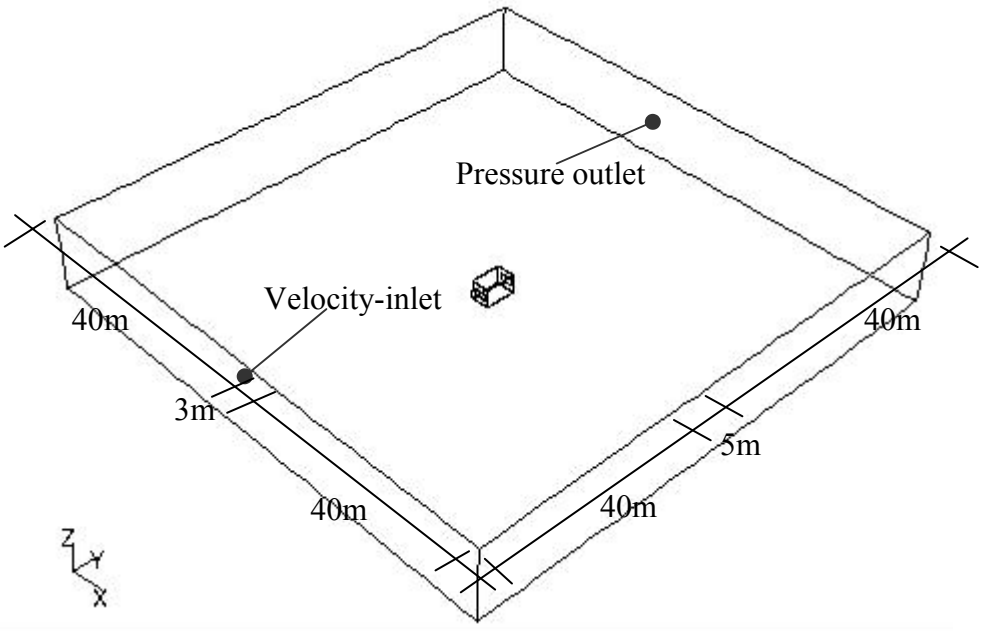

Figure 5.4 Full CFD simulation domain for case 1(North wind direction)

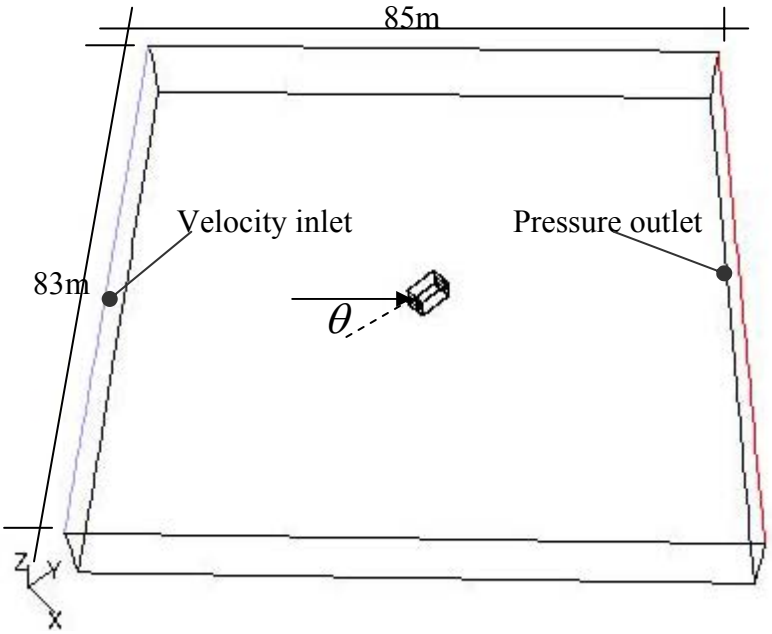

Figure 5.5 Full CFD simulation domain for case 2(θ indicates wind direction)

Three nodes (north, south, and room) are used in the building simulation ESP-r. North and South are the names of wind-induced boundary nodes representing outdoor nodes in north direction and south direction respectively. Room represents the node for the single zone. The ESP-r calculation results (velocity or pressure) are used as boundary conditions for indoor air CFD simulation. The drawback of this process for indoor air CFD simulation is to take the inlet boundary conditions as uniform values to represent the averaged value for boundary conditions. The area weighted velocity magnitude results at the height of 1.5 m (Table 5.2) are compared among full CFD simulation, ESP-r with indoor CFD simulation (velocity boundary conditions), ESP-r with indoor CFD simulation (pressure boundary conditions) and ESP-r simulation only. MFE (mean fractional error), defined in equation (5.4), is used to evaluate different coupling methods. Values of the mean factional error that are equal to 0.67 are equivalent to under/over prediction by a factor of 2. MFE for coupled simulation results and ESP-r results compared with full CFD simulation results are listed in Table 5.2.

$$MFE = 2 \times \frac{|V_P - V_C|}{V_P + V_C} \quad (5.4)$$

The contours and vectors of the airflow at 1.5m above the floor are shown in Figure 5.6 and Figure 5.7 for case 1 (North wind direction) and in Figure 5.9 and Figure 5.10 for case 2 (North East wind direction) at 1.5m above the floor. Figure 5.8 and Figure 5.11 show both outdoor and indoor airflow contours and vectors for case 1 and case 2 at 1.5m above the floor. From the contours and vectors comparison results, it is clear that with proper coupling between building simulation program and CFD program, indoor airflow profile can be accurately predicted for natural ventilation. As can be seen from Figures 5.6, 5.7, 5.9, 5.10, the major difference among three different scenarios (full CFD simulation, ESP-r with velocity inlet CFD simulation, and ESP-r with pressure inlet CFD simulation) appear at the inlet boundary conditions.

The detailed area weighted velocity magnitude results are compared along the height of the room (Figure 5.12) and the length of the room (Figure 5.13) for two cases. The comparison results suggest that indoor CFD simulations using pressure-inlet boundary conditions give better predictions than using velocity-inlet boundary conditions.

By comparing the computing efforts between full CFD simulation (above 12hrs with parallel workstations) and indoor CFD simulation (less than 1 hour with a single computer), the coupling program is more practical to evaluate the detailed thermal comfort level for indoor environment and facade designs in the various planning stages for naturally ventilated buildings.

Case 1 2nd Jan 18:30 (N wind direction)

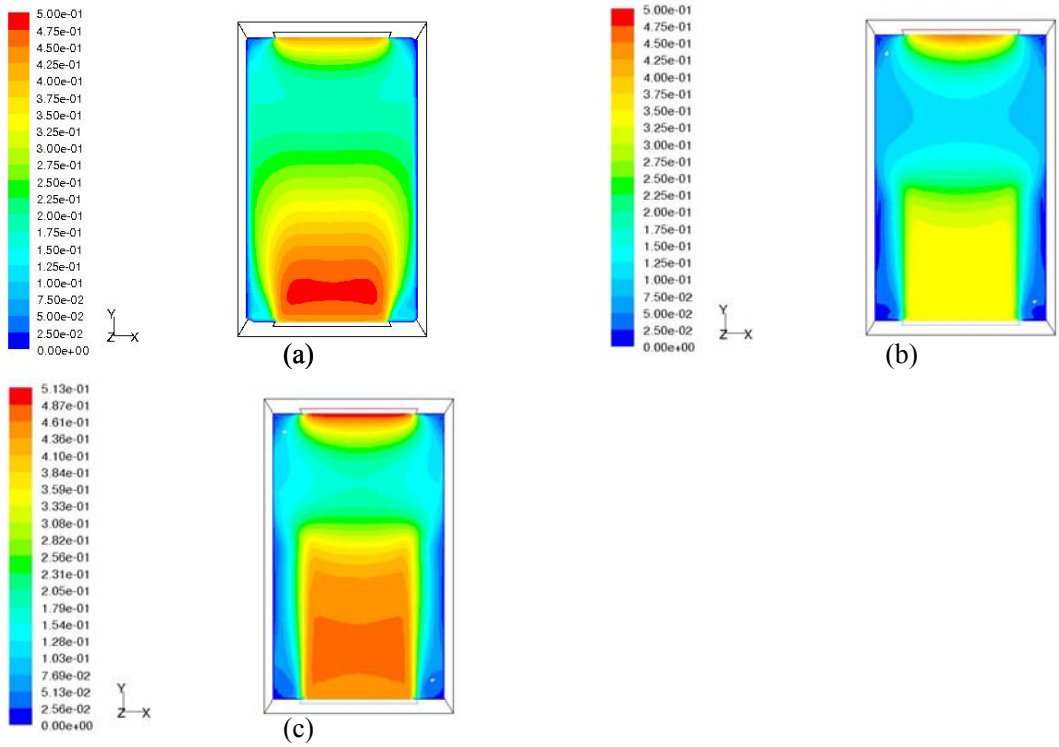

Figure 5.6 Contour of velocity magnitude (m/s) (a) full CFD simulation (b) indoor CFD velocity with velocity boundary conditions (c) indoor CFD simulation with pressure boundary conditions

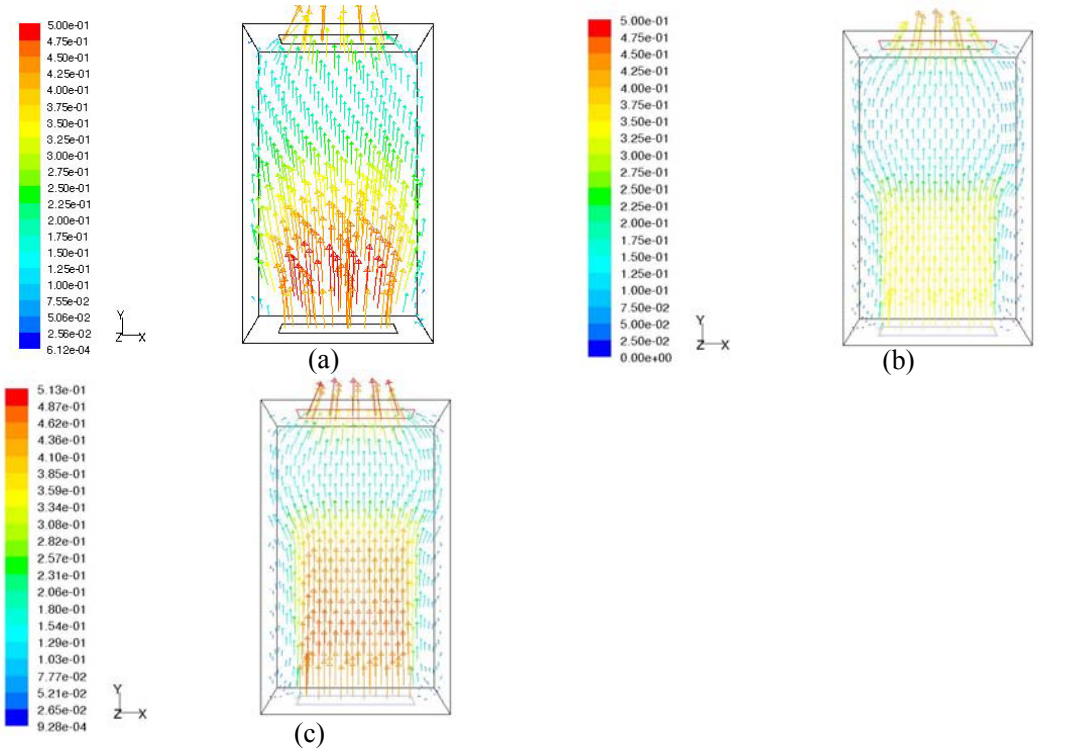

Figure 5.7 Velocity vector contour colored by velocity magnitude (m/s) (a) full CFD simulation (b) indoor CFD velocity with velocity boundary conditions (c) indoor CFD simulation with pressure boundary conditions

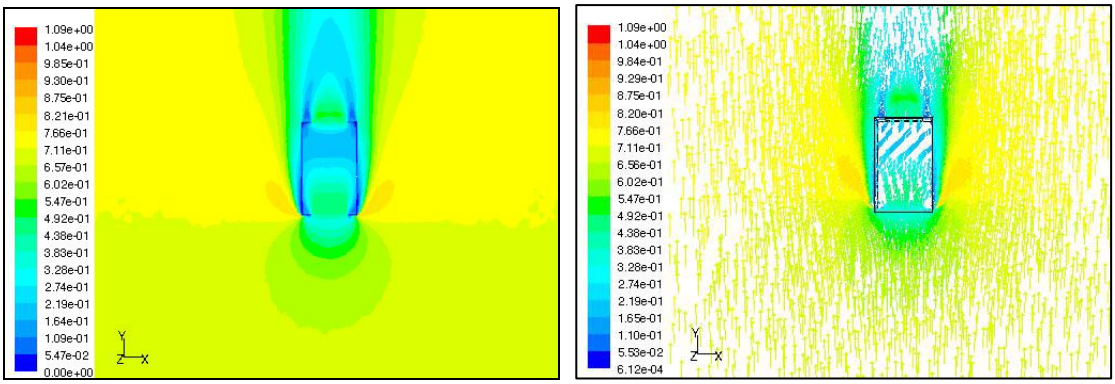

(a) (b)

Figure 5.8 Full CFD simulation (a) velocity contour (b) velocity vector

Case 2 1st Jan 12:30 (NE wind direction)

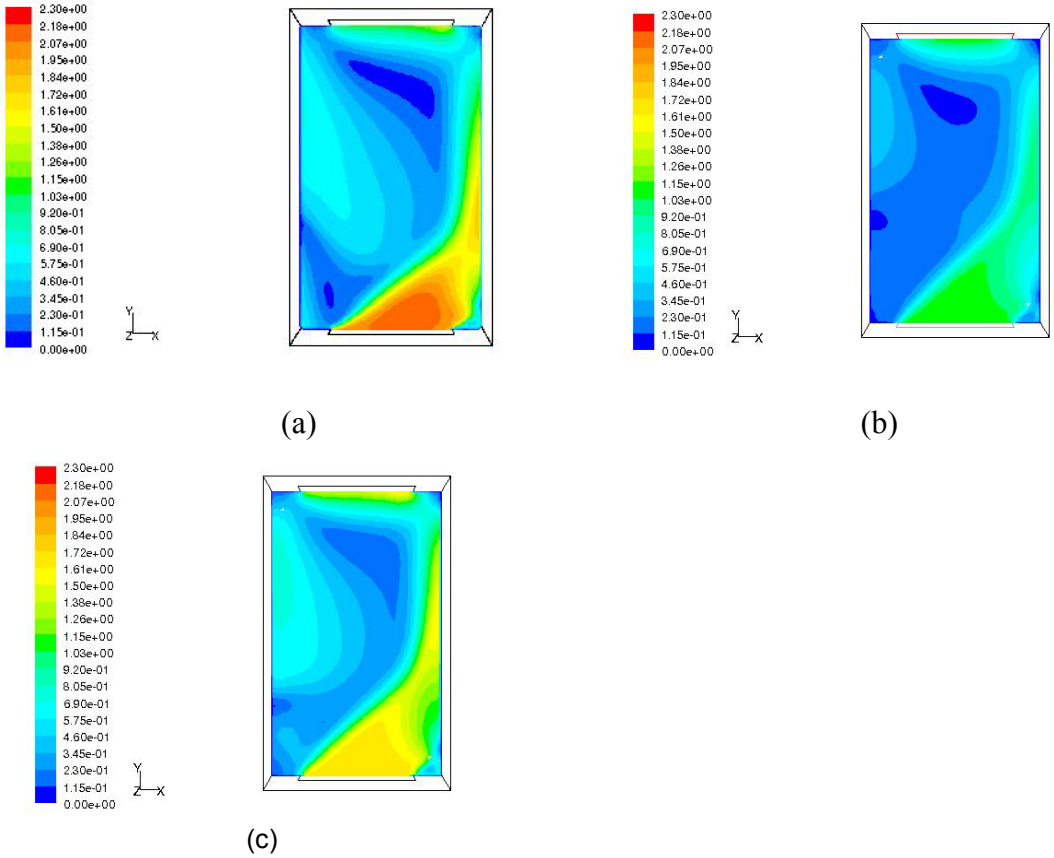

(a) (b)

(c)

Figure 5.9 Contour of velocity magnitude (m/s) (a) full CFD simulation (b) indoor CFD velocity with velocity boundary conditions (c) indoor CFD simulation with pressure boundary conditions

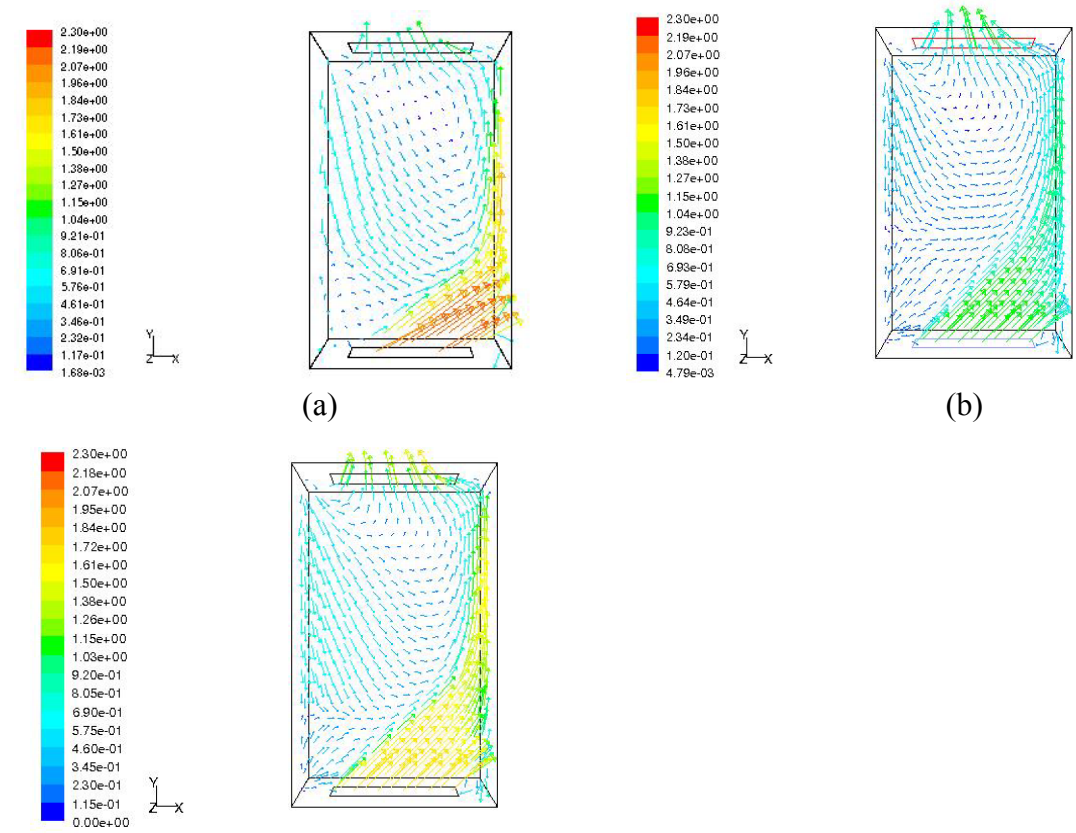

Figure 5.10 Velocity vector contour colored by velocity magnitude (m/s) (a) full CFD simulation (b) indoor CFD velocity with velocity boundary conditions (c) indoor CFD simulation with pressure boundary conditions

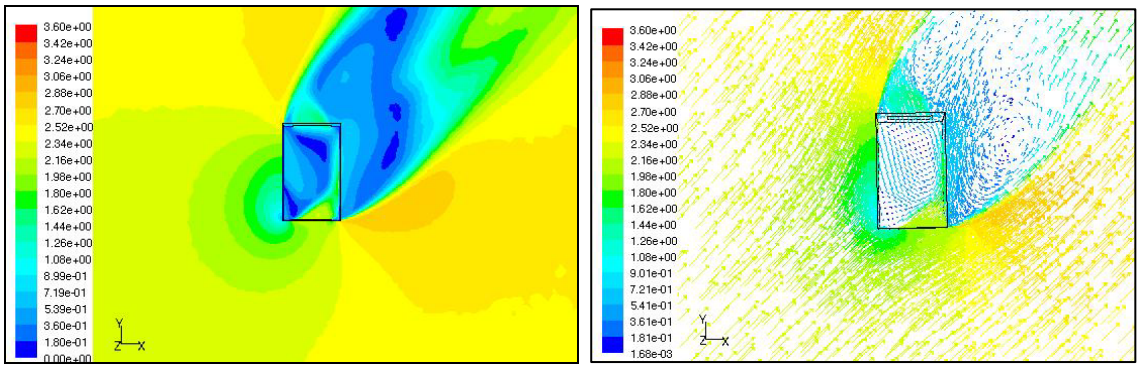

Figure 5.11 Full CFD simulation (a) velocity contour (b) velocity vector

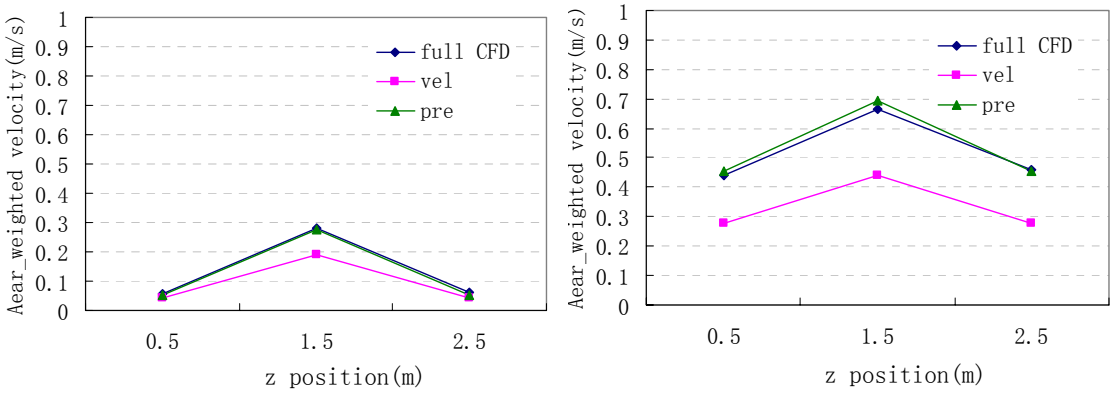

(a) case 1 (b) case 2

Figure 5.12 Area_weighted velocity results comparison along height (z) direction among full CFD simulation, indoor CFD simulation with velocity inlet condition and indoor CFD simulation with pressure inlet condition (a) case 1 (b) case 2

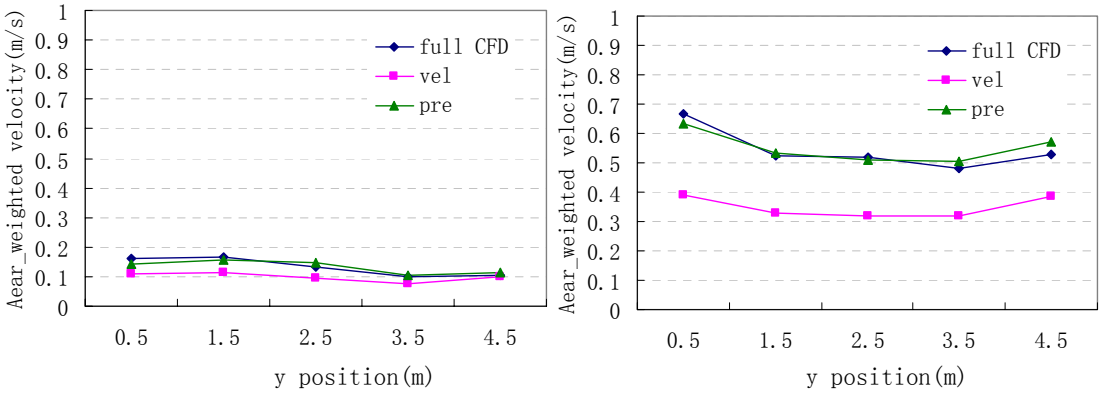

(a) case 1 (b) case 2

Figure 5.13 Area_weighted velocity results comparison along length (y) direction among full CFD simulation, indoor CFD simulation with velocity inlet condition and indoor CFD simulation with pressure inlet condition (a) case 1 (b) case 2

Table 5.2 Result comparison for scenario 1

Area Weighted room velocity (1.5m Height)	Full CFD simulation (m/s)	Indoor CFD with velocity inlet (m/s)	Indoor CFD with pressure inlet (m/s)	ESP-r (m/s)
Case 1: 2nd Jan 18:30	0.28	0.19	0.28	0.09
MFE		38%	0%	103%
Case 2: 1ST Jan 12:30	0.67	0.44	0.70	0.27
MFE		41%	4%	85%

5.3.1.2 Scenario 2

The dimension of the room is 3mx5mx3m (LxWxH), with two opposite openings: north window 2mx1m (WxH) and south door 0.8mx2.1m (WxH), shown in Figure 5.14. The opening locations and dimensions in scenario 2 are different with those in scenario 1. Coupled simulations between FLUENT and ESP-r are performed for this single zone scenario. Similar to scenario 1, the velocity-inlet boundary condition uses the atmosphere boundary profile (1/4 power-law shear flow) for inlet boundary condition and pressure-outlet boundary condition is adopted for the full CFD simulation domain. The two cases same as in scenario 1 (with wind direction 0°(N)and wind direction 45°(NE), which represent the perpendicular wind and angular wind respectively) were used for validation. The climatic conditions for the two cases are listed in Table 5.1.

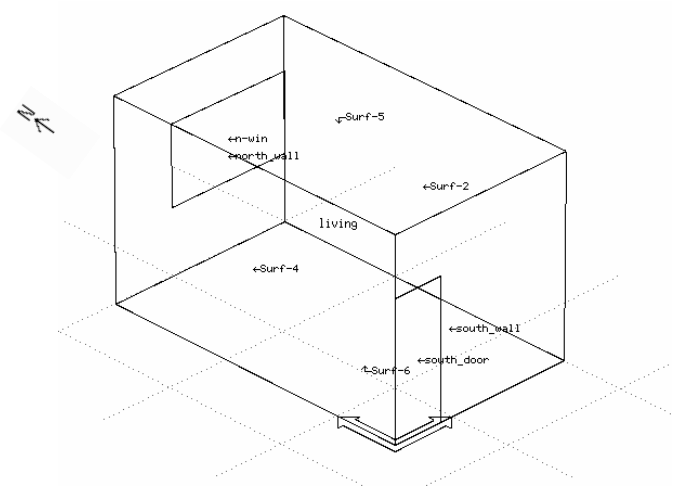

Figure 5.14 A single zone room layout (scenario 2)

The naming conventions of nodes in scenario 2 are the same as those used in scenario 1. The area weighted velocity magnitude results at the height of 1.5 m (Table 5.3) are compared among full CFD simulation, ESP-r with indoor CFD simulation (velocity boundary conditions), ESP-r with indoor CFD simulation (pressure boundary conditions) and ESP-r

simulation only. MFE for coupled simulation results and ESP-r results compared with full CFD simulation results are listed in Table 5.3. The comparing contours and vectors of the velocity magnitude are shown in Figure 5.15 and Figure 5.16 for case 1 (north wind direction) and in Figure 5.18 and Figure 5.19 for case 2 (northeast wind direction). Figure 5.17 and Figure 5.20 indicate both outdoor and indoor airflow contours and vectors of case 1 and case 2 for scenario 2. All the contour and vector profiles are taken at 1.5m above the floor. It can be seen from the results that the non-uniform boundary conditions (values and directions) can be one of major factors to result in discrepancies among full CFD velocity profiles and coupled simulation profiles for natural ventilation. The detailed area weighted velocity magnitude results are compared in Figure 5.21 along height of the room and Figure 5.22 along length of the room for two cases. The comparison results show that indoor CFD simulation taking pressure as boundary conditions (MEF_{MAX}=26%)give better predictions than taking velocity as boundary conditions (MEF_{MAX}=88%) and the estimated airflow velocities using building simulation program are much lower than indoor airflow velocities predicted using the coupled simulations and the full CFD simulations.

Case 1 2nd Jan 18:30 (N wind direction)

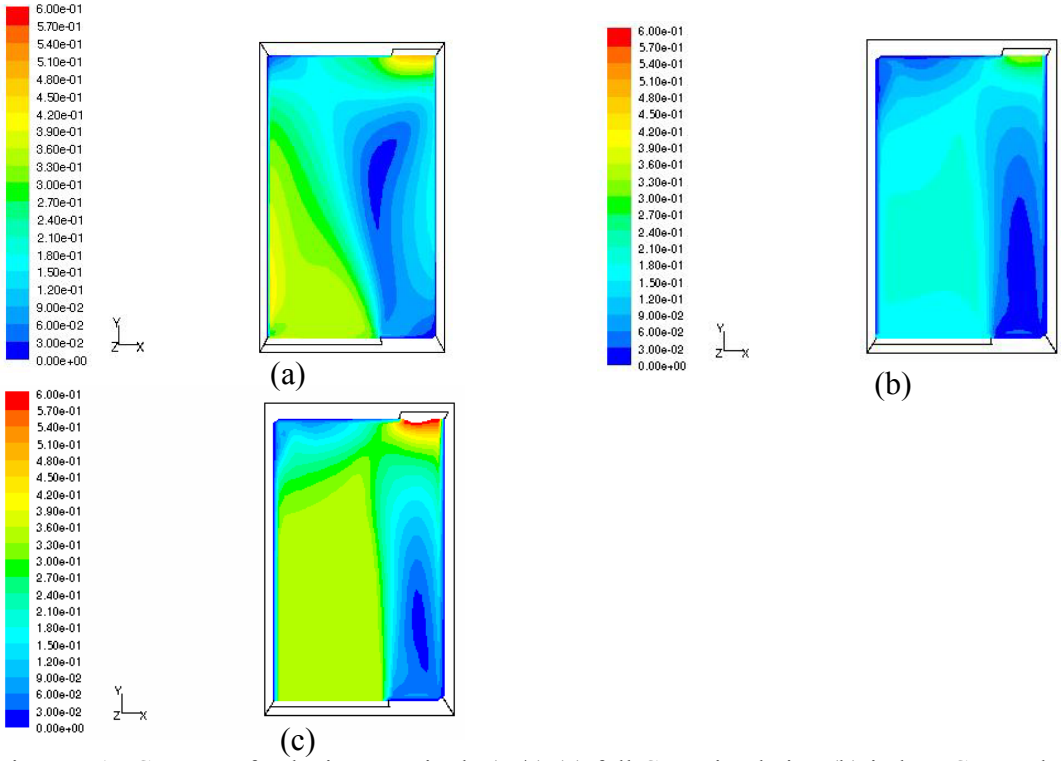

Figure 5.15 Contour of velocity magnitude (m/s) (a) full CFD simulation (b) indoor CFD velocity with velocity boundary conditions (c) indoor CFD simulation with pressure boundary conditions

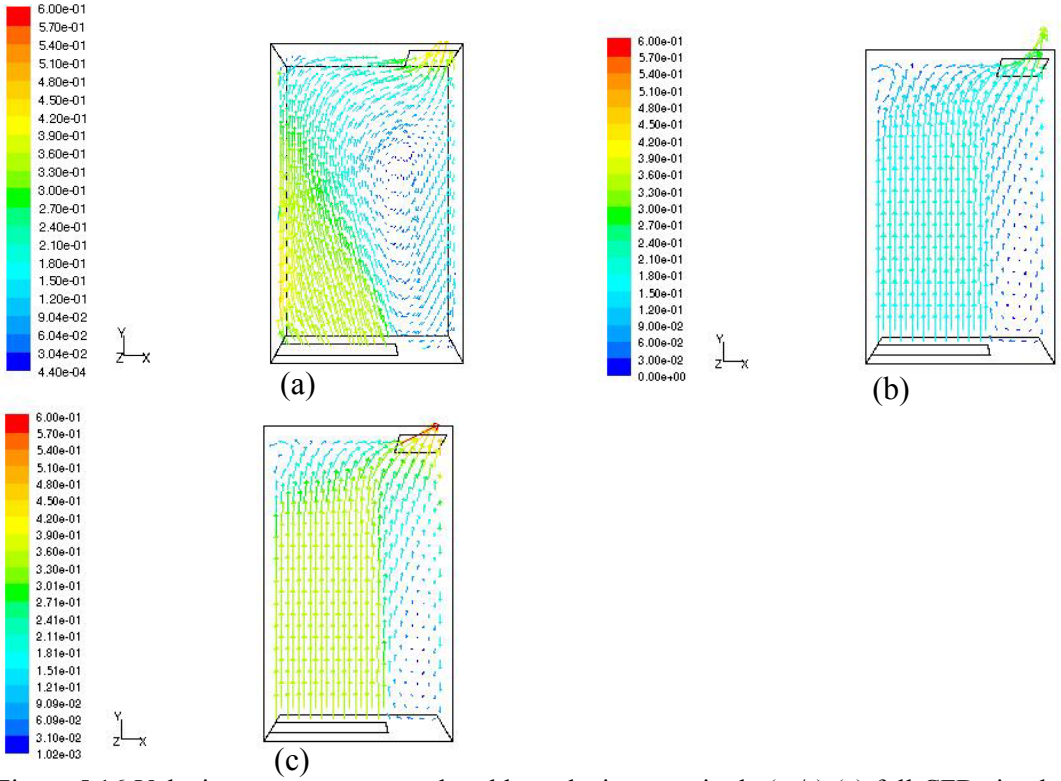

Figure 5.16 Velocity vector contour colored by velocity magnitude (m/s) (a) full CFD simulation (b) indoor CFD velocity with velocity boundary conditions (c) indoor CFD simulation with pressure boundary conditions

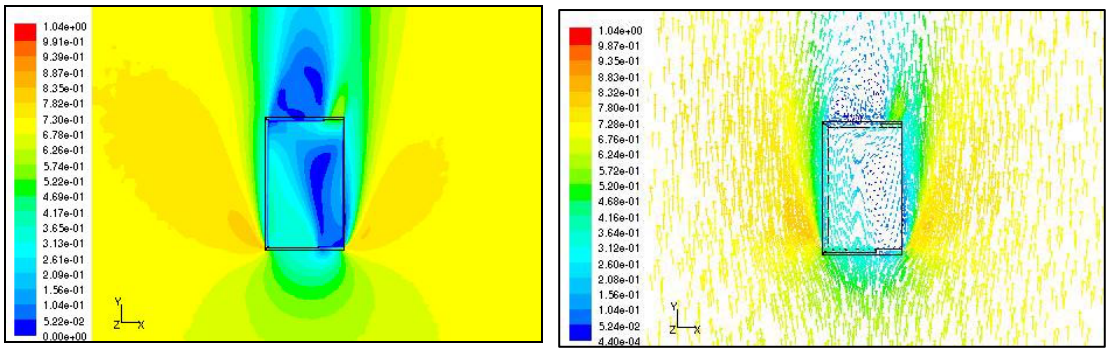

(a) (b)

Figure 5.17 Full CFD simulation (a) velocity contour (b) velocity vector

Case 2 1st Jan 12:30 (NE wind direction)

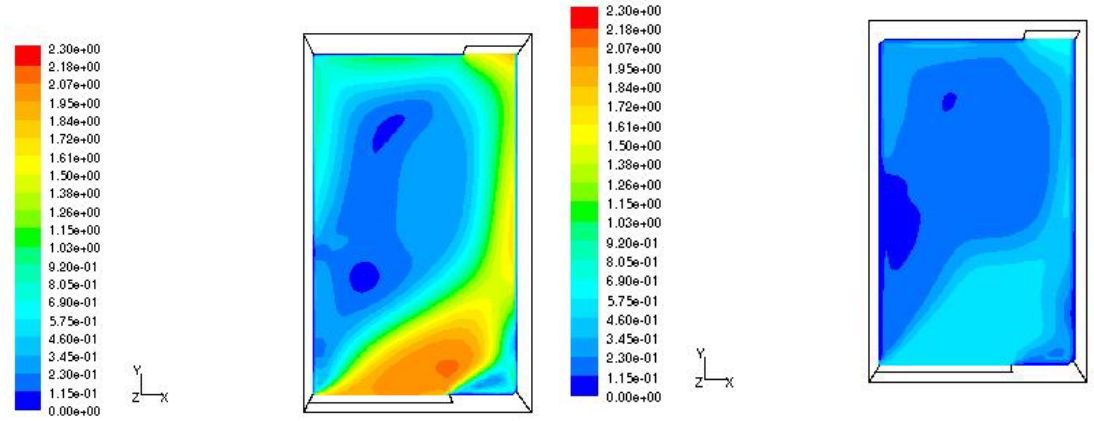

(a) (b)

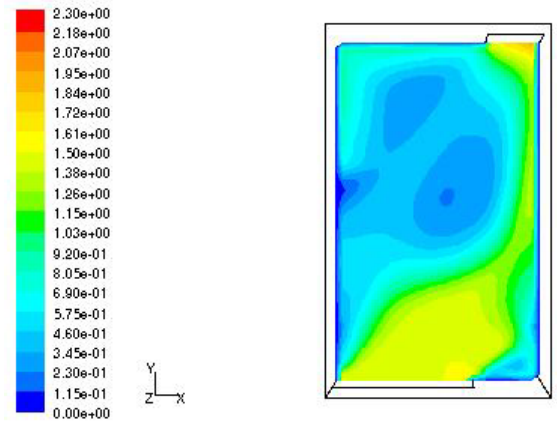

(c)

Figure 5.18 Contour of velocity magnitude (m/s) (a) full CFD simulation (b) indoor CFD velocity with velocity boundary conditions (c) indoor CFD simulation with pressure boundary conditions

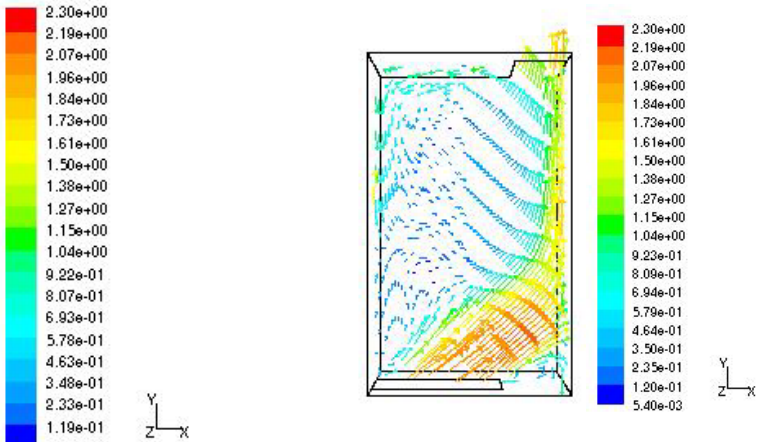

(a) (b)

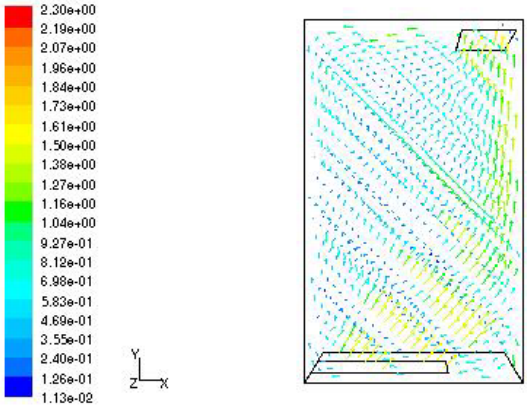

(c)

Figure 5.19 Velocity vector contour colored by velocity magnitude (m/s) (a) full CFD simulation (b) indoor CFD velocity with velocity boundary conditions (c) indoor CFD simulation with pressure boundary conditions

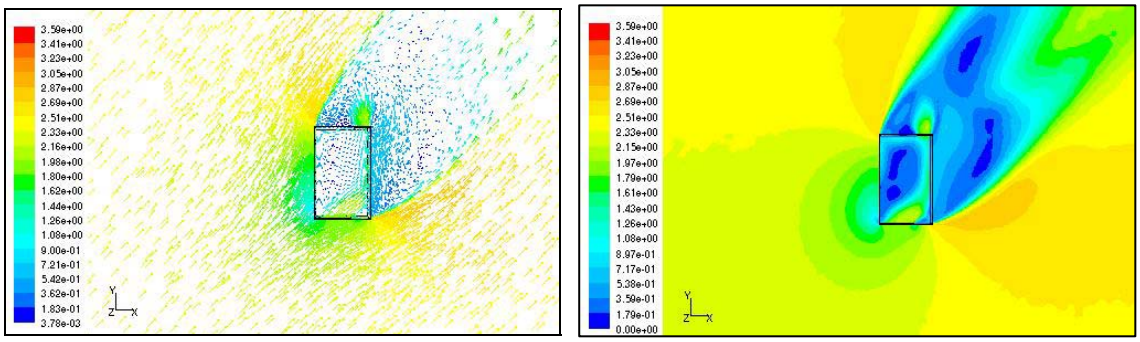

(a) (b)

Figure 5.20 Full CFD simulation (a) velocity contour (b) velocity vector

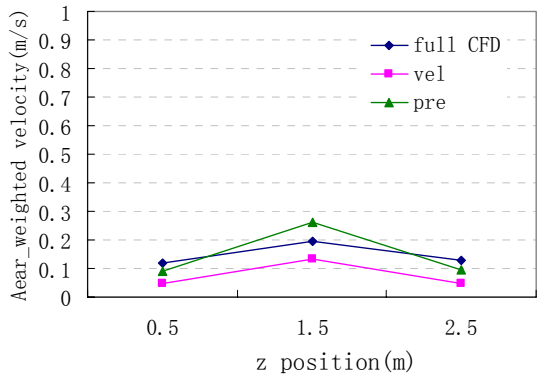

(a) case 1

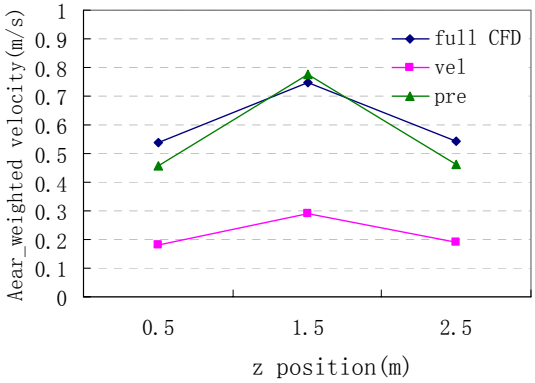

(b) case2

Figure 5.21 Area_weighted velocity results comparison along height (z) direction among full CFD simulation, indoor CFD simulation with velocity inlet condition and indoor CFD simulation with pressure outlet condition (a) case 1 (b) case 2

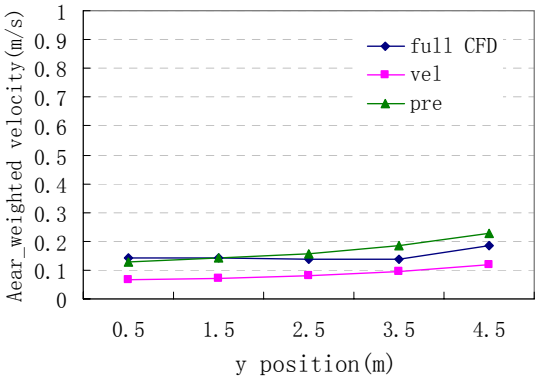

(a) case 1

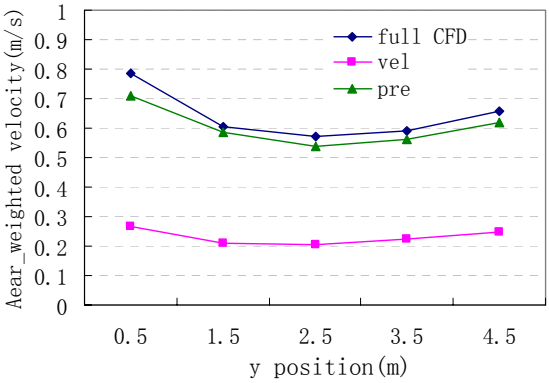

(b) case 2

Figure 5.22 Area_weighted velocity results comparison along length (y) direction among full CFD simulation, indoor CFD simulation with velocity inlet condition and indoor CFD simulation with pressure outlet condition (a) case 1 (b) case 2

Table 5.3 Result comparison for scenario 2

Area Weighted room velocity (1.5m Height)	Full CFD simulation (m/s)	Indoor CFD with velocity inlet (m/s)	Indoor CFD with pressure inlet (m/s)	ESP-r (m/s)
Case 1: 2nd Jan 18:30	0.20	0.13	0.26	0.04
MFE		42%	26%	133%
Case 2: 1ST Jan 12:30	0.75	0.29	0.78	0.12
MFE		88%	4%	144%

5.3.2 Multi-zone scenarios

Multi-zone scenarios are more complicated than single zone scenarios since one of the openings in a zone as an outlet (inlet) is the inlet (outlet) in another zone. Boundary conditions for this internal opening are significant and difficult to predict. Since the comparison results of single zone scenarios show that taking pressure as opening boundary conditions is more accurate than taking velocity as opening boundary conditions, only pressure boundary conditions are taken into consideration in multi-zone scenarios. The pressure boundary conditions for internal openings are further divided into three types, which are tested and compared between the coupled simulation results and the full CFD simulation results. These three types of internal pressure conditions are determined as follows: taking neighboring node pressure as boundary condition (*pre*), taking the average value of two connected node pressures (*pre-ave*) as boundary condition and simulating the multi-zones as a whole taking internal openings as internal condition for indoor CFD (*pre-room*). Two multi-zone scenarios are investigated and validated below.

5.3.2.1 Scenario 3

Scenario 3 is a three-zone naturally ventilated room including zone 1: north living, zone 2: south kitchen and zone 3: block. The dimension of each zone is 3mx5mx3m (LxWxH). In the aspect of airflow paths, north living zone and south kitchen are connected by an internal door and the block zone is not connected with other zones. The layout of the multi-zone case is shown in Figure 5.23. Coupled ESP-r and FLUENT simulations are processed within two connected zones or a particular zone. The full CFD computations for both indoor and outdoor

airflow simulation are also performed for validation of coupled simulations. The velocity inlet boundary condition for full CFD simulation uses the 1/4 shear flow profile to model the atmospheric boundary layer. Pressure-outlet boundary condition is used for the full CFD simulation domain. The wind direction setup of the two cases are the same as scenario 1, with wind direction 0°(N)and wind direction 45°(NE).The climatic conditions for the two cases are listed in Table 5.1.

The airflow network in scenario 3 comprises four nodes (north, south, and living and kitchen) in the building simulation ESP-r. North and South are the names of the wind-induced boundary nodes representing outdoor node in north direction and south direction respectively. The nodes, living and kitchen, indicate the windward zone and connected passive zone, respectively.

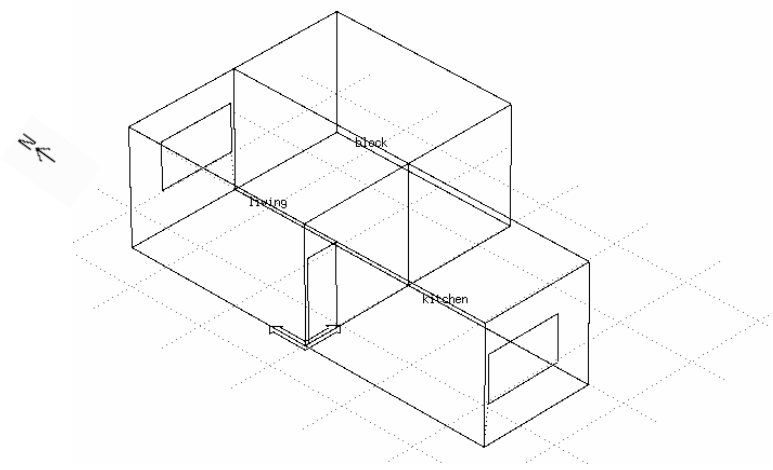

Figure 5.23 A three-zone room with two opposite windows layout (Scenario 3)

The ESP-r simulation results provide boundary conditions for indoor CFD simulation. The area weighted velocity magnitude results at the height of 1.5 m (Table 5.4 for windward zone and Table 5.5 for connected passive zone) are compared among full CFD simulation, coupled

ESP-r and indoor CFD simulation in a particular zone (*pre, pre-ave, pre-room*), ESP-r simulation only. MFE for coupled simulation results and ESP-r results compared with full CFD simulation results are listed in Tables 5.4 and 5.5. The comparing contours and vectors of the velocity magnitude are shown in Figure 5.24 and Figure 5.25 (for living zone); Figure 5.26 and Figure 5.27 (kitchen zone) for case 1 with North wind direction and in Figure 5.29 and Figure 5.30 (living zone); Figure 5.31 and Figure 5.32(kitchen zone) for case 2 with North East wind direction. Figure 5.28 and Figure 5.33 show both outdoor and indoor airflow contours and vectors for case 1 and case 2. All the contour and vector profiles for scenario3 are taken at 1.5m level above the floor.

The detailed area weighted velocity magnitude results for case 1 and case 2 are compared in Figure 5.34, and 5.35 and Figure 5.36, and 5.37 along height and length for living zone and kitchen zone respectively. It can be seen from comparison results that with proper coupling between the building simulation and CFD program with *pre-ave* and *pre-room* methods, the indoor airflow profile can be well predicted for natural ventilation. The results show that coupling program results are consistent with the full CFD simulation results. The coupling program could better predict the average velocity in the room than using building simulation program alone. However, the coupling program may not be able to accurately predict the velocity profile near the inlet. The *pre* method shows the largest errors between full CFD and coupled simulations. The indoor airflow prediction for the windward zone by using coupling program is more accurate than that for the connected passive zone.

Case 1 2nd Jan 18:30 (N wind direction)

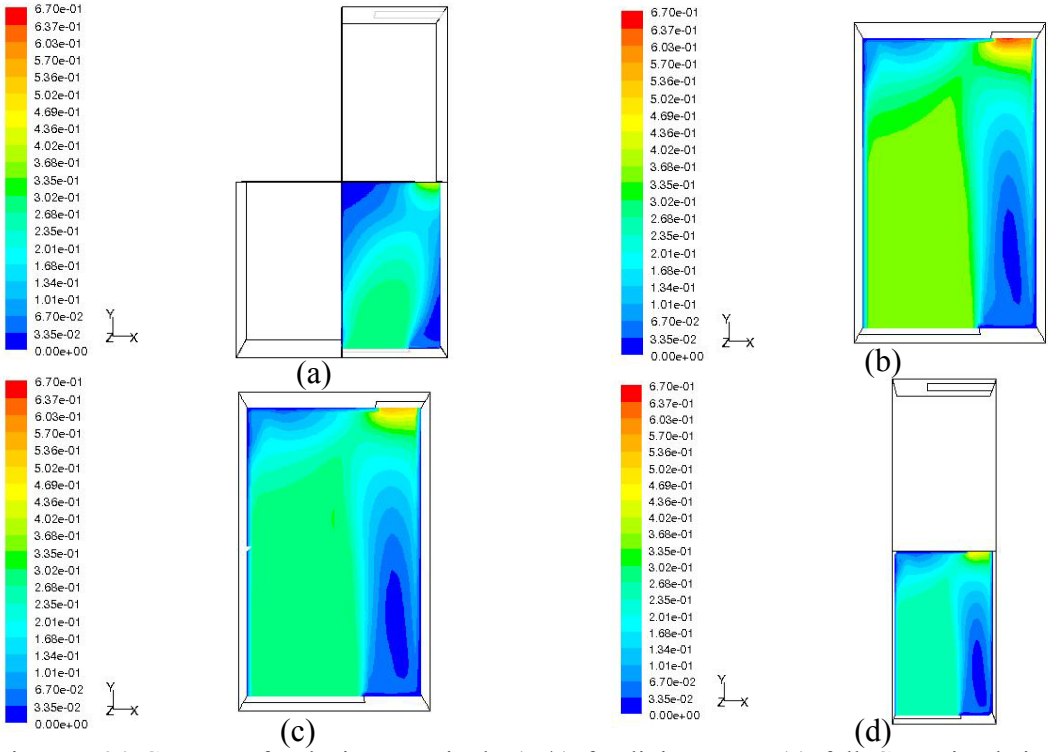

Figure 5.24 Contour of velocity magnitude (m/s) for living room (a) full CFD simulation (b) indoor CFD simulation with pressure boundary conditions (c) indoor CFD simulation with average pressure boundary conditions (d) indoor CFD simulation for multi-zones

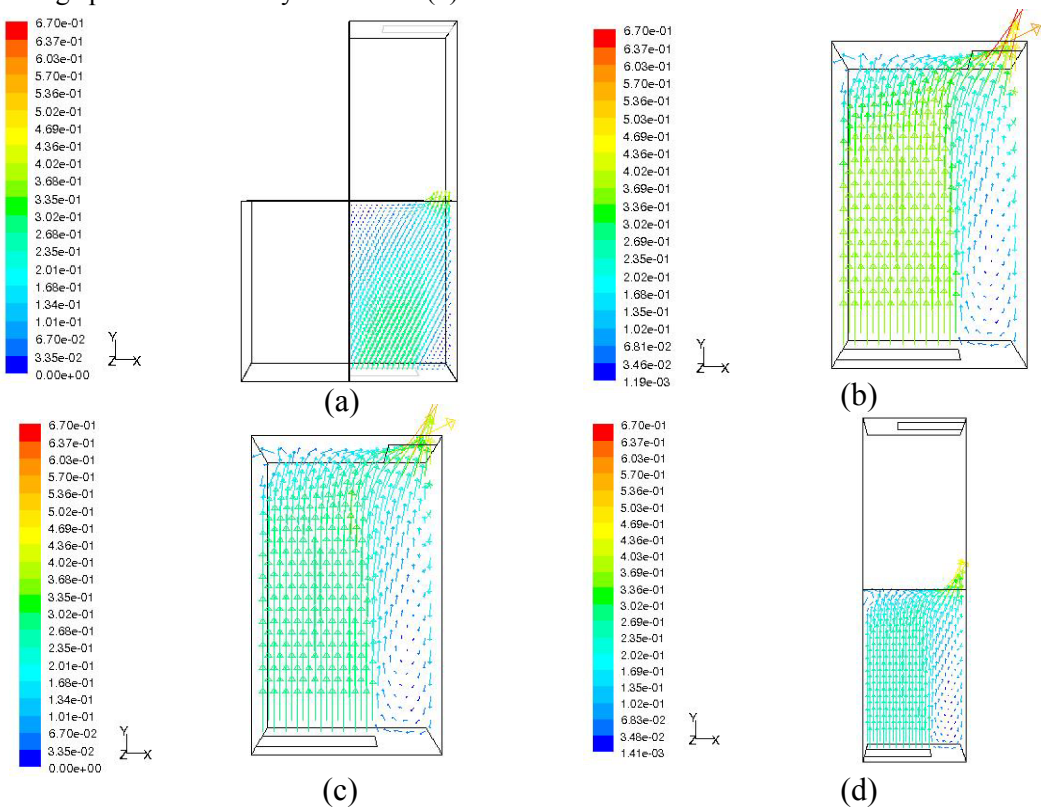

Figure 5.25 Velocity vector contour colored by velocity magnitude (m/s) for living room (a) full CFD simulation (b) indoor CFD simulation with pressure boundary conditions (c) indoor CFD simulation with average pressure boundary conditions (d) indoor CFD simulation for multi-zones

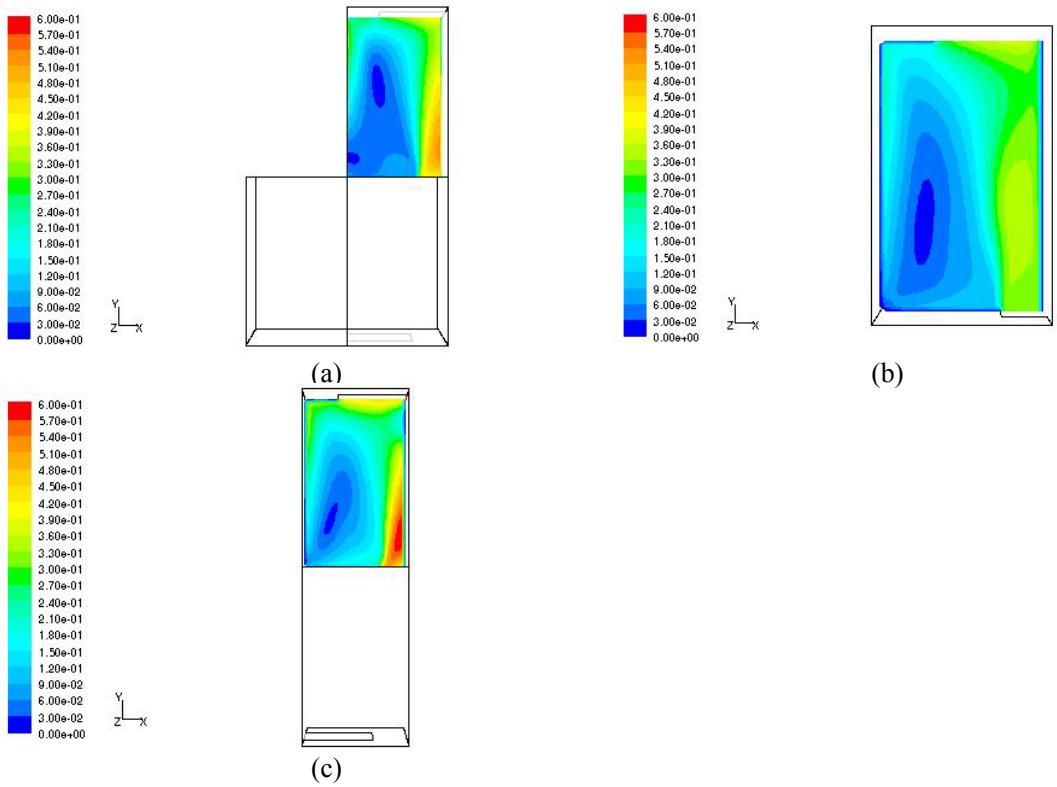

Figure 5.26 Velocity contour colored by velocity magnitude (m/s) for kitchen room (connected zone) (a) full CFD simulation (b) indoor CFD simulation with average pressure boundary conditions (c) indoor CFD simulation for multi-zones

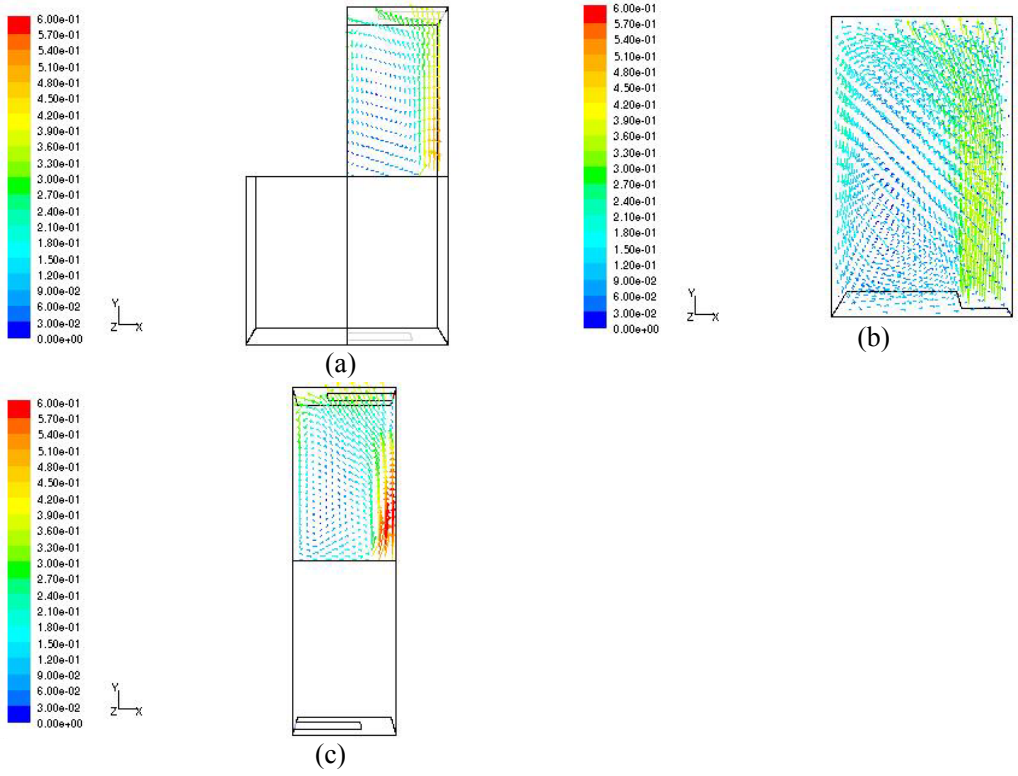

Figure 5.27 Velocity contour colored by velocity magnitude (m/s) for kitchen room (connected zone) (a) full CFD simulation (b) indoor CFD simulation with average pressure boundary conditions (c) indoor CFD simulation for multi-zones

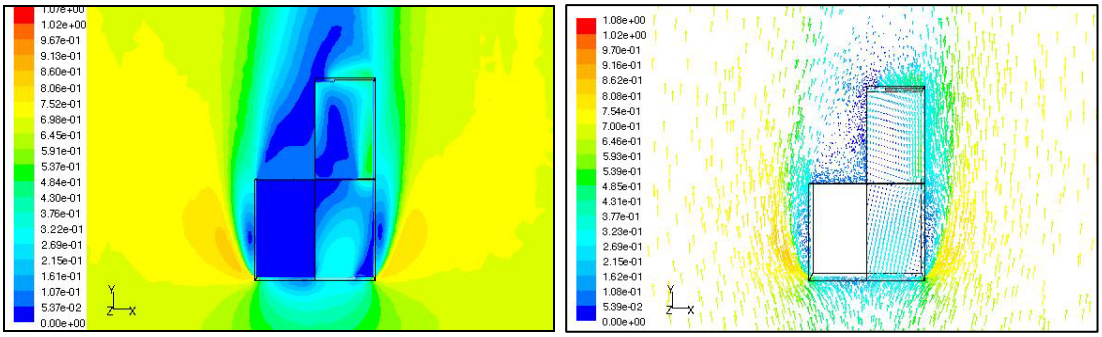

(a) (b)

Figure 5.28 Full CFD simulation (a) velocity contour (b) velocity vector

Case 2 1st Jan 12:30 (NE wind direction)

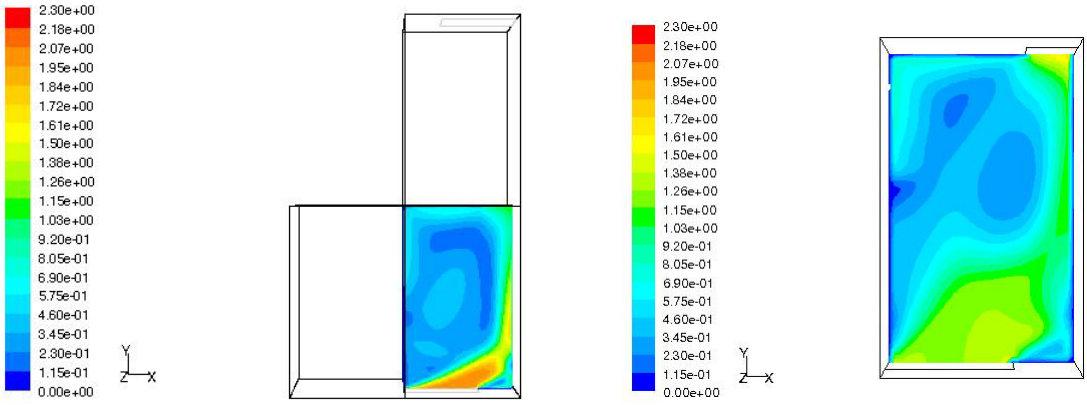

(a) (b)

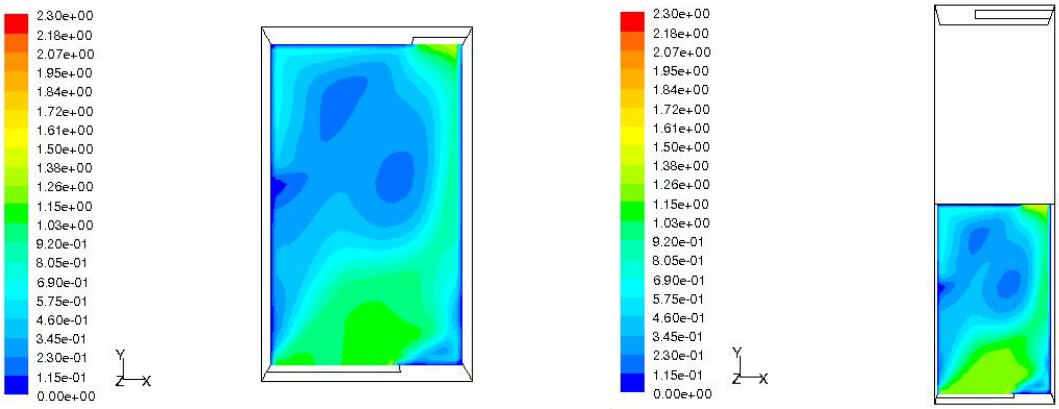

Table 0.┌ ©(d)

Figure 5.29 Contour of velocity magnitude (m/s) for living room (a) full CFD simulation (b) indoor CFD simulation with pressure boundary conditions (c) indoor CFD simulation with average pressure boundary conditions (d) indoor CFD simulation for multi-zones

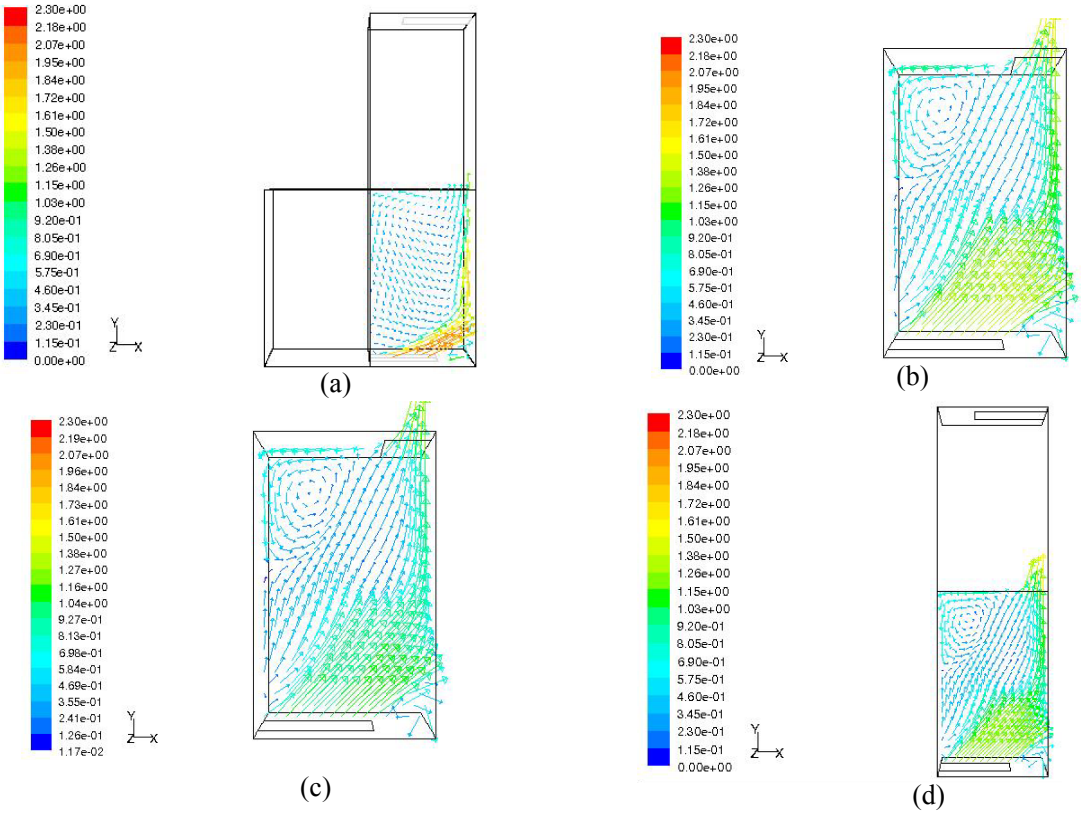

Figure 5.30 Velocity vector contour colored by velocity magnitude (m/s) for living room (a) full CFD simulation (b) indoor CFD simulation with pressure boundary conditions (c) indoor CFD simulation with average pressure boundary conditions (d) indoor CFD simulation for multi-zones

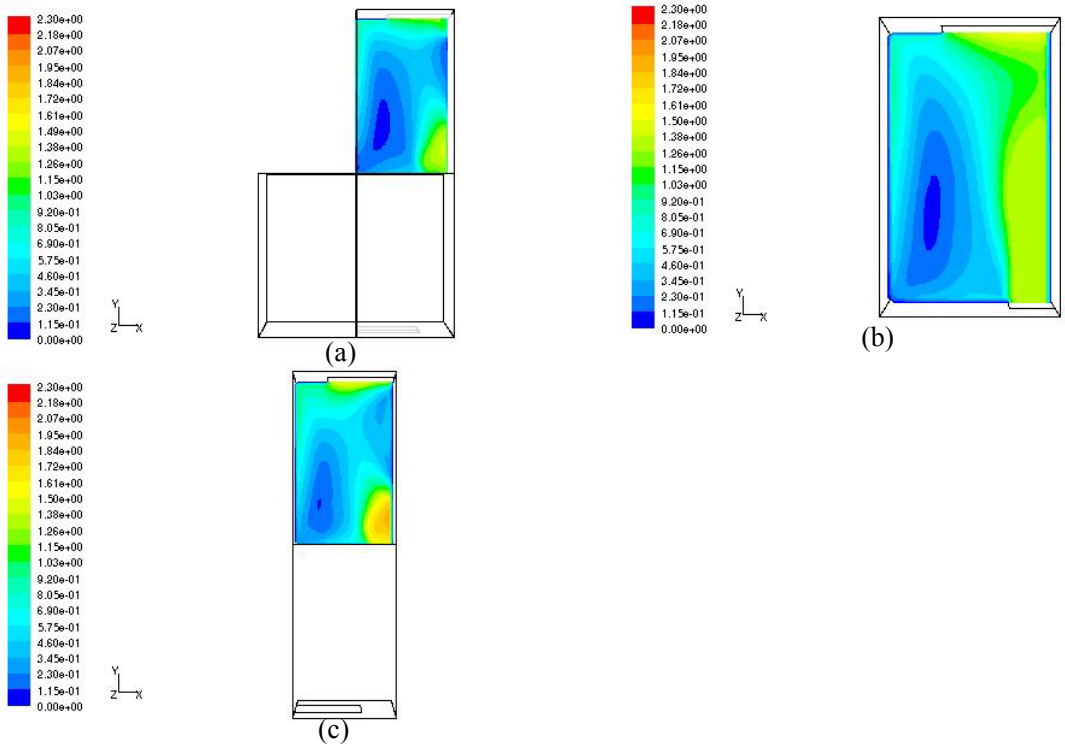

Figure 5.31 Velocity contour colored by velocity magnitude (m/s) for kitchen room (connected zone) (a) full CFD simulation (b) indoor CFD simulation with average pressure boundary conditions (c) indoor CFD simulation for multi-zones

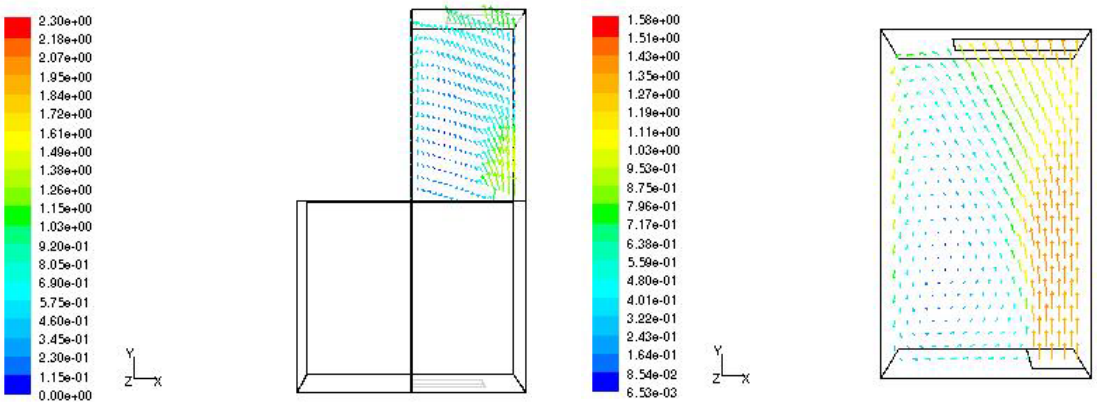

(a) (b)

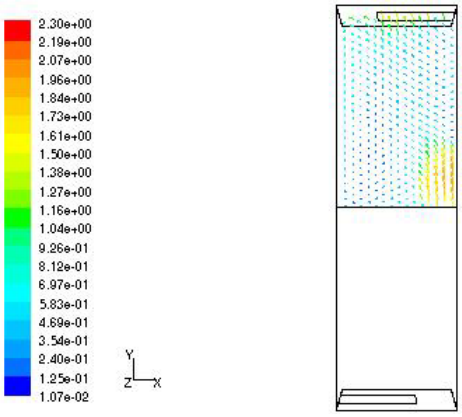

©

Figure 5.32 Velocity vector colored by velocity magnitude (m/s) for kitchen room (connected zone) (a) full CFD simulation (b) indoor CFD simulation with average pressure boundary conditions (c) indoor CFD simulation for multi-zones

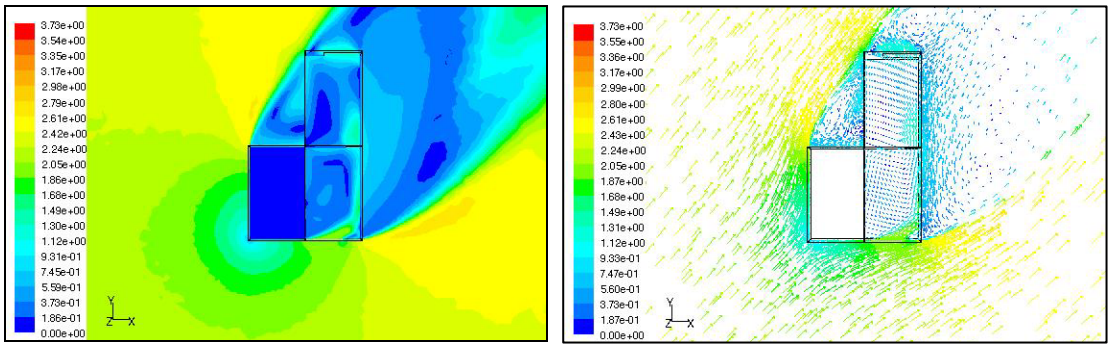

Table 0. ┌ (b)

Figure 5.33 Full CFD simulation (a) velocity contour (b) velocity vector

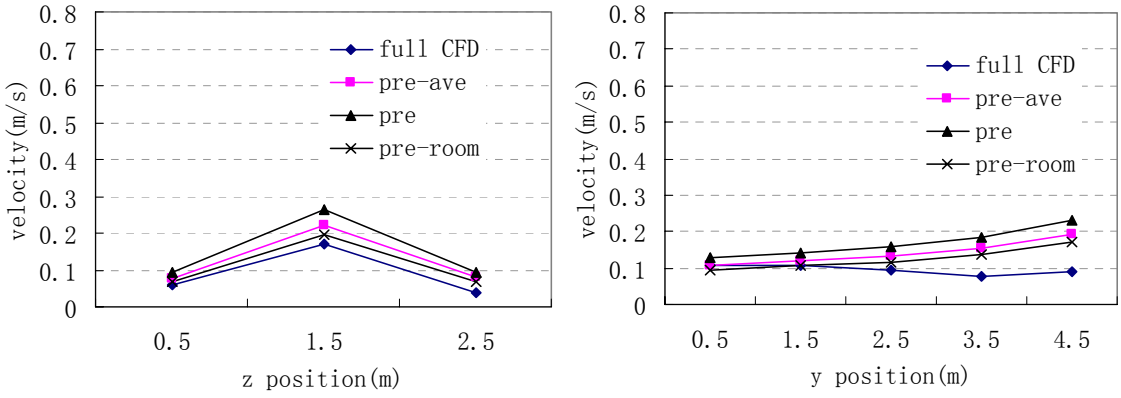

Figure 5.34 Area_weighted velocity results comparison along vertical (z) direction and length (y) direction for living room in case 1 among full CFD simulation, indoor CFD simulation with average pressure boundary condition, indoor CFD simulation with pressure boundary condition, and indoor CFD simulation for the whole room.

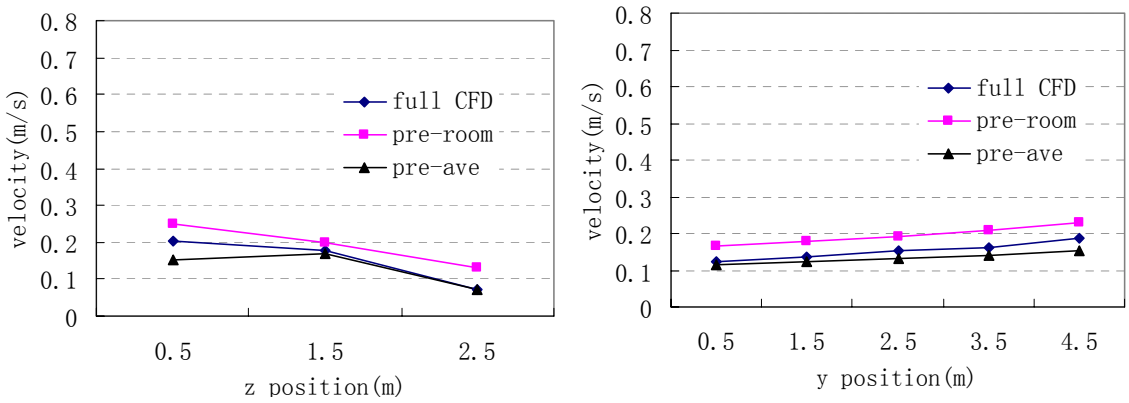

Figure 5.35 Area_weighted velocity results comparison along vertical (z) direction and length (y) direction for kitchen room(connected zone) in case 1 among full CFD simulation, indoor CFD simulation with average pressure boundary condition, indoor CFD simulation with pressure boundary condition, and indoor CFD simulation for the whole room.

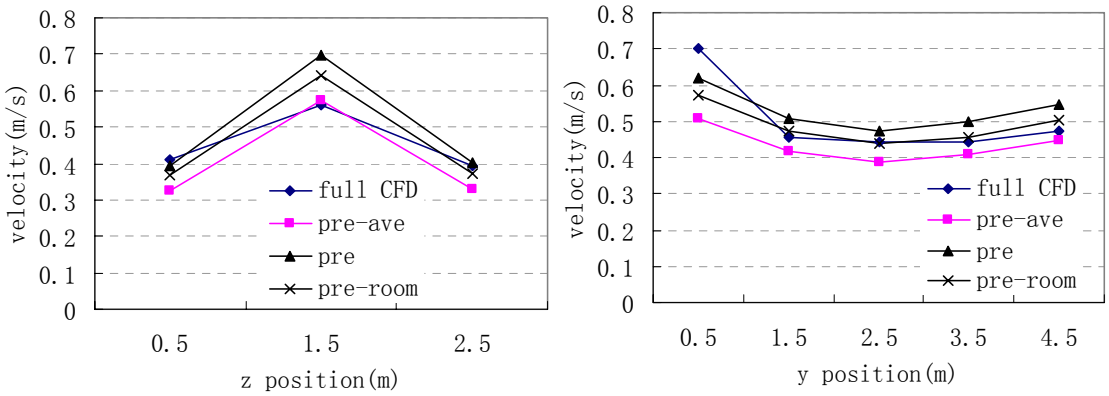

Figure 5.36 Area_weighted velocity results comparison along vertical (z) direction and length (y) direction for living room in case 2 among full CFD simulation, indoor CFD simulation with average pressure boundary condition, indoor CFD simulation with pressure boundary condition, and indoor CFD simulation for the whole room.

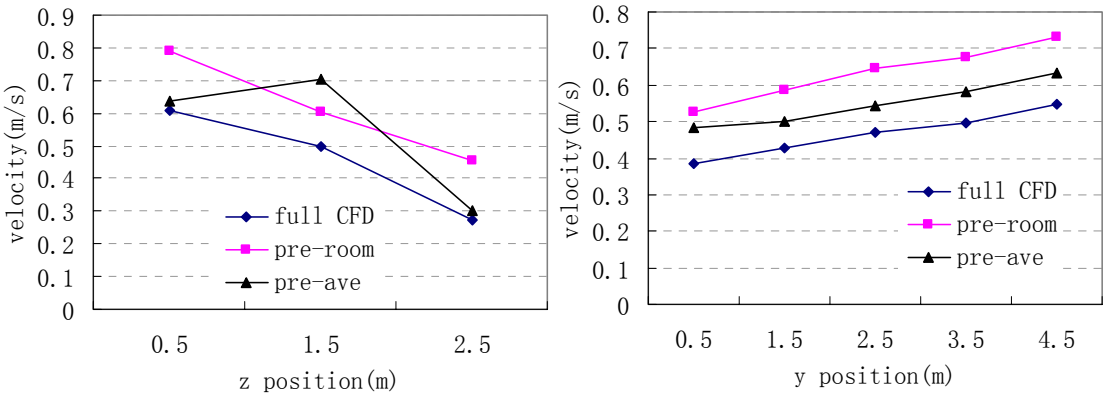

Figure 5.37 Area_weighted velocity results comparison along vertical (z) direction and length (y) direction for kitchen room (connected zone) in case 2 among full CFD simulation, indoor CFD simulation with average pressure boundary condition, indoor CFD simulation with pressure boundary condition, and indoor CFD simulation for the whole room.

Table 5.4 Result comparison (living room)

Area Weighted room velocity (1.5m Height)	Full CFD simulation (m/s)	Indoor CFD with pressure inlet (m/s)	Indoor CFD with pressure –ave (m/s)	Indoor CFD with pressure-room (m/s)	ESP-r (m/s)
Case 1: 2nd Jan 18:30	0.17	0.26	0.22	0.19	0.09
MFE		41%	26%	11%	69%
Case 2: 1ST Jan 12:30	0.56	0.70	0.57	0.64	0.29
MFE		22%	2%	13%	64%

Table 5.5 Result comparison (kitchen room)

Area Weighted room velocity (1.5m Height)	Full CFD simulation (m/s)	Indoor CFD with pre-ave (m/s)	Indoor CFD with pressure-room (m/s)	ESP-r (m/s)
Case 1: 2nd Jan 18:30	0.18	0.17	0.20	0.09
MFE		6%	11%	67%
Case 2: 1ST Jan 12:30	0.50	0.70	0.60	0.29
MFE		33%	18%	53%

5.3.2.2 Scenario 4

In this scenario, a typical residential flat in Singapore is simulated by using full CFD simulations and coupled simulations between BS and CFD. The layout of the flat is shown in Figure 5.38. Eight nodes are used for airflow network simulation in ESP-r, including living room, common1, master room, kitchen, and another four boundary nodes (north, south_common1, south_master room and south_kitchen).

The full CFD computations for both indoor and outdoor airflow simulation are carried out for validation. The velocity inlet boundary condition for both indoor and outdoor CFD simulation uses the atmosphere boundary profile and pressure-outlet boundary condition is adopted for the full CFD simulation domain. Same as in other scenarios, two cases (case 1: with wind direction 0°(N)and case 2: wind direction 45°(NE)) are used for validation. The climatic conditions for the two cases are listed in Table 5.1.

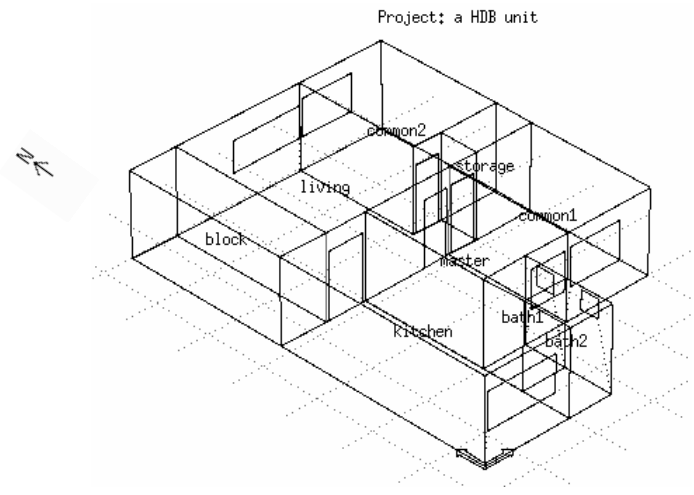

Figure 5.38 A HDB flat in Singapore layout

The ESP-r simulation results provide boundary conditions for indoor CFD simulations. The area weighted velocity magnitude results at the height of 1.35 m shown in Table 5.6 are

compared for full CFD simulation, ESP-r with indoor CFD simulations in a particular zone using *pre-ave*, and *pre-room* methods and ESP-r simulation only. MFE for coupled simulation results and ESP-r results compared with full CFD simulation results are listed in Table 5.6. The comparing contours and vectors of the velocity magnitude are shown in Figure 5.39 and Figure 5.40 for case 1 and in Figure 5.43 and Figure 5.44 for case 2 respectively. Figure 5.41 and Figure 5.42 show both outdoor and indoor airflow contours and vectors for case 1 and Figure 5.45 and Figure 5.46 are for case 2. All the contour and vector profiles are taken at 1.35m above the floor. The detailed area weighted velocity magnitudes along height and length are compared Figure 5.47 Figure 5.48 for case 1 and case2, respectively.

From the comparison, it can be seen that coupled simulations predict reasonable results for natural ventilation. The *pre-room* method (MFE_{MAX} =20%) gives more accurate results than the *pre-ave* method (MFE_{MAX} =34%). Coupled simulation can predict much better results for the average velocity in the room than building simulation program alone. However, the coupling program may not be able to accurately predict the velocity profile near the inlet.

Case 1 2nd Jan 18:30 (N wind direction)

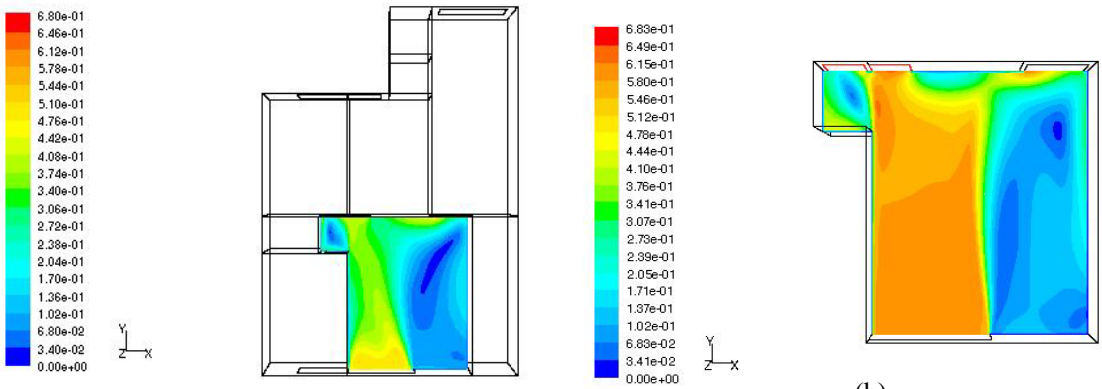

(a) (b)

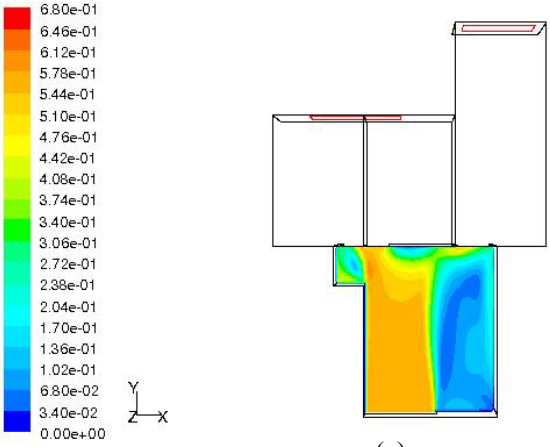

(c)

Figure 5.39 Air velocity contour of living room in unit 606 with (a) full CFD computation (b) coupling program with pressure-average boundary condition (c) coupling program with full-room

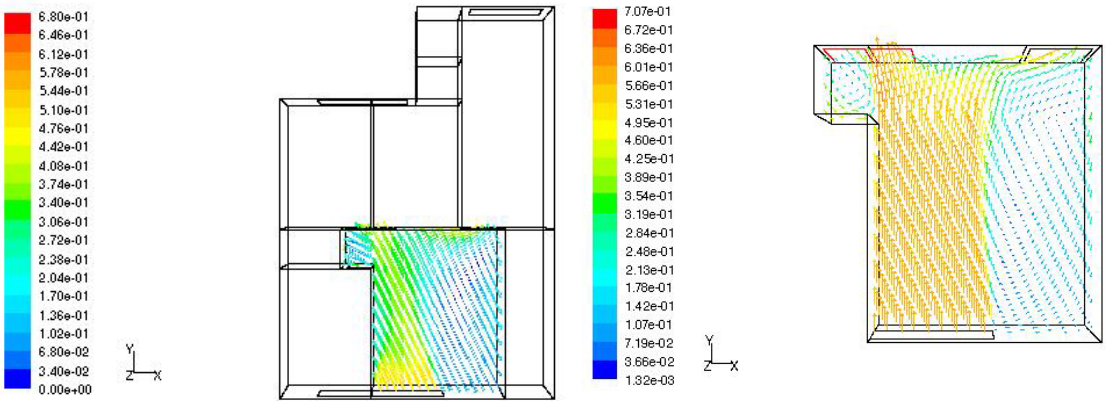

(a) (b)

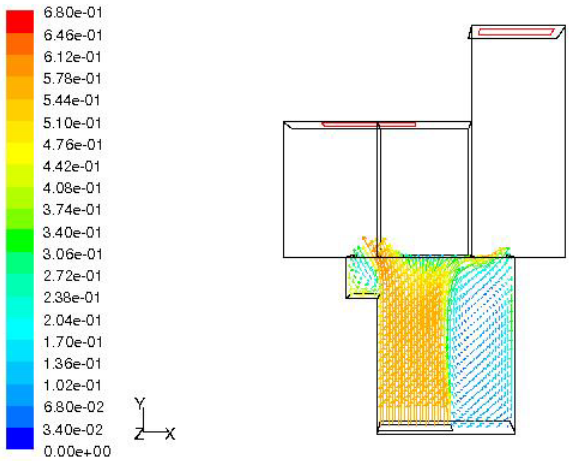

(c)

Figure 5.40 Air velocity contour of living room in unit 606 with (a) full CFD computation (b) coupling program with pressure-average boundary condition (c) coupling program with full-room

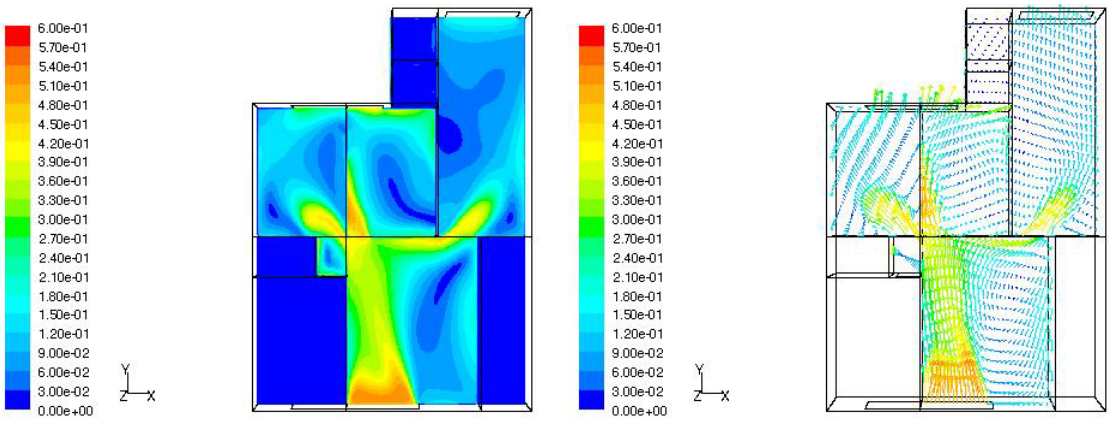

Figure 5.41 Air velocity contour and vector of unit 606 with full CFD computation

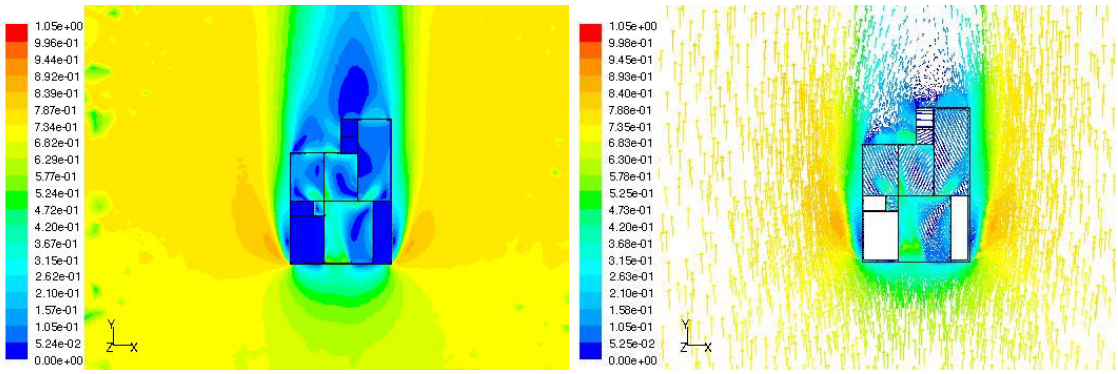

Figure 5.42 Air velocity contour and vector of the outdoor computation domain with full CFD computation

Case 2 1st Jan 12:30 (NE wind direction)

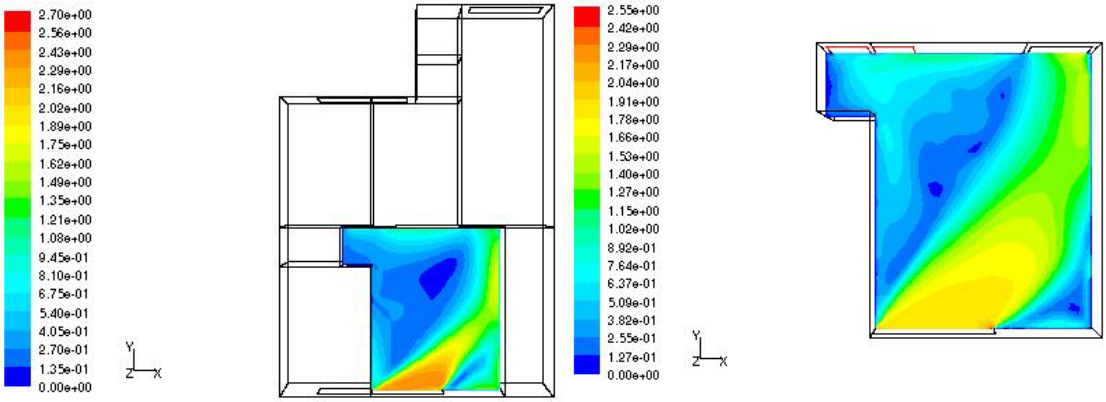

(a) (b)

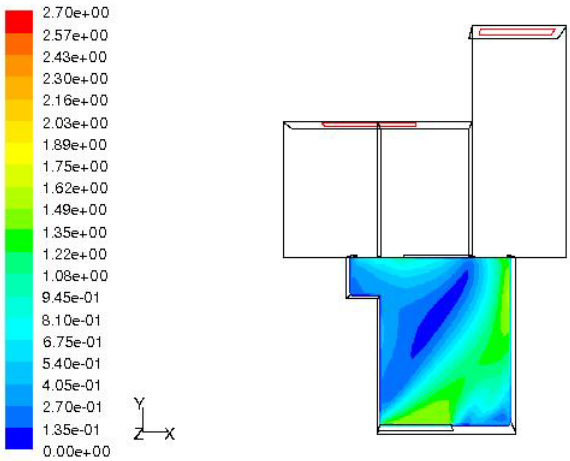

(c)

Figure 5.43 Air velocity contour for living room in case 2 with (a) full CFD computation (b) coupling program with pressure-average boundary condition (c) coupling program with full-room

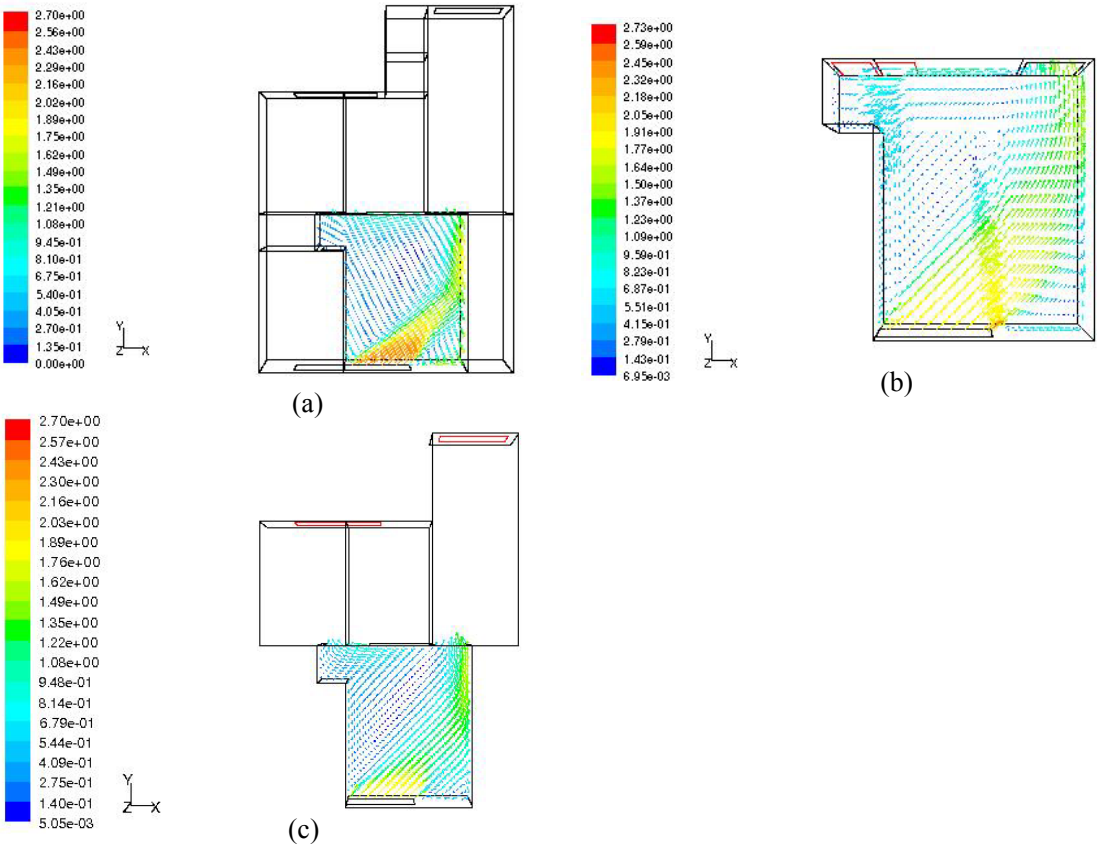

(a) (b)

(c)

Figure 5.44 Air velocity vector for living room in case 2 with (a) full CFD computation (b) coupling program with pressure-average boundary condition (c) coupling program with full-room

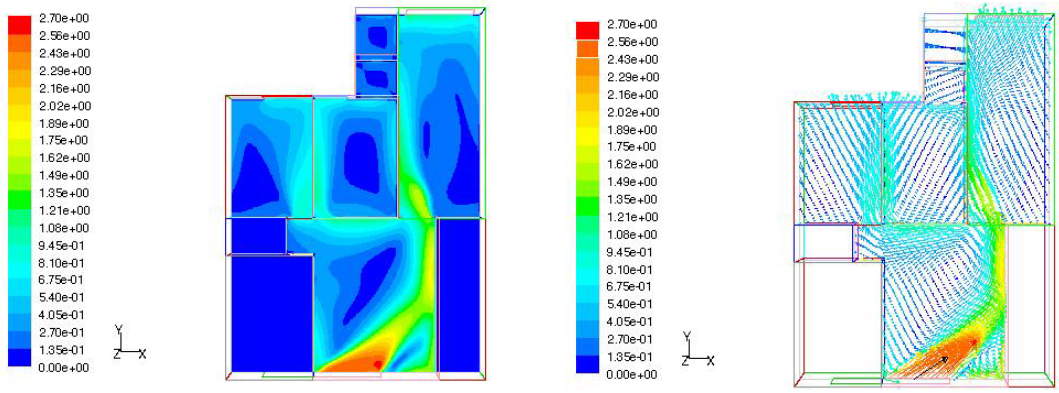

Figure 5.45 Air velocity vector and contour of flat 606

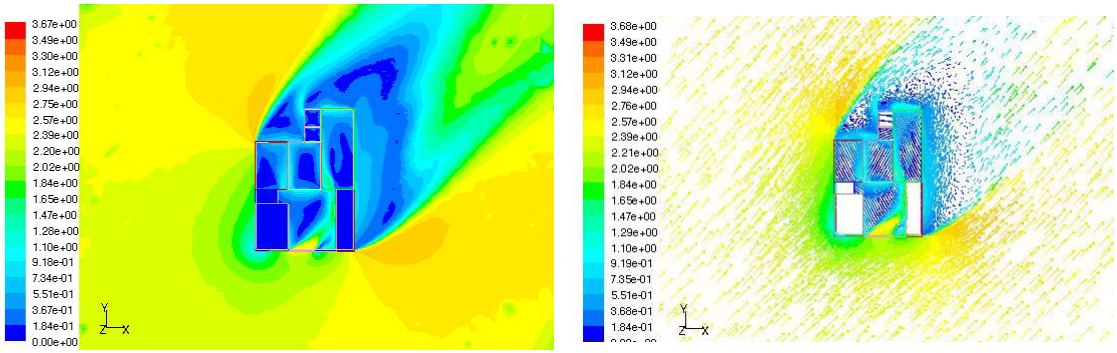

Figure 5.46 Air velocity vector and contour of full CFD computation domain

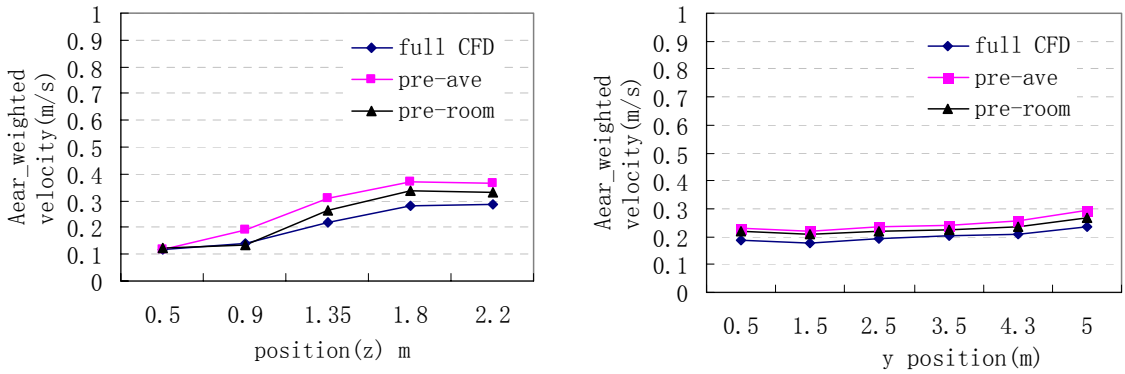

Figure 5.47 Area_weighted velocity results comparison along vertical (z) direction and length (y) direction for living room in case 1 among full CFD simulation, indoor CFD simulation with average pressure boundary condition and indoor CFD simulation for the whole room.

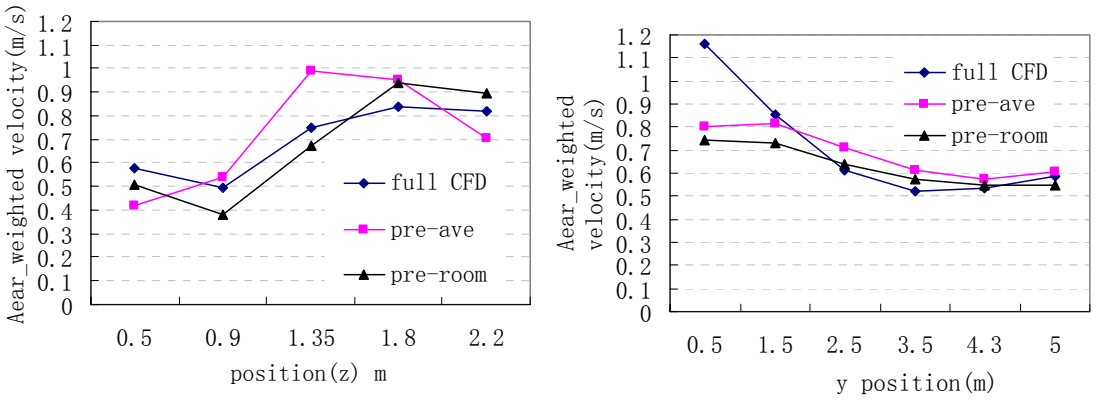

Figure 5.48 Area_weighted velocity results comparison along vertical (z) direction and length (y) direction for living room in case 2 among full CFD simulation, indoor CFD simulation with average pressure boundary condition and indoor CFD simulation for the whole room.

Table 5.6 Result comparison (living room)

Area Weighted room velocity (1.35m Height)	Full CFD simulation (m/s)	Indoor CFD with pre-ave (m/s)	Indoor CFD with pressure-room (m/s)	ESP-r (m/s)
Case 1: 2nd Jan 18:30	0.22	0.31	0.27	0.05
MFE		34%	20%	128%
Case 2: 1ST Jan 12:30	0.75	0.99	0.67	0.17
MFE		28%	11%	126%

5.3.3 Discussion

The simulation results of coupling program for four different scenarios including the single zone cases and multi-zone cases have been compared with full CFD simulation results. The results show that coupled simulations can better predict the indoor airflow simulations than building simulation program alone (airflow network) and the simulation results are reasonable comparing with full CFD simulations. Coupled simulations should take pressure as opening boundary conditions for better results. The *pre-room* method is preferred for multi-zone cases.

5.3.4 Discrepancy factors

Although coupling program can predict the indoor airflow profile with satisfying accuracy, there are still some deviations between the coupling program results and full CFD simulation results. The coupling program may not be able to accurately predict the velocity profile near the inlet. The discrepancy between coupling program and full CFD simulation for connected leeward zones is larger than that for windward zones. The inaccuracies of coupling program can be attributed to the following five aspects: pressure coefficients, inlet boundary conditions, discharge coefficients, pressure loss coefficients, and the impacts of surrounding layout on wind incident angles.

5.3.4.1 Pressure coefficients

Pressure coefficients in building simulation program are important to define the boundary conditions for natural ventilation simulations. The database are the collections of Cp value from typical buildings with various dimensions and surrounding conditions, which may not be accurate for specific configuration and may involve the inaccuracies. De Wit and Augenbroe (2002) concluded that uncertainty in wind pressure coefficients on the output of a building simulation model was one of the dominant factors for the modeling uncertainty. The nodal network method is to solve the airflow within a network of connected pressure nodes when boundary pressures are given. Therefore, network airflow modeling is to calculate the mass flows through pressure drops by an interactive approach till the nodal mass residuals are negligible (Clarke, 2001). Predictions of airflow with coupled simulations are the same as all modeling techniques which are highly sensitive to boundary conditions. Therefore, accurate

prediction of pressure coefficients is important for multi-zone airflow simulation programs. The simulation of the natural ventilation flows in buildings requires accurate knowledge of the wind pressure distribution over building envelope.

5.3.4.2 Non-uniform boundary conditions

From the velocity contours and vectors, it can be seen that the inlet boundary conditions for indoor CFD simulation determines the accuracy of the predicted detailed indoor airflow. However, the uniform inlet boundary conditions, as stated above, have been used for indoor CFD simulation, which is deviated from the full CFD simulation and realistic airflow. The accurate indoor opening conditions cannot be provided even with the division of opening into multiple small sizes in building simulation (Tan, 2005). The inlet boundary condition for full CFD simulation has been analyzed using case 1 in scenario 2 (single zone with wind from north) as an example. Wind incident angles to the north window, velocity magnitude distributions, and pressure distributions along the width of north window at 1.5 meter level above the floor are shown in Figure 5.49, Figure 5.50 and Figure 5.51 respectively. It can be observed from the distribution profiles that boundary conditions are actually non-uniform for all the variables, especially near the edges of the openings. As can be seen from Figure 5.49, wind incident angles are difficult to be accurately described. The wind direction is from normal north for case1, which is perpendicular to the north window, while the wind incident angles changes when wind reaches the location near the opening due to the disturbance of the room to the flow field.

The non-uniform inlet boundary profile obtained from full CFD simulation is involved to improve the pressure boundary condition imposed for coupled simulation. The improved simulation results along the height and length of the room for case1 in scenario 2 are shown in Figure5.52. It can be seen from the results that the accuracy of indoor simulation can be improved by non-uniform inlet conditions. Figure 5.53 shows the velocity contour and vector profiles of the revised pressure inlet boundary condition. Comparing that with Figure 5.16 and Figure 5.17, it is obvious that the airflow patterns predicted with the revised pressure condition is more accurate.

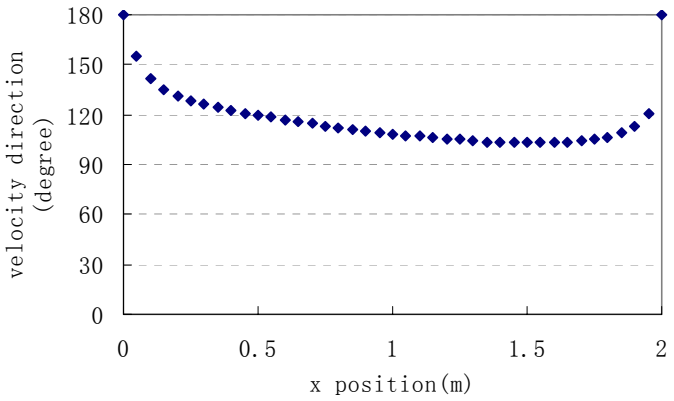

Figure 5.49 Wind incident angles along the width of the opening

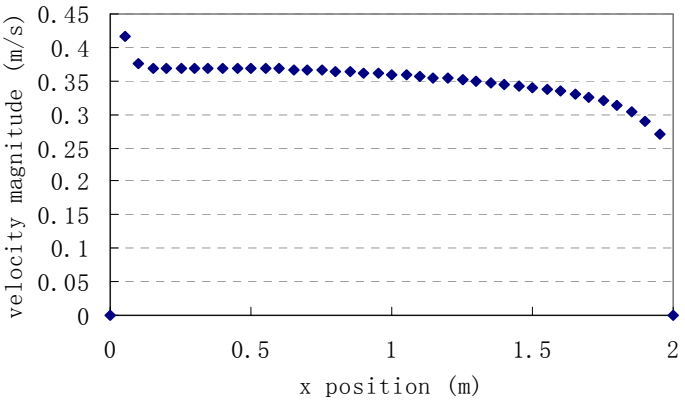

Figure 5.50 Velocity magnitude distributions along the width of the opening

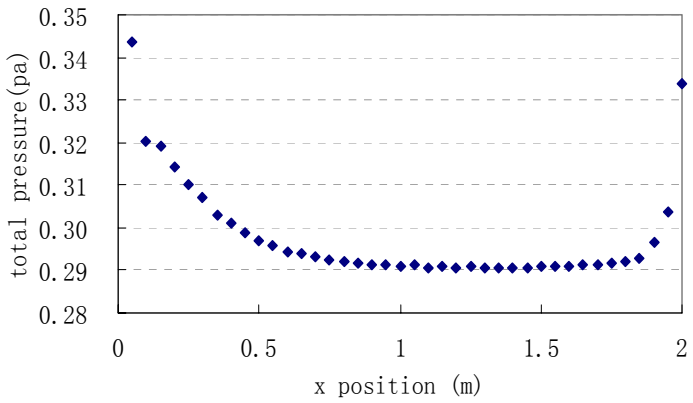

Figure 5.51 Pressure distributions along the width of the opening

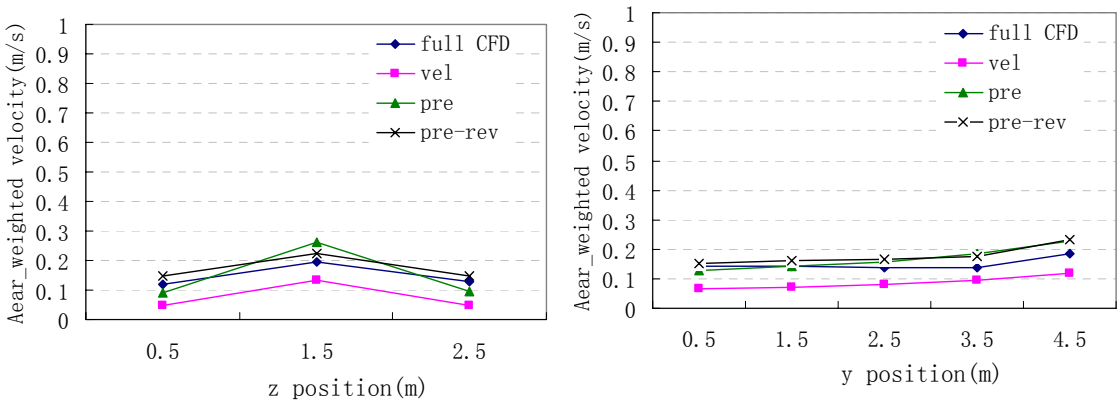

Figure 5.52 Area_weighted velocity results comparison along vertical (z) direction and length (y) direction for scenario 2 in case 1 among full CFD simulation, indoor CFD simulation with averaged velocity boundary condition (vel) indoor CFD simulation with average pressure boundary condition (pre) and improved boundary condition with full CFD boundary profile (pre-rev)

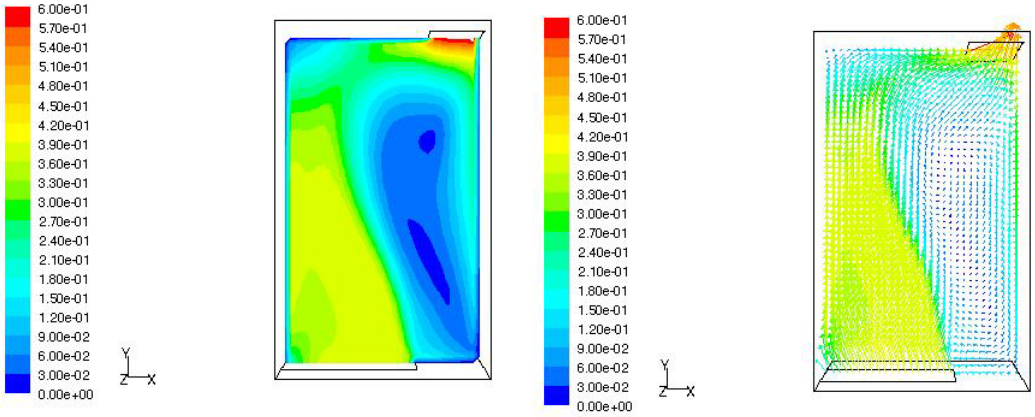

Figure 5.53 Velocity contour and vector profile for revised pressure inlet boundary condition for indoor CFD simulation

5.3.4.3 Discharge coefficients

The discharge coefficients are significant for mass flow calculation, and velocity calculation in airflow network simulation. However, the discharge coefficients are the empirical values for specific airflow openings which normally adopt 0.65 to estimate airflow rates governed by pressure differences.

5.3.4.4 Pressure losses through openings

Another difficult part to achieve accurate indoor simulation by coupled simulation is to reasonably estimate the pressure losses through openings in CFD simulations, namely the difference between internal pressure and external pressure at the opening. When the flow enters a straight tube or conduit, it separates by inertia from the inner surface close behind the entrance, which leads to a decrease in the jet cross section (jet contraction) and constitutes the major sources of the inlet pressure losses. According to the pressure loss coefficient in the conventional method, a turbulent draft flow into stagnant indoor space through an opening will lose a large part of its mean kinetic energy; however, the pressure loss coefficient in cross ventilation modeling is much smaller and therefore, empirical pressure coefficients for openings in handbooks are not suitable for cross ventilation study using CFD.

5.3.4.5 The impacts of surrounding layout on wind incident angle

In coupled simulations, the boundary wind direction is assumed to be the same as local wind directions near buildings, which are used to arrange the inlet velocity vectors for CFD simulations. However, wind incident angles to openings are not always consistent with the

main wind directions from far fields and it is actually affected by the surrounding layouts and surrounding buildings. Three different room layouts have been investigated as shown in Figure 5.54. It could easily be seen from the comparison results of full CFD simulations (Figure 5.55) that layouts have significant impacts on wind incident angles to openings.

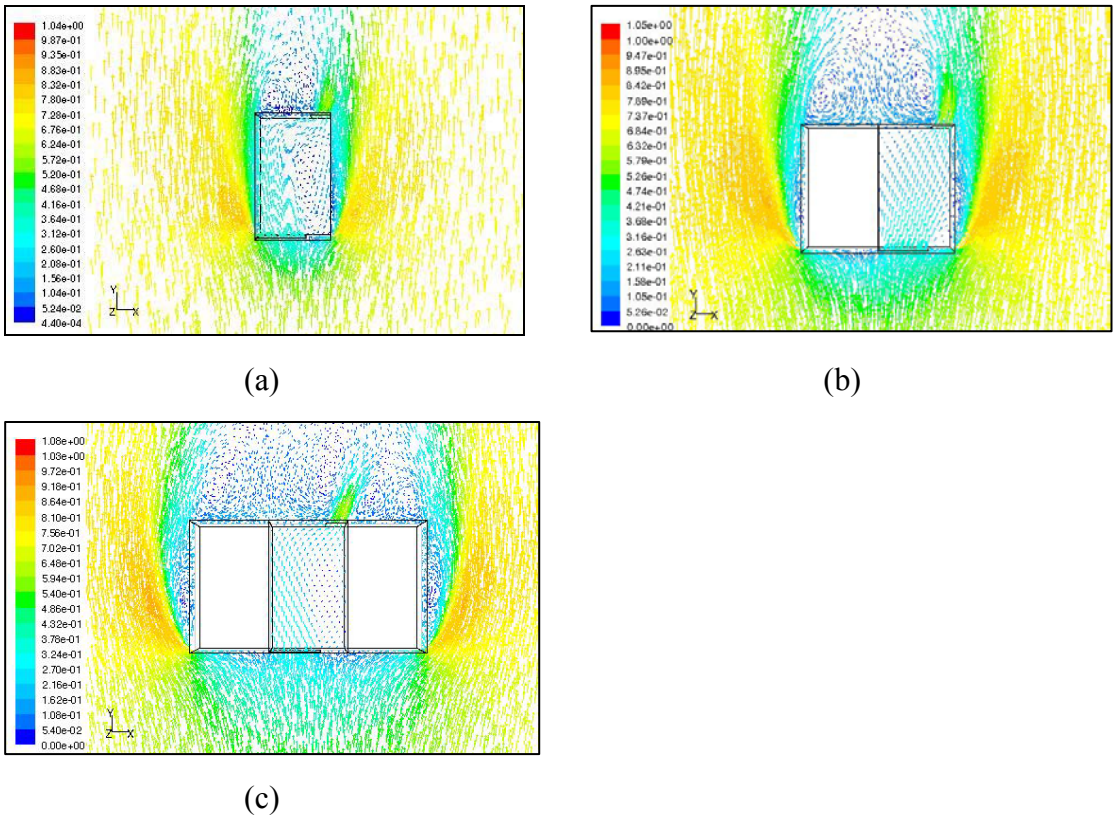

(a) (b)

(c)

Figure 5.54 Three room layouts for wind incident angle investigation
(a) one zone (b) two zones (c) three zones

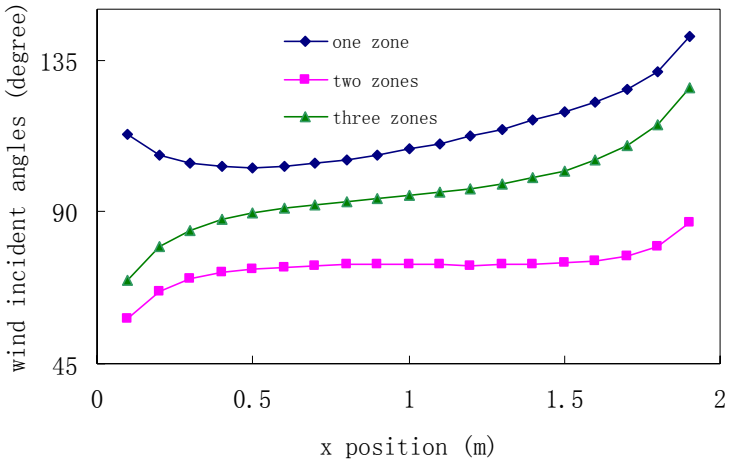

Figure 5.55 Wind incident angles along the width of the opening for three layouts

5.4 Coupled simulations validated with field measurement

A typical HDB building near National University of Singapore has been selected as the subject for field measurements, building simulations and coupled simulations to verify the effectiveness of coupling program between BS and CFD for natural ventilation prediction.

5.4.1 Field measurement results

The HDB block601 is located in Clementi, West coast (Figure 5.56 (a)). It is facing 18 degree northwest and the height of the building is 38.7 meters. A sixth level 4-room unit is used for field measurements. Field measurements were taken at the centre point of the living room and surfaces of facades. The digital multi-channel data logger from BABUC as shown in Figure 5.56 (b) was used to record indoor thermal parameters, including dry bulb temperature, indoor velocity, relative humidity, globe temperature and wet bulb temperature at 20 minute interval. Eight thermal coupling wires (T type) connected with HOBO data loggers (Figure 5.56 (d)) were used to measure the surface temperature both inside and outside of external walls in the living room and the kitchen room at 10 minute interval (Figure 5.56 (c)).

(a) (b) (c) (d)

Figure 5.56 (a) Block 601 and surrounding buildings (b) Babuc layout in the living room (c) Thermal couple wires for surface temperature (d) HOBO data logger

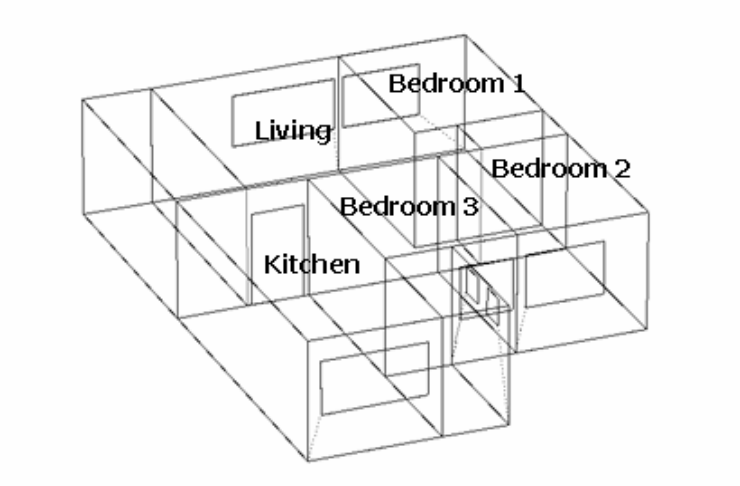

Figure 5.57 The layout of the four-room HDB unit

Table 5.7 Facade material properties

	Material	Thickness (mm)	Thermal transmittance (W/km^2)	Name in ESP-r
North /South external wall	Concrete hollow block wall	100	1.68	RCwall
Internal wall	Concrete hollow block wall	100	1.68	RCwall
Gable End wall	Gable end cavity wall	260	1.29	Gable wall
Glass	6mm antisun glass	6	5.44	Single glass

There are three bedrooms in the unit (Figure 5.57). For the purpose of validation, the doors of bedroom connected with the living room are closed. The internal doors are in good airtightness. Therefore, the airflow network in the unit comprises two boundary nodes (north and south nodes) and two internal nodes (living room node and kitchen node). The airflow route of the unit through the living room and kitchen room is North->living room ->kitchen ->South or South->kitchen->living room->North. The construction material properties are listed in Table 5.7.

The weather data were obtained from NUS weather station, located on the rooftop of building E2 (Faculty of Engineering) of the National University of Singapore, Kent Ridge campus. The geographical coordinates are approximately: 1 deg18 min N (latitude) and 103 deg 46 min E (longitude). The vertical height of the weather station above the ground is 25.3 m (at the cup anemometer position).

The simplified Equation (3.6) is used to describe the relationship between building height wind speed and wind speed measured from Meteorological station at a standard height of 10m.

$$\frac{v_l}{v_{10}} = kz_l^{\ a}$$

v_l ---building height wind speed (m/s)

v_{10} ---wind speed measured from Meteorological station at a standard height of 10m (m/s)

z_l ----building height (m)

k, a ----constants dependent on terrain. Here, we use the terrain coefficients for urban, k=0.35 and a=0.25.

The NUS weather station is located on a small ridge. The position of the instruments does not conform to WMO (1983) guidelines for weather stations in open terrain or recommendations for urban areas. The modified wind speed equation (5.5) for the building height wind speed is used.

$$\frac{v_l}{v_{nm}} = \left(\frac{z_l}{z_{nm}} \right)^a \qquad (5.5)$$

v_{nm} --- wind speed measured from NUS weather station (m/s)

z_{nm} ----NUS weather station height (25.3 m)

5.4.2 Pressure coefficient prediction for high-rise residential buildings

Pressure coefficient (Cp) of external surfaces is a significant parameter for accurate prediction of natural ventilation with coupling program between BS and CFD.

External airflow simulations were carried out for a typical HDB building-Block 601 in Singapore to obtain the Cp values at the sixth floor. Eight cases have been simulated for predicting pressure coefficients. Each case has particular incidence angle of 0º, 45 º, 90 º, 135 º, 180º, 225 º, 270 º, 315º from the building (Figure 5.58). A pressure coefficient set in building simulation typically comprises 16 values at 22.5 º intervals. Therefore, the other eight pressure coefficients are interpolated from the obtained values by CFD simulations. The dimensions of the building cluster are around 90.4m (L) x 13m (W) x 38.7m (H). Therefore, the computational domain for windward part is around 500m, for each side part is around 400m, and for leeward part is around 700m. This ensures that the turbulent flows behind the building are fully developed. A total number of two million mesh elements are generated for each case and the meshes around the building are illustrated in Figure 5.59. The realizable

$k-\varepsilon$ turbulence model is used for outdoor airflow simulation and 1/4 shear flow is adopted for inlet boundary condition.

The pressure coefficients of external surface temperature could be calculated by the following Equation (3.9):

$$C_p = \left(\frac{p - p_\infty}{1/2 \rho V_r^2} \right)$$

Where p is the pressure at the external surface, p_∞ is the pressure at free stream and V_r is the reference wind speed above the roof. The predicted Cp results will be input into the building simulation, taken as boundary conditions.

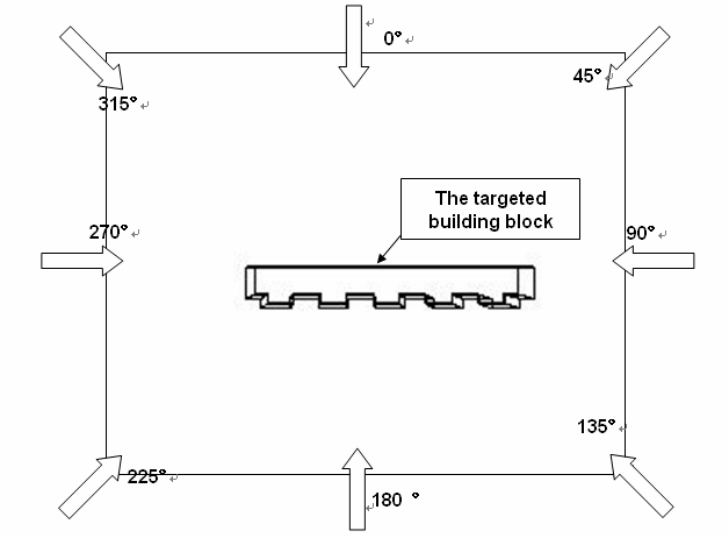

Figure 5.58 Computational methodology for various wind directions

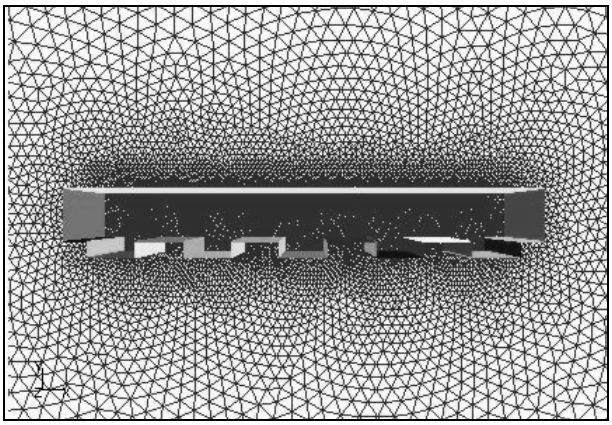

Figure 5.59 Building model in west coast built in GAMBIT

5.4.3 ESP-r simulations

The HDB building is modelled in ESP-r (a 14-storey residential building). The subject of the ESP-r simulation is the living room of a HDB unit on the sixth floor. The purpose of the simulation is to compare the ESP-r simulation results with field measurements. There are altogether 22 zones in the building model (Figure 5.60). Each neighbouring level of the sixth level, such as the fourth level, fifth level, seventh level and eighth level, are divided into two zones, including left zone and right zone. The sixth level includes 10 zones for each specific unit layout. The other distant levels have to be combined together due to the limitation of maximum-zones and geometric models in the ESP-r. The windows in living room and in kitchen zone are adopted half area (1.44m^2) as airflow network components. The building material setting is consistent with the specific materials in the real building. The solar absorptance of external walls is set to 0.3 (white color surface) and the emissivity is set to 0.9.

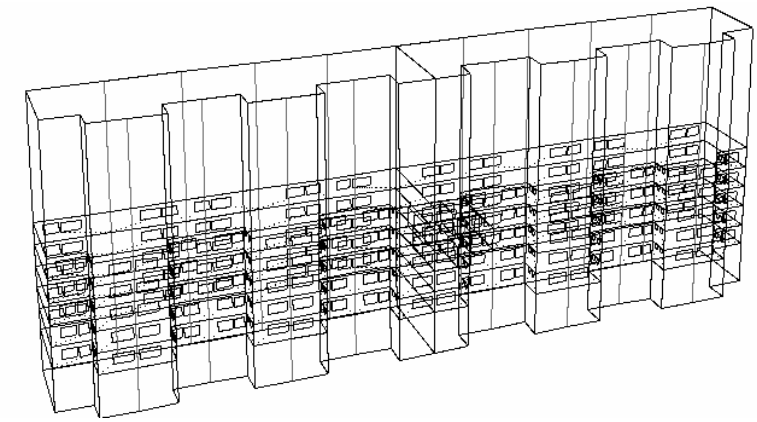

Figure 5.60 HDB block601 ESP-r model

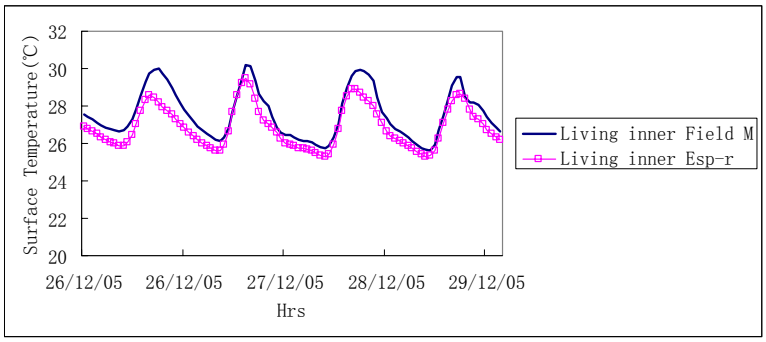

Figure 5.61 Internal surface temperature of living room comparison between measurement and building simulation

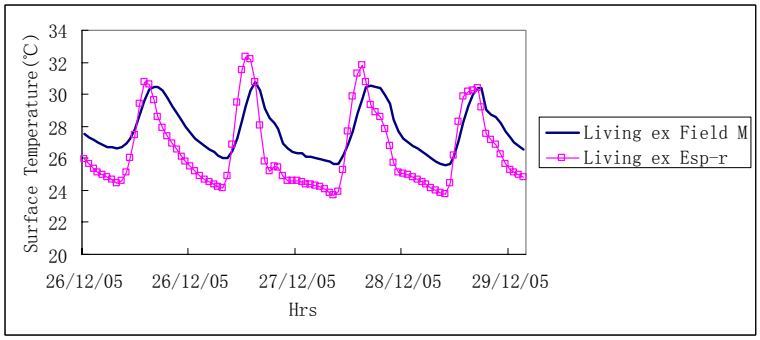

Figure 5.62 External surface temperature of living room comparison between measurement and building simulation

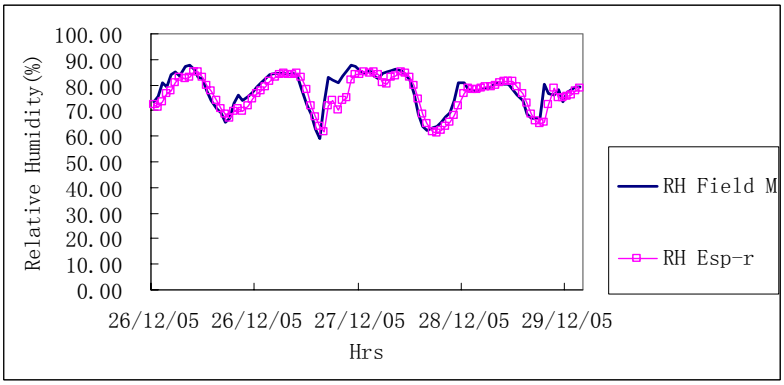

Figure 5.63 Relative Humidity result comparison between measurement and building simulation

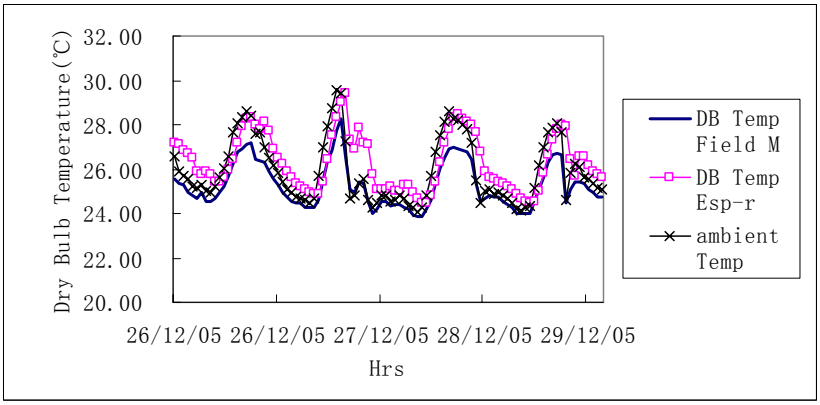

Figure 5.64 Dry bulb temperature result comparison between measurement and building simulation

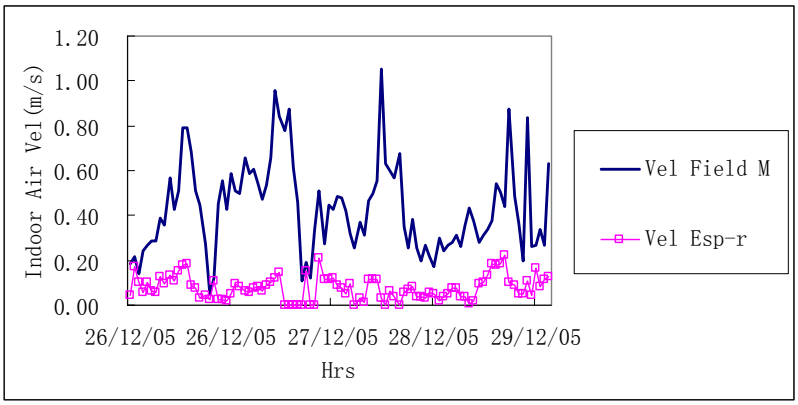

Figure 5.65 Indoor air velocity result comparison between measurement and building simulation

The simulation results of ESP-r compared with field measurement from Dec 26, 2005 to Dec 29, 2005 have been shown in Figures 5.61-5.65. The internal surface temperature and external surface temperature calculated with ESP-r have been compared with the measured surface temperature (shown in Figure 5.61 and Figure 5.62). The comparison indicates that the internal surface temperatures with building simulations agree well with the measured data and the external surface temperatures show fluctuations around the measured external surface temperature. The relative humidity simulation results agree well with measurements (Figure 5.63). The comparison for dry bulb temperatures for the living room is shown in Figure 5.64. From the results, it can be seen that building simulation tends to predict slightly higher zone temperature than field measurement results. Figure 5.65 shows the indoor air velocity results between field measurement and building simulation. The indoor velocity is estimated from the inlet velocity calculated by ESP-r using the following Equation (5.6). As can be seen from the comparison results, the predicted indoor air flow is much lower than the measuring data.

$$V(m/s) = \frac{Inlet\ Velocity \times Inlet\ Area}{\text{sec}\,tion\ area\ of\ the\ room} \quad (m/s) \qquad (5.6)$$

5.4.4 Coupled simulations

It has been noticed that the multi-zone model in ESP-r cannot accurately predict the indoor air velocity, which would probably affect the prediction of other indoor thermal parameters. Therefore, to improve the accuracy of natural ventilation prediction, the coupled simulations between ESP-r and CFD are adopted. The predicted indoor environment (indoor air velocity and dry bulb temperature) with coupling program between building simulation (ESP-r) and computational fluid dynamics(CFD), has been compared with the field measuring data and is shown in Figure 5.66 and Figure 5.67.

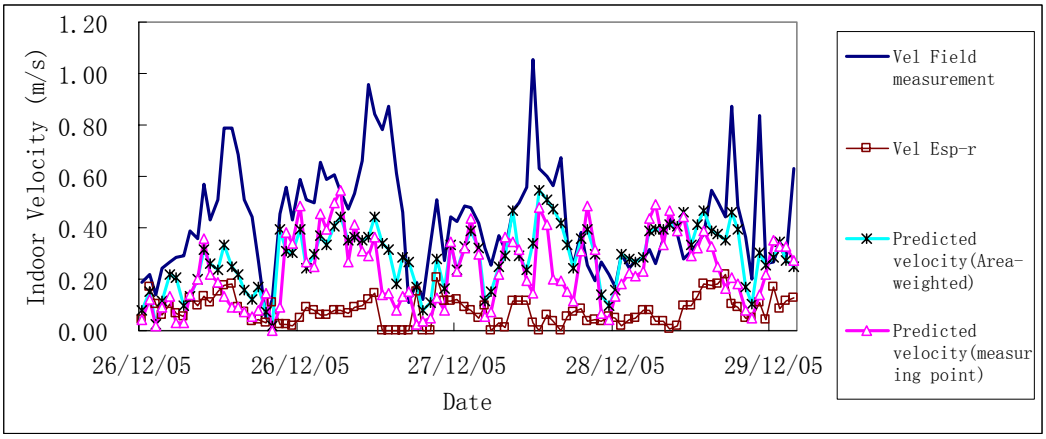

Figure 5.66 Indoor air velocity comparison among Field measurement, ESP-r simulation only and coupled ESP-r-CFD simulation

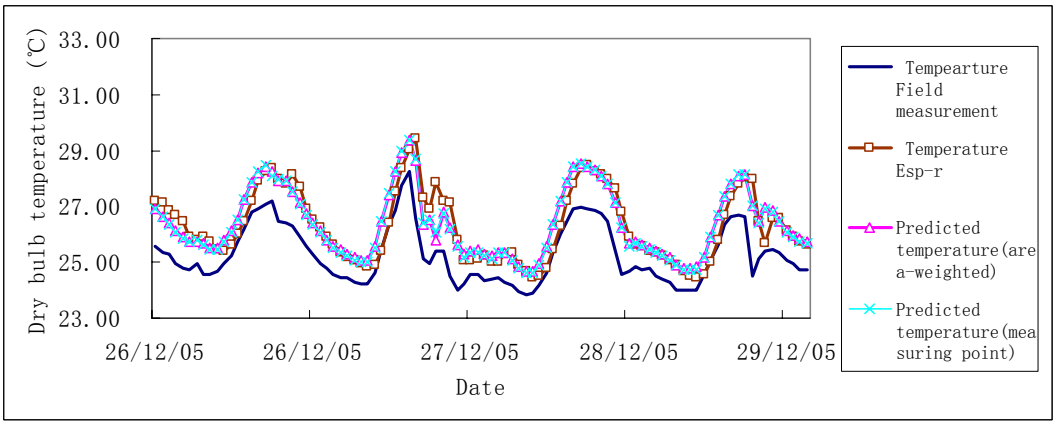

Figure 5.67 Indoor air temperature comparison among Field measurement, ESP-r simulation only and coupled ESP-r-CFD simulation.

Figure 5.66 shows the comparison of indoor air velocity among field measured data, ESP-r simulation results and coupling program results from Dec 26, 2005 to Dec 29, 2005. The field measurement results are taken at the level of 1.5m above the floor near the centre of the room. The predicted area-weighted velocity at 1.5m above the floor and the predicted indoor air velocity at the specific measuring point are obtained by using BS-CFD coupling program for a time series simulation. Compared with the field measurement results, the predicted indoor air velocities by ESP-r are quite low, although the results show good correlation between the predicted velocity by ESP-r and measured data. These results confirm that building simulation (airflow network) cannot accurately predict mass airflow rate and indoor air velocity. This can be attributed to simply using a set of empirical equations governed by pressure differences for mass flow rate prediction of different kinds of components connecting airflow in the building simulation. Therefore, mass flow rate passing by each component cannot be accurately estimated. The underestimation becomes more obvious especially for cross ventilation conditions, under which air velocities around openings and indoor air flow rates can be highly increased. In the airflow network simulation, mass flow rates are calculated based on empirical equations related with the types of components and only mass conservation equation is considered, but momentum equation and turbulence equation are not reflected in the airflow network. It can be seen from the comparison results (Figure 5.66) that with the use of coupling program, the indoor air velocity prediction can be largely improved and the predicted air velocity with BS-CFD coupling program can provide the designers more reliable indoor air velocity results. However, at the peak measured values in the daytime, discrepancies between field measurement and coupling program predicted velocity are

observed. Generally speaking, it is a characteristic of the airflow velocity that greater fluctuations in the speed of gusts occur when the mean air velocity is higher. Normally, in the field measurement, the peak values indicate very high fluctuations of indoor air velocity at those periods. The coupling program takes uniform steady pressure boundary conditions for apertures at each time interval, which is applicable for most of the indoor time, but for highly fluctuating cases, the pressure conditions at the openings could not be simply taken at a uniform constant value in each time interval. To obtain accurate results of highly fluctuating cases, unsteady full CFD simulations for both indoor and outdoor at a small time step or large eddy simulation may be required. However, computational time will be largely increased and static coupled simulations with uniform boundary conditions are sufficient for most naturally ventilated facade design purposes. In general, it could be concluded that BS-CFD coupling program can predict indoor air velocity in a more accurate way than BS alone.

Figure 5.67 shows the comparison results of indoor air dry bulb temperature among field measurement results and ESP-r simulation results and coupling program results from Dec 26 –Dec 29, 2005. The area-weighted indoor air dry bulb temperature and the dry bulb temperature at the specific measuring point are obtained by using BS-CFD coupling program. From the results, it can be seen that the predicted dry bulb temperature by ESP-r is quite close to that predicted by coupling program, which is mainly controlled by outdoor ambient temperature.

From the comparison results, it can be concluded that the coupling program can largely improve the accuracy of indoor air velocity prediction and further improve thermal comfort evaluation.

5.5 Summary of coupled simulations

A coupling program between ESP-r and FLUENT and a text-mode interface were developed. In this chapter, coupled simulations are validated with full CFD simulation and field measurements. The coupling program can improve indoor thermal environment prediction due to the better prediction of natural ventilation taking wind as the major force. Comparing with full CFD simulation (both indoor and outdoor airflow simulation), the coupling program can largely reduce the computational cost. For a very simple multi-zone case, it takes about 12 hours with parallel computer work stations. However, coupled simulation can be completed with in 1 hour for a time step with a general computer. In addition, the impacts of solar radiation on facade heat gains can be easily considered with coupled simulations. It can also improve the accuracy of the airflow prediction for wind driven natural ventilation based on building simulation program. It is an optimal way to rapidly and accurately obtain the indoor thermal environment for naturally ventilated buildings.

Chapter 6 Thermal performance of different facade designs for naturally ventilated residential buildings in Singapore

Singapore is situated on the 1.2° latitude with relatively high temperature ranging from 23℃ to 34℃ and high relative humidity averaging 84% over the year. Natural ventilation is an important sustainable strategy in Singapore as 86% of the population is living in HDB (Housing & Development Board) flats, which are designed to be naturally ventilated. This chapter aims to investigate the feasibility of natural ventilation in a hot-humid climate country and provides useful facade design guidelines for naturally ventilated residential buildings in Singapore. The optimal material properties, window to wall ratios and shading devices for high-rise residential buildings in Singapore are predicted using building simulations and coupled simulations based on thermal comfort criteria.

6.1 Is natural ventilation applicable in Singapore?

The purpose of this climatic study is to examine the feasibility of natural ventilation in Singapore. Local climatic analyses are important for natural ventilation study. Four parameters: dry bulb temperature, relative humidity, wind speed and solar radiation are analyzed.

6.1.1 Selection of typical year data

For thermal analyses of local climate data, thermal conditions of one typical year data set (8760 hours) of weather conditions are required. Several kinds of typical weather data are currently available and the criteria for constructing a typical year weather data vary from one database to another.

Canadian Weather files for Energy Calculations (CWEC), produced by Numerical Logics, contain hourly weather observation representing an artificial one-year period specially designed for building energy calculations. International Weather files for Energy Calculations (IWEC) are derived from up to 18 years of DATSAV3 hourly weather data originally archived at the U.S. National Climatic Data Center (NCDC). The weather data are supplemented by solar radiation estimated on an hourly basis from earth-sun geometry, hourly weather elements, and particularly the cloud amount information. Solar and Wind Energy Resource Assessment (SWERA) developed high quality information on solar and wind energy resources in 13 developing countries. Typical Meteorological Year 2 (TMY2) was derived from a 1961-1990 period of record. The TMY2s are data sets of hourly values of solar radiation and meteorological elements for a one year period. California Climate Zones 2 (CTZ2) updated weather data for 16 California climate zones for use to demonstrate compliance with Title 24 with approved building energy simulation programs.

Typical meteorological year is based on an empirical approach that selects individual months from a long period (30 years or more). Data sets occurring with the maximum frequency may be chosen to be included in the typical year. Since there are only limited amount of weather

data available in Singapore, a different criteria for construction of typical year weather data is applied. In this study, year 2001 weather data has been tested as a typical year data because it is the latest weather data available and has minimum amount of missing data. This reduces the amount of reconstruction and manipulation of data. To ensure that year 2001 weather data can be used as a typical year data, the testing steps listed below, following Lam (1997), were taken to test the dataset.

a) The number of instances where dry bulb temperature or global radiation in a particular hour in a year exceeds the maximum or falls below the minimum of the other years is counted and shown on Figure 6.1 and Figure 6.2, respectively. Any unusual traits in the hourly data of that year can be detected. Year 2001 does not show any unusual characteristics.

b) The differences in the amount of dry bulb temperature and global radiation for each of the above instances are added separately for those above the maximum or below the minimum values. Year 2001 does not show any unusual trends, as shown in Figures 6.3-6.6.

c) The frequency of occurrence of particular wind conditions for each month has been calculated. Occurrence frequency in January is shown in Figure 6.7 and occurrence frequencies for other months are shown in Figures App.1.1-App.1.11. Year 2001 does not show any unusual trends.

d) The year 1997 and year 1998 data show some unusual high dry bulb temperature and wind velocity in some months. Therefore, it is concluded that the use of year 2001 as a typical year is reasonably valid.

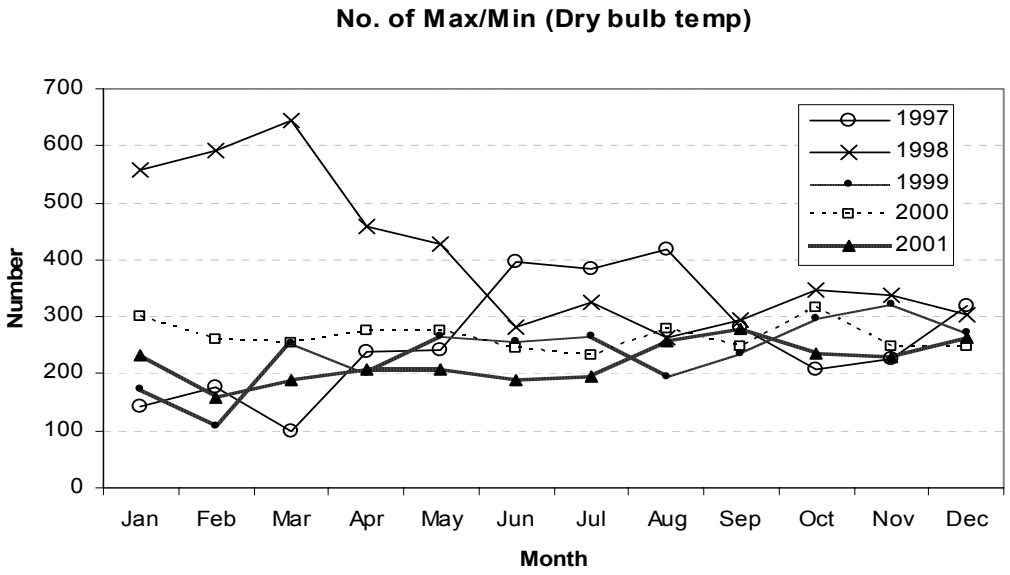

Figure 6.1 The number of hourly instances that the dry bulb temperature for each month of the year exceeds the maximum or falls below the minimum of the other years.

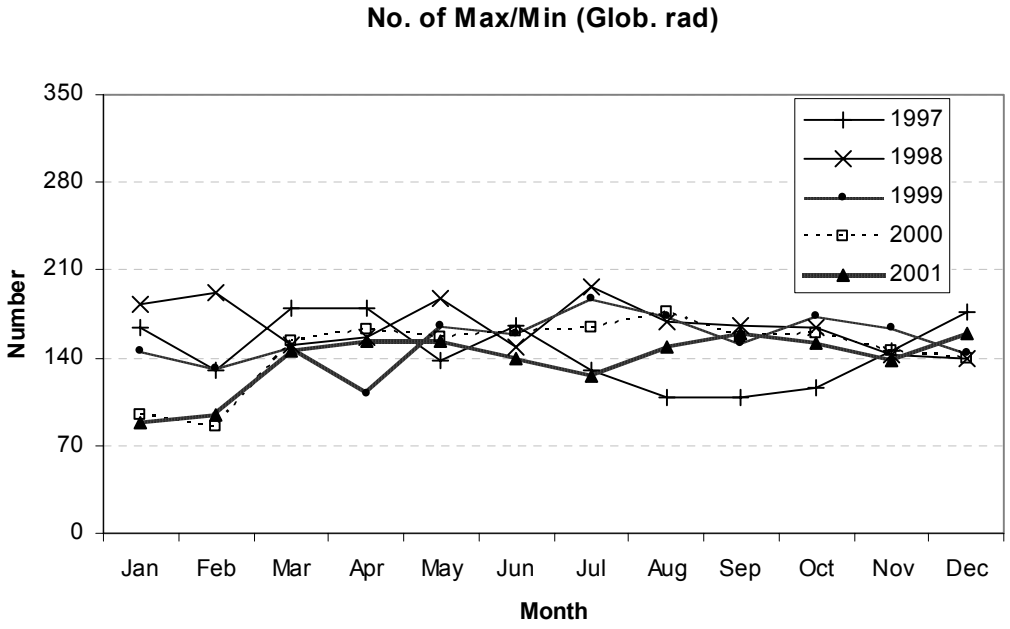

Figure 6.2 The number of hourly instances that the horizontal global radiation for each month of the year exceeds the maximum or falls below the minimum of the other years.

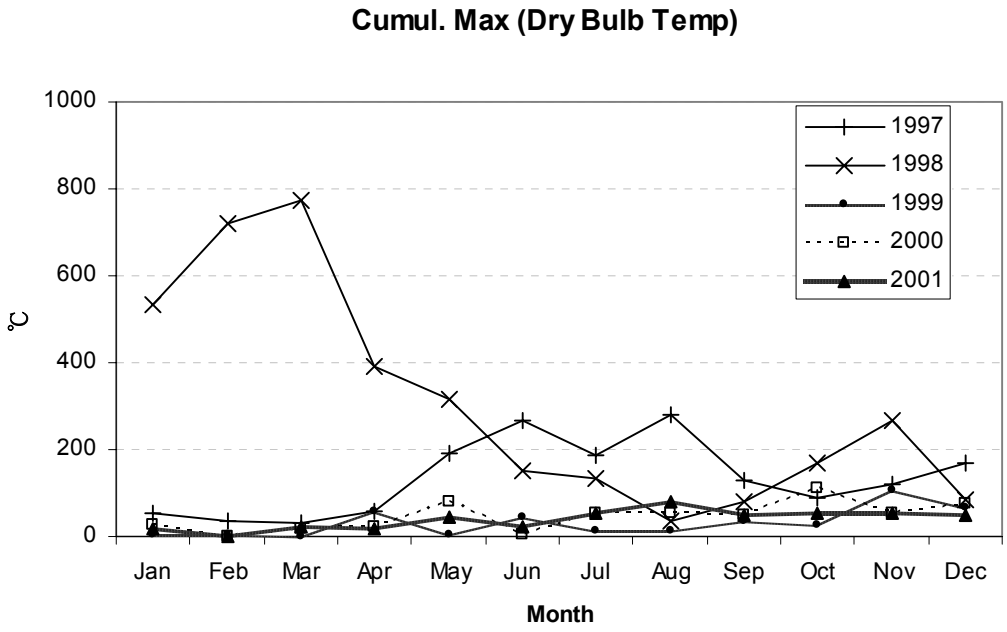

Figure 6.3 The cumulative amount by which the dry bulb temperature for each month of the year exceeds the maximum of the other years.

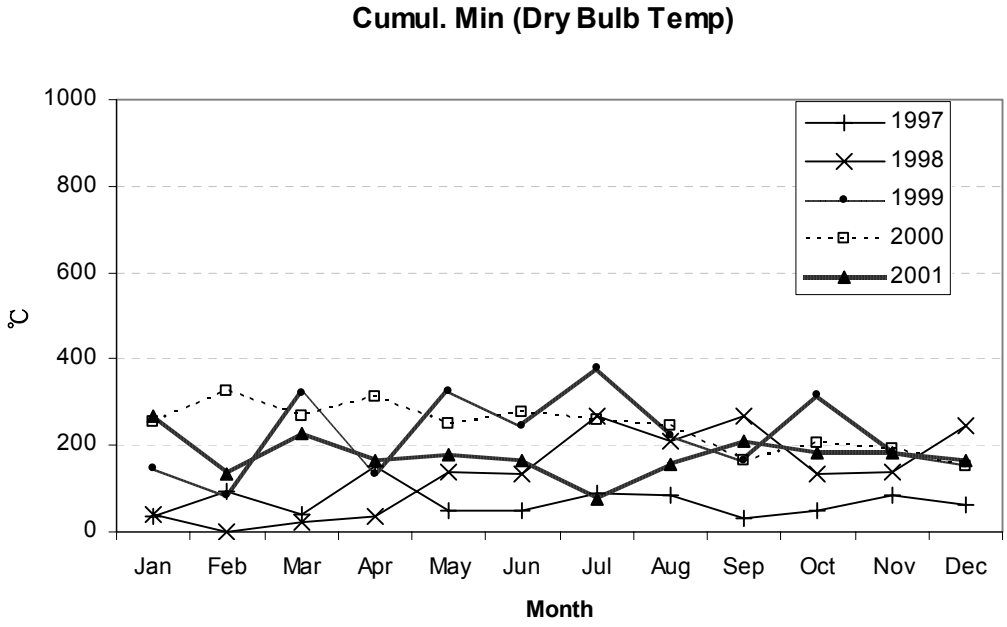

Figure 6.4 The cumulative amount by which the dry bulb temperature for each month of the year falls below the minimum of the other years.

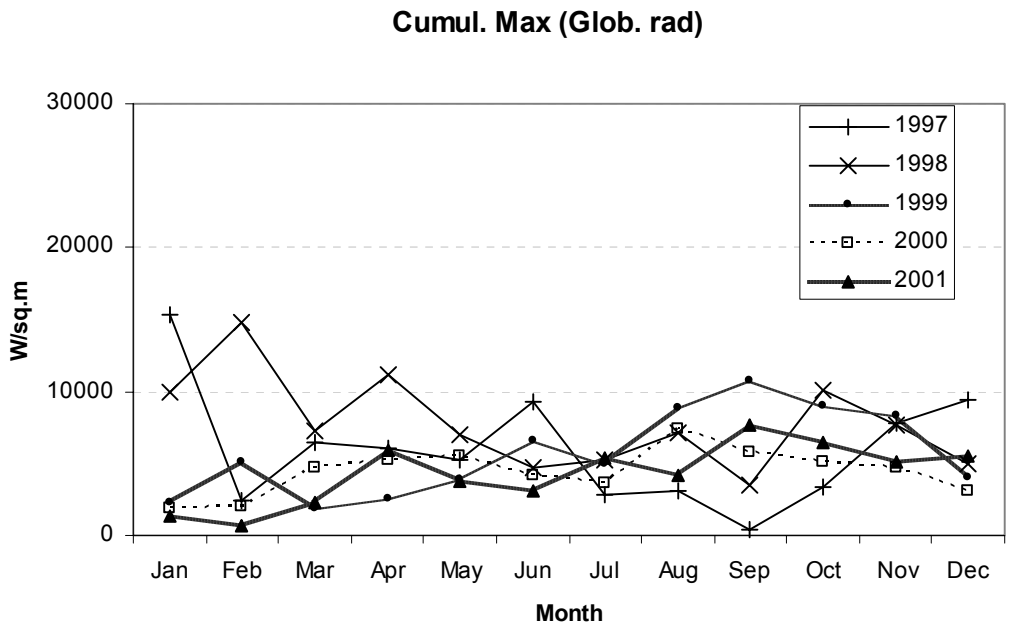

Figure 6.5 The cumulative amount by which the horizontal global radiation for each month of the year exceeds the maximum of the other years.

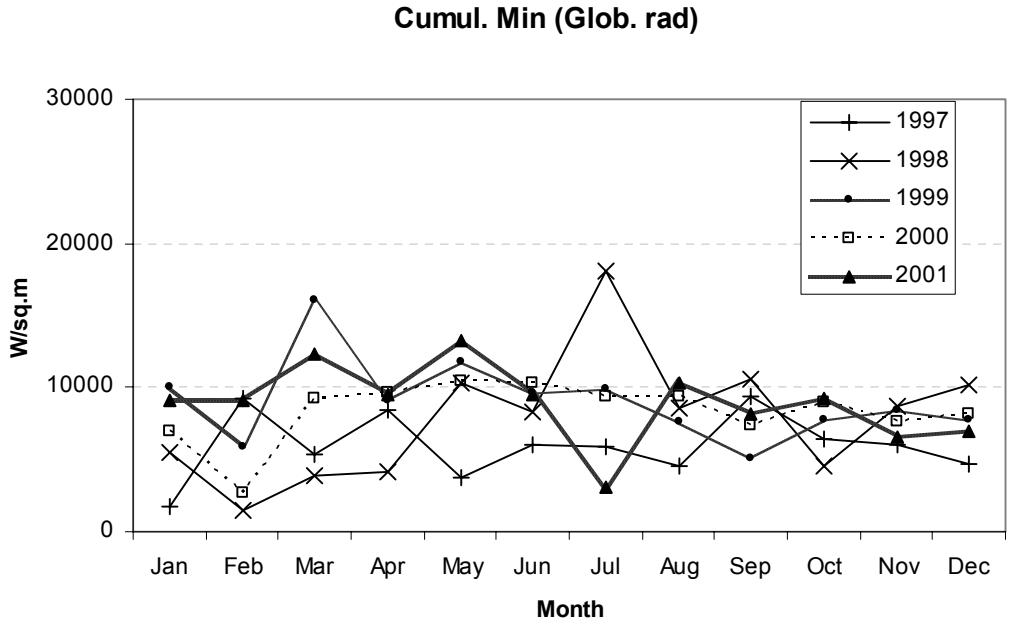

Figure 6.6 The cumulative amount by which the horizontal global radiation for each month of the year falls below the minimum of the other years.

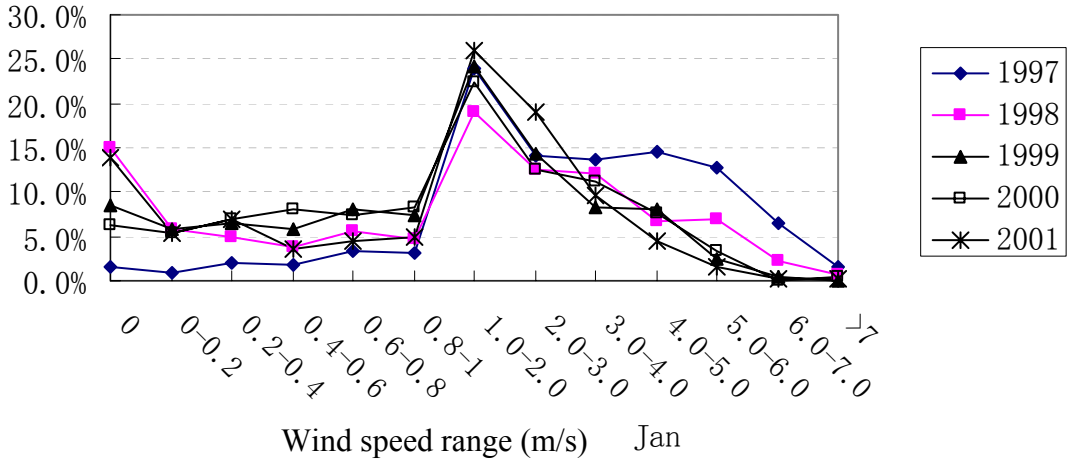

Figure 6.7 The frequency of occurrence of particular wind conditions in Jan.

6.1.2 Thermal analyses of typical year weather data

6.1.2.1 Wind data analyses

Thermal comfort chart (Feriadi, 2003) suggested that wind be used for passive cooling in hot-humid climate. Wind is a stochastic phenomenon that can change in a short period in both speed and direction. Figure 6.8 shows the distribution of selected ranges of wind speed over a whole year. Figure 6.9 reveals that on average, wind speed is low during the night time and early morning. The mean yearly wind speed is below 1m/s during the time 22:00-6:00 in a day while the ambient temperature is low. Figure 6.9 also shows that high wind speed usually occurs at noon time when the ambient temperature is high.

To illustrate the distribution of wind speed as a function of wind direction, wind rose graphs are plotted for each month of the typical year data. A wind rose graph for January is illustrated in Figure 6.10 as an example. Wind rose graphs for other months are shown in Appendix 2 (Appendix2.1-2.11). 0° indicates that the wind comes from due north direction

and 90° indicates that wind comes from due east direction. It is evident that the prevailing wind directions in Singapore are north and south over the whole year. Wind direction in the range of 270°- 30° dominates January, February, March, November and December with comparable high wind speed. Wind direction in the range of 120°-210° dominates May, June, July, August and September. In April, wind speed is relatively low and there is no prevailing wind direction. In October, wind direction is mainly in southwest (i.e.150°-210°, 240°-270°). Singapore is situated on the 1.2° north latitude and higher solar radiation occurs on east and west facing façades than on north and south facing façades. Unique monsoon conditions throughout the whole year with north or south direction provides naturally optimum façade designs for naturally ventilated buildings. This characteristic of the wind profile makes it possible for Singapore to achieve satisfactory thermal comfort in naturally ventilated buildings. It is recommended that large openings should be located in north and south sides for cross ventilation while appropriate building construction materials should be provided for east and west external walls to avoid high solar heat gain.

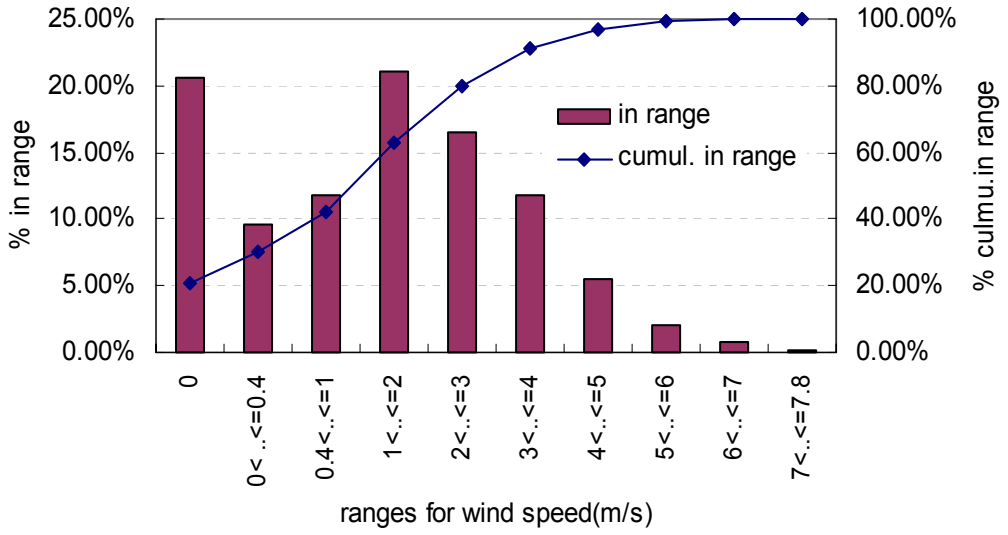

Figure 6.8 Frequency of wind speed in Year 2001

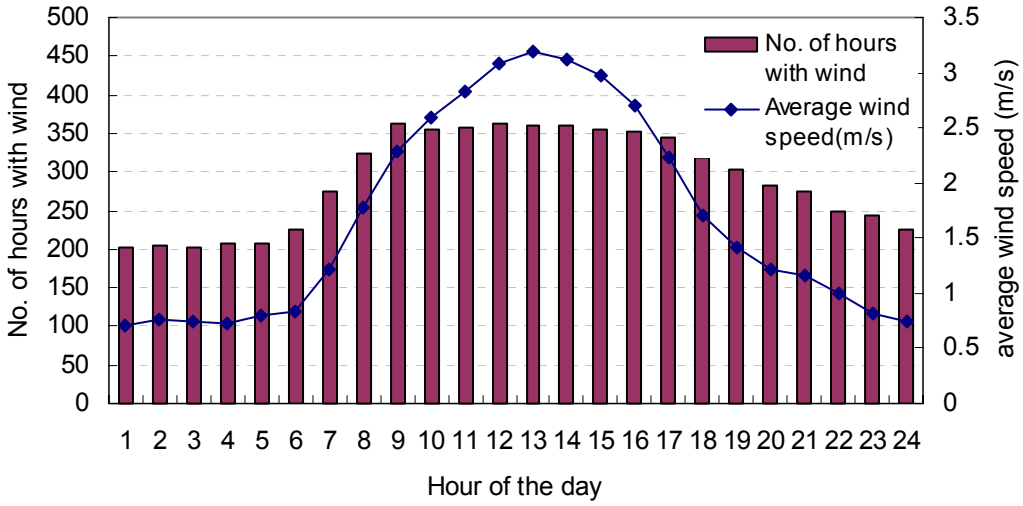

Figure 6.9 Average occurrence and wind speed distribution over 24 hours of a day in Year 2001

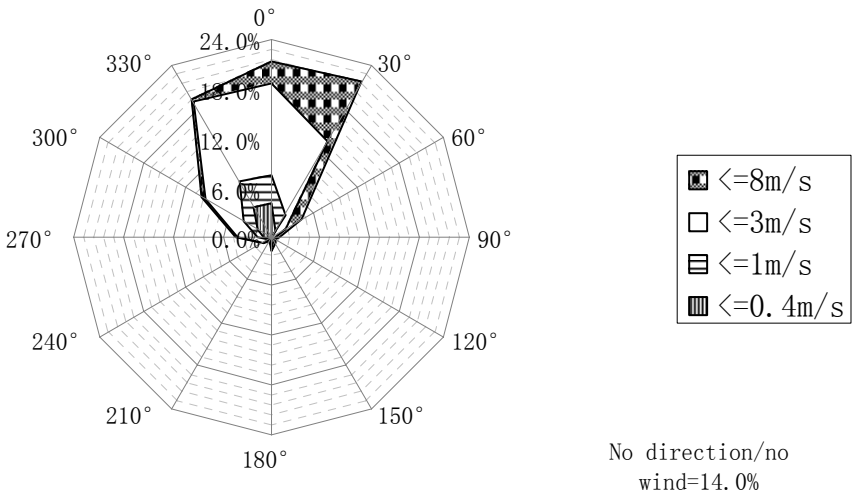

Figure 6.10 Frequency of wind speed above selected values per direction (Jan)

6.1.2.1 Thermal comfort prediction based on thermal comfort chart

In this approach, the outdoor air temperature is assumed to be equal to indoor air temperature and outdoor relative humidity is assumed to be equal to indoor relative humidity. The two hypotheses could be met when indoor heat sources are negligible. Conditions of the air represented by dry-bulb air temperature and relative humidity for outdoor climate have been

registered on the thermal comfort chart (Feriadi, 2003) to investigate the possibility of thermal comfort through natural ventilation in Singapore within each month.

Table 6.1 Percentage of hourly outdoor air out of neutral comfort zone in day or night

	% out of neutral comfort zone	
Month	Day	Night
Jan	27.0%	1.6%
Feb	13.4%	0.0%
Mar	26.1%	15.7%
Apr	45.1%	19.4%
May	51.5%	31.9%
Jun	38.2%	20.8%
Jul	36.4%	21.1%
Aug	40.1%	25.0%
Sep	32.4%	19.7%
Oct	28.0%	16.1%
Nov	25.8%	6.4%
Dec	20.3%	3.1%
Total	32.1%	15.2%

The hourly temperature and RH on Thermal comfort chart in February and May are illustrated in Appendix 3 (Figure App3.1 and Figure App3.2). It can be observed that weather conditions during the period of night time and rainy daytime are mainly on the top left of thermal comfort chart, in which thermal comfort is easy to be satisfied with low air velocity. Table 6.1 shows the percentage of hourly outdoor air condition out of neutral comfort zone (1m/s air velocity) in day or night. It can be seen from the results that about 67.9% daytime and 84.8% nighttime outdoor air conditions in the year are inside neutral comfort zone. Therefore, thermal comfort could be naturally satisfied within the ranges. The rest hours in the year are outside neutral comfort zone. The percentage out of neutral comfort zone is highest in May up

to 51.5% of daytime and 31.9% of nighttime. The lowest percentage 13.4% of daytime occurs in February.

6.1.2.2 Thermal comfort estimation on thermal comfort regression model

Thermal comfort is the outstanding criteria for natural ventilation evaluation. Thermal comfort regression model (Wang and Wong, 2005a), expressed by Equation 6.1, is employed.

$$PMV = -11.7853 + 0.4232 \times Temp - 0.57889V \quad (6.1) \text{ (same as Equation 2.3)}$$

where, *Temp* (℃) indicates the indoor air temperature and *V* (m/s) refers to indoor air velocity measured at 1.2 m above the ground. The term *PMV* refers to the average (mean) response of a group exposed to a given climatic conditions rather than individual responses.

The indoor air temperature is assumed to be the same as the outdoor environment temperature in this thermal comfort estimation approach. The required air velocity for the indoor thermal comfort (consider the neutral condition PMV=0) was calculated based on the regression model. The monthly average required indoor air velocity for thermal comfort has been shown in Figure 6.11. High air velocity (0.8-1.2 m/s) is frequently required to reach thermal comfort at noon time (11:00-14:00).

According to the required air velocity and outdoor wind speed, the required velocity coefficient Cv in Singapore for each month in typical year was calculated, as shown in Figure 6.12. Higher Cv requirements occur in April (0.66) and June (0.61) around 9:00 am in the morning. During the night time and early morning (after 21:00 or before 7:00), the required Cv (around 0.1-0.2) for thermal comfort is much lower.

However, there are 154 hours in the typical year, in which air velocity is required but the wind speed outside is below detection limit. During these hours, thermal comfort has to be achieved by other means such as appropriate construction materials and shading devices or mechanical ventilation if needed.

The required air velocities and air velocity coefficients for indoor thermal comfort obtained from climate analyses can be used for façade designs for naturally ventilated buildings in Singapore.

Based on the thermal analyses with thermal comfort chart and regression model, it can be noticed that there are two strategies to achieve satisfactory thermal comfort. Firstly, with suitable façade designs of qualified construction materials and shading devices, indoor temperature could be reduced comparing with outdoor temperature. Secondly, optimizing window to wall ratio to provide high airflow rates compensates high temperatures. In addition, thermal comfort zone is wider than neutral zone (Feriadi, 2003). Nicol and Humphreys (2002) indicated comfort zone may be much wider when adaptive opportunities such as changing clothing or opening windows are adopted for naturally ventilated buildings. Therefore, it is applicable to achieve satisfactory indoor thermal comfort by natural ventilation in Singapore with smart façade designs in residential buildings, with negligible heat sources.

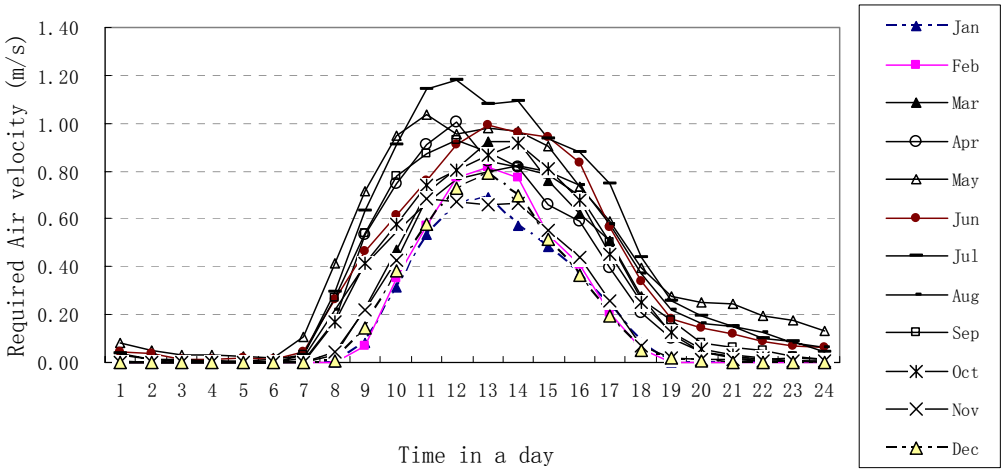

Figure 6.11 Required average monthly indoor air velocity in a day

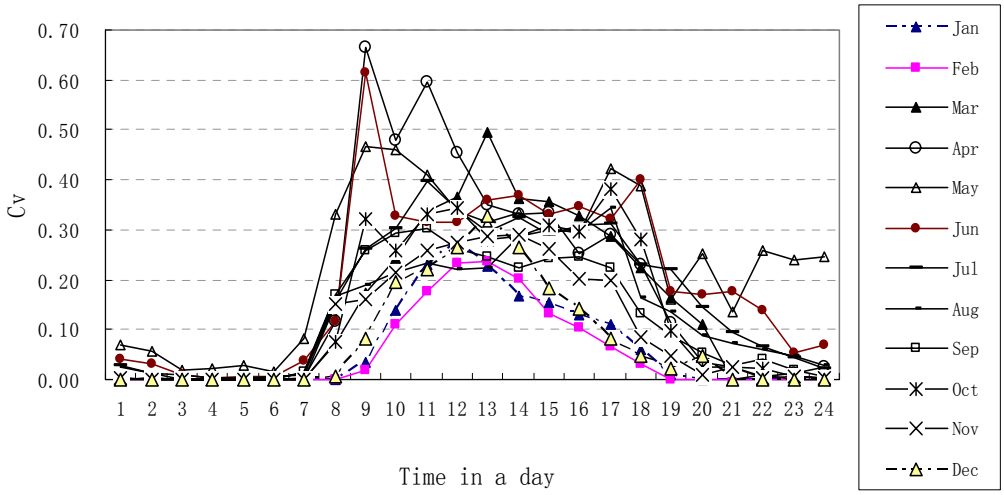

Figure 6.12 Required average monthly Cv distribution in a day

6.2 U-value determination

Thermal resistance of façade plays an important role in reducing solar heat gain and maintaining a good indoor thermal environment. As Singapore is located in the tropical region, the indoor thermal comfort is highly concerned by the occupants, especially in the non-air-conditioned buildings. However, there is no clear standard for U-value of façade materials for naturally ventilated buildings. Therefore, it is necessary to investigate on the impacts of U-value of facade materials on indoor environment for the non-air-conditioned buildings. Since thermal impacts of U-value are mainly on indoor location nearby openings

and the impacts of facade material properties on indoor averaged thermal environment (centre of the room) are relatively small, thermal impacts of U-value are investigated near the openings (within 200mm distance from openings in room).

High rise residential building HDB274C model (Figure 6.13 and Figure 6.14) was built for the parametric studies on U-values by a series of TAS simulations. A bedroom with one external wall at the 10^{th} floor in the buildings is selected as the simulation subject. In this study, U-value ranges from 1.5 W/K·m^2 to 3.5 W/K·m^2 at 0.5 intervals. WWR (Window to Wall Ratio) varies from 0.1 to 0.4. Three orientations: north, east and west are investigated. The indoor ambient temperature and mean radiant temperature near the openings are affected by changing the U-value. The criterion that temperature difference between mean radiant temperature and indoor ambient air temperature should be less than 2 degrees (Chrenko, 1953) to avoid the perception of thermal asymmetry by occupants is adopted to evaluate the thermal performance of external wall with various U-values. In the simulation, the weather file 2001 was adopted. The hottest day in typical year 2001 was selected. The highest solar radiation was 979w/m^2 and outdoor ambient temperature was 33.8 °C.

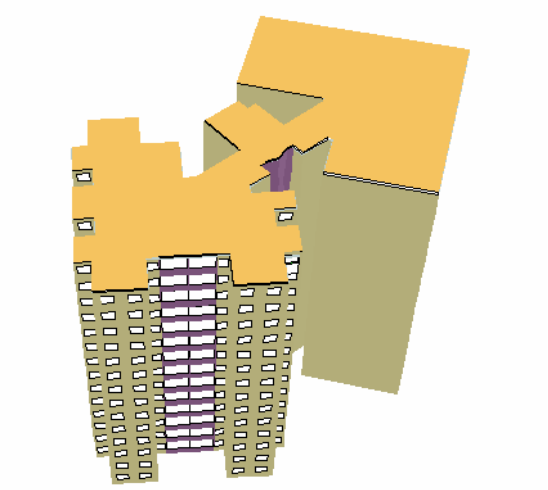

Figure 6.13 HDB274C model in TAS simulation

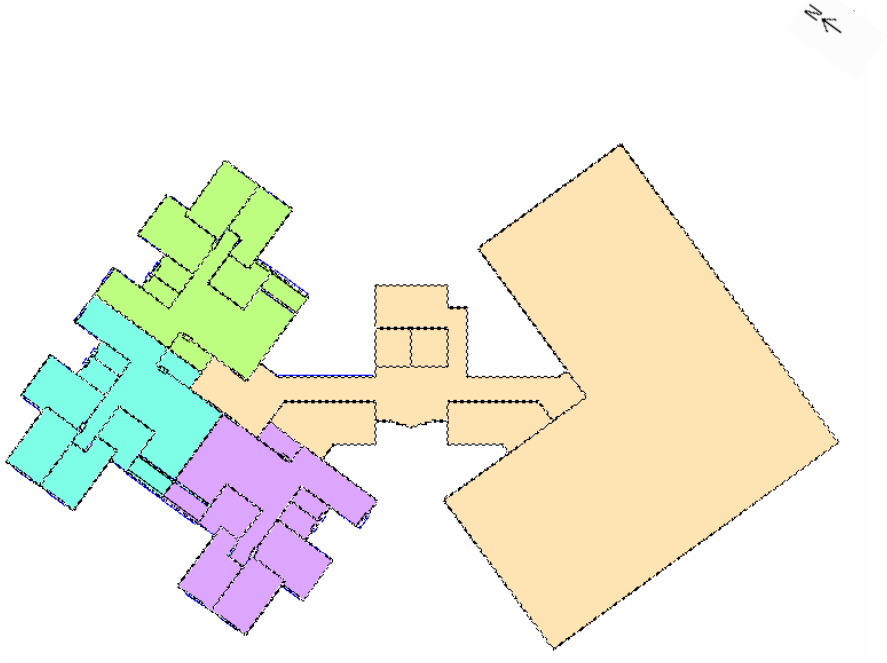

Figure 6.14 Floor plan and indoor layout of Jurong west Block 274C

6.2.1 East oriented external wall

Figure 6.15 shows the difference between the indoor mean radiant temperature and ambient temperature (ΔT) when WWR=0.1. When the U-value of external wall was kept below 2W/m^{2}K, the ΔT was less than 2°C during most time except in the morning and late evening. In the late evening, since the ambient air temperature is low, it cannot be concluded that the indoor thermal comfort is not satisfied due to higher ΔT (>2°C). In the morning period, it is noticed that even the U-value of external wall is 1.5W/m^{2}K, the ΔT is still as high as 3.5℃. Thus, window shading device is added to reduce the temperature difference between MRT and ambient temperature.

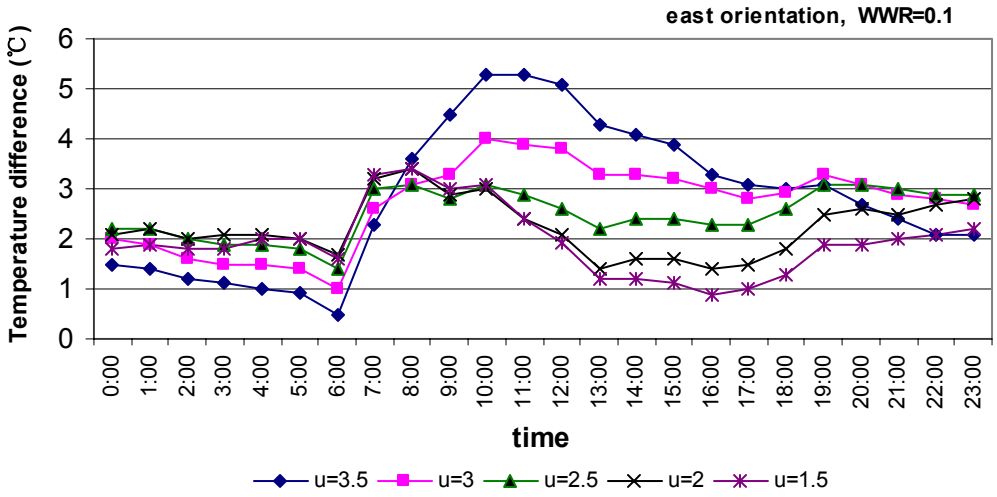

Figure 6.15 Difference between mean radiant temperature and indoor ambient temperature (WWR=0.1)

Figure 6.16 shows the ΔT when the U-value of external wall is 2 W/m^{2}K, and the window shading devices are applied for the window with a WWR value of 0.1. It can be seen using the 300mm horizontal window shading device dramatically decreases the ΔT comparing with the situation that there is no shading device. Hence, the 2 W/m^{2}K is the acceptable U-value for east oriented external wall with a WWR value of 0.1 and the 300mm horizontal shading device has to be used at the same time.

Figures 6.17-6.19 show the effect of window shading device when the U-value of east external wall is 2 W/m^{2}K and the window size varies from WWR=0.2 to WWR=0.4. From Figure 6.17, it can be observed that when the WWR is increased from 0.1 to 0.2, the ΔT can be controlled under 2°C when the external wall has a U value of 2 W/m^{2}K and a 300mm horizontal window shading device is used. Figure 6.18 shows that when the window size is increased to WWR=0.3, the 900mm shading device can provide good effect. However, from Figure 6.19, it can be observed that when the WWR is 0.4, ΔT exceeds 2°C slightly during the morning, even though the 900mm shading device is adopted.

In conclusion, suitable U-value for east external wall is less than 2 W/m^{2}K. Window shading device is necessary as long as there is window on the external wall. When the WWR is less than or equal 0.2, 300mm horizontal shading is enough. When the WWR=0.3, 900mm horizontal shading has to be used to control the ΔT under 2℃ for all the hours. When the WWR is larger than 0.4, indoor thermal comfort cannot be ensured in during morning hours.

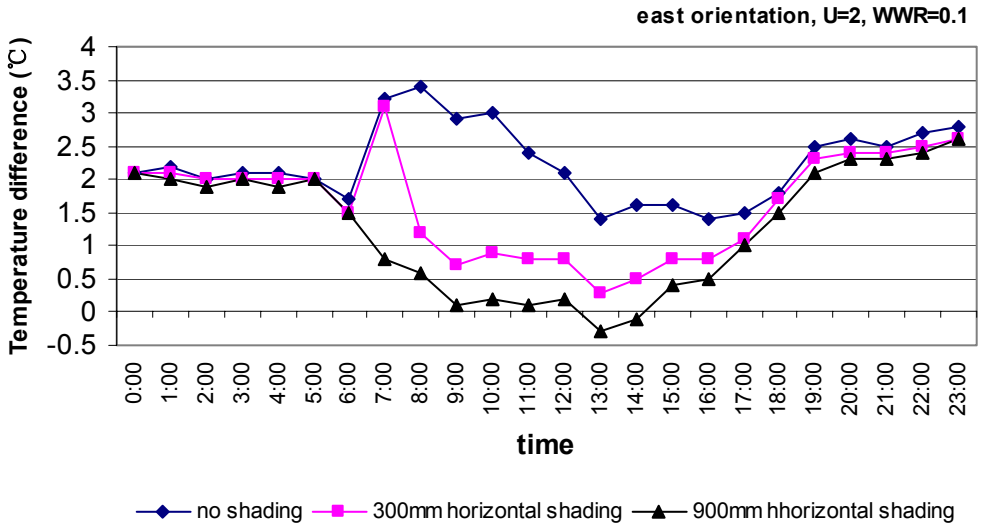

Figure 6.16 Difference between mean radiant temperature and ambient temperature when the window shading device was adopted (WWR=0.1)

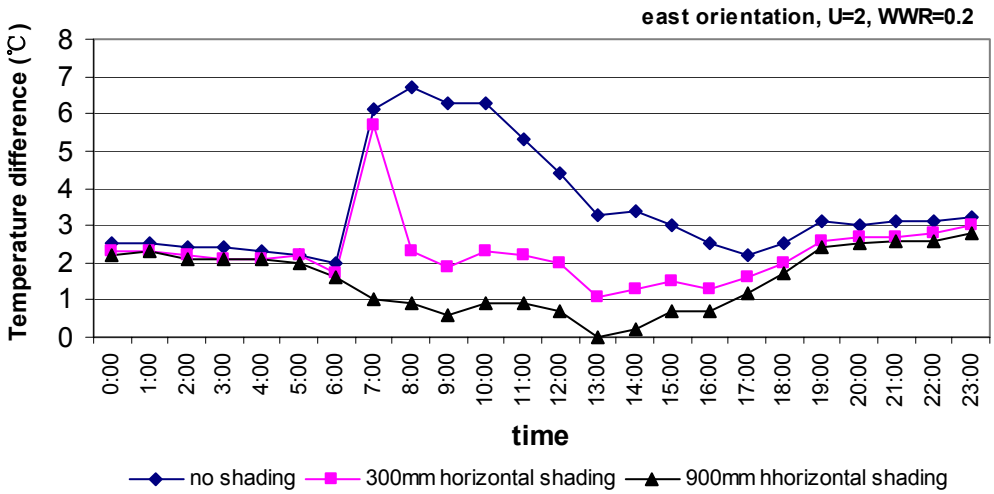

Figure 6.17 Difference between mean radiant temperature and ambient temperature when the window shading device was adopted (WWR=0.2)

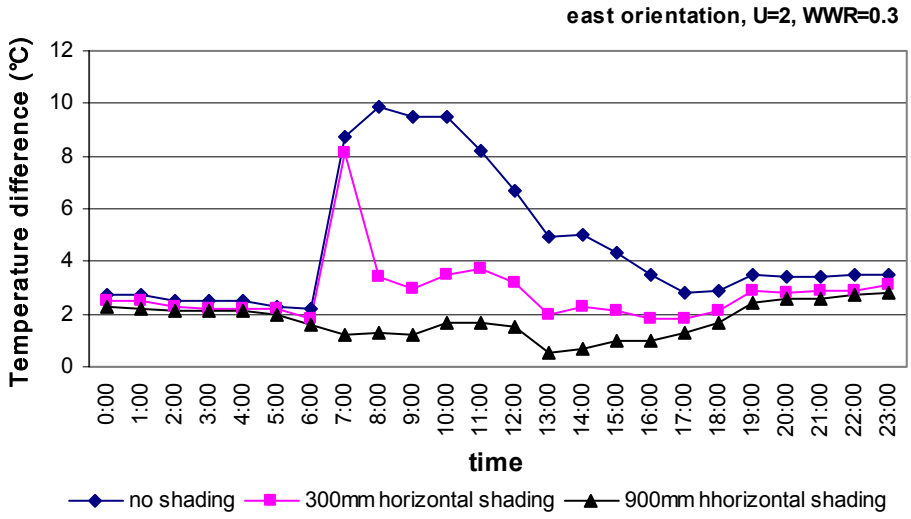

Figure 6.18 Difference between mean radiant temperature and ambient temperature when the window shading device was adopted (WWR=0.3)

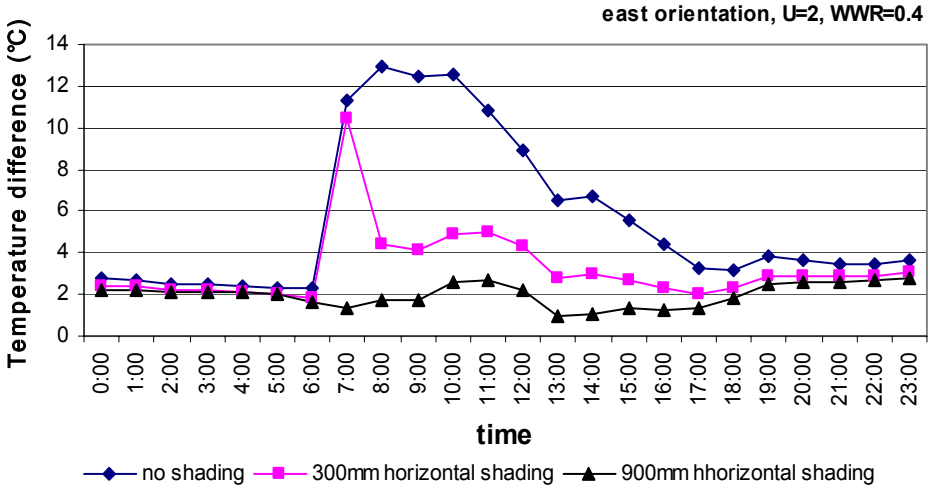

Figure 6.19 Difference between mean radiant temperature and ambient temperature when the window shading device was adopted (WWR=0.4)

6.2.2 West oriented external wall

Figure 6.20 shows the difference between the indoor mean radiant temperature and ambient temperature (ΔT) when WWR=0.1. From Figure 6.20, it can be observed that, when the U-value of west external wall is 2 W/m^{2}K, ΔT is less than 2°C during the whole day except in the late evening.

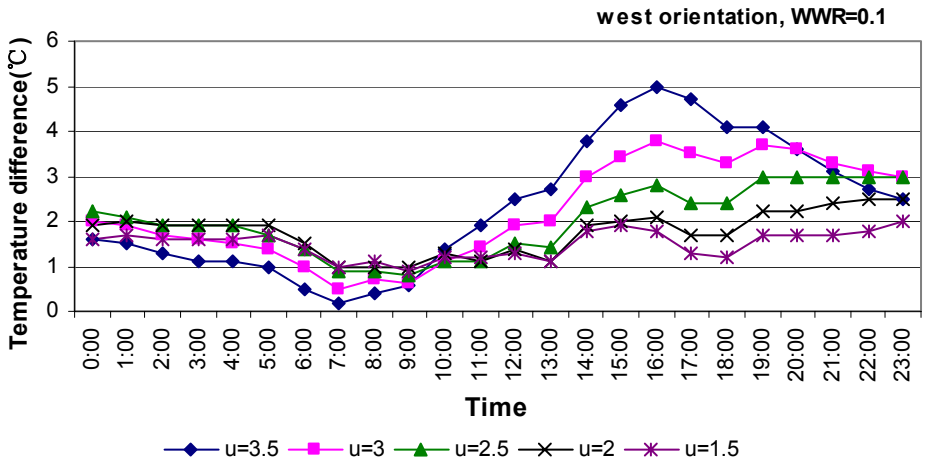

Figure 6.20 Difference between mean radiant temperature and indoor ambient temperature (WWR=0.1)

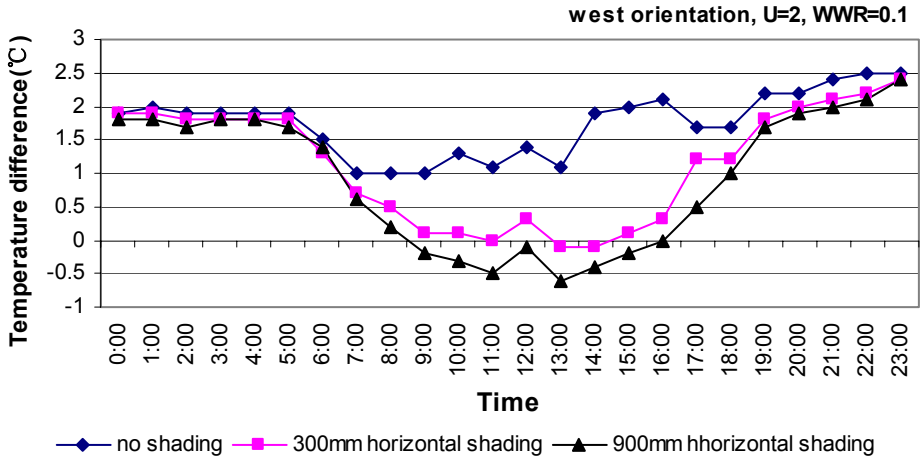

Figure 6.21 Difference between mean radiant temperature and ambient temperature when the window shading device was adopted (WWR=0.1)

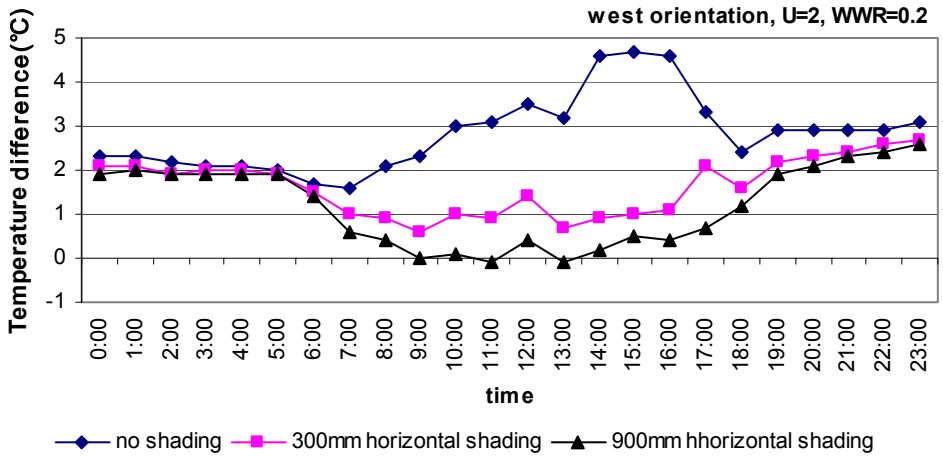

Figure 6.22 Difference between mean radiant temperature and ambient temperature when the window shading device was adopted (WWR=0.2)

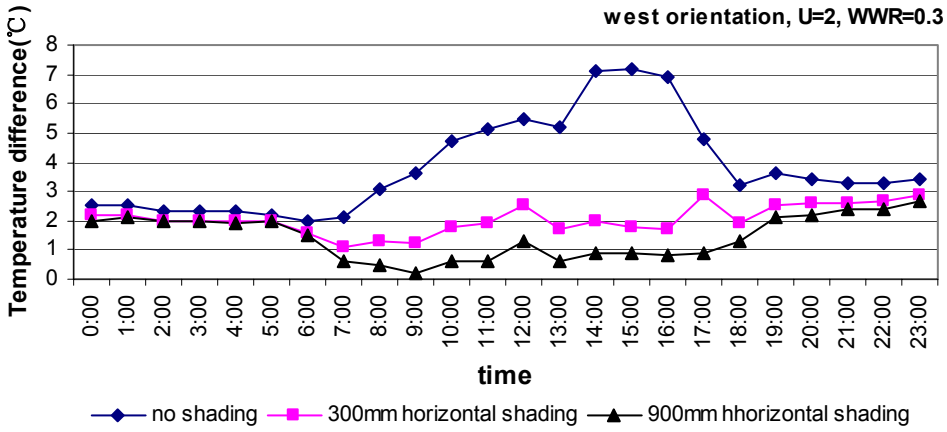

Figure 6.23 Difference between mean radiant temperature and ambient temperature when the window shading device was adopted (WWR=0.3)

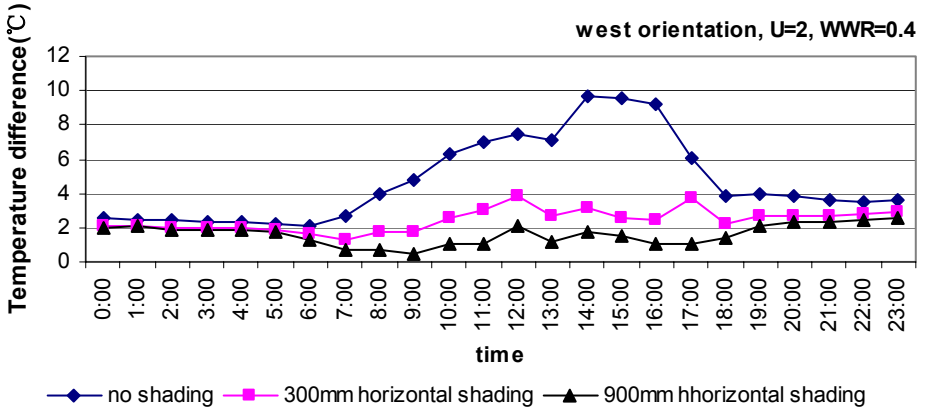

Figure 6.24 Difference between mean radiant temperature and ambient temperature when the window shading device was adopted (WWR=0.4)

Figures 6.21-6.24 show the effects of window shading devices for the west oriented windows. It can be observed from Figure 6.21 and Figure 6.22 that when the U-value of west external wall is 2 W/m^{2}K and WWR=0.1 and 0.2, ΔT can be controlled under 2°C during the entire day with 300mm horizontal window shading device. Figure 6.23 and Figure 6.24 show that when WWR is larger than or equal to 0.3, 900mm horizontal shading device is necessary to avoid thermal asymmetry.

6.2.3 North oriented external wall

Figure 6.25 shows ΔT as a function of time when WWR=0.1. When the U-value of north external wall is 2.5 W/m^{2}K, ΔT is always below 2°C before 7pm. As explained before, that the ΔT is greater than 2°C at night does not necessarily indicate that the indoor thermal comfort is not good because ambient air temperature is relatively low at night. Hence, 2.5 W/m^{2}K is assumed as the suitable U-value for the north oriented external.

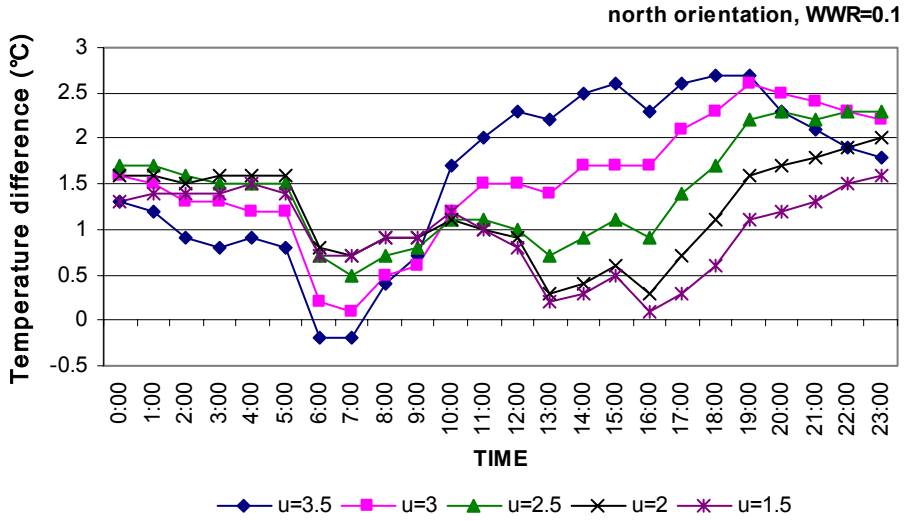

Figure 6.25 Difference between mean radiant temperature and indoor ambient temperature (WWR=0.1)

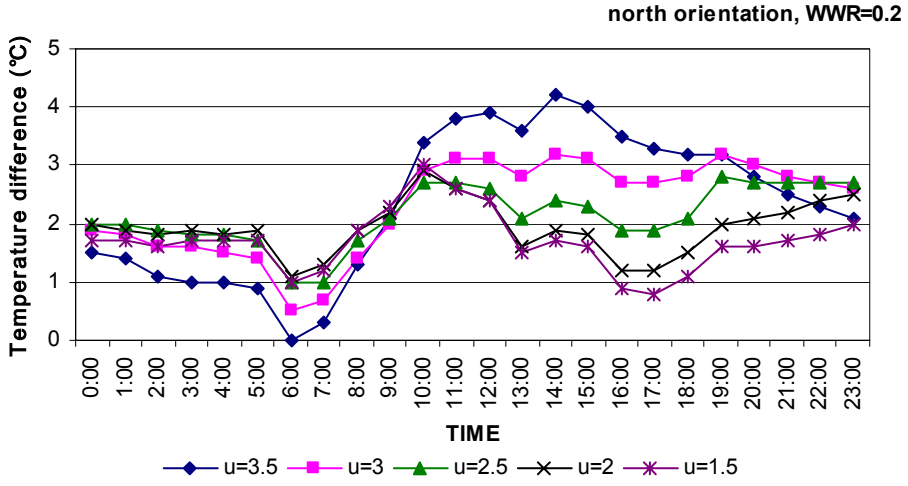

Figure 6.26 Difference between mean radiant temperature and indoor ambient temperature (WWR=0.2)

Figure 6.26 show the ΔT when WWR=0.2. It can be observed that when the window size was increased to WWR=0.2, ΔT exceeds 2°C in late afternoon and thus, shading device is required.

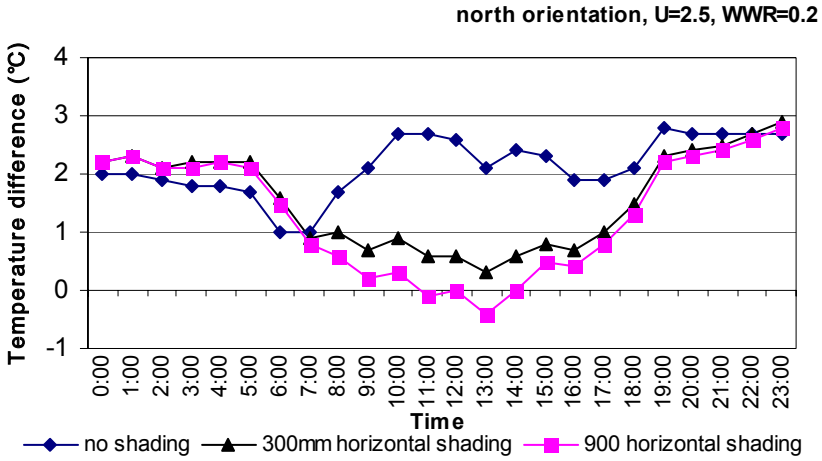

Figure 6.27 Difference between mean radiant temperature and ambient temperature when the window shading device was adopted (WWR=0.2)

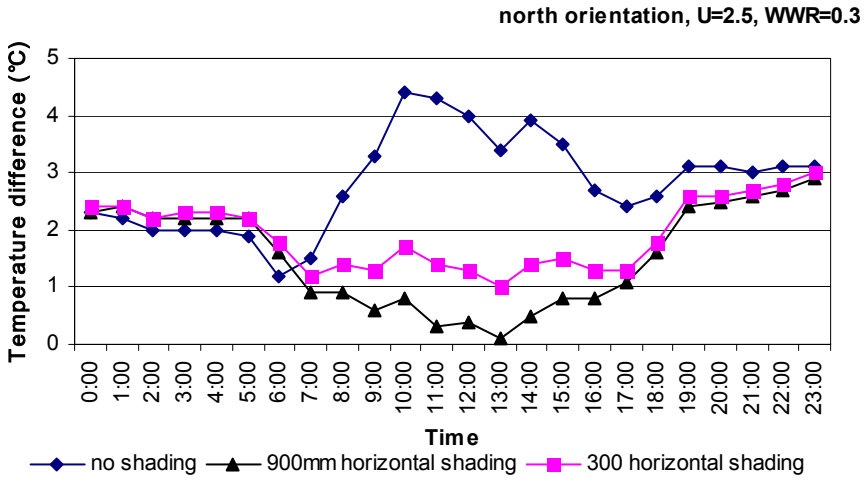

Figure 6.28 Difference between mean radiant temperature and ambient temperature when the window shading device was adopted (WWR=0.3)

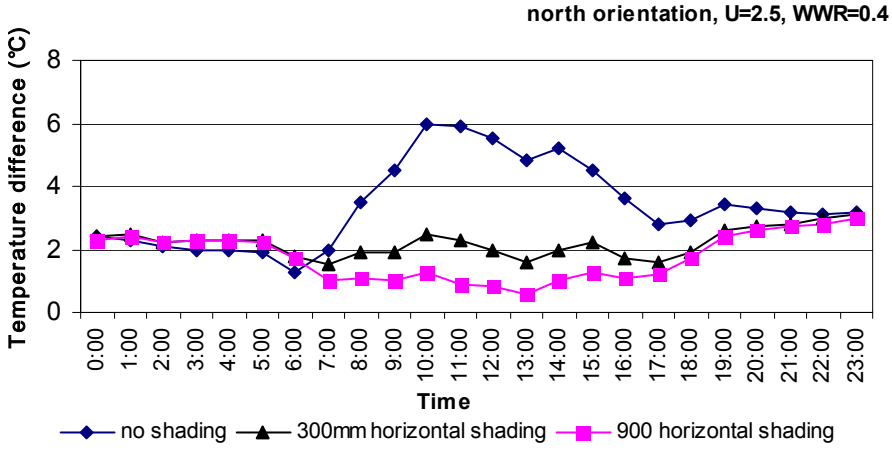

Figure 6.29 Difference between mean radiant temperature and ambient temperature when the window shading device was adopted (WWR=0.4)

Figures 6.27-6.29 show that when the U-value of north external wall is 2.5W/m^{2}K and the WWR is less than 0.4, 300mm horizontal shading device is enough to maintain a good indoor thermal comfort.

Since the solar radiation on north orientation is very similar with that on south orientation for equatorial regions, the results of suitable U-value and shading device performance obtained above are also available for the south orientation. Hence, from the analyses above, it can be concluded that for the north and south orientation, the suitable U-value for external wall is 2.5 W/m^{2}K. The window shading device is needed when WWR=0.2. 300mm horizontal shading is enough for the window when WWR is less than or equal to 0.4.

6.2.4 The acceptable U-value for facade

Required U-value of facade materials for naturally ventilated buildings is summarized.

Table 6.2 Acceptable U-value

	East Orientation	**West orientation**	**North orientation**	**South orientation**
WWR=0.1	U=2W/m^{2}K **300mm** horizontal shading	U=2W/m^{2}K **300mm** horizontal shading	U=2.5W/m^{2}K No shading is needed	U=2.5W/m^{2}K No shading is needed
WWR=0.2	U=2W/m^{2}K **300mm** horizontal shading	U=2W/m^{2}K **300mm** horizontal shading	U=2.5W/m^{2}K **300mm** horizontal shading	U=2.5W/m^{2}K **300mm** horizontal shading
WWR=0.3	U=2W/m^{2}K **900mm** horizontal shading	U=2W/m^{2}K **900mm** horizontal shading	U=2.5W/m^{2}K **300mm** horizontal shading	U=2.5W/m^{2}K **300mm** horizontal shading
WWR=0.4	U=2W/m^{2}K **900mm** horizontal shading	U=2W/m^{2}K **900mm** horizontal shading	U=2.5W/m^{2}K **300mm** horizontal shading	U=2.5W/m^{2}K **300mm** horizontal shading

6.3 Thermal comfort evaluation by coupled simulations for facade design parametric studies

In previous section, it was found that U-value for the east and west facing facade should be no more than 2W/m^{2}k and for north and south should be no more than 2.5W/m^{2}k to avoid the perception of asymmetry near openings. Preliminary study (Wang and Wong, 2005b) with a series of building simulations in Singapore indicates full day ventilation is an effective ventilation strategy for hot-humid climate.

However, indoor air velocity, one of the significant parameters in thermal comfort for naturally ventilated buildings, cannot be accurately predicted and fully addressed by building simulation alone. Therefore, the impacts of window sizes on indoor air velocity cannot be accurately predicted by building simulations. With the aids of the developed coupling program in Chapter 5, coupled simulations between building simulations and computational fluid dynamics can quickly and accurately predict indoor thermal environment for natural ventilation studies.

In the following parametric study, three prominent facade design parameters, including orientations, window to wall ratios and shading device dimensions, are investigated by coupled simulations between building simulation (ESP-r) and CFD simulation (FLUENT). Thermal comfort regression model (Equation 6.1) for Singapore is used to evaluate different facade designs.

Since the coupled simulations involve computational fluid dynamics to improve resolution and accuracy of the results, the computational time is also increased. Currently, coupled simulation for the whole typical year takes about one and a half to two-month computation time for one particular zone. Thus, it may not be realistic to optimize various facade designs based on simulation results for the whole year. In this parametric study, the two methods: typical-week method and typical-hour method are adopted to predict indoor thermal environment with various façade designs based on thermal comfort index.

HDB building block601, west coast, the same one used for field measurement and further validation of the coupled simulations described in Chapter 5 is used in this parametric study. A typical living room in the HDB residential buildings on the sixth floor, which holds one external wall, is the targeted subject for the parametric study. The layout of the HDB unit is shown in Figure 6.30. The living room has five openings: one window within the facade, one door connected with kitchen and the other three doors are connected with bedroom 1, bedroom 2 and bedroom 3, respectively. The window and door connecting to the kitchen are assumed to be fully open and the other three doors connected with bedrooms are assumed to be close. The window within the facade in kitchen is assumed to be fully opened for 24 hours.

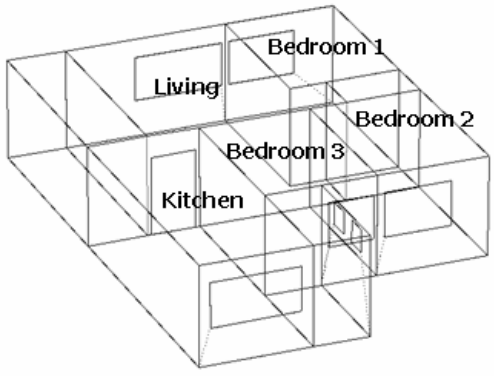

Figure 6.30 The layout of the four-room HDB unit

6.3.1 Thermal comfort evaluation by typical-week method

Two typical weeks in May (dry season) and October (raining season) are selected to test for thermal comfort with various façade designs. From the climatic data analyses in Singapore that is described in previous sections, the largest percentage of thermal discomfort in the typical year occurs in May for Singapore. The choosing outlines of typical weeks in the two months are listed as follows:

a) The number of instances where the global radiation, dry bulb temperature, or wind speed in a particular hour in the week exceeds the maximum or falls below the minimum of the other weeks is added.

b) The differences in the amount of global radiation, dry bulb temperature and wind speed for each of the above instances are added separately for those above the maximum or below the maximum values.

By detailed comparisons of the above parameters, any unusual traits in the day of the week for each hour can be detected. Two typical weeks (18th -24th May and 18th -24th Oct) are selected for long term indoor thermal comfort evaluation. The percentage of hours within the thermal comfort zone in each typical week is taken as the criteria for façade design evaluation.

In this parametric study, the combination effects of several façade design parameters in naturally ventilated buildings, including four different orientations (north, south, west and east), three various window to wall ratios (0.12, 0.24 and 0.3) and three horizontal shading

dimensions (0, 600mm, 900mm), are taking into considerations. The window to wall ratio in kitchen is the same as the one in the investigated living room. Concrete hollow block wall, which is widely used in building construction in Singapore, is taken as both external and internal wall materials in the building. Thermal transmittance of the 100mm concrete hollow block wall is 1.89 W/m^2K. Indoor heat sources including equipments, lighting, and occupants are negligible in the unit. In total, twenty-six various façade design scenarios were investigated and fifty-two cases were simulated for indoor thermal comfort evaluation for the two typical weeks in dry and raining seasons.

6.3.1.1 Demonstration of simulation results with coupling program

With coupled simulations, indoor thermal environment can be predicted in details. The results for an hour case with the aids of the coupling program are shown here for demonstration. It is 9 AM on 18th May with the ambient temperature of 30.7 ℃ and wind direction 77º and wind speed of 1.4m/s. The demonstrated facade design case is east facing room with window to wall ratio 0.24 and no shading device. Figures 6.31-6.34 illustrate detailed indoor temperature, velocity magnitude, velocity vector and PMV index of the living room 1.2m above the floor, respectively. From the PMV index in Figure 6.34, it can be seen that indoor thermal comfort are non-uniform and the area with higher air velocity provides better indoor thermal comfort than the stagnant spaces.

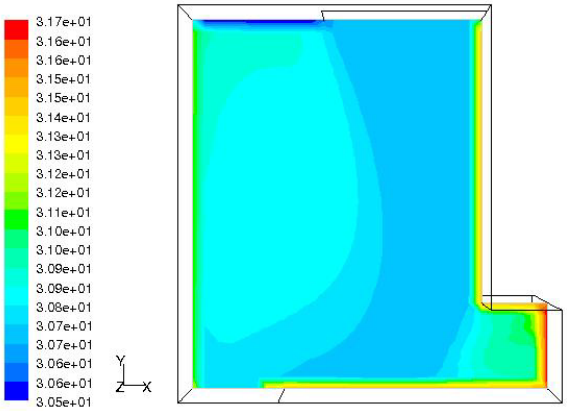

Figure 6.31 Contour of indoor temperature (℃)

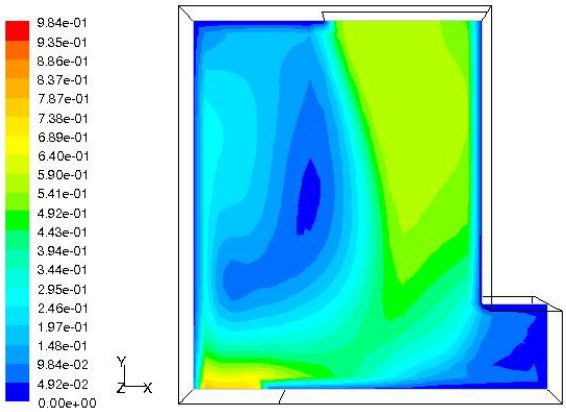

Figure 6.32 Contour of indoor velocity magnitude (m/s)

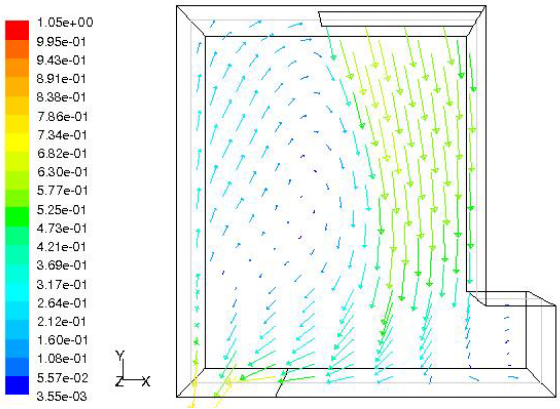

Figure 6.33 Velocity vectors colored by velocity magnitude (m/s)

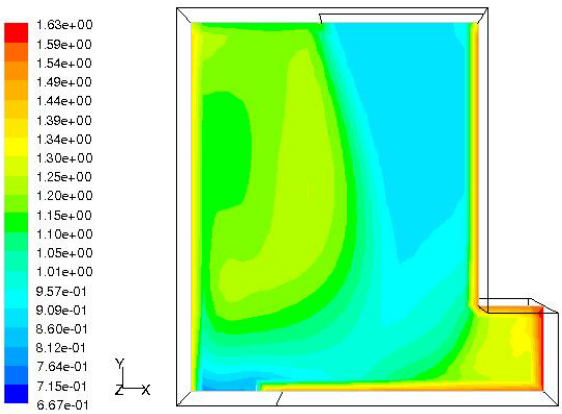

Figure 6.34 Contour of PMV (indoor thermal comfort index)

6.3.1.2 Thermal comfort percentage for various facade designs

A series of coupled simulations are carried out for twenty-six facade design options. Coupled simulations for each particular facade design are performed for two typical weeks (18th-24th May and 18th-24th Oct), and the simulation results for each case are analyzed based on thermal comfort index (Equation 6.1) and represented by thermal comfort percentage in both typical weeks.

The simulation results for satisfactory thermal comfort percentage in the two typical weeks are shown in Tables 6.4-6.7 for four different orientations. It can be seen from the results that south facing and north facing units have much better indoor thermal environment than east facing and west facing units in Singapore. The results also show that the thermal comfort conditions in raining season are much better than those in the dry season. This can be attributed to two reasons: the ambient temperatures in the raining season are normally lower than those in the dry season; and solar heat gains in the raining season are less since the raining season happens in the winter time.

Table 6.3 Thermal comfort percentage in two typical weeks in north orientation

WWR	SHADING	Thermal comfort percentage	
		Typical week in May	Typical week in Oct.
0.121	0	52.98	80.23
0.121	600	55.95	80.95
0.24	0	66.07	88.09
0.24	600	70.8	88.09
0.3	0	66.67	88.09
0.3	600	72.02	88.09

Table 6.4 Thermal comfort percentage in two typical weeks in south orientation

WWR	SHADING	Thermal comfort percentage	
		Typical week in May	Typical week in Oct.
0.121	0	72.62	81.54
0.121	600	72.62	83.33
0.24	0	78.57	83.9
0.24	600	78.57	86.9
0.3	0	77.97	84.52
0.3	600	77.97	86.9

Table 6.5 Thermal comfort percentage in two typical weeks in east orientation

WWR	SHADING	Thermal comfort percentage	
		Typical week in May	Typical week in Oct.
0.121	0	52.97	54.16
0.121	600	55.35	56.28
0.24	0	64.88	69.04
0.24	600	66.07	70.24
0.3	0	64.88	69.04
0.3	600	66.07	69.6
0.3	900	66.07	70.24

Table 6.6 Thermal comfort percentage in two typical weeks in west orientation

WWR	SHADING	Thermal comfort percentage	
		Typical week in May	Typical week in Oct.
0.121	0	46.42	57.14
0.121	600	46.42	58.93
0.24	0	53.57	62.27
0.24	600	54.17	64.28
0.3	0	53.57	63.09
0.3	600	54.17	63.09
0.3	900	55.35	63.09

As can be seen from the results (Table 6.3) in May, indoor thermal comfort environment can be largely improved by 13% with the increase of WWR from 0.12 to 0.24 and indoor satisfactory thermal comfort percentage is improved when shading device is added. However, when the window to wall ratio is further increased to 0.3, there is no obvious improvement in thermal conditions when shading device is not added. This is because the improvement in thermal comfort due to the increase of indoor air velocity with large window to wall ratios is cancelled by the increase of indoor temperature due to larger amount of heat gains through window openings. Therefore, shading devices for large openings are important to block direct solar radiations. As can be seen from the results, with the 600mm horizontal shading device above the window, indoor thermal comfort environment can be further improved. For the thermal conditions in October (rainy season), the effects of shading device on thermal comfort are not obvious.

Thermal comfort percentage in south orientation is shown in Table 6.4. Thermal comfort conditions for south facing room are generally good in both dry and raining seasons. There is an obvious improvement in thermal comfort when the window to wall ratios is increased to 0.24 and 600mm horizontal shading device is needed for better thermal comfort when solar is in the south hemisphere.

Table 6.5 and Table 6.6 illustrate the results of thermal comfort percentage for east and west orientations. Compared with the other two orientations, satisfactory thermal comfort percentages in the two typical weeks for east and west facing room are much lower. Same as north and south orientations, the increase of window to wall ratios to 0.24 can largely improve

indoor thermal comfort by increasing indoor air velocity. Horizontal shading devices are needed for both orientations to further improve the indoor thermal comfort. However, with the increase of the length of shading device to 900mm, thermal comfort percentage in the typical week in May for west orientation is still not satisfactory enough to meet thermal comfort requirements in most of the time. Under this condition, mechanical fans have to be used to improve indoor thermal comfort. Thus, east or west facing rooms should be avoided for residential buildings for the purpose of thermal comfort and energy consumption in Singapore. By any means, the improvement of façade designs in naturally ventilated buildings can largely alleviate the burden of energy crises and provide a natural and comfortable indoor environment.

In summary, the investigation on façade design parameters including orientations, window to wall ratios, and the dimensions of shading device recommends that south and north facing units have much better indoor thermal environment than east facing and west facing units in Singapore. The increase of window to wall ratio to 0.24 could improve indoor thermal conditions to a large extent. Horizontal shading devices are needed for the four orientations for further improvement in indoor thermal comfort.

6.3.2 Thermal comfort evaluation by typical-hour method

In order to provide facade design engineers or architects user-friendly tools to estimate the indoor thermal environment according to the particular design, the year 2001 weather data are used as typical weather conditions for this parametric study to build up indoor velocity

charts and thermal comfort index charts for various facade designs. The procedures of choosing typical weather conditions are as follows:

a) Hourly outdoor dry bulb temperature and solar radiation (Figure 6.35) in the typical year have been averaged based on the weather data for the whole year.

b) In this typical averaged day, the peek values on outdoor dry bulb temperature and solar radiation appear at twelve o'clock. This outdoor dry bulb temperature and solar radiation pair is taken as the elements of typical weather condition.

c) The wind data are divided into sixteen categories based on wind directions, in which eight categories (see Table 6.7): N(north), S(south), W(west), E(east), NW(northwest), NE(northeast), SW(southwest), and SE(southeast) are selected for typical weather conditions. Year-averaged wind speeds in these eight directions are used as wind data in this study.

d) Therefore, averaged wind data in eight wind directions combined with averaged outdoor dry bulb temperature and solar radiation pair are used for parametric facade design studies as typical weather conditions.

Table 6.7 Averaged wind data in sixteen wind directions in the typical year

Wind direction	0（N）	22.5	45 (NE)	67.5	90(E)	112.5	135(SE)	157.5
Mean (m/s)	1.715	2.74	2.534	1.89	1.888	2.675	2.7	2.46
Number of data points	563	703	377	156	151	204	380	444
Wind direction	180(S)	202.5	225(SW)	247.5	270(W)	292.5	315(NW)	337.5
Mean (m/s)	2.35	2.29	2.187	1.965	1.975	1.592	1.304	1.396
Number of data points	796	806	427	238	311	376	448	577

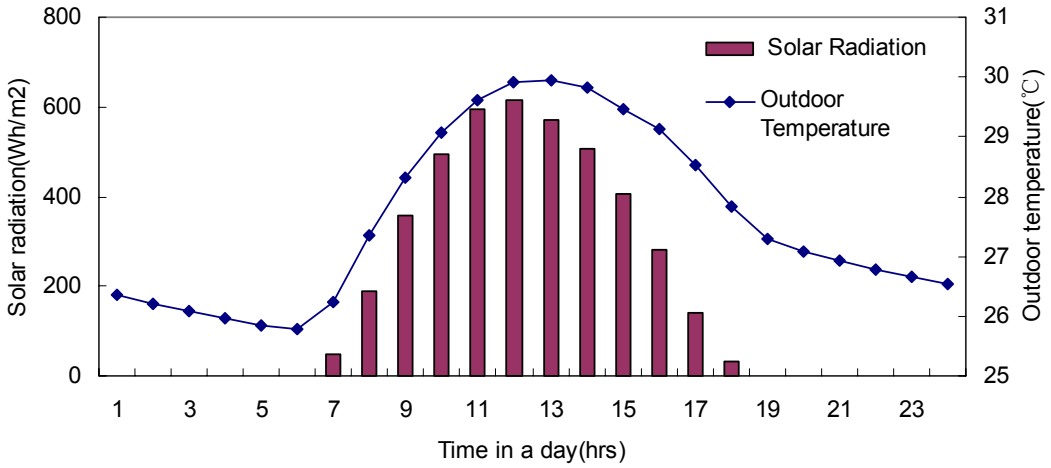

Figure 6.35 Outdoor average temperature and solar radiation profile in the whole year

In this parametric study, 48 cases were investigated for indoor thermal comfort. North, south, east and west orientations are investigated as the orientation parameter. Four WWR values, 0.12, 0.24, 0.3, and 0.36, are investigated for each orientation. Horizontal shading device lengths of 0 (no shading), 300 and 600mm are investigated for north and south orientation facades and device lengths of 0, 600 and 1200mm are investigated for east and west orientation facades. The window to wall ratio for the kitchen is taken to be the same as the one in living room when it is equal to 0.12, 0.24, and 0.3. When the window to wall ratio is equal to 0.36 for the living room, the window to wall ratio for kitchen remains to be 0.3. Thermal conductivity 1.89 W/m^2 K is chosen to be the thermal property of external hollow block wall.

Therefore, eight typical weather conditions (typical hours) are built up and set into weather data files. For each case, coupled simulations are executed for these typical hours.

6.3.2.1 Indoor air velocity results

The main parameter affecting indoor air velocity is the window size, which is expressed as WWR (window to wall ratios) in the study. Four different WWR values, 0.12, 0.24, 0.3 and 0.36 are investigated for cross ventilation. The window sizes are 1.2mx1.2m (WXH) for both sides (WWR=0.12), 2.4mx1.2m for both sides (WWR=0.24), 3mx1.2m (WWR=0.3) for both sides, and 3.6mx1.2m for one side, which is consistent with facade orientation and 3mx1.2m for the other side, which is in the opposite orientation (WWR=0.36). As shown in Figures 6.36-6.43, when the wind direction is strictly parallel to opening orientation, very little wind can be induced into the room. However, the wind speed is largely increased when wind direction is oblique to the openings. Another interesting result, which is rather counter intuitive, is that with the increase of WWR, indoor air velocities are not always increased. When WWR is increased from 0.3 to 0.36, indoor air velocities are either increased or decreased depending on wind directions and facade orientations. For example, in the north wind direction, when facade is north facing (inlet window size is larger than outlet size), the indoor air velocity is decreased as the WWR is increased to 0.36, but when the facade is south facing (inlet window size is smaller than outlet size), the indoor air velocity is increased as the WWR is increased to 0.36. Similar results can be observed for other wind directions, either normal or oblique to openings. It can be concluded from the results that large outlet window size can promote higher wind speed, which is consistent with the other studies (Allard, 1998). When the inlet size is the same as outlet size, with the increase of WWR, the indoor air velocity are increased.

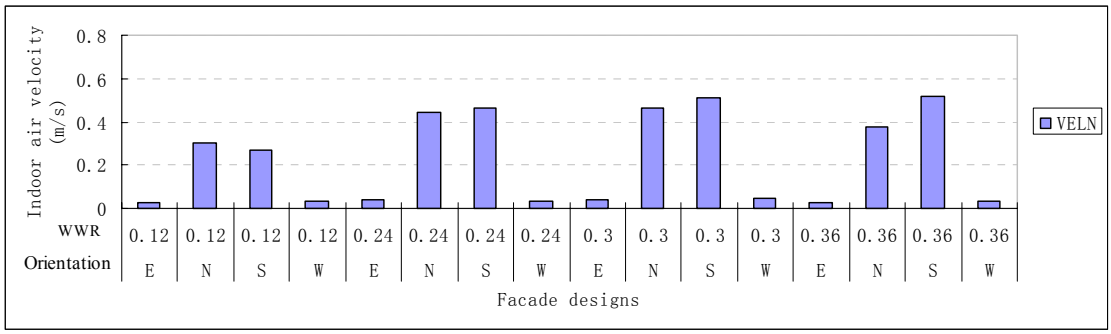

Figure 6.36 Averaged indoor air velocity with north wind direction for various designs

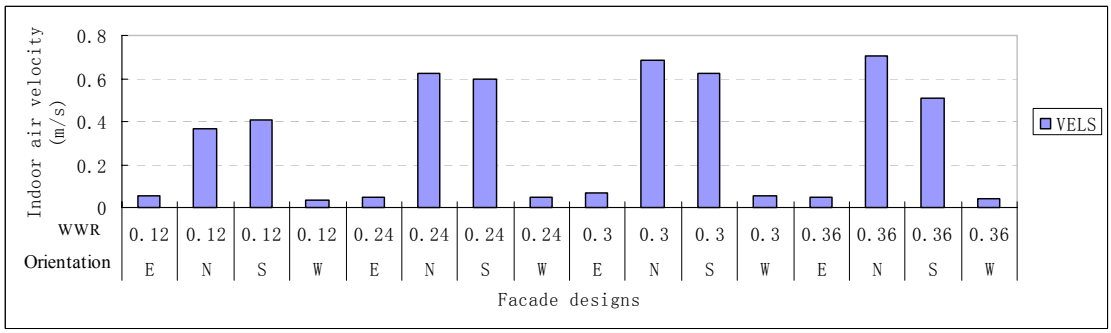

Figure 6.37 Averaged indoor air velocity with south wind direction for various designs

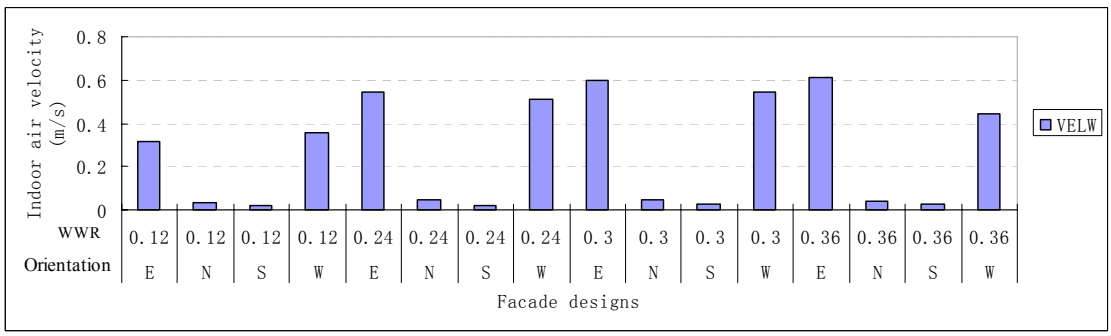

Figure 6.38 Averaged indoor air velocity with west wind direction for various designs

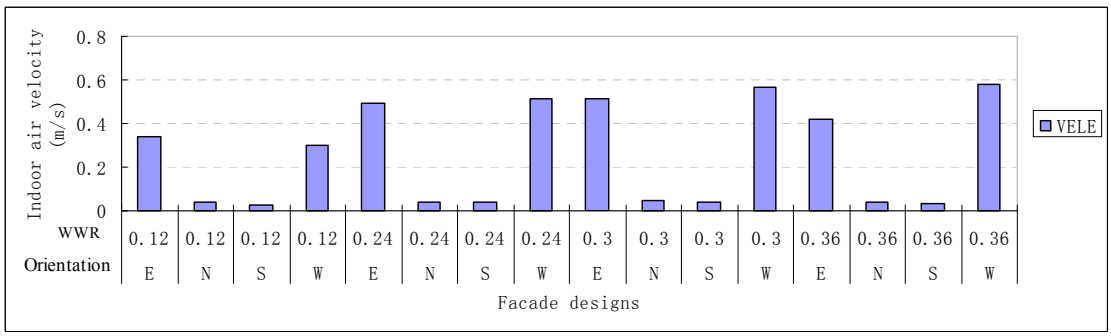

Figure 6.39 Averaged indoor air velocity with east wind direction for various designs

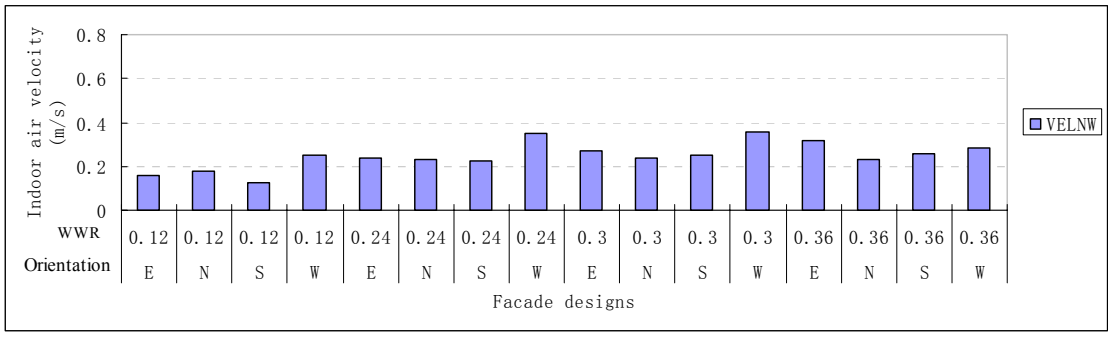

Figure 6.40 Averaged indoor air velocity with north west wind direction for various facade designs

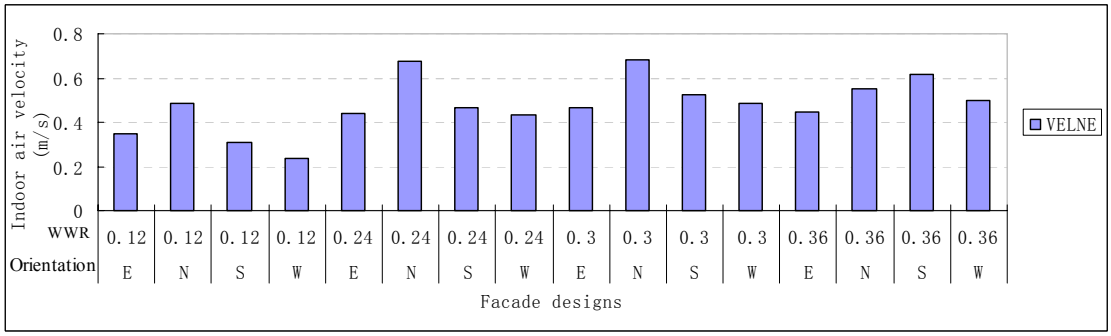

Figure 6.41 Averaged indoor air velocity with north east wind direction for various facade designs

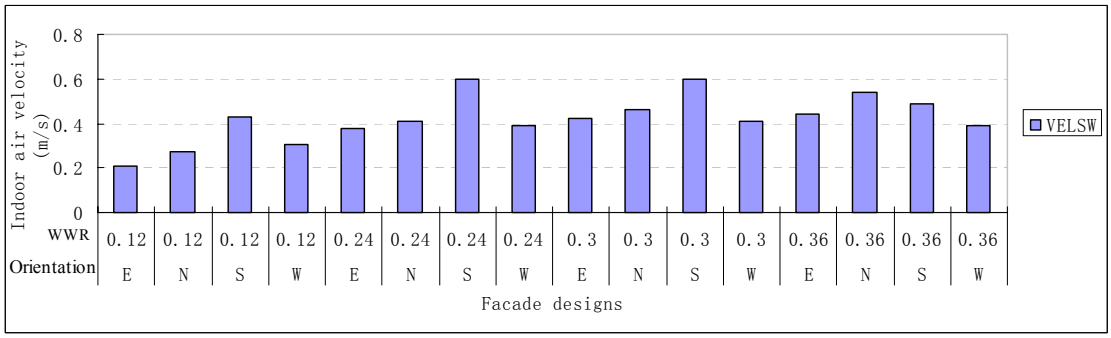

Figure 6.42 Averaged indoor air velocity with south west wind direction for various facade designs

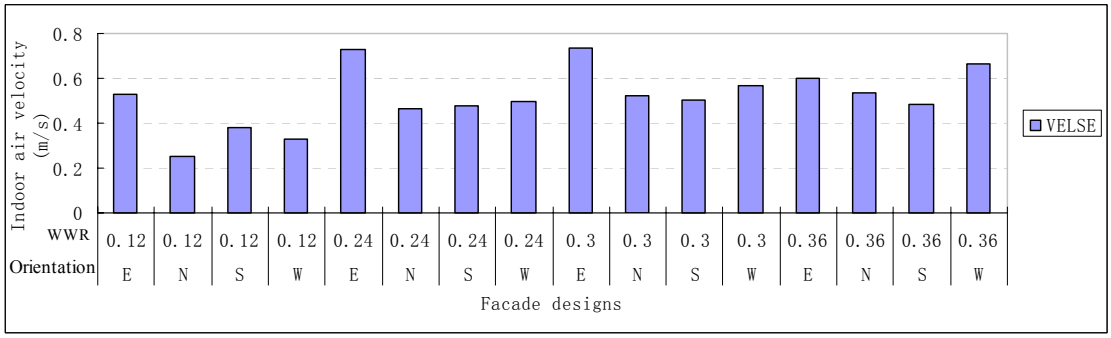

Figure 6.43 Averaged indoor air velocity with south east wind direction for various facade designs

However, for the naturally ventilated buildings in order to provide comfortable indoor thermal environment, it would be biased to particularly pursing high indoor air velocity as there is the risk that with the increase of fenestration sizes, the increase of solar heat gains and heat exchange with outdoor environment can result in thermal discomfort. Therefore, thermal comfort should be taken as a facade design criterion for natural ventilation and be clearly taken into consideration to give a comprehensive evaluation on indoor environment.

6.3.2.2 Mean radiant temperature distribution (MRT)

The distribution of mean radiant temperature for various facade designs in east facade orientation is illustrated in Figure 6.44. Indoor mean radiant temperature results for all the 48 cases are shown in Figure App.4.1. It can be seen from the results that MRT increases with the increases of window sizes. For east or west orientated facades, the effects of shading devices on the reduction of mean radiant temperature are significant, especially when the facade has large WWR. In this study, the shading device is only applied on the window that has the same facing with facade and there is no shading device for the opposite window. It can be seen from Figure 6.44 that comparing with the case that has a WWR value of 0.36 and without shading devices, the case with WWR=0.36 and 1200mm horizontal shading device can reduce indoor mean radiant temperature up to 1.2 degrees. Therefore, shading devices are strongly recommended for some worse facade orientations such west and east.

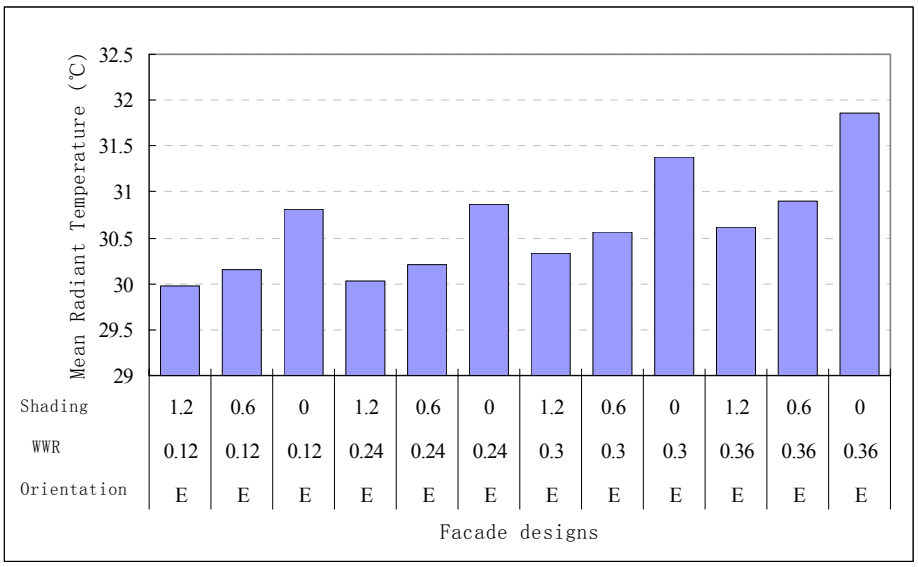

Figure 6.44 Mean radiant temperature distribution for various facade designs in east facade orientation

6.3.2.3 Thermal comfort distribution

In the following section, thermal comfort index for the eight wind directions are predicted based on coupled simulation results. Thermal comfort distributions are illustrated and analyzed for each wind direction.

1) North and south wind directions

North and south are the main wind directions for Singapore in the whole year. The optimum facade designs for each facade orientation with north and south winds are listed in Table 6.8 and Table 6.9, respectively. Thermal comfort distribution of eight cases (composed of maximum and minimum PMV cases for each façade orientation) is illustrated in Figure 6.45 for north wind direction and in Figure 6.46 for south wind direction. Detailed thermal comfort results for all the 48 cases are shown in Figure App.5.1 and Figure App.5.2 for north and south wind directions, respectively.

Table 6.8 Optimum facade designs for N S W E orientations with north wind

Orientation	Optimum WWR	Optimum Shading (horizontal)
N	0.36	300 mm
S	0.24	No shading is needed
W	0.12	1200mm above
E	0.12 or 0.24	1200mm above

Table 6.9 Optimum facade design for N S W E orientations with south wind

Orientation	Optimum WWR	Optimum Shading (horizontal)
N	0.36	No shading is needed
S	0.24	No shading is needed
W	0.24	1200mm above
E	0.12 or 0.24	1200mm above

According to thermal comfort results, the best facade design for north wind direction is WWR=0.36, south facing and with horizontal shading width 300mm and for south wind direction is WWR=0.36, north facing and without shading devices. Generally speaking, north and south facing facades can provide much better thermal comfort than west and east facing facades and thus should be considered as priority.

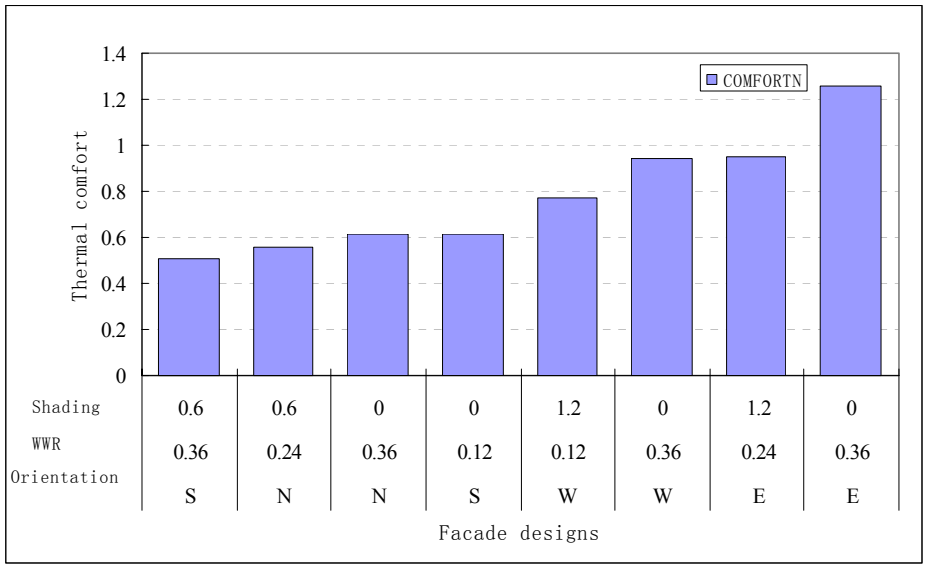

Figure 6.45 Thermal comfort of various facade designs with north wind direction

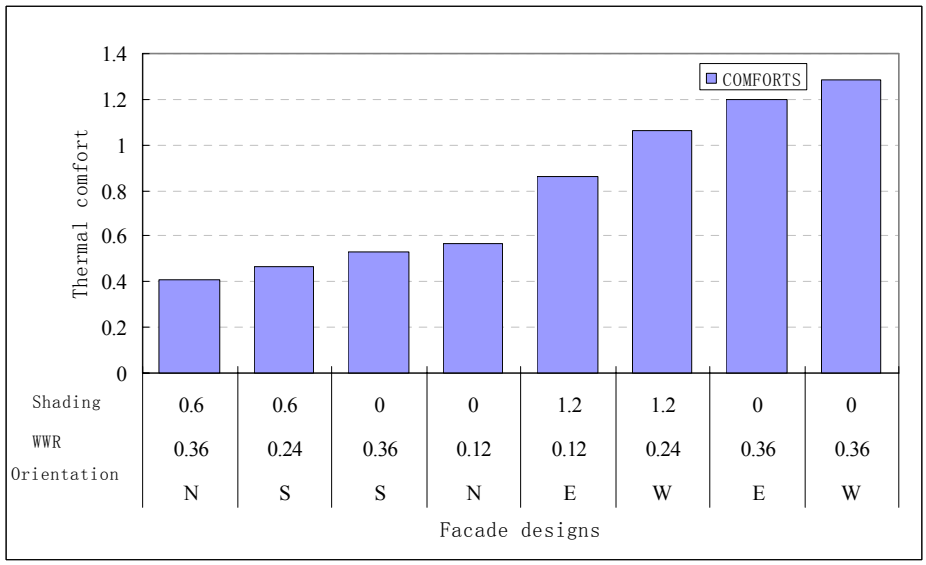

Figure 6.46 Thermal comfort of various facade designs with south wind direction

The impact of orientation

Indoor thermal comfort results are automatically sorted by orientations when wind comes from north or south. With north wind direction, for the same WWR ratio and shading device, the largest difference in the thermal comfort provided due to various facade orientations is from 0.51 (WWR 0.36, 600mm shading device, north) to 1.13 (WWR 0.36, 600mm shading, east). Similarly, with south wind direction, for the same WWR ratio and shading device, the

largest difference for thermal comfort provided due to orientations is from 0.41 (WWR 0.36, no shading device, north)to 1.29 (WWR 0.36, no shading device, west) .

As can be seen in Table 6.9, the optimum WWR and shading dimensions vary according to different facade orientations. For south facing facade, the optimum facade design is WWR=0.36 with horizontal shading width 300mm. For north facing facade, the optimum WWR is 0.24 with or without shading. For west facing facade the optimum WWR is 0.12 with horizontal shading width more than 1200mm and for east facing facade the optimum WWR is 0.24 or 0.12 with horizontal shading width more than 1200mm.

The impact of WWR (window to wall ratio) and shading devices

In addition to facade orientation, WWR and shading devices are also significant parameters on indoor thermal comfort. Since west and east orientations are the worst facing scenarios when winds come from south or north, west and east oriented facades should be paid more attention.

As shown in Figure 6.45 with north wind direction, thermal comfort index increases from 0.772 (optimum facade design) to 0.95 (worst facade design) for west facing facade and it increases from 0.95 (optimum facade design) to 1.26(worst facade design) for east facing facade. It can be seen from Figure 6.46 that with south wind direction, thermal comfort index increases from 1.06 (optimum facade design) to 1.29 (worst facade design) for west facing facade and it increases from 0.86 (optimum facade design) to 1.2(worst facade design) for east facing facade. The results indicate shading devices are highly needed for the west and

east facing facade to improve indoor thermal comfort. For west and east orientations, if local main wind direction is mainly parallel with the facade, large WWR should be avoided even for the naturally ventilated buildings, which results in more solar heat gains, higher surface temperature and higher indoor temperature.

2) West and east wind directions

Thermal comfort distribution of eight cases (composed of maximum and minimum PMV cases for each façade orientation) is illustrated in Figure 6.47 for west wind direction and in Figure 6.48 for east wind direction. Detailed thermal comfort results are shown in Figure App.5.3 and Figure App.5.4 for west wind direction and east wind direction respectively. The optimum facade designs for four orientations are listed in the Table 6.10 (west wind direction) and table 6.11(east wind direction). The best facade design for west wind direction is WWR= 0.3, west facing and with horizontal shading device above 1200mm and for east wind direction is WWR= 0.3, east facing and with horizontal shading device above 1200mm.

Table 6. 10 Optimum facade design for N S W E orientations with west wind

Orientation	Optimum WWR	Optimum Shading (horizontal)
N	0.12	No shading is needed
S	0.12	No shading is needed
W	0.3	1200mm above
E	0.3 or 0.24	1200mm above

Table 6. 11 Optimum facade design for N S W E orientations with east wind

Orientation	Optimum WWR	Optimum Shading (horizontal)
N	0.12	With 300mm above
S	0.12	No shading is needed
W	0.3	1200mm above
E	0.3 or 0.24	1200mm above

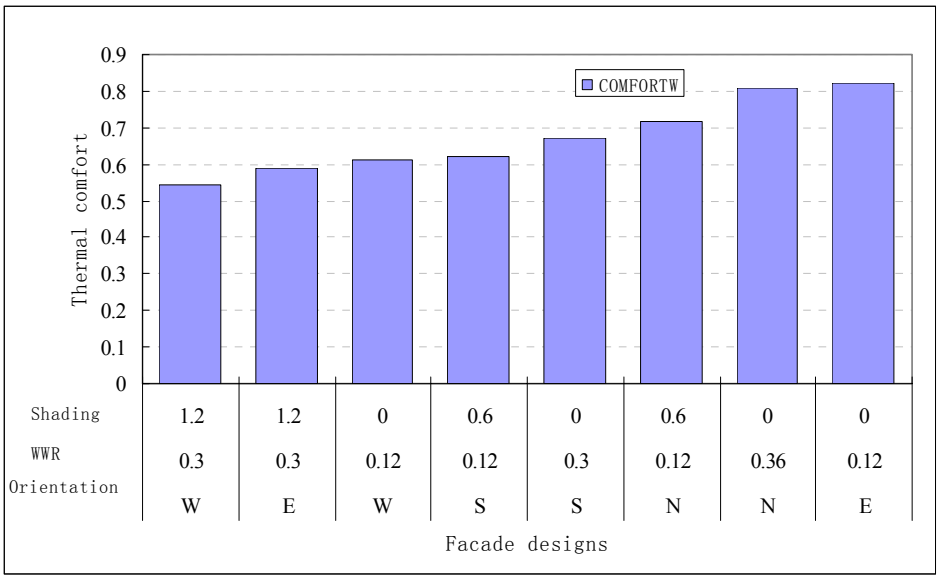

Figure 6.47 Thermal comfort of various facade designs with west wind direction

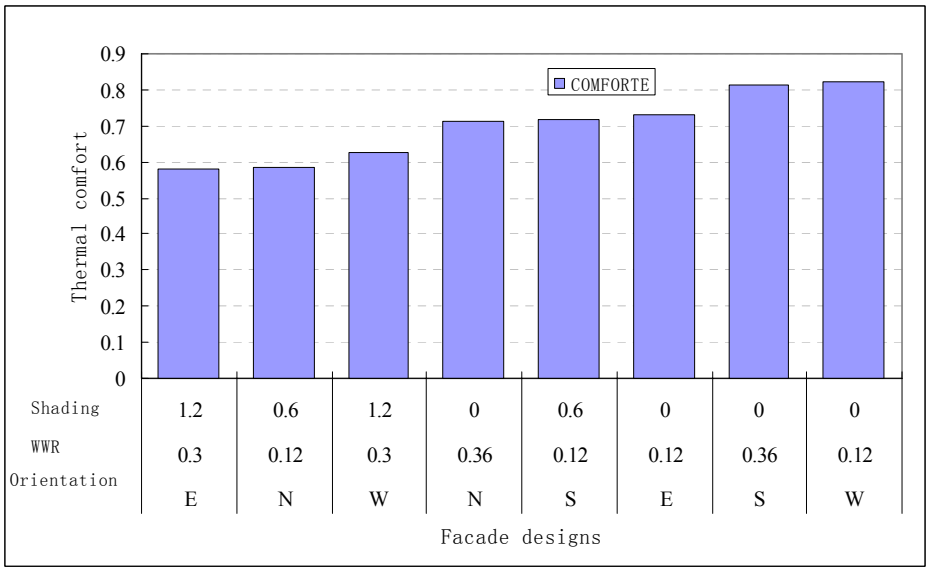

Figure 6.48 Thermal comfort of various facade designs with east wind direction

The impact of Orientation

When the main wind direction is west or east, the impacts of orientations on thermal comfort are not important since west and east orientations, which receive more solar radiations, have the capability to capture wind to improve ventilation rates and indoor thermal comfort. With west wind direction, for the same WWR ratio and shading device, the largest difference for thermal comfort provided due to different orientations is from 0.54 (WWR 0.3, no shading device, west) to 0.78 (WWR 0.3, no shading device, north).

The impact of WWR (window to wall ratio) and shading devices

Shading devices are still very important to improve indoor thermal comfort for the west and east facing facade. As can be seen from Figure 6.47, thermal comfort index increases from 0.59 (optimum facade design) to 0.82(worst facade design) for east facing facade. With east wind direction shown in Figure 6.48, thermal comfort index increases from 0.58 (optimum facade design) to 0.73 (worst facade design) for east facing facade and it increases from 0.625 (optimum facade design) to 0.82 (worst facade design) for east facing facade.

3) Northwest, northeast, southwest and southeast wind directions

The optimum facade designs for each facade orientation are listed in the Table 6.12-6.15, for northwest, northeast, southwest and southeast wind directions respectively. Thermal comfort distribution of eight cases (composed of maximum and minimum PMV cases for each façade orientation) is illustrated in Figures 6.47-6.50. Detailed thermal comfort results are shown in Figure App.5.5-5.8 for different wind directions.

Table 6.12 Optimum facade design for N S W E orientations with northwest wind

Orientation	Optimum WWR	Optimum Shading (horizontal)
N	0.12	No shading is needed
S	0.24	300mm above
W	0.24	1200mm above
E	0.24	1200mm above

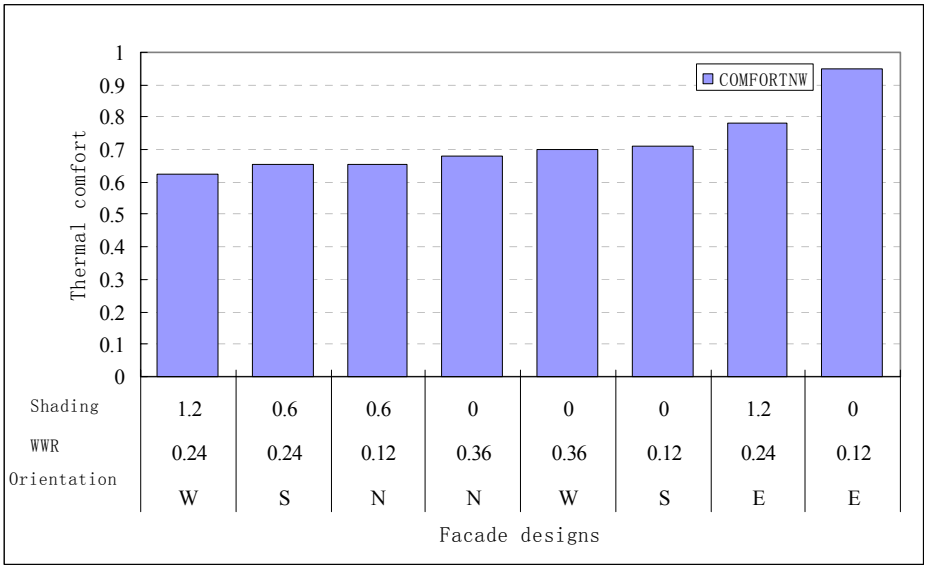

Figure 6.49 Thermal comfort of various facade designs with northwest wind direction

The best facade design for northwest wind direction is WWR= 0.24, west facing and with horizontal shading device above 1200mm. When the main wind direction comes from northwest, the orientation of the facade does not have a large impact on the indoor averaged thermal comfort (Figure 6.49). For the same WWR ratio and shading device, the largest difference for thermal comfort provided due to orientation is from 0.65 (WWR 0.12, no shading device, north) to 0.95 (WWR 0.12, no shading device, east). Shading devices are needed for the west and east facing facade to improve indoor thermal comfort. As can be seen

in Figure 6.49, thermal comfort index increases from 0.78 (optimum facade design) to 0.95 (worst facade design) in east facing facade and it increases from 0.62 (optimum facade design) to 0.70 (worst facade design) in west facing facade.

Table 6.13 Optimum facade designs for N S W E orientations with northeast wind

Orientation	Optimum WWR	Optimum Shading (horizontal)
N	0.24	No shading is needed
S	0.36	No shading is needed
W	0.3	1200mm above
E	0.24	1200mm above

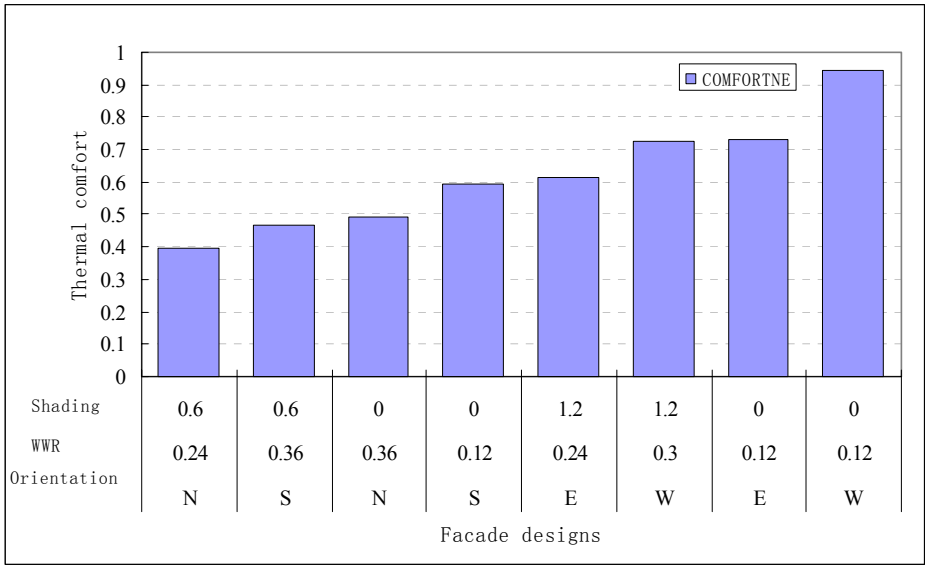

Figure 6.50 Thermal comfort of various facade designs with northeast wind direction

The best facade design for northeast wind direction is WWR= 0.24, north facing and with or without horizontal shading. As can be seen in Figure 6.50, for the same WWR ratio and shading device, the largest difference for thermal comfort provided due to orientation is from

0.46 (WWR 0.12, no shading device, north) to 0.95 (WWR 0.12, no shading device, west). Thermal comfort index increases from 0.64 (optimum facade design) to 0.73 (worst facade design) in east facing facade and it increases from 0.72 (optimum facade design) to 0.95 (worst facade design) in west facing facade.

Table 6.14 Optimum facade design for N S W E orientations with southwest wind

Orientation	Optimum WWR	Optimum Shading (horizontal)
N	0.36	No shading is needed
S	0.24	No shading is needed
W	0.24	1200mm above
E	0.3	1200mm above

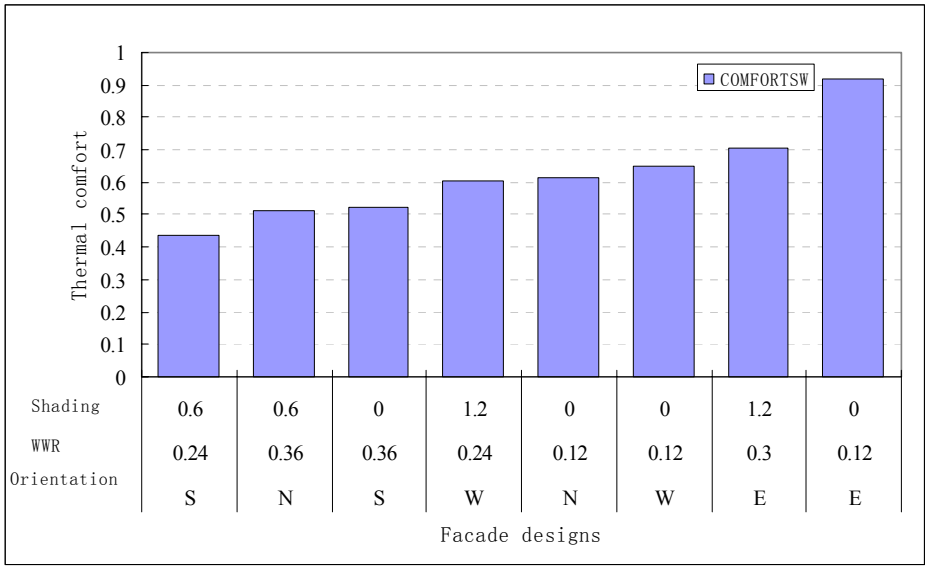

Figure 6.51 Thermal comfort of various facade designs with southwest wind direction

The best facade design for southwest wind direction is WWR= 0.24, south facing and with or without horizontal shading. As shown in Figure 6.51, for the same WWR ratio and shading

device, the largest difference for thermal comfort provided due to orientation is from 0.48 (WWR 0.12, no shading device, south) to 0.92 (WWR 0.12, no shading device, east). Thermal comfort index increases from 0.71 (optimum facade design) to 0.92 (worst facade design) in east facing facade.

Table 6.15 Optimum facade design for N S W E orientations with southeast wind

Orientation	Optimum WWR	Optimum Shading (horizontal)
N	0.3	No shading is needed
S	0.24	No shading is needed
W	0.36	1200mm above
E	0.24	1200mm above

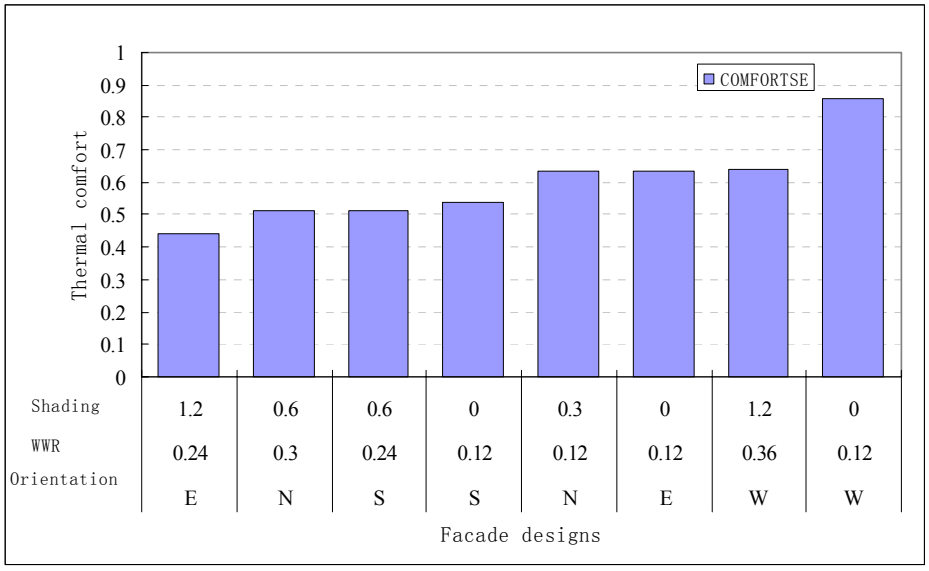

Figure 6.52 Thermal comfort of various facade designs with southeast wind direction

The best facade design for southeast wind direction is WWR= 0.24, east facing and with above 1200mm horizontal shading devices. As shown in Figure 6.52, for the same WWR

ratio and shading device, the largest difference for thermal comfort provided due to orientation is from 0.53 (WWR 0.12, no shading device, south) to 0.86 (WWR 0.12, no shading device, west). From the results (Figure 6.52), it can be seen that WWR (window to wall ratio) and shading devices are significant parameters in facade design. Thermal comfort index increases from 0.44 (optimum facade design) to 0.64 (worst facade design) in east facing facade and it increases from 0.64 (optimum facade design) to 0.86 (worst facade design) in west facing facade.

6.3.3 Design Guidelines

The following recommendation for naturally ventilated buildings in Singapore can be drawn based on the above thermal comfort investigation for various facade designs.

1) The feasibility of natural ventilation for buildings where internal heat sources can be neglected (for example: residential buildings) is confirmed. Based on climatic analyses, there are 52.7% of total hours in the year during which outdoor air condition is inside neutral comfort zone and therefore, thermal comfort could be naturally satisfied. The rest of 47.3% of total hours in the year are outside neutral comfort zone.
2) The U-value of facade materials for north and south orientation should be less than 2.5 W/m^2K and The U-value of facade materials for west and east orientation should be less than $2W/m^2K$ in order to avoid thermal asymmetry near the openings.
3) North and south facing facades can provide much comfortable indoor environment than east and west facing facades in Singapore. Shading devices are needed for east and west facing facades.

4) If residential buildings have to face east or west due to the site limitations, try to build up these buildings in such a way that they are about 45 degree to the west or east to increase ventilation. Direct east and west facing facades should be avoided.

5) The coupled simulations indicate the optimum window to wall ratio is 0.24. Horizontal shading devices are needed for the four orientations for further improvement in indoor thermal comfort.

6) Based on the coupled simulation results of eight typical hours, the weighted thermal comfort results with acceptable U values are summarized in Table 6.16.

Table 6.16 Design guidelines for naturally ventilation residential buildings in Singapore

	East	**West**	**North**	**South**
WWR=0.12	U=2W/m^{2}K **PMV=0.82** Above **600mm** horizontal shading	U=2W/m^{2}K **PMV=0.83** Above **600mm** horizontal shading	U=2.5W/m^{2}K **PMV=0.59** No shading is needed	U=2.5W/m^{2}K **PMV=0.58** No shading is needed
WWR=0.24	U=2W/m^{2}K **PMV=0.75** Above **600mm** horizontal shading	U=2W/m^{2}K **PMV=0.77** **600mm** horizontal shading is needed	U=2.5W/m^{2}K **PMV=0.54** **300mm** horizontal shading is needed	U=2.5W/m^{2}K **PMV=0.53** **300mm** horizontal shading is needed
WWR=0.3	U=2W/m^{2}K **PMV=0.75** Above **1200mm** horizontal shading	U=2W/m^{2}K **PMV=0.78** Above **1200mm** horizontal shading	U=2.5W/m^{2}K **PMV=0.54** **300mm** horizontal shading	U=2.5W/m^{2}K **PMV=0.54** **300mm** horizontal shading
WWR=0.36	U=2W/m^{2}K **PMV=0.81** Above **1200mm** horizontal shading	U=2W/m^{2}K **PMV=0.83** Above **1200mm** horizontal shading	U=2.5W/m^{2}K **PMV=0.56** **300mm** horizontal shading	U=2.5W/m^{2}K **PMV=0.56** **300mm** horizontal shading

Chapter 7 Conclusions and future works

The work presented in this thesis can be summarized in the two parts: 1) The development of an external coupling program between building simulation (BS) and computational fluid dynamics (CFD) for naturally ventilated buildings; 2) The investigation of naturally ventilated residential buildings in Singapore for better thermal comfort. This chapter discusses and summarizes the results of the research work described in previous chapters. The major contributions of this work are reviewed and suggestions for future works are discussed further.

7.1 Summary and Results

In Chapter 4, different turbulence models are tested to predict pressure coefficients (Cp). The realizable $k-\varepsilon$ two equation turbulence model can well predict Cp values of external facades and also has the advantages of fast calculation and easy convergence. Different turbulence modeling methods (standard $k-\varepsilon$ two equation model, RNG $k-\varepsilon$ two equation models, realizable $k-\varepsilon$ two equation model, Reynold stress model) were used to predict mean pressure coefficients of external surfaces. The simulation results were compared with the experiment results done by AIJ group (1994). It was concluded that realizable $k-\varepsilon$ two equation model can accurately predict Cp while standard $k-\varepsilon$ model does not predict Cp of the horizontal roof well. The predicted Cp of external facade by the realizable $k-\varepsilon$ model could be fed into building simulation program as boundary conditions for airflow network simulation.

In terms of coupling strategies, by comparing two different coupling strategies (velocity as boundary condition and pressure as boundary conditions for indoor CFD) between BS and CFD, taking pressure results of apertures from BS as indoor CFD boundary conditions is a reliable strategy for natural ventilation prediction (see Chapter 5). Single–zone, multi-zone, and building block cases were simulated and the coupling results were validated with full CFD simulation (both indoor and outdoor) to verify the reliability of the pressure coupling strategy. The field measurement results of a typical residential building in Singapore were used to validate the coupling program in a time series. The consistency of measured data and the coupling program results proved the effectiveness of the coupling program.

In Chapter 6, the feasibility of natural ventilation application in Singapore was analyzed based on typical year 2001 weather data. It was concluded that comfort indoor environment can be achieved with better facade designs for naturally ventilated buildings in Singapore. The U-value of facade materials was investigated for naturally ventilated buildings to avoid thermal asymmetry. Based on these preliminary studies, a set of facade designs for high-rise naturally ventilated residential buildings, with various orientations, window to wall ratios and shading devices, were investigated by using the coupled simulations and evaluated with thermal comfort index. Interestingly, among different the facade design parameters, window to wall ratio is the most critical for naturally ventilated buildings. The coupled simulations indicate the optimum window to wall ratio is equal to 0.24 for full day ventilation. It can be attributed to the fact that both indoor air velocity and solar heat gains are highly affected by the window to wall ratios. It was also found that horizontal shading devices are necessary for the four orientations for better indoor thermal comfort to reduce indoor heat gains.

7.2 Contributions

The major contributions of this thesis are summarized here.

- Development of coupled simulation methodology to predict indoor thermal comfort in naturally ventilated building by providing detailed results. The coupling program with text-mode interface is able to provide a more quick and accurate way to predict long term natural ventilation in high rise residential buildings.
- Confirmation of the reliability of realizable $k-\varepsilon$ two equation model in predicting Cp of external facades. With the use of realizable $k-\varepsilon$ two equation model, computation cost is largely reduced and convergence can easily be achieved.
- Confirmation of the feasibility of natural ventilation with full day ventilation or night time ventilation strategies being applied in residential buildings in Singapore for indoor thermal comfort.
- Several facade design guidelines for naturally ventilated residential buildings in Singapore are put forward based on indoor thermal comfort criteria and coupled simulation results.
- Relationships between acceptable thermal comfort (or indoor air temperature / indoor air velocity) and different facade designs are provided for architects in detail in easy-to use graphs and table tools.

7.3 Limitations

There were some limitations in the research. Firstly, for coupled simulations, pressure loss coefficients at the openings were not being considered since for cross ventilation pressure drops at the apertures are much smaller compared with those in single sided ventilation and there had been

no available literature about pressure loss coefficients for natural ventilation under cross ventilation. Secondly, the inlet boundary conditions were considered to be uniform in the coupling program, which may not be the real situation, especially for jet flow with angles. Thirdly, for facade parametric studies, only horizontal shading devices were investigated in the parametric studies. However, for the west and east facing facade with more solar radiations, horizontal shading devices may not be good enough to block most of the solar heat gains.

7.4 Suggestions and future works

This study developed a coupling program with text-mode interface for natural ventilation prediction. To further improve its qualities and enhance the applicability of the coupling program, further studies in these areas are expected:

One possible avenue of future work is the extension of the coupling program between BS and CFD using dynamic coupling. In dynamic coupling, the indoor air temperature and mass flow rate by the current coupled simulations will be further fed back into building simulation until the results are converged to further improve the accuracy of coupling program. The accuracy of the simulation results using steady coupling and dynamic coupling should be compared by using field measurement results as well as the full CFD simulations.

Another interesting area of future work is the investigation of velocity profiles, pressure profiles and direction profiles at apertures from different wind directions. With the input of more detailed pressure profiles at the openings, the accuracy of coupling program is expected to be further improved. Therefore, investigations of detailed inlet profile with different wind

directions, which are related to the average values for inlet condition, will be able to find non-uniform inlet profiles to further improve calculation accuracy of coupling program.

In addition, further investigation with the coupling program on various types of shading devices, not only horizontal shading devices, but vertical fins and the combination of horizontal ones and vertical ones, should be done for detailed understanding of facade performance in naturally ventilated buildings.

7.5 Conclusions

This thesis has developed a coupling method between building simulation and CFD simulation. The main contributions of the work are in the development and application of the coupling program and a text-mode interface for naturally ventilated high rise residential buildings. The coupling program between BS and CFD can be used by researchers or engineers for accurate prediction of natural ventilation.

Façade designs for natural ventilation is a challenging task, which is related to indoor thermal comfort and domestic energy consumption. There are several important façade design parameters. However, it would probably be biased to simply take one parameter into account and neglect others. The coupling program between BS and CFD simulation can accurately and efficiently predict indoor thermal environment in detail and can be used as a convenient tool for façade design evaluation of naturally ventilated buildings. Thermal comfort could be used as the criteria to evaluate the combination effect of different façade design parameters.

References

Aasem, E. O. (1993).Practical Simulation of Buildings and AIr-Conditioning Systems in the Transient Domain. PhD Thesis.University of Strathclyde.

Allard, F. (1998). Natural ventilation in buildings—A design handbook. James & James Ltd, UK.

ASHRAE.(2004). Thermal environmental conditions for human occupant. Atlanta, ASHRAE, USA.

AIJ Working Group. (1994). Numerical prediction of wind loading on buildings and structures. Division for Wind Loading Design. Architecture Institute of Japan. (in Japanese)

Baker, N., and Standeven, M. (1996).Thermal comfort for free-running buildings. Energy and buildings, 23, 175-182.

Beausoleil-Morrison, I (2001). The Adaptive Coupling of Heat and Air Flow Modelling Within Dynamic Whole-Building Simulation. PhD Thesis. University of Strathclyde.

Bojic, M., and Yik, F. (2005).Cooling energy evaluation for high-rise residential buildings in Hong Kong. Energy and buildings, 37 (4), 345-351.

Bouchlaghem, N. (2000). Optimizing the design of building envelopes for thermal performance. Automation in Construction, 10(1). 101-112.

Building and Construction Authority (2004). Guidelines on Envelop Thermal Transfer Value for Buildings. Singapore.

Brager, G.S., and De Dear, R.J. (1998). Thermal adaptation in the built environment: a literature review. Energy and Buildings, 27, 83-96.

Burnett, J., Bojic, M. and Yik, F., (2005). wind-induced pressure at external surfaces of a high-rise residential building in Hong Kong, Building and Environment 40765-777

Chandra, S., and Kerestecioglu,A.A. (1984). Heat transfer in naturally ventilated rooms data from full-scale measurements. ASHRAE Transactions 90. 211-224.

Chen, Q. (2004). Using computational tools to factor wind into architectural environment design. Energy and Buildings, 39(8), 1000-1009.

Chen, Q.(1995). Comparison of different K-e models for indoor air flow computations. Numerical heat transfer, Part B, 28,353-369.

Chen, Q. and Xu, W. (1998) A zero equation turbulence model for indoor airflow simulation. Energy and Buildings,28,137-144.

Cheung, C.K., Fuller, R.J., and Luther, M.B. (2005). Energy-efficient envelope design for high-rise apartments. Energy and buildings, 37 (1), 37-48.

Chow, T. T. (1995) Air-Conditioning Plant Component Taxonomy by Primitive Parts. PhD Thesis. University of Strathclyde.

Chrenko, F.A. (1953). Heated ceilings and comfort. Journal of the Institute of Heating and Ventilating Engineers. 20, 375-396 ; 21, 145-154.

Clarke J A. (1977) Environmental systems performance. PhD thesis. University of Strathclyde

Clarke JA, and McLean D.(1988). ESP-A building and plant energy simulation system. Strathclyde: Energy Simulation Research Unit. University of Strathclyde.

Clarke J A. (2001)Energy Simulation in Building Design.. Butterworth-Heinemann. Oxford. 2nd Edition.

Crawley D.B., Lawrie L.K., Pederson C.O., and Winkelmann F.C. (2000). EnergyPlus: energy simulation program. ASHRAE Journal 42(4). 49-56.

Corrado, V., Serra,V., and Vosilla, A.(2004). Performance analysis of external shading devices. In Proceedings of PLEA 2004, Netherlands.

Cockcroft J.P. (1979), Heat Transfer and Air Flow in Buildings, PhD Thesis, University of Glasgow, Glasgow U.K.

De Dear, R.J., and Brager, G.S. (1998). Developing an adaptive model of thermal comfort and preference, Field studies of thermal comfort and adaptation, ASHRAE Technical Data Bulletin 14(1) (1998)27-49; ASHRAE Transactions 104(1) (1998).

De Dear, R.J., and Brager, G.S. (2002). Thermal comfort in naturally ventilated buildings: revisions to ASHRAE standard 55.Energy and buildings, 34, 549-561.

De Wit, Sten and Augenbroe, G. (2002). Analysis of uncertainty in building design evaluations and its implications. Energy and Buildings. 34, Issue 9, 951-958

Dutt, A.J., De Dear R.J. and Krishnan Parthiphan. (1992). Full scale and model investigation of natural ventilation and thermal comfort in a building. Journal of Wind Engineering and Industrial Aerodynamics. 41-44. 2599-2609

Djunaedy, E. (2005). External coupling between building energy simulation and computational fluid dynamics. Ph.D. thesis. Technische University of Eindhoven, April, 2005

EDSL (Environmental Design Solution Limited). (1989). TAS simulation manuals

ESRU(Energy simulation research unit) (2002).ESP-r: User's guide version 10 series. University of Strathclyde.

Evola, G and Popov, V. (2005). Computational analysis of wind driven natural ventilation in buildings. Energy and buildings. Volume 38, Issue 5, May 2006, Pages 491-501

Fanger, P.O. (1970). Thermal comfort: Analysis and application in Environmental Engineering. Danish Technical Press.

Fanger,P.O., and Toftum, J.(2002). Extension of the PMV model to non-air-conditioned buildings in warm climates. Energy and Buildings, 34, 533-536.

Feriadi,H.(2003). Thermal comfort for natural ventilated residential buildings in the tropical climate. PhD dissertation. National University of Singapore.

Feustel, HE. (1999). COMIS—an international multi-zone air-flow and contaminant transport model. Energy and buildings. 30, 3-18.

FLUENT user' s guide version 6.2. FLUENT Inc.

Givoni, B. (1978).L'Homme, l' Architecture et le Climat. Eyrolles, Paris (French Edition).

Givoni, B. (1981). Man, Climate and Architecture, second edition. Van Nostrand Reinhold Company. USA.

Carrilho-da-Graca, G, Chen, Q., Glicksman, L.R. and Norford, L.K. (2002). Simulation of wind driven ventilative cooling systems for an apartment building in Beijing and Shanghai. Energy and Buildings, 34(1), 1-11.

Gritzki, R., Seifert, J., Richter, W., and Rosler, M.(2004). Determination of the air change rate for natural ventilation with regard to energy efficiency and building physics.In Proceedings of roomvent, Portugal.

Grosso, M.(1992). Wind pressure distribution around buildings: a parametrical model. Energy and Buildings. 18. 101-131.

Häggkvist, K., Svensson, U., and Taesler, R.(1989). Numerical simulations of pressure fields around building Building and Environment. 24(1) , 65-72.

Hand, J .W.(1998). Removing Barriers to the Use of Simulation in the Building Design Professions. PhD Thesis.University of Strathclyde.

Hanjalic, K. and Launder, B.E. (1972). A Reynolds stress model of turbulence and its application to asymmetric shear flows. Journal of Fluid Mechnaics. 52, 609-638.

Hensen, J. (1991). On the Thermal Interaction of Building Structure and Heating and Ventilating System. PhD Thesis. University of Eindhoven.

Herrlin, M. (1990). Solution Methods for Air Flow Networks, in COMIS Fundamentals, Lawrence Berkeley Laboratory Report.

Hittle D.C. (1979). Building load analysis and system thermodynamics (BLAST) users manual. Technical Report E-153. Vol. 1 and 2. US army Construction Engineering Research Laboratory (USA-CERL), Champaign, IL.

Holmbom, A. (1982). Numerical predictions of flow over two-dimensional obstacles. WREL water resources engineering Luleå.

Iaccarino, G., Ooi, A., Durbin, P.A., and Behnia, M. (2003). Reynolds averaged simulation of unsteady separated flow. International Journal of Heat and Fluid Flow. 24, 147-156.

Jiang, Y. & Chen, Q. (2001). Study of natural ventilation in buildings by large eddy simulation. Journal of Wind Engineering and Industrial Aerodynamics. 89,1155-1178.

Jiang, Y. & Chen, Q. (2002). Effect of fluctuating wind direction on cross natural ventilation in buildings from large eddy simulation. Building and environment. 37, 379-386.

Jiang, Y., Alexander, D., Jenkins, H., Arthur, R., and Chen, Q. (2003). Natural ventilation in buildings: measurement in a wind tunnel and numerical simulation with large-eddy simulation. Journal of Wind Engineering and Industrial Aerodynamics. 91, 331-353.

Kelly, N .J.(1998) Towards a Design Environment for Building-Integrated Energy Systems: The Integration of Electrical Power Flow Modelling with Building Simulation. PhD Thesis, University of Strathclyde.

Kim, S.-E. and Choudhury, D. (1995). A near-wall treatment using wall functions sensitized to pressure gradient. In ASME FED Vol.217. Separated and Complex Flows. ASME.

Lam, K.P. (1997). Mapping of the sky luminance distribution and computational prediction of daylighting performance in Singapore. National University of Singapore.

Launder, B.E. and Spalding, D.B. (1974). The numerical computation of turbulent flows. Computer Methods in Applied Mechanics and Engineering. (3). 269-289.

Liddament, M.W. (1986). Air infiltration calculation techniques - an applications guide, IEA Air Infiltration And Ventilation Centre (AIVC), Bracknell (UK).

Lin, B., Tan, G., Wang, P., Song L., Zhu Y., and Zhai G. (2004). Study on the thermal performance of the Chinese traditional vernacular dwellings in Summer. Energy and buildings, 36, 73-79.

Lin, H. (2006) Tropical and subtropical characteristics of building energy and climatic context of architecture. INTA conference, 2006, Jogjakarta, Indonesia

Lakehal, D and Rodi, W (1997). Calculation of the flow past a surface-mounted cube with two-layer turbulence models. Journal of Wind Engineering and Industrial Aerodynamics 67&68, 65-78.

LBNL (Lawrence Berkeley National Laboratory). (1982). The DOE2.1A Reference Manual. Berkeley, CA.

Lorenzetti, David M.(2002).Computational aspects of nodal multizone airflow systems Building and Environment. 37(11), 1083-1090.

MacQueen, J.(1997).The Modelling and Simulation of Energy Management Control Systems. PhD Thesis. University of Strathclyde.

Mallick, F.H.(1996).Thermal comfort and building design in the tropical climate, Energy and buildings ,23, 161-167.

Melaragno, M. (1982). Wind in Architectural and Environmental Design. Van Nostrand Reinhold, New York.

Mitalas GP, and Stephenson DG. (1967). Room thermal response factors. ASHRAE Transactions. 73(1).

Muniz, P. A.(1985). The geometry of external shading devices as related to natural ventilation, daylighting and thermal comfort, with particular reference to tropical hot humid climates. PH.D. dissertation. Virginia Polytechnic Institute and State University. University Microfilms international.

Shuzo, M., Akashi, M. and Hayashi. (1990). Examing the k-e model by means of a wind tunnel test and large-eddy simulation of the turbulence structure around a cube. Journal of Wind Engineering and Industrial Aerodynamics. 35, 87-100

Nakhi, A. E.(1995) Adaptive Construction Modelling Within Whole Building Dynamic Simulation. PhD Thesis. University of Strathclyde

Negrao, C. O. R.(1995) Conflation of Computational Fluid Dynamics and Building Thermal Simulation. PhD Thesis. University of Strathclyde.

Nicol, J.F., and Humphreys, M.A. (1973).Thermal comfort as part of a self-regulating system. Building Research and Practise (J CIB), 6(3), 191-197.

Nicol, J.F., and Humphreys, M.A. (2002). Adaptive thermal comfort and sustainable thermal standards for buildings. Energy and Buildings, 34, 563-572.

Nicol, F., (2004).Adaptive thermal comfort standards in the hot-humid tropics. Energy and Buildings, 36(7), 628-637.

Ozdeniz, M and Hancer, P. (2005). Suitable roof constructions for warm climates—Gazimagusa case. Energy and Buildings, 37 (6), 643–649.

Patankar S.V. and Spalding D.B. (1972). A calculation procedure for heat, mass and momentum transfer in three-dimensional parabolic flows. International Journal of Heart and Mass Transfer. (15).1787-1806.

Patankar S.V. (1980). Numerical Heat Transfer and Fluid Flow, McGraw-Hill.

P.W.D. (The development & building control division) (1979). Handbook on energy conservation in buildings and building services. The Division, Singapore.

Reed, R. (1953). Design for natural ventilation in hot humid weather. Housing and building in hot-humid and hot-dry climate. B.R.A.B. Conference Report No.5, Washington, May 1953.

Seifert, J., Axley, J., Li, Y., and Rosler, M. (2004).The effect of wall porosity on the flow rate in a building ventilated by cross wind, proceedings of roomvent, Portugal.

Shih, T.-H., Liou, W. W., Shabbir, A., Yang, Z., and J. Zhu. A New k- ϵ Eddy Viscosity Model for High Reynolds Number Turbulent Flows - Model Development and Validation. *Computers Fluids*, 24(3):227-238, 1995.

Simiu, E. and Scanlan, R.H. (1986). Wind effects on structures: an introduction to wind engineering, Wiley-Interscience, Chichester ,UK.

Srebric, J., Chen, Q. and Glicksman, L.R. (2000). A coupled airflow and energy simulation program for indoor thermal environment studies. ASHRAE Transactions 106(1) 465-476

Sreshthaputra, A. (2003). Building design and operation for improving thermal comfort in naturally ventilated buildings in a hot-humid climate. PhD dissertation. Texas A&M University.

Sreshthaputra, A., Haberl, J. and Andrews, M. J. (2004). Improving building design and operation of a Thai Buddhist temple. Energy and Buildings, 36 (6),481-494.

Stephenson DG and Mitalas GP. (1967) Cooling load calculation by thermal response factor method. ASHRAE Transactions. 73(1)

Tang, D. (1985). Modelling of Heating and Air-Conditioning Systems. PhD dissertation. University of Strathclyde.

Tan, G (2005). Study of natural ventilation design by integrating the multi-zone model with CFD simulation. PhD dissertation. MIT

Tetsuro, T., Hiromasa, K., Shinji, K., Kojiro, N., Shigehiro, S. and Takeshi, O. (1997). Numerical prediction of wind loading on buildings and structures –Activities of AIJ cooperative project on CFD. 67&68 671-685

Tantasavasdi, C., Srebric, J., and Chen, Q. (2001). Natural ventilation design for houses in Thailand. Energy and Buildings, 33, 815-824.

Versteeg, H.K. and Malalasekera. W.(1995). An introduction to computational fluid dynamics : the finite volume method. Harlow, Essex: Longman Scientific & Technical

Walker, I.S. and Wilson, D.J. (1994). Practical methods for improving estimates of natural ventilation rates. 15th AIVC conference. Buxton. Great Britain. 27-30 Sep, 1994.

Wang, L. and Wong, N. H. (2005a). Thermal analysis of climate environments based on weather data in Singapore for naturally ventilated buildings. the 10th International conference on Indoor Air Quality and Climate, Beijing, 2005

Wang, L. and Wong, N. H. (2005b). The impacts of facade and ventilation strategies on indoor thermal environment for a naturally ventilated residential building in Singapore, the 10th International conference on Indoor Air Quality and Climate, Beijing, 2005

WMO (1983). Guide to Meteorological Instruments and Methods of Observation. World Meteorological Organization No.8, 5th edition, Geneva Switzerland.

Wong, N.H. and Khoo, S.S. (2003). Thermal comfort in classrooms in the tropics. Energy and Buildings,35,337-351.

Xia, Y.Z., Zhao, R.Y., and Jiang, Y. (1999). Thermal comfort in naturally ventilated houses in Beijing.HVAC &R ,29(4), 1-5(in Chinese).

Yakhot, V. and Orszag, S. A. (1986). Renormalization group analysis of turbulence: basic theory. *Journal of Scientific Computing*, 1:3-11

Zhai, Z., Hamilton, S.D., Huang, J., Allocca, C., Kobayashi, N., and Q.Chen.(2000). Integration of indoor and outdoor airflow study for natural ventilation design using CFD, Proceedings 21st AIVC annual conference, "Innovations in ventilation technology", 26-29Sep 2000, paper 13

Zhai Z. (2003). Developing an integrated building design tool by coupling building energy simulation and computational fluid dynamics programs. PhD Thesis. Massachusetts Institute of Technology.

Zhu, Y., and Lin, B. (2004). Sustainable housing and urban construction in China, Energy and buildings, 36(12), 1287-1297.

REFEREED JOURNAL PUBLICATIONS

1. **Liping Wang** and Nyuk Hien Wong Coupled simulations for naturally ventilated residential buildings, Automation in Construction (Accepted)
2. **Liping Wang,** Nyuk Hien Wong and Shuo Li Facade design optimization for naturally ventilated residential buildings in Singapore, Energy and buildings (In print)
3. **Liping Wang** and Nyuk Hien Wong Coupled simulation for naturally ventilated rooms between building simulation (BS) and computational fluid dynamics (CFD) for better prediction of indoor thermal environment, Building and Environment (In print)
4. **Liping Wang** & Nyuk Hien Wong Investigation of the possibility of applying natural ventilation for thermal comfort in residential buildings in Singapore, Architectural Science Review (In print)
5. **Liping Wang** and Nyuk Hien Wong The impacts of facade and ventilation strategies on indoor thermal environment for a naturally ventilated residential building in Singapore, Building and Environment (In print)
6. Nyuk Hien Wong and **Liping Wang**, Aida Noplie Chandra, Anupama Rana Pandey and Wei Xiaolin Effects of double glazed façade on energy consumption, thermal comfort and condensation for a typical office building in Singapore, Energy and buildings, Volume 37, Issue 6, June 2005
7. Angui Li, Phillip Jones, Pingge Zhao, and **Liping Wang** Heat transfer and natural ventilation from single-sided heated solar chimney for buildings, Journal of Asian Architecture and Building Engineering, Volume 3, No.2, 2004

REFEREED CONFERENCE PUBLICATIONS

1. **Liping Wang** and Nyuk Hien Wong, The impacts of facade designs: orientations, window to wall ratios and shading devices on indoor environment for naturally ventilated residential buildings in Singapore. the 23st International conference on Passive and Low energy architecture , Geneva, 6-8 September, 2006

2. **Liping Wang** and Nyuk Hien Wong, Natural ventilation simulation by using coupling building simulation and CFD simulation program for accurate prediction of indoor thermal environment the 23st International conference on Passive and Low energy architecture , Geneva, 6-8 September, 2006
3. **Liping Wang** and Angui Li, A numerical study of Trombe wall for enhancing stack ventilation in buildings. the 23st International conference on Passive and Low energy architecture , Geneva, 6-8 September, 2006
4. **Liping Wang** and Nyuk Hien Wong, Coupling between the CFD simulation and building simulation for better prediction of natural ventilation, the 2nd International conference on sustainable architecture and urban design in tropical regions, Jogjakarta, April, 2006
5. **Liping Wang** and Nyuk Hien Wong, A coupling method to increase the accuracy of natural ventilation prediction in thermal simulation program, 2nd International conference on sustainable architecture and urban design in tropical regions, Jogjakarta, April, 2006
6. **Liping Wang** and Nyuk Hien Wong, The impacts of facade and ventilation strategies on indoor thermal environment for a naturally ventilated residential building in Singapore, the 10th International conference on Indoor Air Quality and Climate, Beijing, 2005 (the paper has been selected in the conference to submit to the international journal)
7. **Liping Wang** and Nyuk Hien Wong, Thermal analysis of climate environments based on weather data in Singapore for naturally ventilated buildings, the 10th International conference on Indoor Air Quality and Climate, Beijing, 2005
8. Angui Li, H Jing and **Liping Wang**, Experimental investigation and CFD prediction on heat transfer and natural convection from single-sided heated solar chimney, the 10th International conference on Indoor Air Quality and Climate, Beijing, 2005
9. **Liping Wang** & Angui Li, A numerical study of vertical solar chimney for Enhancing stack ventilation in buildings, the 21st International conference on Passive and Low energy architecture , the Netherlands, 19-22 September, 2004

Appendix 1 The frequency of occurrence of particular wind conditions

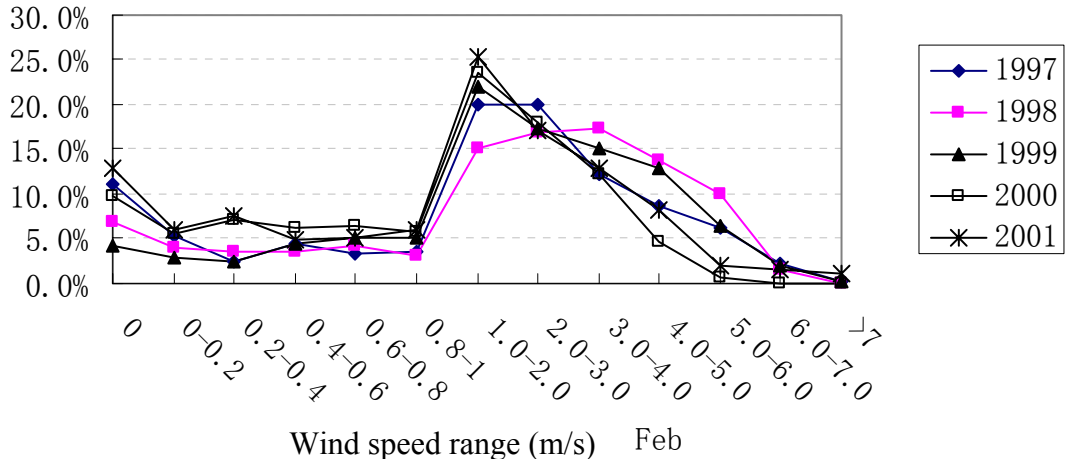

Figure App.1.1 The frequency of occurrence of particular wind conditions in Feb.

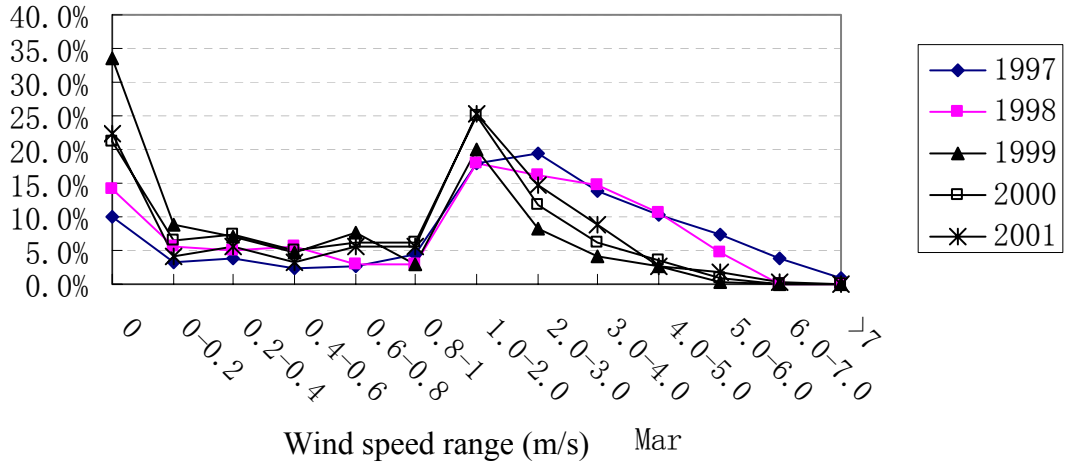

Figure App.1.2 The frequency of occurrence of particular wind conditions in Mar.

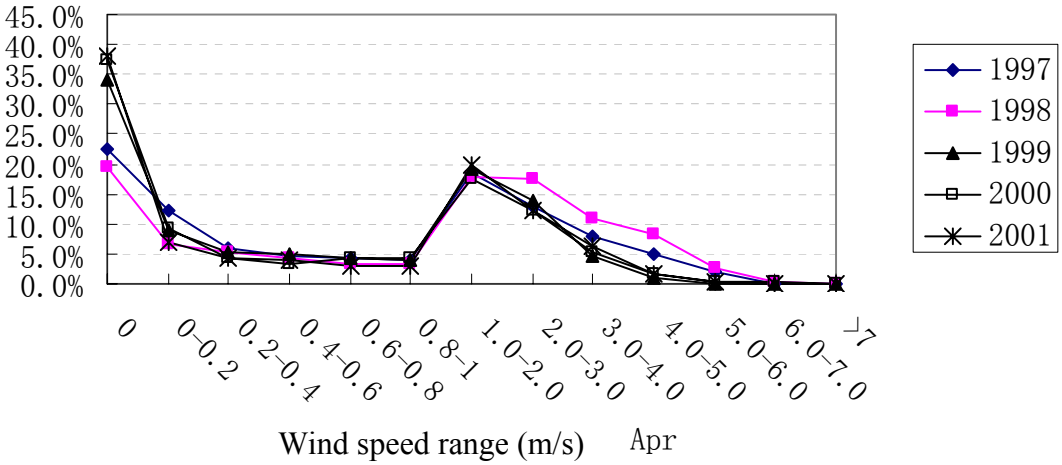

Figure App.1.3 The frequency of occurrence of particular wind conditions in Apr.

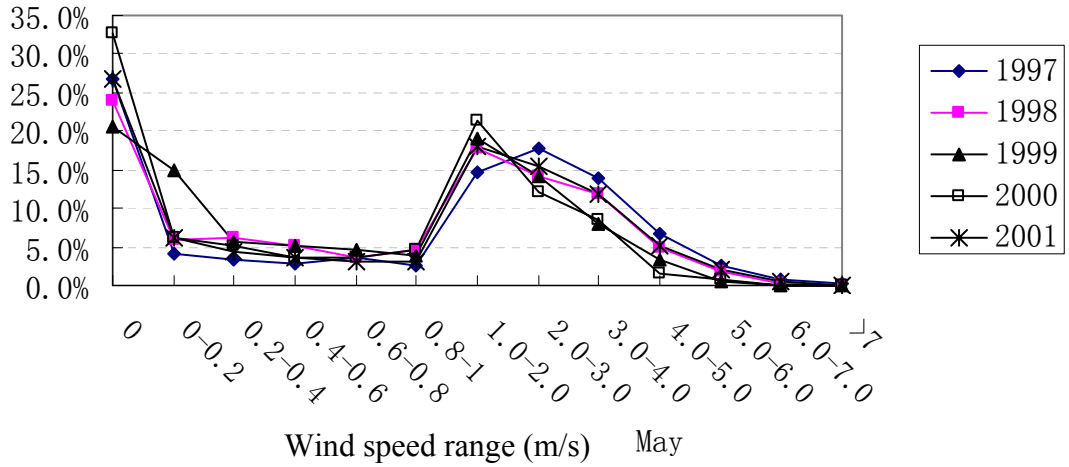

Figure App.1.4 The frequency of occurrence of particular wind conditions in May.

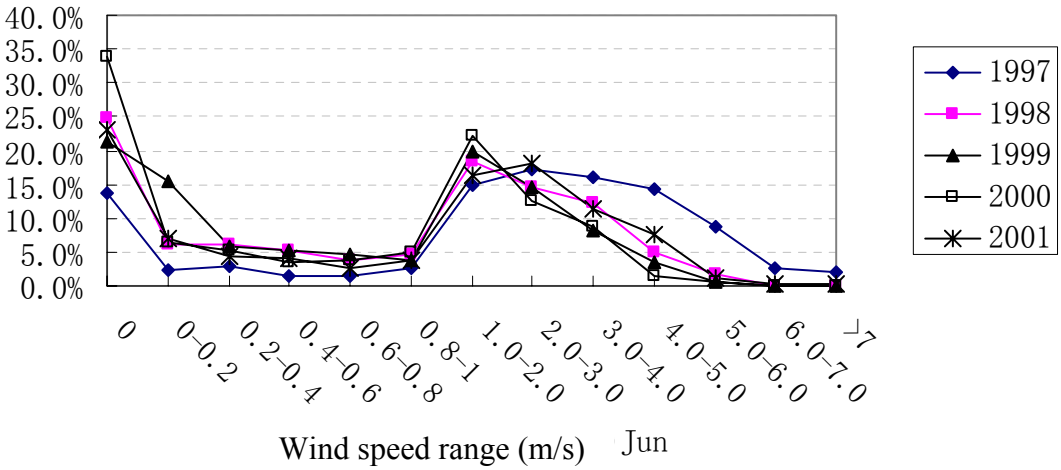

Figure App.1.5 The frequency of occurrence of particular wind conditions in Jun.

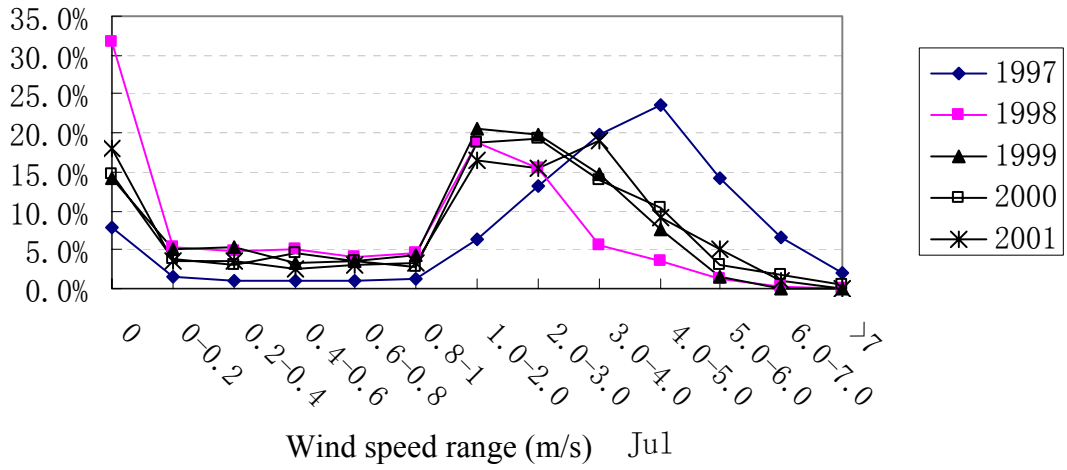

Figure App.1.6 The frequency of occurrence of particular wind conditions in Jul.

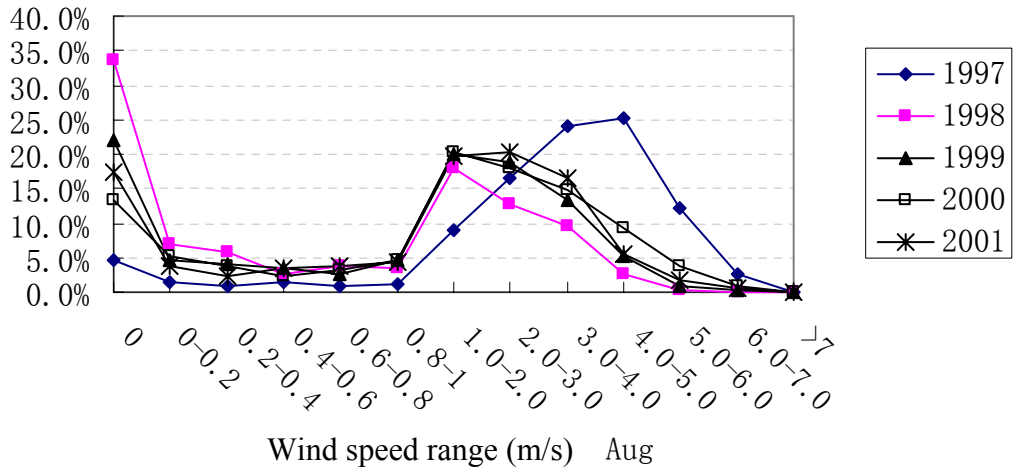

Figure App.1.7 The frequency of occurrence of particular wind conditions in Aug.

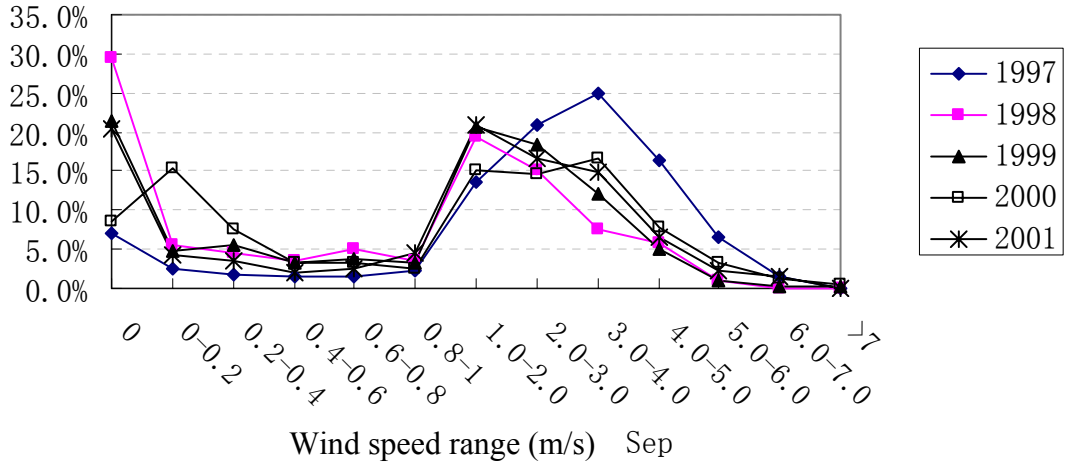

Figure App.1.8 The frequency of occurrence of particular wind conditions in Sep.

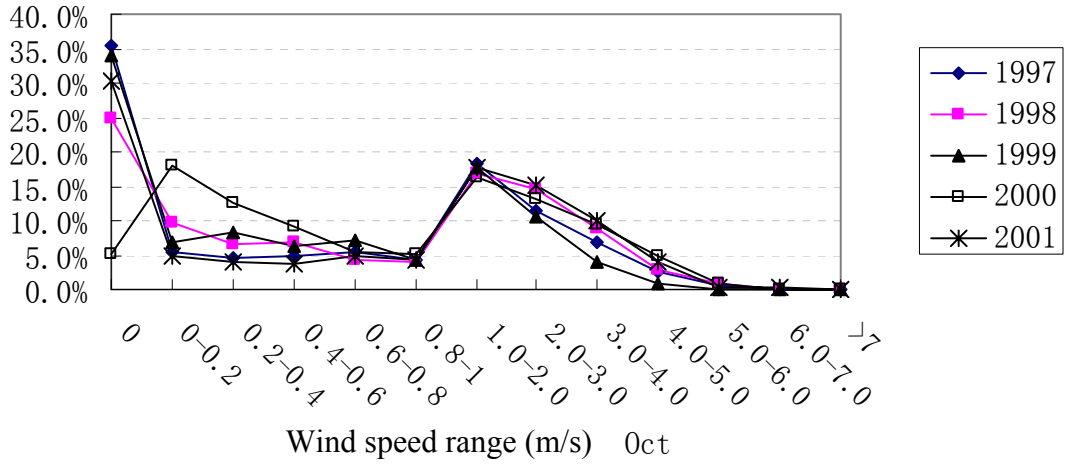

Figure App.1.9 The frequency of occurrence of particular wind conditions in Oct.

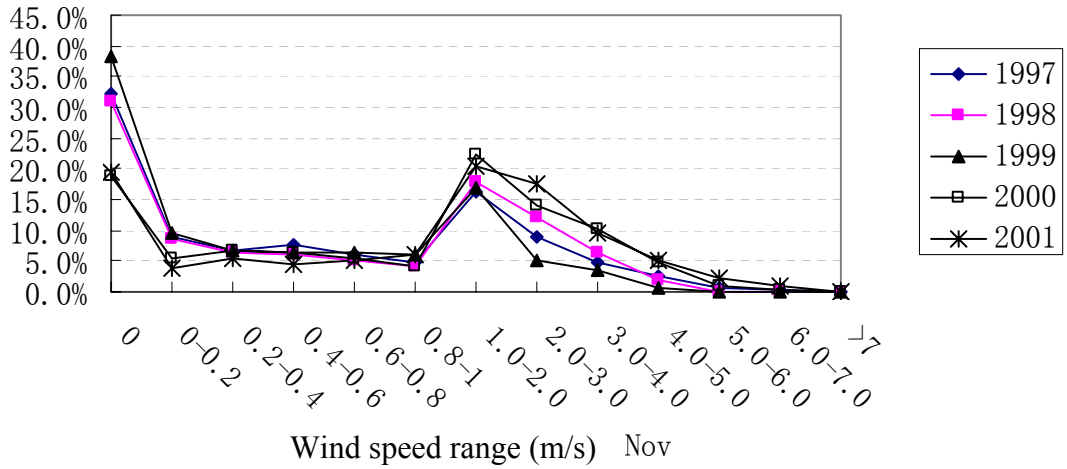

Figure App.1.10 The frequency of occurrence of particular wind conditions in Nov.

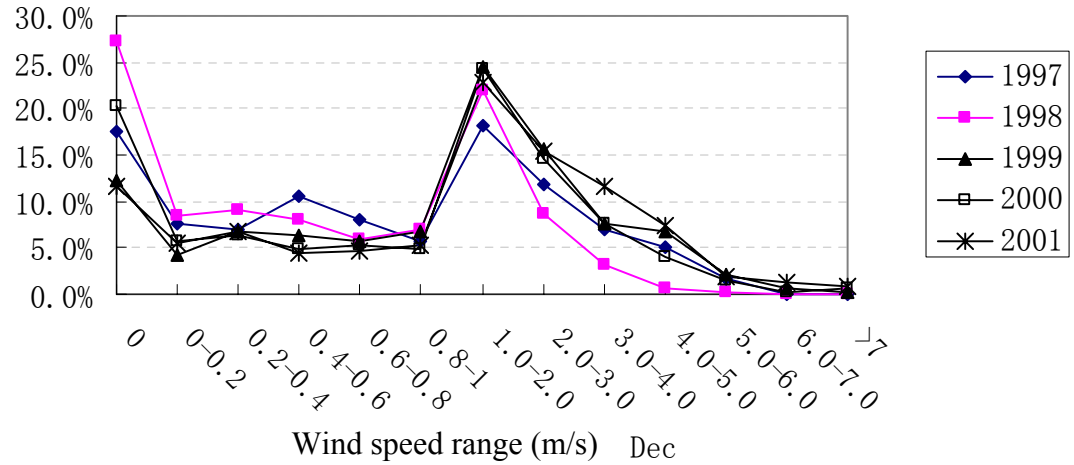

Figure App.1.11 The frequency of occurrence of particular wind conditions in Dec.

Appendix 2 Wind roses for months

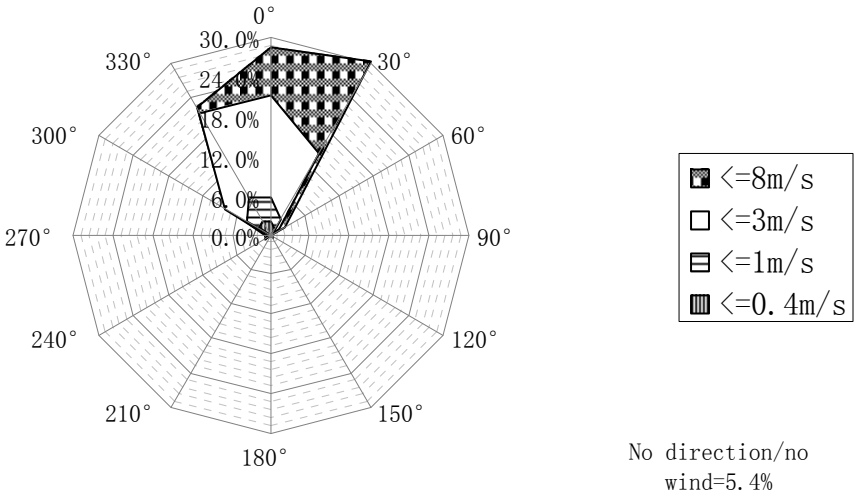

Figure App.2.1 Frequency of wind speed above selected values per direction (Feb)

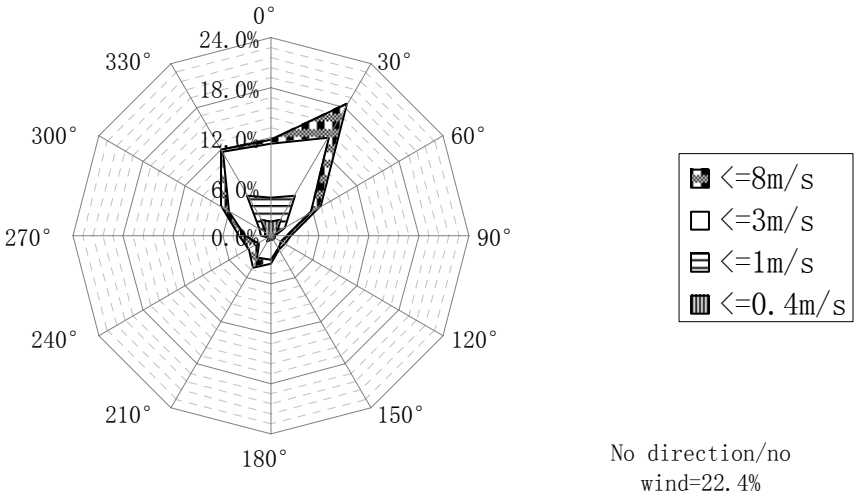

Figure App.2.2 Frequency of wind speed above selected values per direction (Mar)

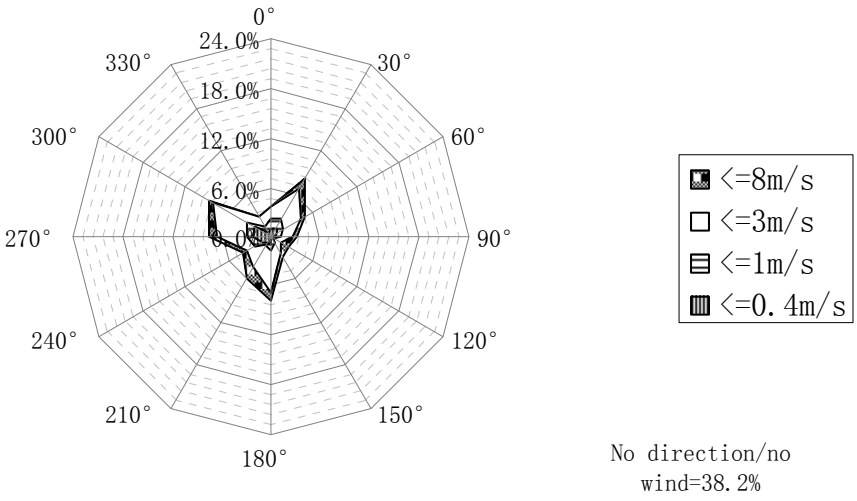

Figure App.2.3 Frequency of wind speed above selected values per direction (Apr)

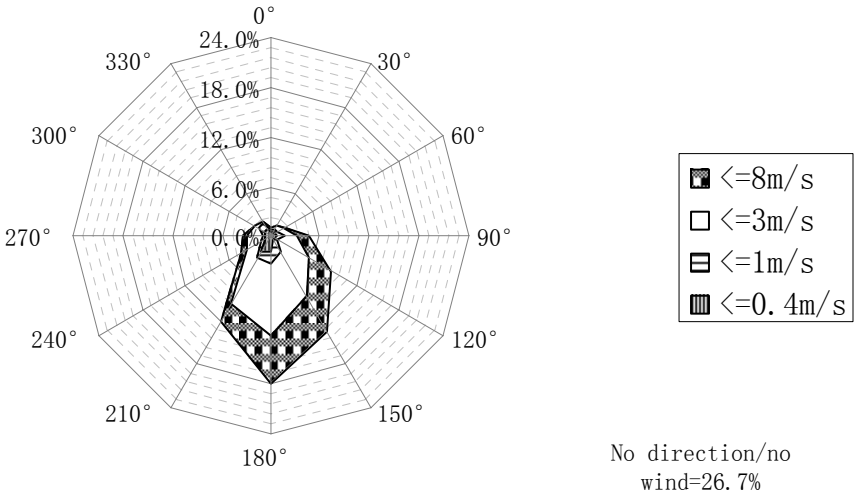

Figure App.2.4 Frequency of wind speed above selected values per direction (May)

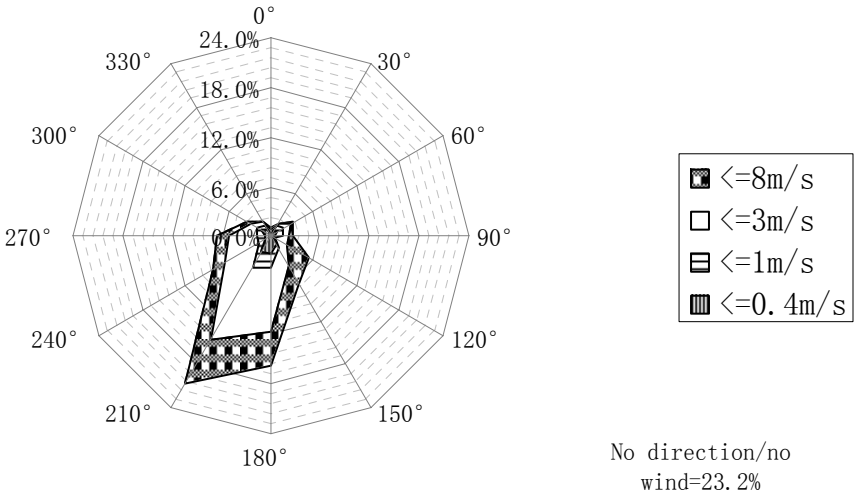

Figure App.2.5 Frequency of wind speed above selected values per direction (Jun)

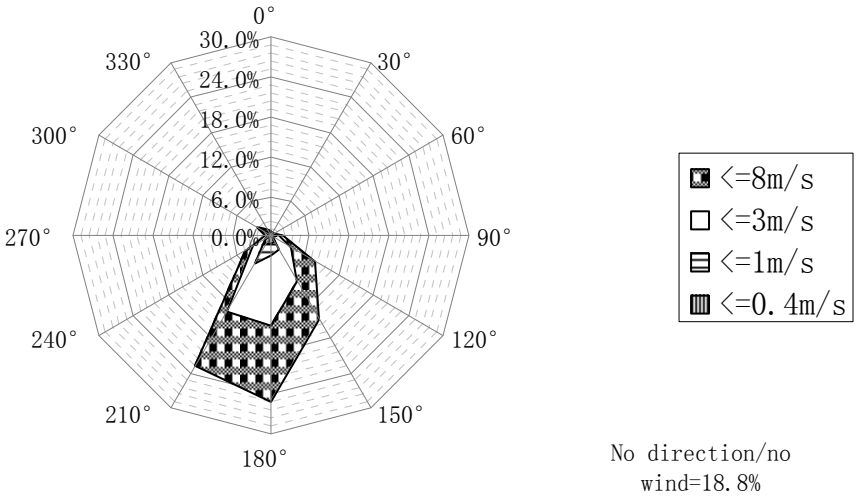

Figure App.2.6 Frequency of wind speed above selected values per direction (Jul)

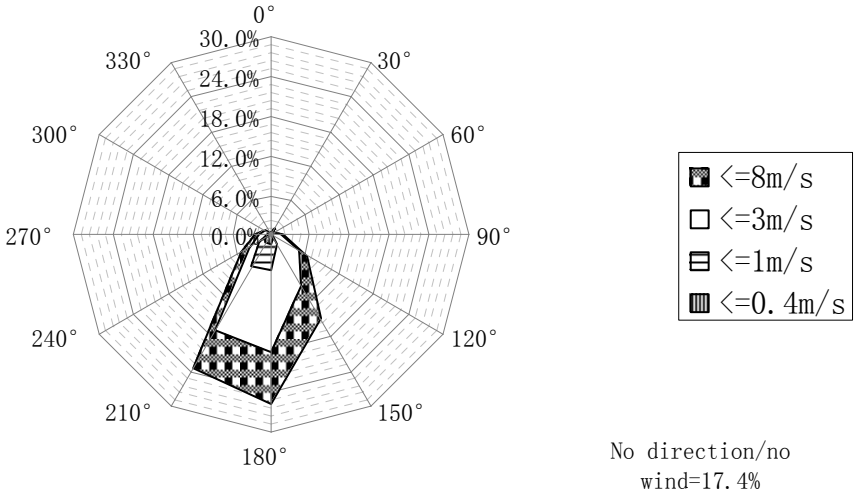

Figure App.2.7 Frequency of wind speed above selected values per direction (Aug)

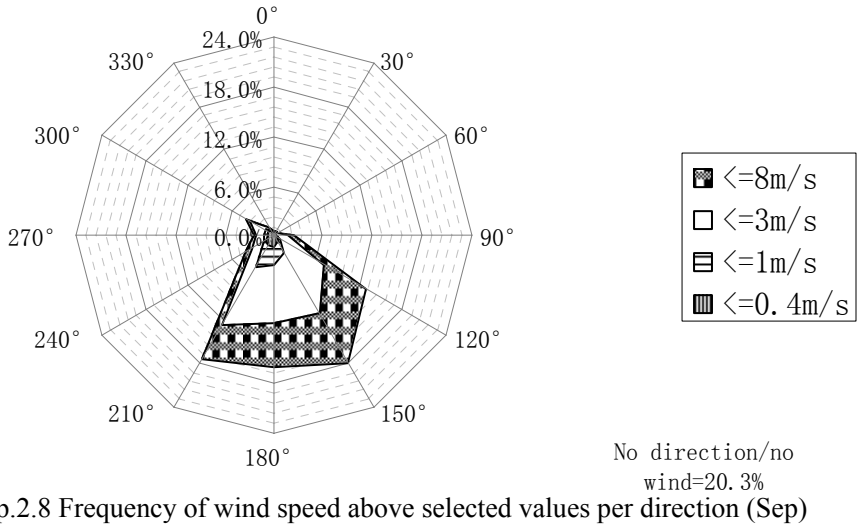

Figure App.2.8 Frequency of wind speed above selected values per direction (Sep)

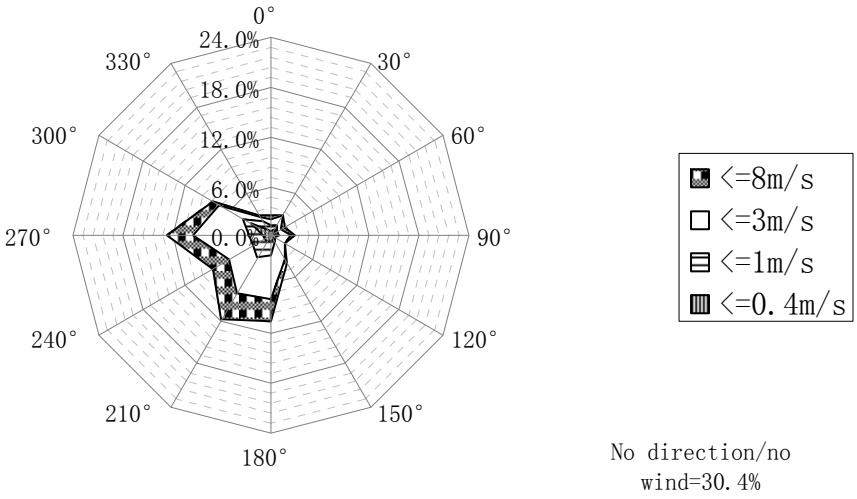

Figure App.2.9 Frequency of wind speed above selected values per direction (Oct)

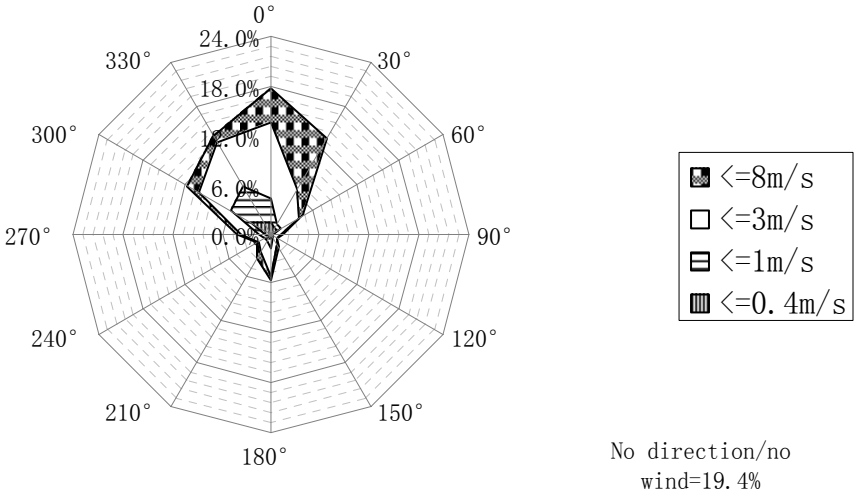

Figure App.2.10 Frequency of wind speed above selected values per direction (Nov)

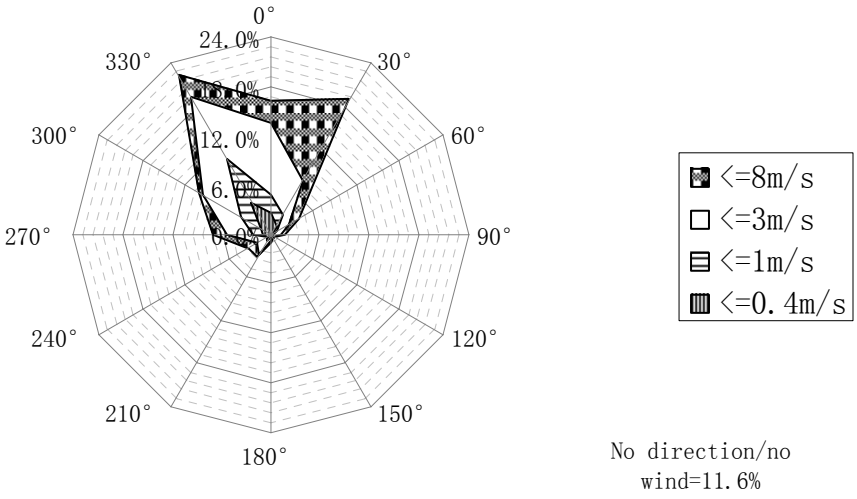

Figure App.2.11 Frequency of wind speed above selected values per direction (Dec)

Appendix 3 Thermal comfort analyses for months

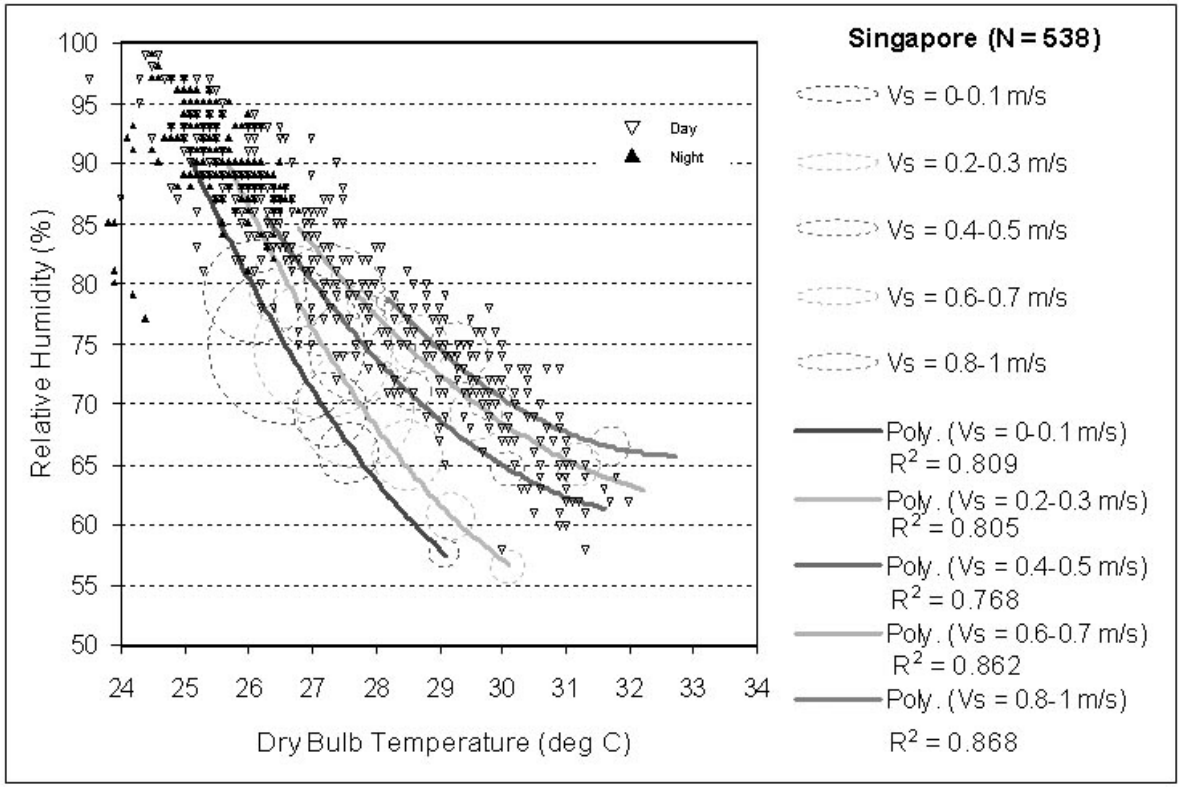

Figure App.3.1 Hourly temperature and RH on Thermal comfort chart in February (Modified from Feriadi, 2003)

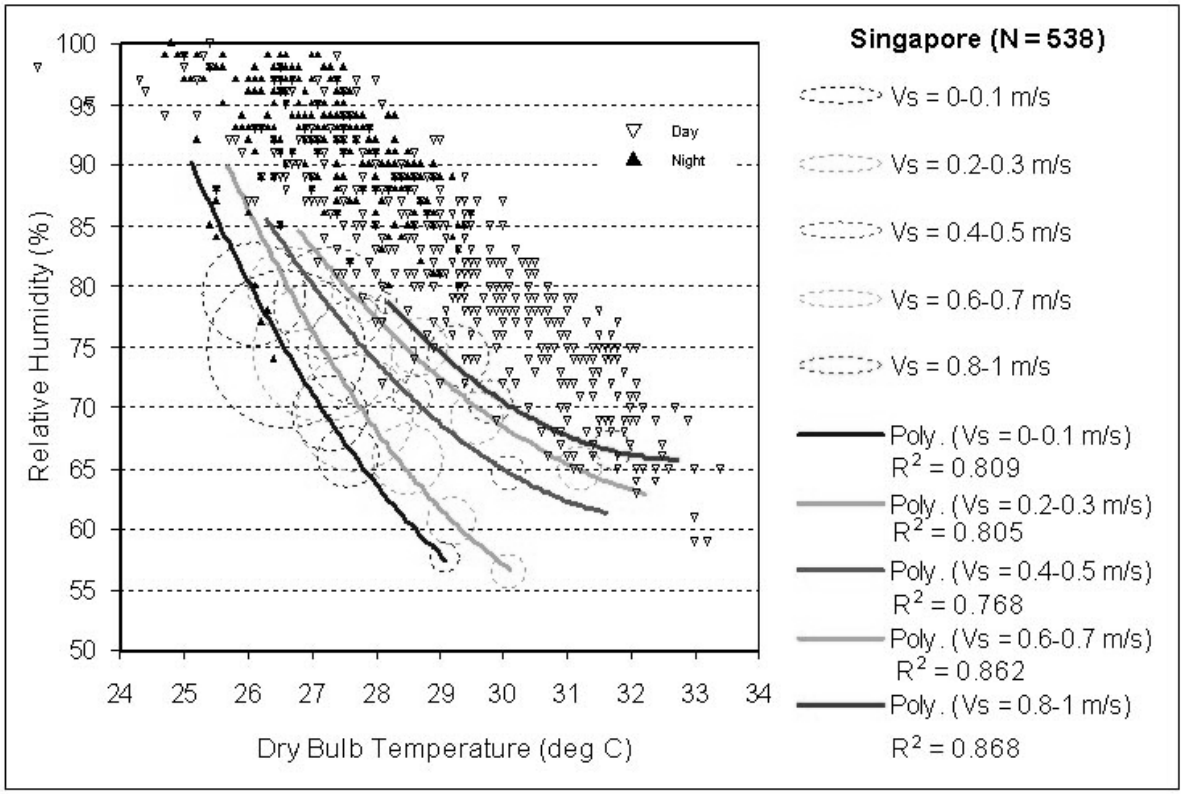

Figure App.3.2 Hourly temperature and RH on Thermal comfort chart in May (Modified from Feriadi, 2003)

Appendix 4 Mean radiant temperature distribution for various facade designs

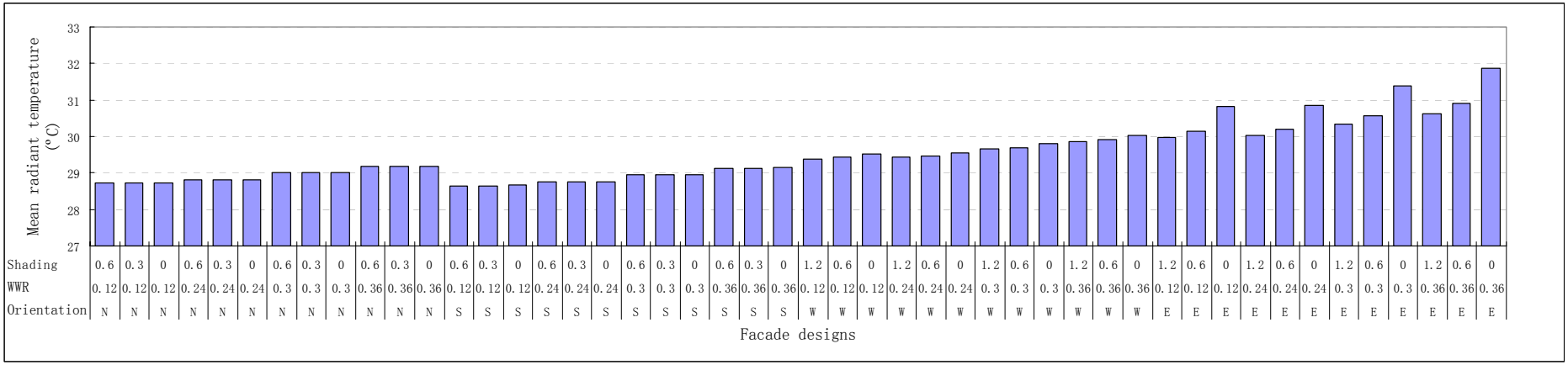

Figure App.4.1 Mean radiation temperature distribution for various facade designs (48 cases)

Appendix 5 Thermal comfort index of various facade designs

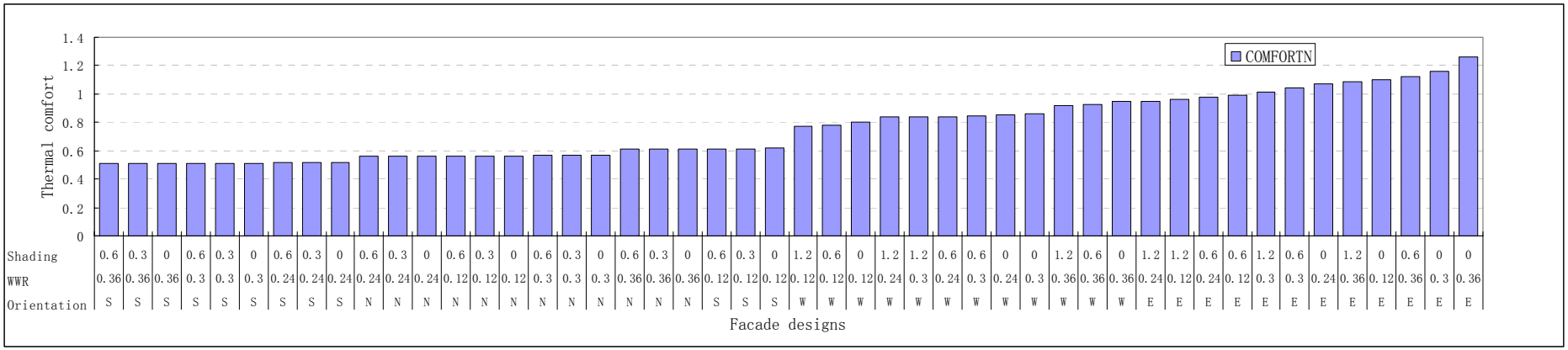

Figure App.5.1 Thermal comfort of various facade designs with north wind direction (48 cases)

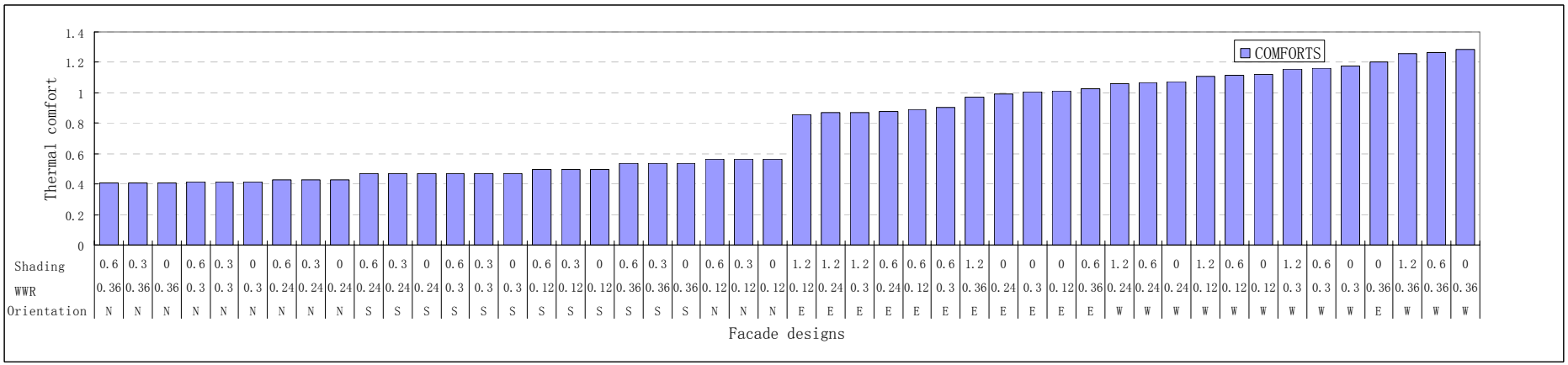

Figure App.5.2 Thermal comfort of various facade designs with south wind direction (48 cases)

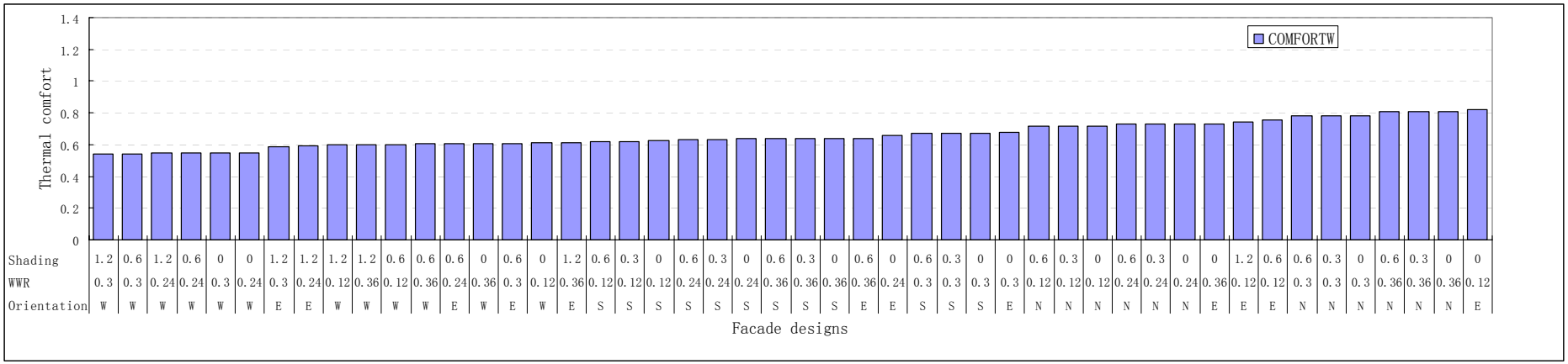

Figure App.5.3 Thermal comfort of various facade designs with west wind direction (48 cases)

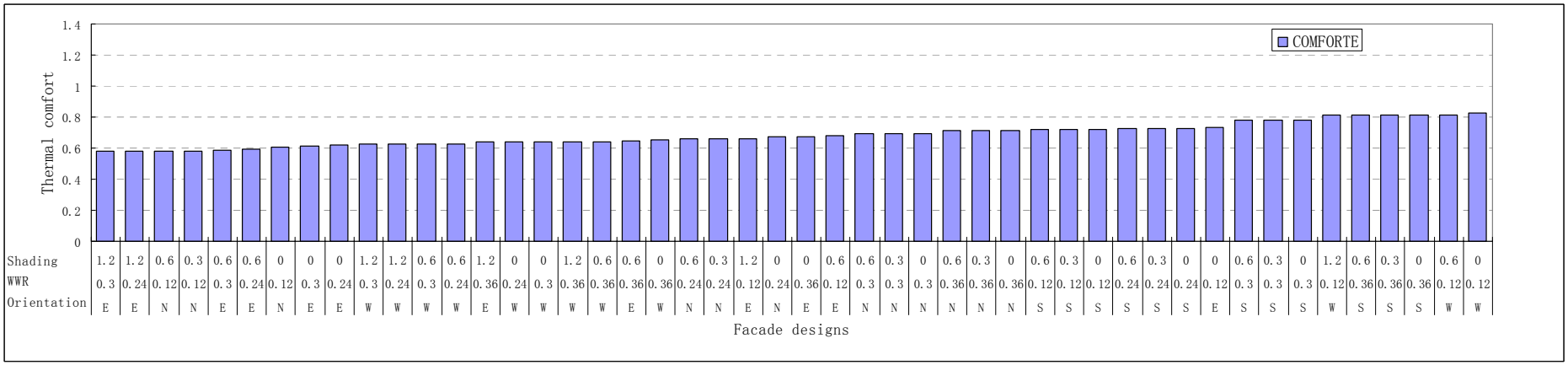

Figure App.5.4 Thermal comfort of various facade designs with east wind direction (48 cases)

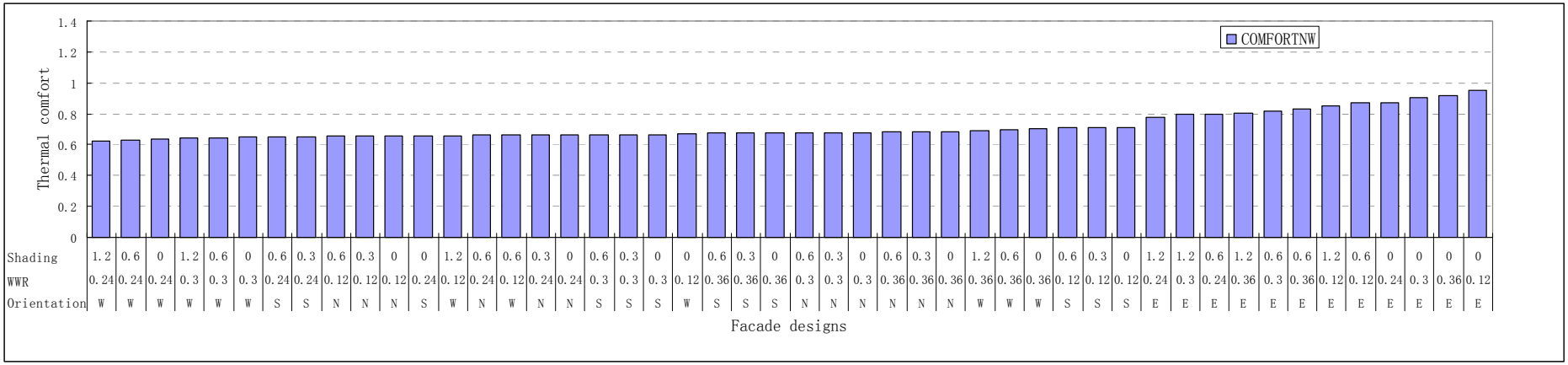

Figure App.5.5 Thermal comfort of various facade designs with northwest wind direction (48 cases)

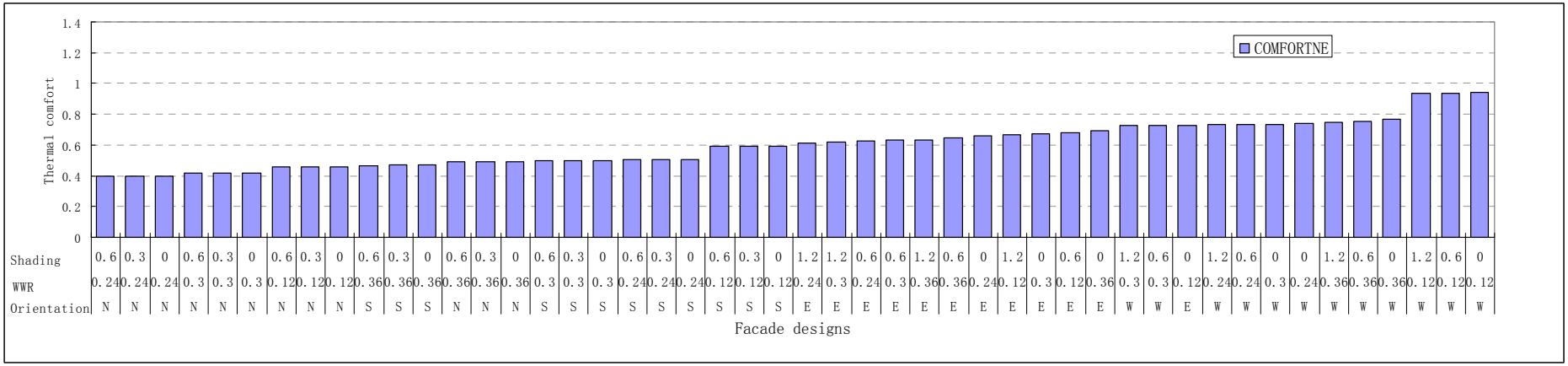

Figure App.5.6 Thermal comfort of various facade designs with northeast wind direction (48 cases)

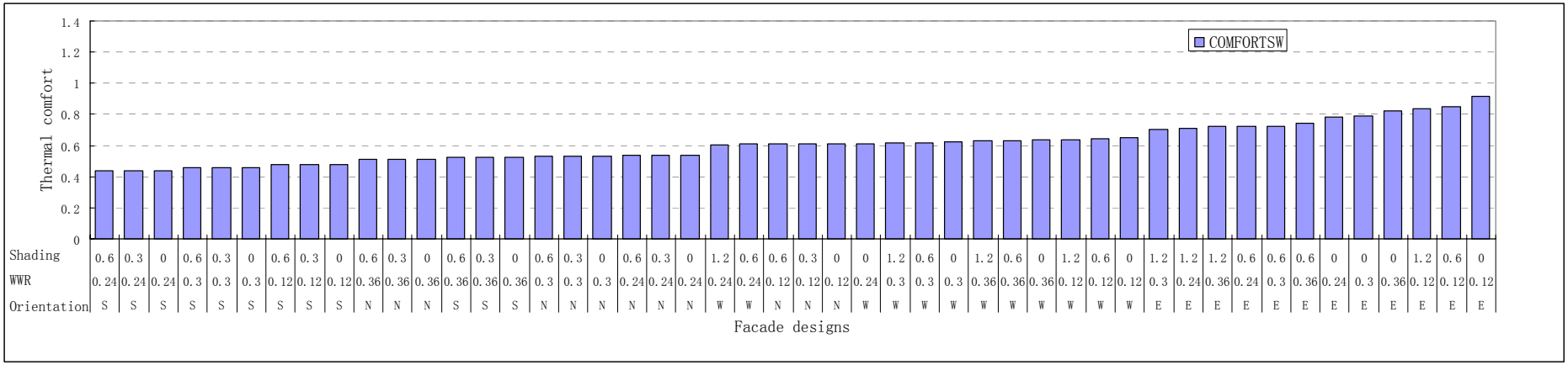

Figure App.5.7 Thermal comfort of various facade designs with southwest wind direction (48 cases)

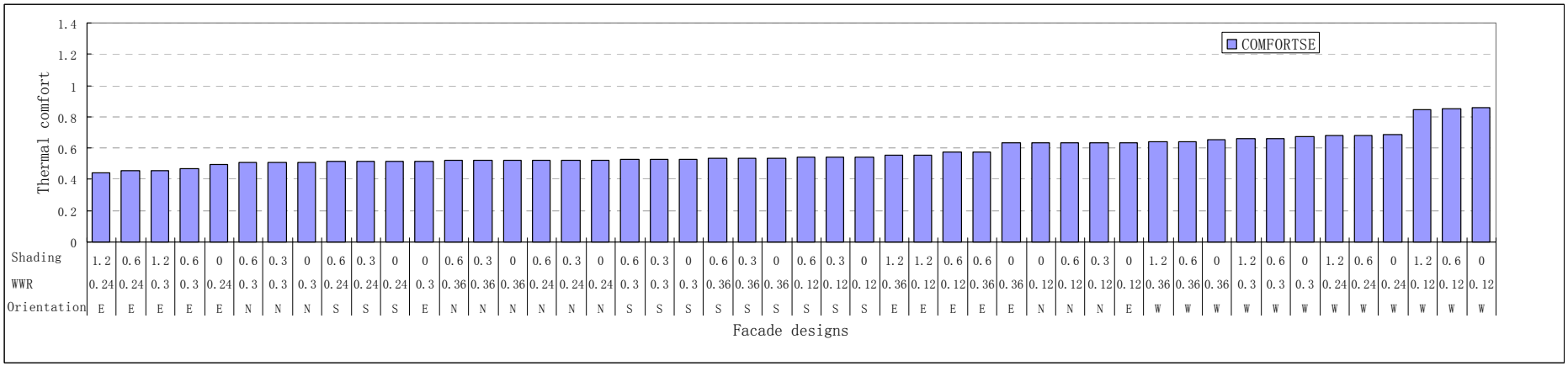

Figure App.5.8 Thermal comfort of various facade designs with southeast wind direction (48 cases)

Appendix 6 The flowchart for natural ventilation study in Singapore

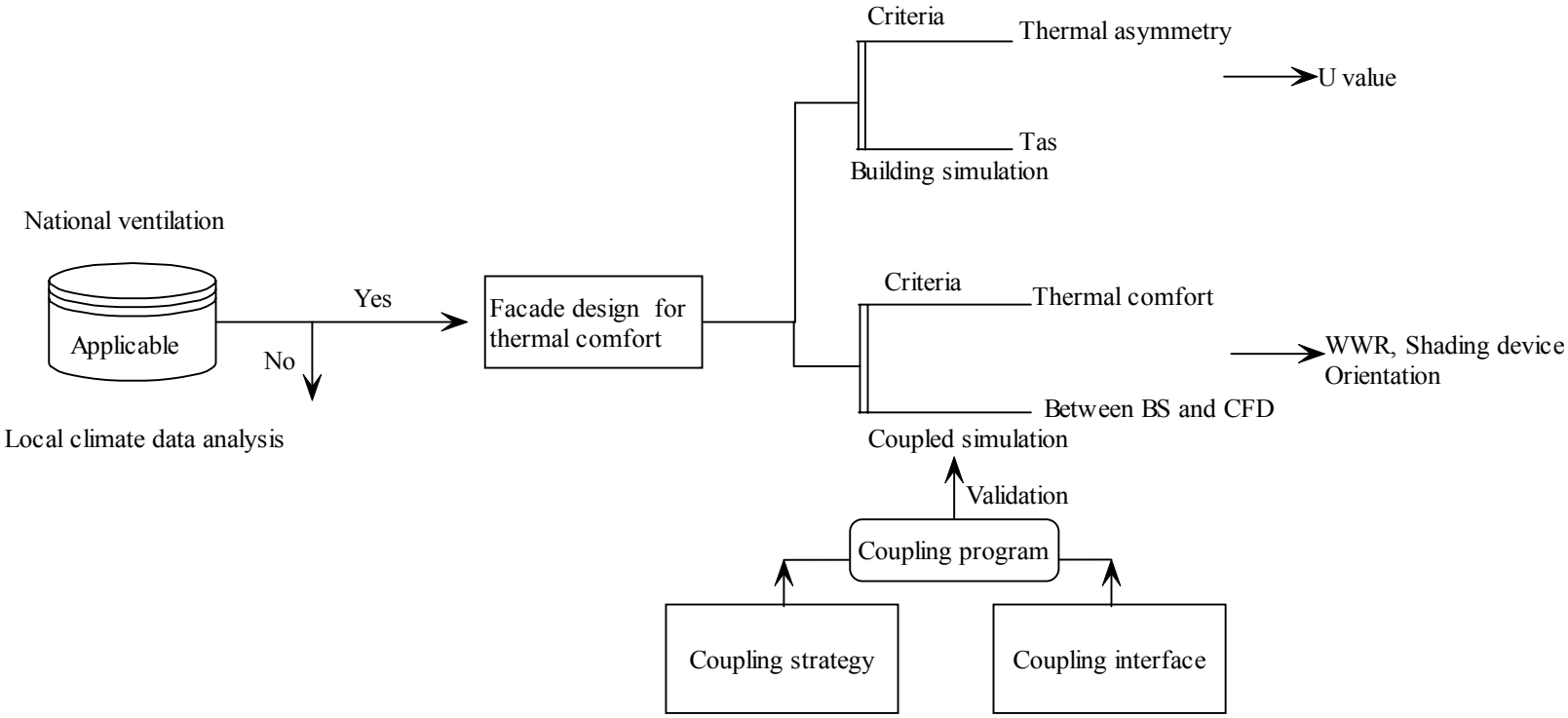

Figure App.6.1 The flowchart for natural ventilation study in Singapore